SISSA
Scuola
Internazionale
Superiore di
Studi Avanzati

Physics Area - PhD course in
Astroparticle physics

Dynamics of phase transitions in the early universe and cosmological consequences

Candidate:
Miguel Vanvlasselaer

Advisor:
Prof. Aleksandr Azatov
Co-advisor:
Prof. Andrea Romanino

Academic Year 2021-22

Contents

List of Figures

List of Tables

Abstract

The advent of gravitational waves (GW) astronomy opens the possibility of probing experimentally the first second of the universe. As a consequence, having a theoretical control over all the early universe events that may have occurred and the putative GW signal that would have been produced at those events has become an urgent matter. The main aim of this thesis is to study the dynamics of First Order Phase Transition (FOPT) with relativistic bubble walls in correlation with the three following processes: GW emission, baryogenesis and production of Dark Matter (DM). After recalling the basics of cosmology, of thermal field theory and of FOPTs in the early universe in the first chapter, in the second chapter, we discuss at length the pressure on the domain wall of the bubble in the ultra-relativistic limit. In so doing we identify and discuss in depth three contributions to this pressure: from particles gaining a mass in the transition, from heavy states with mass up to $\sqrt{\gamma_w v_{\rm trans} T_{\rm nuc}}$ emitted during the transition, and from the emission of ultra-soft gauge bosons obtaining a mass in the transition. We subsequently apply those results to find the full pressure in the case of a generic PT and in the case of the ElectroWeak Phase Transition (EWPT). In a third chapter, we come back to the process of production of heavy states and we show that those heavy states, once produced, can be stable and constitute a viable super-heavy DM candidate. We study the relic abundance matching observations in the context of dark PT (by dark we mean a transition which is neither EWPT neither QCDPT) and in the context of the EWPT. In the fourth chapter, we complete the study of the production of heavy states by going to one-loop level. We show that if an imaginary phase is present in the Yukawa matrix, CP-violation can occur in the process of production, opening a possible route for baryogenesis. As a proof of principle, we then provide two different models realising baryogenesis via relativistic bubble walls. The first model uses the breaking of the $U_L(1)$ lepton number during a dark PT at high scale to generate relativistic walls and baryogenesis. The second model postulates a heavy extension of the standard model (SM) with new source of CP and baryon number breaking and a strong EWPT with relativistic EW bubble wall to induce baryogenesis. In all our models we left the phase transition sector as an unknown, only assuming that the wall would become ultra-relativistic. In the last chapter, we provide a model of the EWPT augmented by a singlet scalar with Z_2 symmetry which realises ultra-relativistic bubble walls, upon allowing some tuning in the parameters. With this model in hand we revisit our scenarios of production of DM and baryogenesis and estimate the tuning within those classes of models.

Aknowledgments

I would like to thank first my parents, who had to endure a series of physics explanation since few years. They had (from time to time) the patience to pretend to listen to me and to nod their head as they heard about Black holes, baryogenesis, cosmic microwaves background and Higgs boson.

Second I would like to thank my mentor Alex for his patience, from time to time tormented, when confronted with my mistakes and misunderstandings, and his numerous pieces of advice even when I pretended to know well.

I would like also to thank my Trieste friends and/or colleagues: Natalia and its excitement for physics, Anto and its many interests for painting and art, Lotte and its never-ending lust for learning, Matteo and its taste for parties and simple enjoyements, Titouan because he shaked and impressed me so many times, Pauline and all her stories, Regis because of his fighting spirit, Irina and her refreshing spirituality (that should not disappear with age!), Olga because she sees beauty in places I would have never thought of (and that should not disappear with age neither), Jon because of its legendary moving honesty, Vanessa because she brought me on untravelled roads, Giulio because he was a great partner of work, Sabyasachi because his convictions broke a bit my certitudes and finally all my dead friends from the books, that from time to time come and talk to me (believe or not).

To all of them, dead and alive, I wish the best.

Introduction

The early evolution of the universe is believed to be a very quiet era during which the hot plasma would have closely followed thermal equilibrium stages. After inflation and the (possibly strongly out-of-equilibrium) stage of reheating, the plasma in the universe would have quickly thermalised at a very high temperature. This stage is the *Hot Bang* of the Big Bang theory. Reheating was followed by a period of cooling driven by the slow expansion of the universe. Compared to this weak expansion, the strong couplings of the Standard Model (SM) enforced equilibrium until very low temperatures. At temperature of the order of the hundred of GeV, the thermal effects are not able any more to stabilise the Higgs potential and the Higgs acquires a VEV, breaking the EW symmetry. Though this transition could in principle introduce strong departure from equilibrium, lattice computations suggest that, for realistic masses of the Higgs, the transition was actually a smooth cross-over, only coming with very mild departure from equilibrium. The situation is similar, at around hundreds of MeV, when the quark-gluon plasma confines. Lattice simulations of the SM indicates that the QCD phase transition should be a smooth cross-over. As a consequence, Standard Model of Particles physics (SM) combined with the Standard Model of Cosmology (SMC) seem to pave the way to a very calm history for the early universe, like an ocean without any storm.

However, issues of the SM with SMC hints toward the necessity of strong departure from equilibrium in the early universe. The first one, and arguably the strongest one, is the necessity for baryogenesis, which is realised only if it is embedded in an event involving strong departure from thermal equilibrium. The very existence of matter today, combined with the well-known third Sakharov condition seems thus to beg for a strongly out-of-equilibrium event in the early universe.

Similar hints seem to come from the Dark Matter (DM) sector. As we will review, thermal freeze-out mechanism with SM-like weak couplings is under increasing pressure by the non-detection of DM in multiple experiments. Even if, of course, there are many ways out of this experimental exclusion, this observation motivated physicists to explore deeper other mechanisms of production of DM, among which many display strong departures from thermal equilibrium.

Finally, a third revolution motivated us to study in depth the out-of-equilibrium dynamics of the early universe: the recent discovery of Gravitational Waves (GW) and the numerous projects for forthcoming GW observers, which would cover a large range of frequencies and amplitudes. This opens a new avenue for the poetically called *Heavenly Laboratory* of Kolb and Turner and opens up the possibility of soon discovering a Stochastic Background of GW (SGWB) that would have been produced by some out-of-equilibrium event in the first second of the universe. Even if there is no one-to-one correspondence between SGWB and out-of-equilibrium processes, the two are however connected and many out-of-equilibrium processes have been studied in the context of SGWB production. Conversely, the processes producing SGWB can often be also recycled as mechanism for baryogenesis and non-thermal DM production.

One of those processes are the First-Order Phase Transitions (FOPTs), where two phases of a fluid (in the present case the early universe plasma) are neatly separated by an interface and a release of latent heat occurs around the

region of the interface. FOPTs and their dynamics will be the topic of this thesis. They have been correlated with the large production of GW and the spectra emitted have been abundantly studied in the literature in the prospect of future detection at observers like LISA. On the other hand, they constitute one of the leading candidates for baryogenesis, production of InterGalactic Magnetic field, Production of Primordial Black Holes and production of non-thermal DM. Their complicated dynamics with the hot plasma and the very different regimes of expansion of the bubble walls make them a fertile ground for theoretical investigation. Thus, in the view of the importance of the bubble wall velocity for several observables, like GW or baryogenesis, in Chapter 2, we study the dynamics of the bubble wall expansion and the pressure exerted by the plasma. Specifically, we study in detail the regime of *ballistic expansion*, the regime of expansion when the bubble wall managed to reach relativistic velocities and plasma particles can be treated as collisionless classical particles all throughout the wall. We will discuss the three dominant contributions to the pressure on the bubble wall expansion in this regime. In so doing, on the top of the leading order effect, we will unveil the effect of heavy physics coupled to the light physics via a portal and show that those heavy physics effects cannot in general be neglected. Since it was the source of a recent debate in the literature, we will also discuss at length the scaling of the next-to-leading order contribution and show some avenues for new investigation.

In Chapter 3, we restart from the same mechanism of production of heavy states discussed in Chapter 2 and show that the heavy states produced during the expansion of the bubble wall can constitute all DM density observed. We discuss the possible interplay with the unavoidable usual Freeze-Out (FO) mechanism and show that DM with correct abundance but with masses in large excess with respect to Griest-Kamionkowski bound can be produced. We find that dark PT with scale up to $\sim 10^8$ GeV can induce the observed DM abundance. To conclude, we also emphasize the positive correlation with strong GW signal.

In Chapter 4, we use the same mechanism of production of heavy states and take advantage of the fact that those states are strongly out-of-equilibrium when produced, thus naturally satisfying the third Sakharov condition for baryogenesis. In this chapter, we first compute the expected CP violation occurring at one-loop level and then embed this raw production mechanism in two different models of baryogenesis with relativistic bubble walls. In the first model, the breaking of the $U_L(1)$ lepton number during a dark PT at high scale generates relativistic walls and induces baryogenesis. In the second model, we assume a heavy extension of the standard model (SM) with new source of CP and baryon number violation and a strong EWPT with relativistic EW bubble wall. We show that those two ingredients combined induce baryogenesis. We discuss the different constraints of each of those models and finally emphasize their special detectability, namely via strong GW signal.

In the last chapter 5, we build a model of FOPTs with long supercooling and ultra-relativistic bubble walls. We consider the simplest extension of the SM, the addition of a real singlet with a Z_2 symmetry and focus on the 2-steps PT, where the singlet obtains a VEV in a first PT and then relaxes to zero while the EW is broken in a second PT. We emphasize that in this context, the second PT can be strongly supercooled and induce very relativistic bubble walls. We then revisit the DM production mechanism of Chapter 3 and the baryogenesis second model of Chapter 4 in this context. We conclude that such a possibility requires some amount of fine-tuning.

Even if the study of this thesis is ultimately confined to a restricted area of FOPT with relativistic walls[1], it is worth keeping in mind the global picture and the goal of our investigation: learn about the dynamics of the early universe, and in the end being able to draw conclusion about microscopic interaction and the SM!

[1]Because I am not omniscient!

Acronym	Full name
PT	Phase Transition
FOPT	First-Order Phase Transition
DM	Dark Matter
GW	Gravitational Waves
SGWB	Stochastic Gravitational Waves Background
SM	Standard Model (of particle physics)
BSM	Beyond the Standard Model (of particle physics)
SMC	Standard Model of Cosmology
CS	Cosmic Strings
DW	Domain Walls
FI	Freeze-In
FO	Freeze-Out
BE	Bubble-Expansion
VEV	Vacuum Expectation Value
EWPT	Electroweak Phase Transition
EWBG	Electroweak baryogenesis
NDA	Naive Dimensional analysis
FCNC	Flavor Changing Neutral Currents

Table 1: Acronyms and translation used in this thesis.

0.1 List of publications during the PhD

List of publications presented in this thesis

1. [1] **Bubble wall velocity: heavy physics effects**, Aleksandr Azatov and Miguel Vanvlasselaer JCAP01(2021)058

2. [2]**Dark Matter production from relativistic bubble walls.** Azatov, A., Vanvlasselaer, M. and Yin, W. J. High Energ. Phys. 2021, 288 (2021). https://doi.org/10.1007/JHEP03(2021)288

3. [3]**Baryogenesis via relativistic bubble walls.** Azatov, A., Vanvlasselaer, M. and Yin, W. J. High Energ. Phys. 2021, 43 (2021). https://doi.org/10.1007/JHEP10(2021)043

4. [4]**Ultra-relativistic bubbles from the simplest Higgs portal and their cosmological consequences**, Azatov, A. and Barni, G. and Chakraborty, S. and Vanvlasselaer, M. and Yin, W. preprint: arxiv 2207.02230.

List of publications not presented in this thesis but written (or almost finished) during the PhD of the author

1. [5] **Phase transitions in perturbative walking dynamics.**, Azatov, A., Vanvlasselaer, M. J. High Energ. Phys. 2020, 85 (2020). https://doi.org/10.1007/JHEP09(2020)085

2. **Cooling of neutron stars via WZW term**, Gupta, A., Chakraborty, S. and Vanvlasselaer, M. In preparation. preprint: arxiv 220X.XXXXX

3. **Trapping the electroweak scale**, Trifinopoulos, S and Vanvlasselaer, M. In preparation. preprint: arxiv 2209.XXXXX.

Chapter 1

Fundamentals

In this first chapter we introduce the basic quantities, definitions and formalisms that we will use in the other chapters of this thesis. The basic playground of this thesis is the early universe plasma and the associated out-of-equilibrium processes. After a quick review of the thermal history of the universe and the thermodynamics of it, we will introduce the basic tools to compute one loop-level potentials. However, the precise study of the early universe, from its thermal evolution to its complex possible out-of-equilibrium processes require theoretical tools beyond the ordinary 4D Quantum Field Theory. We thus also introduce the so-called *Thermal Field Theory* (TFT), or *Finite-Temperature Quantum Field Theory*. After those preliminaries, we apply those tools to the special case of FOPTs in the early universe and provide a quick review of the FOPT bubble dynamics. We finish by providing the result of the state of the art of GW emitted by FOPT bubble. This introductory chapter is mostly a review and does not contain anything new, as a consequence it can be safely skipped by the expert reader.

Contents

1.1 Notations

Here and all throughout this thesis we will work in natural units and take the usual convention of setting

$$\hbar = c = k_B = 1. \tag{1.1}$$

Also, Table 1.4 contains most of the notations that we will keep fixed in this thesis. The other ones will be defined on the spot.

1.2 Thermal history of the universe

In this section, we would like to give an account of some of the necessary quantities involved the early universe computations as well as an overview of the standard thermal evolution of the universe, which demands rudiments of statistical physics and gravity.

1.2.1 Expansion and symmetries of the universe

The most basic notion for the universe history is the expansion of the universe, discovered by *Edwin Hubble* in 1920's via the redshift of distant galaxies. The famous linear dependence of the redshift z on the luminosity distance d_L[2] takes the form

$$H_0 d_L \approx z, \qquad H_0 \approx 100h \quad \text{km}s^{-1}\text{Mpc}^{-1} \tag{1.2}$$

where the reduced Hubble $h \approx 0.7$ is still today the source of heated debates. This induces that the size of the observable universe today is order $H_0^{-1} \sim 3000h^{-1}$ Mpc.

On the top of the expansion of the universe, a second critical concept for our understanding of the universe is the *cosmological principle*: this means that the matter distribution at sufficiently large scales is *isotropic* and *homogeneous*. The clearest proof for such homogeneity and isotropy (at least at the last scattering surface) is the very high homogeneity of the CMB temperature, with $\delta T/T \sim 10^{-5}$. Surveys of bright matter (galaxies) also support homogeneity for scales larger than around ~ 100 Mpc, which means that any sphere of a radius of ~ 100 Mpc would contain around the same mass[3].

[2]Here, let me do some historical comment: there has been a ferocious resistance to the non-fixity of the universe, maybe the most famous being the Einstein one, via the introduction of the Cosmological Constant. It is perhaps surprising that the notion of non-fixity was introduced in Biology with Lamarck and Erasmus Darwin, around 1820's, defended in philosophy by the historical dialectics of Hegel, around the same time and introduced in the study of values by Nietzsche in the end of the 19th century. We could even wonder why historical thinking took so long to become pregnant in one of the oldest field of intellectual inquiry: cosmology.

[3]Notice that, amusingly, before reaching the sacro-saint status of principle, the isotropy and homogeneity assumptions were merely introduced for the sake of simplifying the equations.

Quantity name	Symbol
Higgs Doublet	$\mathcal{H}$
Physical Higgs degree of freedom	h
Hubble constant	H
Collision term in Boltzmann Eq.	$\mathcal{C}$
Velocity of the bubble wall	v_w
Internal number of dof of the particle i	g_i
Mixing angle between ψ and Ψ	$\theta_{\psi\Psi}$
Heaviside Theta function	Θ
Boost factor of the bubble wall to the plasma frame	γ_w
reduced Planck mass	$M_{\rm pl}$
Mass of the Higgs in the true vacuum	m_h
Mass of the particle of *higgsed side*[1]	m_h
mass of the particle in the *symmetric side*	m_s
Length of the bubble wall (in the wall frame)	L_w
Cosmological Constant	Λ
Reheating temperature *after inflation*	T_R
Reheating temperature *after the PT*	$T_{\rm reh}$
Nucleation temperature	$T_{\rm nuc}$
Percolation temperature	$T_{\rm per}$
Typically scalar DM candidate	ϕ
Typically light fermion	χ or ψ
Typically heavy fermion	N
Typically dark scalar having transition	φ
Scalar singlet under the SM gauge group	s
Difference of energy between the false and the true vacuum at zero T	ΔV
Probability of interaction $i \to j$	$P(i \to j)$
Plasma pressure on the bubble wall	$\mathcal{P}$
Pressure of a fluid	p
Density of the particle i	n_i
Energy density	ρ
Renormalisation scale	μ_R
Stress-energy/Energy-momentum tensor	$T_{\mu\nu}$
Distribution function of the particle i	f_i

Table 1.1: Important Notations that we will keep fixed throughout the thesis. Other definitions will be defined on the spot.

With those two concepts, we are ready to reconcile the master equation of GR, the *Einstein equation*, with the cosmological evolution. The Einstein equation is given by

$$R_{\mu\nu} - \frac{1}{2}\mathcal{R}g_{\mu\nu} = -8\pi G_N T_{\mu\nu} + \Lambda g_{\mu\nu} \qquad \text{(Einstein equation)} \tag{1.3}$$

where $g_{\mu\nu}$ is the metric and as a convention, we use a mostly minus metric for flat space $(+,-,-,-)$. In Eq.(1.3), $R_{\mu\nu}$ is the curvature tensor of space-time, $\mathcal{R}$ is the Ricci scalar, G_N the gravitation constant, $T_{\mu\nu}$ the stress-energy tensor of the matter in the universe and Λ is the Cosmological Constant. Imposing homogeneity and isotropy notoriously restricts the number of degrees of freedom of the Einstein equation Eq.(1.3) to only one. This is the "Friedmann-Robertson-Lemaitre-Walker metric":

$$ds^2 = dt^2 - a^2(t)\left[\frac{dr^2}{1-kr^2} + r^2 d\theta^2 + r^2 \sin^2\theta d\phi^2\right] \qquad \text{(FRLW metric)} \tag{1.4}$$

where k can be $0, 1, -1$ and defines three types of geometries for the universe and the degree of freedom a encapsulates the possibility of expansion or contraction of the universe.

The stress-energy tensor T^ν_μ has to be diagonal by isotropy and homogeneity considerations:

$$T^\nu_\mu = \text{diag}(\rho(t), -p(t), -p(t), -p(t)) \tag{1.5}$$

and is only parametrized by the energy density ρ and the pressure p of the fluid in the universe. In the context of a FRLW metric and using the diagonal stress-energy tensor Eq.(1.5), the *Einstein Equation* easily[4] leads to the so-called Friedmann equations for the expansion parameter a:

$$\begin{aligned} \left(\frac{\dot{a}}{a}\right)^2 &= \frac{8\pi G_N \rho_{\text{tot}} + \Lambda}{3} - \frac{k}{a^2} \qquad \text{(First Friedmann equations)} \\ \frac{\ddot{a}}{a} &= -\frac{4\pi G_N}{3}(\rho_{\text{tot}} + 3p_{\text{tot}}) + \frac{\Lambda}{3} \qquad \text{(Second Friedmann equations),} \end{aligned} \tag{1.6}$$

from which it becomes natural to define the Hubble constant, which is all but constant,

$$H \equiv \frac{\dot{a}}{a} \qquad \text{(Hubble constant).} \tag{1.7}$$

The physical content can be made clearer if we use the first equation to transform the second, and using an equation of state of the form $p = w\rho$. We obtain the relation driving the evolution of ρ_{tot}, assuming a constant equation of state w:

$$\dot{\rho}_{\text{tot}} = -3H(\rho_{\text{tot}} + p_{\text{tot}}) = -3H\rho_{\text{tot}}(1+w). \tag{1.8}$$

We can read the evolution of the Hubble expansion from the first equation in Eq.(1.6). Defining $\rho_\Lambda = \frac{3\Lambda}{8\pi G_N}$ and $\rho_k = -\frac{k}{8\pi G a^2}$, the Friedmann equations are often rewritten

$$\begin{aligned} H^2 = \sum_i \frac{8\pi G_N \rho_i}{3} \qquad \Rightarrow \qquad \frac{H^2}{H_0^2} &= \Omega_0^R a^{-4} + \Omega_0^m a^{-3} + \Omega_0^k a^{-2} + \Omega_0^\Lambda \\ H^2 + \dot{H} &= -\frac{4\pi G_N \rho_{\text{tot}}}{3}(1+3w) \end{aligned} \tag{1.9}$$

[4] More or less easily ...

dominating component	$\rho(a) \propto H^2 \propto a^{-n}$	$t \propto a^m$
Radiation	$n = 4$	$m = 1/2$
Matter	$n = 3$	$m = 2/3$
Kination	$n = 6$	$m = 1/3$
Curvature	$n = 2$	$m = 1$
Cosmological constant	$n = 0$	$a \propto \exp Ht$

Table 1.2: Expansion of the universe for different type of fluid dominating the expansion.

where the index 0 means the value of the variable evaluated today and we have normalised $a_0 = 1$. We have also defined the ratio of the density over the critical density, the density when the universe is flat

$$\Omega_i \equiv \frac{\rho_i}{\rho_c}, \qquad \rho_c \equiv \frac{3H^2}{8\pi G_N}. \tag{1.10}$$

Remarkably enough, taking the conservation of the stress-energy tensor $T^{\mu\nu}_{;\nu} = 0$ gives the first law of thermodynamics

$$d(\rho a^3) = -pd(a^3) \Rightarrow d[a^3(\rho + p)] = a^3 dp \qquad \text{(First law)} \tag{1.11}$$

which is turn leads to the energy density evolution

$$\dot{\rho} = -3H(1 + w)\rho \qquad \text{(Energy density evolution)} \tag{1.12}$$

that we already obtained in Eq.(1.8). The solutions of 1.8 (if w does not depend on the time) are really simple:

$$\rho \propto a^{-3(1+w)} \qquad a \propto t^{2/3(1+w)} \qquad \text{(Universe expansion regimes)} \tag{1.13}$$

Specially interesting cases are displayed in Table 1.2.

1.2.2 Thermal description of the early universe

Since we expect very mild departure from equilibrium in the early universe, a very good description of this early plasma takes advantage of thermodynamic evolution tools. Let us begin by defining the *density*, *energy density* and *pressure* of some component i of the early universe plasma:

$$n_i = g_i \int \frac{d^3p}{(2\pi)^3} f_i(p) \qquad \text{(Number density)} \tag{1.14}$$

$$\rho_i = g_i \int \frac{d^3p}{(2\pi)^3} E(p) f_i(p) \qquad \text{(Energy density)} \tag{1.15}$$

$$P_i = g_i \int \frac{d^3p}{(2\pi)^3} \frac{|\mathbf{p}|^2}{3E(p)} f_i(p) \qquad \text{(Pressure)} \tag{1.16}$$

where i designates some component of the fluid and g_i is the number of degrees of freedom of i. In those expressions, the *equilibrium distribution function* $f_i(p, T)$ takes a specific form

$$f^{\text{eq}}(p, T) = \frac{1}{e^{(E-\mu)/T} \pm 1} \tag{1.17}$$

where $E = \sqrt{\mathbf{p}^2 + m^2}$ is the energy of the particle, m its mass and μ its *chemical potential*. The $+$ $(-)$ sign holds for fermions (bosons). This distribution is valid if the component is at chemical and kinetic equilibrium at temperature T. At this point, it is good to notice that the Hubble expansion sets a scale in the early universe. By convention, we call *in equilibrium* a reaction which has a rate faster than the expansion rate H. Mathematically, this rough condition is

$$\Gamma_{\rm int} \gg H \qquad \text{(Equilibrium condition)}. \tag{1.18}$$

Reactions that strongly violate this condition are *frozen-out*. This can be seen straightforwardly from the Boltzmann equations, as we will do soon.

Let us dig a bit in the numenclature. If some particle changing interaction $i + j \leftrightarrow m + n$ is in equilibrium then the following relation among chemical potential holds

$$\mu_i + \mu_j = \mu_m + \mu_n. \tag{1.19}$$

This is the *chemical equilibrium*. On the other hand, *kinetic equilibrium* refers to an equality of temperature between two fluids, which is enforced if scattering interactions between the two fluids are in equilibrium. For example i, j component will be in kinetic equilibrium if the reaction $i + j \leftrightarrow i + j$ is in equilibrium. In this case, the two fluids are characterized by the same temperature. Chemical equilibrium is typically a stronger requirement than kinetic equilibrium. Now we can come back to the expression for the equilibrium distribution in Eq.(1.17): This form is enforced if the species is in kinetic equilibrium with itself. That is to say if interaction redistributing energy, for example $i + i \leftrightarrow i + i$ are in equilibrium.

It is known that quantities in Eq.(1.21) have simple form in two particular limits. Let us first neglect the chemical potential μ[5]. i) if $m_i \gg T_i$ (non-relativistic particle)

$$\begin{aligned} n_i &= g_i \left(\frac{m_i T_i}{2\pi}\right)^{3/2} e^{-m_i/T_i} \qquad \text{(Number density)} \\ \rho_i &= m_i n_i \qquad \text{(Energy density)} \\ P_i &= n_i T_i \qquad \text{(Pressure)} \end{aligned} \tag{1.20}$$

and we observe that $w \equiv P/\rho \to 0$ in this case: the particles go pressureless. On the other hand, ii) if $m_i \ll T_i$ (relativistic particle), the mass can be ignored overall and we have

$$\begin{aligned} n_i &= c_i \frac{g_i \zeta(3)}{\pi^2} T_i^3 \qquad \text{(Number density)} \\ \rho_i &= d_i \frac{g_i \pi^2}{30} T_i^4 \qquad \text{(Energy density)} \\ P_i &= \frac{\rho_i}{3} \qquad \text{(Pressure)} \end{aligned} \tag{1.21}$$

with $c_i = 1(3/4)$, $d_i = 1(7/8)$ for bosons (fermions). We observe that the energy in non-relativistic sector is exponentially smaller than in the relativistic sector, so we can safely neglect the non-relativistic sector when we will compute the energy density[6]. From those results, we define the energy in the radiation sector

$$\rho_{\rm rad} = \frac{\pi^2}{30} g_\star T^4, \qquad g_\star \equiv \sum_{i \in \text{boson}} g_i \left(\frac{T_i}{T}\right)^4 + \frac{7}{8} \sum_{j \in \text{fermion}} g_j \left(\frac{T_j}{T}\right)^4 \tag{1.22}$$

[5]Cases with large chemical potential are not expected to arise in the early universe, but for example in very dense medium like neutron stars, so we ignore them for our purpose.

[6]A exception of great importance to this approximation is frozen-out DM, which we know cannot be neglected!

where T is the temperature of the bath, and T_i is the temperature of the particle i. This permits to account for difference of temperatures between two decoupled sectors. A simple computation provide the following result for the Hubble and the time during *radiation domination*

$$H = \sqrt{\frac{\rho_{\rm rad}}{3M_{\rm pl}^2}} \approx 1.66 g_\star^{1/2} \frac{T^2}{M_{pl}} \tag{1.23}$$

$$t \approx 0.3 g_\star^{-1/2} \frac{M_{\rm pl}}{T^2} \sim \left(\frac{T}{\rm MeV}\right)^{-2} {\rm s}. \tag{1.24}$$

and we emphasize that $M_{\rm pl}$ is the reduced Planck mass. We can now turn to the entropy density in the early universe. One of the first important claims is: *as long as local thermal equilibrium (LTE) is maintained, entropy per comoving volume is constant.* This law is exactly what makes the entropy density so useful for the early universe studies.

The second law of thermodynamic writes

$$TdS = d(\rho V) + pdV \qquad \Rightarrow dS = \frac{d[(\rho+p)V]}{T} - \frac{V}{T}dp \qquad \text{(Second law)} \tag{1.25}$$

Using the permutation of derivatives in the previous expression gives

$$\frac{\partial^2 S}{\partial T \partial V} = \frac{\partial^2 S}{\partial V \partial T} \qquad \Rightarrow dp = \frac{\rho+p}{T} dT \tag{1.26}$$

and upon plugging in the second law

$$dS = \frac{d[(\rho+p)V]}{T} - \frac{V(\rho+p)dT}{T^2} = d\left[\frac{(\rho+p)V}{T} + \text{const}\right]. \tag{1.27}$$

This is a beautiful result, which means that (up to an additive constant)

$$S = a^3 \frac{\rho+p}{T} \qquad \text{(Entropy definition)}. \tag{1.28}$$

Moreover, upon combining the first law in Eq.(1.11) and Eq. (1.26), we obtain that

$$dS = d(a^3 s) = 0. \tag{1.29}$$

Using the definition of Eq.(1.28) and the expression of radiation density, we obtain that

$$s = \frac{2\pi^2}{45} g_{\star,S} T^3, \qquad g_{\star,S} = \sum_{i \in \text{boson}} g_i \left(\frac{T_i}{T}\right)^3 + \frac{7}{8} \sum_{j \in \text{fermion}} g_j \left(\frac{T_j}{T}\right)^3. \tag{1.30}$$

This means that the quantity $g_{\star S} T^3 a^3$ is constant in the early universe evolution. So, as long as entropy is conserved, the following relation holds

$$T \propto g_\star^{-1/3} a^{-1}. \tag{1.31}$$

This will motivate the later definition of the *baryon number*, divided by the entropy,

$$\frac{n_B}{s} \equiv \frac{n_b - n_{\bar{b}}}{s} \tag{1.32}$$

Quantity name	Symbol	Expression
Hubble	H	$H(T)^2 = \frac{1}{3M_{\rm pl}^2}(\rho_{\rm rad} + \rho_{\rm vac})$
Radiation density	$\rho_{\rm rad}$	$\rho_{\rm rad} = \frac{\pi^2}{30} g_\star T^4$
Relativistic entropic dof	$g_\star$	$\sum_{i\in B} g_i \left(\frac{T_i}{T_\gamma}\right)^4 + \frac{7}{8}\sum_{j\in F} g_j \left(\frac{T_j}{T_\gamma}\right)^4$
Entropy density	s	$s = \frac{2\pi^2}{45} g_{\star S} T^3$
Relativistic entropic dof	$g_{\star S}$	$\sum_{i\in B} g_i \left(\frac{T_i}{T_\gamma}\right)^3 + \frac{7}{8}\sum_{j\in F} g_j \left(\frac{T_j}{T_\gamma}\right)^3$
Critical density	ρ_c	$\rho_c \equiv \frac{3H_0^2}{8\pi G_N}$
Relative density	Y_X	$Y_X \equiv \frac{n_X}{s}$
Energy fraction	Ω_X	$\Omega_X \equiv \frac{\rho_X}{\rho_c}$

Table 1.3: Summary of the different quantities important in the thermodynamical description of the early universe and their definitions that will be used in this thesis.

since it is a conserved quantity in equilibrium.

We already mentioned that kinetic equilibrium is enforced between two components if scatterings manage to keep the same temperature for the two fluids. A nice example is provided by the neutrinos, which interact with the thermal bath of electrons via $e\nu \leftrightarrow e\nu, e^+e^- \leftrightarrow \bar{\nu}\nu, ...$ Those interaction have a typical rate controlled by the weak interaction G_F:

$$\Gamma_{\nu e} \sim G_F^2 T^5, \tag{1.33}$$

which will typically fall below the Hubble expansion around $T \sim 1$ MeV. At this point, T (of the photon bath) and T_ν of the neutrinos do not need to be the same anymore. As a consequence, when the electrons becomes non-relativistic and decay, the entropy is transferred to the photons only, which are reheated with respect to the neutrinos. In the photon bath, $g_\star$ jumps from $11/2$ to 2 and we can apply Eq.(1.31) to the photon temperature. This means that

$$\frac{T}{T_\nu} = \left(\frac{11}{4}\right)^{1/3} \approx 1.4 \tag{1.34}$$

At this point, it is instructive to consider the value of some of those quantities today

$$\begin{aligned} g_\star^0 &= 2 + \frac{7}{8} \times 2 \times 3 \times \left(\frac{4}{11}\right)^{4/3} \approx 3.36 \\ g_{\star,S}^0 &= 2 + \frac{7}{8} \times 2 \times 3 \times \left(\frac{4}{11}\right) \approx 3.9 \\ s^0 &\approx 3000\text{cm}^{-3} \qquad n_\gamma^0 \approx 400\text{cm}^{-3} \end{aligned} \tag{1.35}$$

Since we will discuss it at length in the chapter on DM production, we will not approach in this introduction the slightly more involved phenomenon of freeze-out.

1.2.3 Universe Highlights

Now, with all the theoretical tools that we have gathered, we are able to tell the expected history of the first second of the universe. The list that we are going to present becomes more and more speculative as we go down, from the very well understood BBN to the very speculative Peccei-Quinn symmetry breaking and inflation:

- $T \sim 10 - 0.1$ **MeV,** $t \sim$ **second-minutes: Big Bang Nucleosynthesis (BBN)**: The neutrons and the protons combine in nuclei to form the light elements: D, He^3, He^4, Li^7. This is a very well understood era of cosmology and the predicted abundance of each species matches very well the prediction: large injection of entropy after BBN would ruin this agreement. We will thus consider that BBN is then the final edge of our playground and we will not dare to mess with it.

- $T \sim 0.5$ **MeV,** $t \sim$ **second: Decay of the electrons**: The temperature falls below the mass of the electron and annihilation of electron-positron into photons become favorable. The entropy is transferred to the photon bath, which is reheated.

- $T \sim 1$ **MeV,** $t \sim$ **sec: Neutrino decoupling and production of the cosmic neutrino background**: Weak interactions are not able anymore to cope with the expansion of the universe and neutrinos interactions with the photons-electrons bath are frozen.

- $T \sim 300$ **MeV,** $t \sim 10^{-5}$ **sec: QCD phase transition**: When the temperature drops below around $T \sim 300$ MeV, the plasma of quarks and gluons confine into hadrons and mesons. Massive up and down quarks and tiny chemical potentials lead us to believe that this transition is a very smooth cross-over.

- $T \sim 10 - 100$ **GeV,** $t \sim 10^{-8} - 10^{-10}$ **sec: Thermal production of CDM**: This is the moment of the freeze-out of the (formerly?) preferred model of DM, the WIMP. When the temperature falls below the mass of the WIMP, they start to annihilate. This annihilation leads to a decreasing of the rate of interactions, which induces the freeze-out of DM, saving a final *relic abundance*.

- $T \sim 100$ **GeV,** $t \sim 10^{-10}$ **sec: Electroweak phase transition**: When the temperature drops below around $T \sim 100$ GeV, thermal effects are not able to stabilise the potential of the Higgs anymore and electroweak symmetry is broken. Lattice simulations have suggested that this transition, for realistic masses of the Higgs, is also a smooth cross-over. It is also possible that EW symmetry has never been restored in the early universe, like in the scenario of non-symmetry restoration.

- $T \sim 10^{12} - 10^{14}$ **GeV, Peccei-Quinn phase transition**: If the Peccei-Quinn postulated symmetry is really the mechanism solving the strong QCD problem and if the Peccei-Quinn symmetry is restored in the early universe, then it has to be broken at some temperature close to the axion decay constant f_a, if we assume vanilla axion models.

- ? **Inflation.** The universe undergoes a period of exponential inflation driven by the potential of some scalar field. Specifically, the density perturbations are produced by quantum fluctuations in the scalar field. The range of possible reheating temperature and scale for inflation is extremely large, and so we prefer not display any. However, our belief in inflation is a very important piece of the puzzle for all the other fields of research of cosmology: if we believe in inflation, diluting any primordial constituent, the thermal universe becomes independent of the initial conditions. Therefore we need a *dynamical* solution to the questions of baryogenesis, production of DM, ...

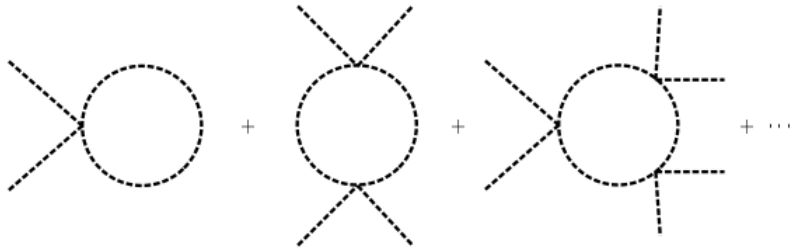

Figure 1.1: Diagrams to be summed for the 1-loop CW potential. Image from [6].

As already emphazised, everything prior to BBN remains highly speculative and open to model-building. More specifically, baryogenesis and DM production could almost happen any time in the time-line that we have proposed. This speculative era will be the playground of this thesis.

1.3 Constructing the one-loop potential at zero temperature

A crucial building block for the understanding of the PT is the potential. Though PT can be triggered by tree-level potentials only, it is known that one-loop effects can drastically modify the type of transition. In this section, following[6], we review shortly how to build the one-loop potential, dubbed CW potential. Let us take the simple example of a real scalar field ϕ, the most general renormalisable Lagrangian takes the form

$$\mathcal{L} = \frac{1}{2}|\partial_\mu \varphi|^2 - V_{\rm tree}(\varphi), \qquad V_{\rm tree}(\varphi) = \frac{1}{2}m_\varphi^2\varphi^2 + c\varphi^3 + \frac{\lambda}{4!}\varphi^4. \tag{1.36}$$

The c-term can be eliminated by simply imposing a symmetry under $\varphi \to -\varphi$, a choice that we make for the simplicity of the illustration. The condition $\lambda > 0$ is necessary for the stability of the potential at large values of the field. On the other hand, the stability of the origin, at tree-level is controlled by the sign of the mass term: if $m_\varphi^2 > 0$ the origin $\langle\varphi\rangle = 0$ is stable and the theory has to be expanded around the origin, if the mass is tachyonic $m_\varphi^2 < 0$, the origin becomes of maximum and the minimum of the theory becomes $\langle\varphi\rangle = \sqrt{\frac{-6m_\varphi^2}{\lambda}}$. This is the so-called broken phase or *higgsed* phase (we will use both terminologies in the remainder of the thesis).

As we might have noticed, there is however a marginal possibility, which was studied by E.Weinberg and S.Coleman: $m_\varphi^2 = 0$[7, 8]. In this case, at tree-level, the potential around the origin is very flat and it becomes controlled by the loop corrections. The fastest way to compute the potential at 1-loop is to use the *1PI* action. Without reconstructing the full 1PI formalism, we can simply use the formula

$$V_{1-\rm loop} = -\sum_{n=0}^{\infty}\langle\varphi\rangle^n\Gamma^{(n)}(p_i = 0) \tag{1.37}$$

with $\Gamma^{(n)}$ the Fourier transform of the one-particle irreducible n-point green functions. In this specific case, diagramatically, this formula corresponds to the sum over all 1PI with $2n$ (n integer) external legs displayed in the Fig.1.4. This gives

$$V_{1-\rm loop} = i\sum_{n=1}^{\infty}\int\frac{d^4p}{(2\pi)^4}\frac{1}{2n}\left[\frac{(\lambda\langle\varphi\rangle^2/2)}{p^2 - m_\varphi^2 + i\epsilon}\right]^n = -\frac{i}{2}\int\frac{d^4p}{(2\pi)^4}\log\left[1 - \frac{(\lambda\langle\varphi\rangle^2/2)}{p^2 - m_\varphi^2 + i\epsilon}\right] \tag{1.38}$$

Upon *Wick* rotation and defining $ip_E^0 = p^0$, we obtain

$$V_{1-\text{loop}} = \frac{1}{2}\int \frac{d^4p_E}{(2\pi)^4}\log\Big[p_E^2 + m^2(\langle\varphi\rangle)\Big], \qquad m^2(\langle\varphi\rangle) = m_\varphi^2 + \lambda\langle\varphi\rangle^2/2, \tag{1.39}$$

where we have discarded an irrelevant constant. As the integral above is obviously divergent, we now need to renormalise the theory by fixing the value of the coupling λ at some scale μ_R, which is the so-called *renormalisation scale*. Using the dimensional regularisation with $\overline{MS}$ scheme, the final result is

$$V_{CW}(\varphi) = \frac{m^4(\langle\varphi\rangle)}{64\pi^2}\left(\log\frac{m^2(\langle\varphi\rangle)}{\mu_R^2} - c\right) \qquad \text{(Coleman-Weinberg (CW) potential)} \tag{1.40}$$

Here, $c = 3/2$ in $\overline{MS}$. In the case of a pure CW potential (vanishing tree-level mass $m_\varphi = 0$), it can easily be seen that the minimum of that potential is given by $\varphi = \mu_R e^{1/4} \neq 0$, away from the origin. let us again notice that the full (often called *effective*) potential at one-loop is the sum of the tree-level and the 1-loop CW potential:

$$V_{\text{eff}}(\varphi) = V_{\text{tree}}(\varphi) + V_{CW}(\varphi). \tag{1.41}$$

This result can be generalised to a theory containing fermions and gauge bosons or multiple scalars in a very straightforward way. The CW potential for those different species is given by

$$V_{i,CW}(\varphi) = g_i(-1)^{n_i}\frac{M^4(\langle\varphi\rangle)}{64\pi^2}\left(\log\frac{M^2(\langle\varphi\rangle)}{\mu_R^2} - c_i\right) \tag{1.42}$$

where $c_i = 3/2(5/6)$ for fermions and scalars (gauge bosons), $n_i = 1(0)$ for fermions (scalars and gauge bosons), g_i is the number of degrees of freedom of the species i and M is the mass of the species running in the loop. The effective potential naturally becomes

$$V_{\text{eff}}(\varphi) = V_{\text{tree}}(\varphi) + \sum_i V_{i,CW}(\varphi). \tag{1.43}$$

1.3.1 Hierarchy problem

As we have seen, at the quantum level, the potential of a field described by the model in Eq.(1.36).

$$\mathcal{L} = \frac{1}{2}|\partial_\mu\varphi|^2 - V_{\text{tree}}(\varphi), \qquad V_{\text{tree}}(\varphi) = \frac{1}{2}m_\varphi^2\varphi^2 + c\varphi^3 + \frac{\lambda}{4!}\varphi^4. \tag{1.44}$$

This has a typical scale at m_φ that we put by hand at classical level. The point of the hierarchy problem is really that this scale cannot resist once we add the loop corrections. Indeed assume that we couple the φ to some other scalar ϕ via $\lambda_{\phi\varphi}\phi^2\varphi^2$, which is always allowed by symmetries, but that ϕ has a very large mass $M_\phi \gg m_\varphi$, the very same computation than in the discussion above can by performed if we have ϕ running into the loops.

$$m^2(\langle\varphi\rangle) = m_\phi^2 + \lambda_{\phi\varphi}\langle\varphi\rangle^2/2. \tag{1.45}$$

Upon plugging into the CW potential, a new quadratic term appears

$$\frac{\lambda_{\phi\varphi}M_\phi^2\langle\varphi\rangle^2}{64\pi^2}\left(\log\frac{M_\phi^2}{\mu_R^2} - c_i\right) \sim \frac{\lambda_{\phi\varphi}M_\phi^2\langle\varphi\rangle^2}{64\pi^2} \tag{1.46}$$

which corrects the m_φ^2 by an amount $\frac{\lambda_{\phi\varphi}M^2}{32\pi^2}$. This justifies the statement that in QFT heavy scale physics *attract* the scale of light physics.

Or course, since QFT cannot predict the value of observed masses, we can add a counterterm to kill the new contribution from high physics: (we do not include all the factors, since this is quite irrelevant for the explanation)

$$m_{\rm obs}^2 = m_\varphi^2 + \frac{\lambda_{\phi\varphi}M_\phi^2}{32\pi^2} + \delta m^2 \tag{1.47}$$

and fine tuning the δm^2 such that $m_{\rm obs}^2 \sim m_\varphi^2$. This issue generically advocated in twofold: first, if there is a hierarchy between m_φ^2 and M_ϕ^2, the cancellation between the second and the third term in Eq.(1.47) becomes considerable, in the sense that we need to fix many decimals in the quantity δm^2. Second, assume that such a fixing has been done and scales have been separated, now the smallest change in the parameters of heavy physics would ruin the tuning and destroy the separation of scale. We can say that there is a huge sensitivity of light physics to the parameters of heavy physics.

This second point is really the crux of the issue: the principle of separation of scales says that description of physics at some scale should not depends crucially on the tuning of parameters in a heavy sector. This is the so-called *hierarchy problem of QFT* which in the SM concerns the Higgs bosons, if it is indeed a scalar field.

1.3.2 On-shell regularisation scheme

Above we used the dimensional regularisation scheme. Let us now present another very useful scheme of regularisation. If we impose the following renormalisation condition,

$$\left.\frac{dV_{\rm eff}}{d\varphi}\right|_{\varphi=v} = 0, \qquad \left.\frac{d^2V_{\rm eff}}{d\varphi^2}\right|_{\varphi=v} = m_\varphi^2 \ . \tag{1.48}$$

where v is the minimum in the tree-level potential. we can observe easily that the CW potential becomes

$$V_{CW} = \sum_i \frac{n_i(-1)^F}{64\pi^2}\left[M_i^4\left(\log\frac{M_i^2}{M_{i0}^2} - \frac{3}{2}\right) + 2M_i^2M_{i0}^2\right] \ . \tag{1.49}$$

In this expression, M_i stand for the masses depending on the scalar fields values, $M_i \equiv M_i(\varphi)$, and M_{i0} are the field values from the tree-level vev, $M_{i0} \equiv M_i(v)$, in the true vacuum of the theory.

Unfortunately, Eq.(1.42) cannot be used directly for contributions of the Goldstone bosons (if there are Goldstone bosons involved in the problem), since their masses vanish in the true vacuum and the CW potential is IR divergent. Let us specialize to the case of the Higgs sector, since this is a place where this issue becomes important. The solution to this issue was suggested in Ref. [9] which emphasized that the physical Higgs mass is defined at $p^2 = m_h^2$ (m_h being the Higgs mass) and the effective potential at $p^2 = 0$ (see for details Ref. [9]). Thus it would be better to use modified renormalization condition

$$\left.\frac{d^2V_{\rm eff}}{dh^2}\right|_{h=v} = m_h^2 - \Sigma\left(p^2 = m_h^2\right) + \Sigma\left(0\right) \ , \tag{1.50}$$

where the differences of self-energies are taking into account the running of self-energy from $p^2 = 0$ to $p^2 = m_h^2$. In this case the IR divergences in $\Sigma(0)$ due to the virtual Goldstone bosons are cancelled against the IR divergences

of V_{eff}. In practice, at the end of this renormalization procedure, the contribution of the Goldstone bosons is given by :

$$V_{CW}^{GB}(h) = \sum_{i=G} \frac{n_G}{64\pi^2} M_G^4(h) \left[\log \frac{M_G^2}{m_h^2} - \frac{3}{2} \right] . \tag{1.51}$$

This scheme is particularly useful in the study of BSM potential because the loop-corrections are defined in such a way that they do not modify the position of the true vacuum and the mass at the true vacuum, which are the main observables. We will use this type of potentials in Chapter 5.

1.3.3 Renormalisation group improved potential and what are we resumming?

It is known that a powerful tool for improving the convergence of the series expansion is the *RG improved* potential. In this section we shortly review this important result.

RG improvement for the four-point function If we come back to the computation of the one-loop on Fig.(1.4) and using this time the cut-off regularisation scheme with cut-off Λ

$$\Gamma^{(4)}_{1-\text{loop}}(p_i = 0) = -\lambda + \frac{\lambda^2}{32\pi^2} \int_0^1 dx \left(\log \frac{\Lambda^2}{m_\varphi^2 - sx(1-x)} - 1 \right) + (s \to u) + (s \to t) \tag{1.52}$$

where s, t, u are the usual Mandelstam variables. After this regularisation, the four-point function basically needs to be renormalised. We define again a renormalisation scale μ_R such that

$$\Gamma^{(4)}(s = t = u = -\mu_R^2) = -\lambda(\mu_R). \tag{1.53}$$

As a consequence, Eq.(1.52) becomes

$$\Gamma^{(4)}(s,t,u) = -\lambda(\mu_R) + \frac{\lambda(\mu_R)^2}{32\pi^2} \int_0^1 dx \log \frac{m_\varphi^2 + \mu_R^2 x(1-x)}{m_\varphi^2 - sx(1-x)} + (s \to u) + (s \to t) \tag{1.54}$$

In this context μ_R serves as a sliding scale that adapts to the typical energy s in the center of mass in such a way that the log in Eq.(1.52) is never large. However, it is obviously an unphysical parameter and observable should ne depend on it, so that we need to require $d\Gamma^{(4)}(s,t,u)/d\mu_R = 0$. This gives

$$\left[\mu_R \frac{\partial}{\partial \mu_R} + \beta_\lambda \frac{\partial}{\partial \lambda} \right] \Gamma^{(4)} = 0, \qquad \beta_\lambda \equiv \mu_R \frac{d\lambda}{d\mu_R} \tag{1.55}$$

and β takes the form

$$\begin{aligned} \beta &= \frac{3\lambda}{16\pi^2} \int_0^1 dx \frac{\mu_R^2 x(1-x)}{m_\varphi^2 + \mu_R^2 x(1-x)} + \mathcal{O}(\lambda^3) \\ \beta &\approx \begin{cases} \frac{3\lambda}{16\pi^2} & \text{if } \mu_R \gg m_\varphi \\ \frac{3\lambda}{16\pi^2} \left(\frac{\mu_R}{m_\varphi} \right)^2 & \text{if } \mu_R \ll m_\varphi \end{cases} \end{aligned} \tag{1.56}$$

with solutions

$$\lambda(\mu_R) \approx \begin{cases} \frac{\lambda(\mu_0)}{1-\frac{3\lambda(\mu_0)}{16\pi^2}\log\frac{\mu_R}{\mu_0}} & \text{if } \mu_R \gg m_\varphi \\ \text{constant} & \text{if } \mu_R \ll m_\varphi \end{cases} \tag{1.57}$$

where we introduced μ_0 as a reference scale. So, if we fix the reference scale at $\mu_0 = m_\varphi$ and evaluate the integral at large energy $s = -E^2$ with $\lambda \equiv \lambda(m_\varphi)$, the RG-improved four-point function is given by

$$\Gamma^{(4)}_{\rm RG}(E) = -\frac{\lambda}{1-\frac{3\lambda}{16\pi^2}\log\frac{E}{m}} \qquad \text{(RG-improved 4-points function).} \tag{1.58}$$

From this expression, we can recover the non-RG improved by expanding the ratio

$$\Gamma^{(4)}_{\rm non-RG}(E) = -\lambda - \frac{3\lambda^2}{16\pi^2}\log\frac{E}{m} \qquad \text{(non-RG-improved 4-points function).} \tag{1.59}$$

At this point, we could wonder: what did we gain in this procedure ? The claim is that the Eq.(1.58) resums all the *leading-logs* (LL) terms that shows up at l-loops in $\lambda\lambda^l \log^l E/m$. Before to go to show this claim, let us explain in which context those logs can be dangerous: It is known that at l-loops, the potential is a polynomial of $\lambda^n \log^n E/m$, with $n < l+1$.We see that for $E \gg m$, the leading-log $\lambda^l \log^l E/m$ is dominating at l-loops. Now, if the hierarchy between E and m, $E \gg m$ becomes so large that $\log E/m$ starts to compete with the suppression $\lambda/16\pi^2$, all the terms $\frac{\lambda^l}{(16\pi^2)^l}\log^l E/m$ becomes equally important. This threatens the perturbative series. However, after the resummation, all those logs are under control and we expect much better convergence of the series.

RG improvement for the potential For the RG-improvement of the potential, the story goes essentially the same. Let us remember that the quartic part of the potential is given by

$$V(\varphi,\mu_R) = \frac{\lambda(\mu_R)}{4!}\varphi^4 + \frac{\lambda(\mu_R)^2}{256\pi^2}\left(\log\frac{\lambda(\mu_R)\varphi^2}{\mu_R^2} - c_i\right) \tag{1.60}$$

with a possible scheme dependent c_i. This constant is set to zero if we choose

$$V(\varphi=\mu_R) \equiv \frac{\lambda(\mu_R)\mu_R^4}{4!} \tag{1.61}$$

and we obtain

$$V(\varphi,\mu_R) = \frac{\lambda(\mu_R)}{4!}\phi^4 + \frac{\lambda(\mu_R)^2}{256\pi^2}\log\frac{\lambda(\mu_R).\phi^2}{\mu_R^2} \tag{1.62}$$

Let us notice that this potential seems to have a zero at very small values of the field φ. This has to be unphysical. At this point, we can notice a simple way to recover the expression of the β:

$$\mu_R\frac{dV}{d\mu_R} = 0, \qquad \beta = \frac{3\lambda}{16\pi^2} \tag{1.63}$$

(where we also used that the anomalous dimension of φ at 1-loop level is zero.)

We can now compute the RG-improved potential by setting $\mu_R = \varphi$, which gets rid of the log and use the value of the coupling after running from a reference scale φ_0 to $\mu = \varphi$. The potential becomes

$$V(\varphi) = \frac{\lambda(\varphi)\varphi^4}{4!} \tag{1.64}$$

becomes free of unphysical minima. As a conclusion, to RG-improve our potentials in what follows, we will replace all the constant couplings by running couplings with scales dictated by the problem at hand. A choice that we could typically make is

$$\lambda \to \lambda(\mu), \qquad \mu \equiv \sqrt{\varphi^2 + T^2} \tag{1.65}$$

in a thermal medium.

Though this is not the case in our toy model, if there is some physics that drives the couplings to zero, via the RG evolution at some scale Λ, thus at this scale, the potential will become controlled by radiative effects. This is typically the case if there are several scalars in the theory, see [10, 11, 12]. In this case, we can restart from Eq.(1.64) and integrate the β equation from φ to φ_0, taking β constant

$$\beta \log \frac{\varphi}{\varphi_0} = \lambda(\varphi) - \lambda(\varphi_0). \tag{1.66}$$

Plugging $\lambda(\phi)$ in Eq.(1.64) and expressing the potential in terms of the minimum v, we obtain

$$V(\phi) = \frac{\beta}{4!}\left(\log \frac{\varphi}{v} - \frac{1}{4}\right) \tag{1.67}$$

and we observe that the potential becomes controlled by the β function, so it becomes long and flat, and the mass of the φ field becomes suppressed $m_\varphi^2 \sim \beta v^2$ in the true vacuum.

Resummation of the leading-logs: the proof Let us now go to the formal proof of our previous claim that the RG-improvement would resum the leading logs at all orders in the loop expansion. It is enough to give the proof for the four-point function.

At high energy, we can neglect the masses and the four-point function depends on λ and μ_R/E and we can expand it

$$\Gamma^{(4)} = -\lambda \sum_{n=0} \lambda^n c_n(\mu_R/E) \tag{1.68}$$

with c_n unknown functions of μ_R/E. Starting from $c_0 = 1$ and the *Callan-Symanzik* equation

$$\left(\mu_R \frac{\partial}{\partial \mu_R} + \beta \frac{\partial}{\partial \lambda} - 4\gamma_\phi\right)\Gamma^{(4)} = 0 \tag{1.69}$$

On the other hand, β and λ can itself be expanded

$$\beta = \beta_0\lambda^2 + \beta_1\lambda^3 + ..., \qquad \gamma = \gamma_0\lambda + \gamma_1\lambda^2 \tag{1.70}$$

with $\gamma_0 = 0$. Now let us solve Eq.(1.69) order by order.

$$\begin{aligned} \text{order 1} &: \mu_R \tfrac{\partial}{\partial \mu_R} c_1 = -\beta_0 \qquad \Rightarrow c_1 = -\beta_0 \log \tfrac{\mu_R}{E} + C_1 \\ \text{order 2} &: \mu_R \tfrac{\partial}{\partial \mu_R} c_2 = -2\beta_0 c_1 - \beta_1 + 4\gamma_1 \quad \Rightarrow c_2 = \beta_0^2 \log^2 \tfrac{\mu_R}{E} - (4\gamma_1 - \beta_1 - 2\beta_0 C_1) \log \tfrac{\mu_R}{E} + C_2 \\ \text{order 3} &: ... \end{aligned} \tag{1.71}$$

Proceeding recursively, we see that the four-point function at n-loops is a polynomial of order n in $\log \mu_R/E$ the c_n will have a $\beta_0^n \log^n \mu_R/E$. Resumming the leading logs now becomes very simple:

$$\Gamma^{(4)}_{LL} = -\lambda \sum_{n=0} (\lambda\beta_0)^n \log^n \mu_R/E = -\frac{\lambda}{1-\beta_0\lambda \log \mu_R/E} \tag{1.72}$$

Plugging the value of β_0, we recover the result in Eq.(1.58), closing the proof that the RG-improvement indeed takes care of all the leading logs. This is a beautiful proof.

1.4 Thermal field theory

As we will make abundant use of thermal corrections in this thesis, in this section, we review the Thermal Field Theory (TFT) formalism. We will base our exposition of the TFT on the books [13, 14, 15], the lecture notes[6] and [16]. Thermal field theory permits the computation of field observables, like the vacuum expectation value (VEV) of a field, in a thermal background. For our purpose, the interesting feature is that it allows us to compute the potential of symmetry breaking field.

1.4.1 Basic formalism and basic properties

The essence of the Thermal Field Theory is to introduce a scale in the theory, the temperature of the plasma, T and thus we define the *radius of compactification* $\beta \equiv 1/T$. The main result of TFT is that a 4D QFT at finite-temperature T can be nicely recast into effective 3D QFT with time-dimension compactified on a circle of circumference $\beta = \frac{1}{T}$. We will elaborate on this claim in the next parts of this section. As TFT is designed to study systems at equilibrium with fixed temperature T, volume V and chemical potential μ, we will work in the so-called *grand canonical ensemble*, where the system under study is able to exchange particles and energy with the reservoir and the thermodynamical variables are T, V, μ_i, i designating each of the species of the ensemble. The *statistical density matrix* is given by

$$\hat{\rho} = e^{-(\hat{H}-\sum_i \mu_i \hat{N}_i)/T} \tag{1.73}$$

where the sum is over all the species i in the ensemble, and the grand ensemble average of any operator $\hat{A}$ is given by

$$\langle A \rangle_T = \frac{\text{Tr}[\hat{\rho}_T \hat{A}]}{Z}. \tag{1.74}$$

In this context, the single most important quantity in thermodynamics and the portal to all the other quantities is the *partition function* $Z[T]$, which writes

$$Z[T] \equiv \text{Tr}[e^{-(\hat{H}-\sum_i \mu_i \hat{N}_i)/T}] = \sum_a \int d\phi_a \langle \phi_a | e^{-(\hat{H}-\sum_i \mu_i \hat{N}_i)/T} | \phi_a \rangle \tag{1.75}$$

where the sum runs over all the states. $\hat{H}$ is the Hamiltonian operator and $\hat{N}_i$ the operator number of i particles. To go from the first to the second equality we introduced a complete set of eigenstates, in the form $1 = \sum_a |\phi_a\rangle\langle\phi_a|$ and performed the trace.

The other thermodynamical variables can be directly obtained from the partition function with the following definitions

$$\begin{aligned} \text{(Free energy)} \quad F \equiv -T\ln Z, \qquad \text{(Pressure)} \quad P \equiv T\frac{\partial \ln Z}{\partial V}, \\ \text{(Number of particles i)} \quad N_i \equiv T\frac{\partial \ln Z}{\partial \mu_i}, \qquad \text{(Entropy)} \quad S \equiv \frac{\partial T \ln Z}{\partial T}. \end{aligned} \tag{1.76}$$

As it is well-known, in the path integral formalism, the non-diagonal matrix element relating the state ϕ_a at time $t = 0$ to ϕ_b at time t, $\langle\phi_b|e^{-i\hat{H}t}|\phi_a\rangle$, can be cast in the form[7]

$$\langle\phi_b|e^{-i\hat{H}t}|\phi_a\rangle = \int [d\pi] \int\limits_{\phi(\mathbf{x},0)=\phi_a(\mathbf{x})}^{\phi(\mathbf{x},t)=\phi_b(\mathbf{x})} [d\phi] \exp\left[i\int\limits_0^t dt \int d^3\mathbf{x}\Big(\pi\partial_t\phi - \mathcal{H}(\phi,\pi)\Big)\right]. \tag{1.77}$$

From Eq.(1.75) and (1.77), we see that we can draw a relation between the partition function of the thermodynamical formalism and the matrix element of a QFT, if we set $a = b$, integrate over ϕ_a and perform the changes:

$$\mathcal{H} \to \mathcal{H} - \sum_i \mu_i \mathcal{N}_i \tag{1.78}$$

$$t \to -i\beta = -\frac{i}{T}. \tag{1.79}$$

and use the usual formalism of 4D QFT path integral to compute the partition function with periodic boundary condition set by $1/T$. This justifies the usual saying that the TFT is equivalent to a QFT compactified on a circle of circumference $\beta = 1/T$.

In an analogous way, the time evolution operator translates into

$$\hat{\phi}(\mathbf{x},t) = e^{i\hat{H}t}\hat{\phi}(\mathbf{x},0)e^{-i\hat{H}t} \to e^{\beta\hat{H}}\hat{\phi}(\mathbf{x},0)e^{-\beta\hat{H}} = \hat{\phi}(\mathbf{x},1/T) \tag{1.80}$$

Due to the trace operation, the boundary conditions are such that $\phi(\mathbf{x},0) = \phi(\mathbf{x},1/T)$. The periodicity of the operator can also be found in the thermal Green functions. As an example, let us define the following Green's function

$$G_B(\mathbf{x},\mathbf{y};\tau,0) \equiv Z^{-1}\text{Tr}\{\hat{\rho}T_\tau[\hat{\phi}(\mathbf{x},\tau)\hat{\phi}(\mathbf{y},0)]\} = \langle T_\tau[\hat{\phi}(\mathbf{x},\tau)\hat{\phi}(\mathbf{y},0)]\rangle_T, \tag{1.81}$$

with T_τ the imaginary time ordering operator of the form

$$T_\tau[\hat{\phi}(\mathbf{x},\tau_1)\hat{\phi}(\mathbf{y},\tau_2)] = \theta(\tau_1-\tau_2)\hat{\phi}(\mathbf{x},\tau_1)\hat{\phi}(\mathbf{y},\tau_2) - \theta(\tau_2-\tau_1)\hat{\phi}(\mathbf{y},\tau_2)\hat{\phi}(\mathbf{x},\tau_1). \tag{1.82}$$

Then using the cyclic property of the trace and time evolution of the operator Eq. (1.80), we can easily see that

$$G_B(\mathbf{x},\mathbf{y};\tau,1/T) = G_B(\mathbf{x},\mathbf{y};\tau,0). \tag{1.83}$$

The main consequence of the this equality is to impose a periodicity condition on the field inside the brackets $\phi(\mathbf{x},0) = \phi(\mathbf{x},\beta)$. Thus the periodicity of the fields and of the Green's functions are consequences of the presence of the trace. This induces a discretization of the energy: The so-called *Matsubara modes*

$$\omega_n = 2\pi nT \qquad \text{(bosonic Matsubara modes)} \tag{1.84}$$

[7]We use round letters to denote the function related to the operator, denoted by a hat.

for n being an integer. This result is very important and induces that for bosons, a soft mode with $n = 0, \omega_0 = 0$ exists. The modes with $n > 0$ are called *hard modes*. The presence of the soft modes for bosons will prove to have a strong impact for the series expansion later on. In contrast, the fermions have anti-periodic boundary conditions $\psi(\mathbf{x}, 0) = -\psi(\mathbf{x}, \beta)$, which is reminiscent of the minus sign that fermions pick up when rotated by 2π and Green functions also have

$$G_F(\mathbf{x}, \mathbf{y}; \tau, 1/T) = -G_F(\mathbf{x}, \mathbf{y}; \tau, 0) \tag{1.85}$$

and this induces that *fermions have no soft modes*, since the Matsubara modes are

$$\omega_n = (1 + 2n)\pi T \qquad \text{(fermionic Matsubara modes)}. \tag{1.86}$$

Overall,

$$\begin{cases} \phi(\mathbf{x}, \beta) = \phi(\mathbf{x}, 0), & \omega_n = 2\pi n T, & \text{for bosons ,} \\ \psi(\mathbf{x}, \beta) = -\psi(\mathbf{x}, 0), & \omega_n = (2n+1)\pi T, & \text{for fermions.} \end{cases} \tag{1.87}$$

Going to an interactive theory and switching on a coupling constant, we can expand the exponential in the path integral in powers of the small coupling, if it is small enough, and apply the usual perturbation theory. Carefully keeping track of the combinatorics, we obtain the following modification of the Feynman rules for the diagrams

1. We start as usual by drawing all the connected diagrams
2. To each line, we associate $T \sum_n \int \frac{d^3p}{(2\pi)^3} \mathcal{D}_0(\omega_n, \mathbf{p})$, with $\mathcal{D}_0(\omega_n, \mathbf{p})$ the propagator at tree-level. For a boson it is
$$\mathcal{D}_0(\omega_n, \mathbf{p}) = \frac{1}{\omega_n^2 + \mathbf{p}^2 + m^2} \tag{1.88}$$
3. Each vertex, gives the momentum conservation factor $(2\pi)^3 \frac{\delta_{\omega_{\text{in}}, \omega_{\text{out}}}}{T} \delta(\mathbf{p}_{\text{in}} - \mathbf{p}_{\text{out}})$ times a power of the coupling to be determined by the specific model under consideration, $-\lambda$ in the present case.
4. Determine the combinatorics of the specified diagram in similar way than in QFT.
5. At the end, we still have to add a factor $\beta(2\pi)^3\delta(0)$.

This sets of rules permits to simply apply the reflexes of usual QFT for thermal backgrounds.

1.4.2 Mass corrections, thermal self-energy in Toy model

Now that we have adapted the usual weapons of vacuum QFT to the case of a hot and dense medium, we can repeat the usual computations of QFT in this new setting. Let us thus resume our study of the φ^4-theory of Eq.(1.36), again neglecting the cubic term. In this section, let us go through a very basic, but useful and instructive computation, and that will be useful in the future. Let us compute the finite temperature exact (dressed) propagator $\mathcal{D}(\omega_n, \mathbf{p})$, which is defined in the position space by

$$\mathcal{D}(\mathbf{x}, \tau_1; \mathbf{y}, \tau_2) = \langle \varphi(\mathbf{x}, \tau_1) \varphi(\mathbf{y}, \tau_2) \rangle_T \tag{1.89}$$

Figure 1.2: Hard thermal loop: Diagrams contributing to the mass of the scalar field.

where the brackets denote thermal ensemble average. The undressed propagator can be straightforwardly obtained from the path integral and is given by

$$\mathcal{D}_0(\omega_n, \mathbf{p}) = \frac{1}{\omega_n^2 + \mathbf{p}^2 + m_\varphi^2}. \tag{1.90}$$

Going to the Fourier space, we define the *self-energy* function $\Pi(\omega_n, \mathbf{p})$ in the following way:

$$\mathcal{D}(\omega_n, \mathbf{p}) = \left[\omega_n^2 + \mathbf{p}^2 + m_\varphi^2 + \Pi(\omega_n, \mathbf{p})\right]^{-1} \tag{1.91}$$

$$= (1 + \mathcal{D}_0\Pi)^{-1}\mathcal{D}_0. \tag{1.92}$$

Turning off the interaction would induce $\Pi(\omega_n, \mathbf{p}) = 0, \mathcal{D} = \mathcal{D}_0$. We would like now to compute the first order correction to the self energy $\sim \lambda$, that is to say the diagram in Fig. 1.2. Applying the Feynman rules recalled above, we obtain

$$\Pi_{1-\text{loop}} = 12\lambda T \sum_n \int \frac{d^3p}{(2\pi)^3} \frac{1}{\omega_n^2 + \omega^2}, \qquad \omega = \sqrt{\mathbf{p}^2 + m_\varphi^2}, \tag{1.93}$$

and the sum is to be performed over *Matsubara* frequencies. At the end of the day, after regulating and performing the integral and the sum, the result splits into two contributions: the first contribution is the usual *vacuum contribution to the mass* Π_{vac}

$$\Pi_{\text{vac}} = \frac{3\lambda}{4\pi^2}\left[\Lambda_c^2 - m_\phi^2 \log \frac{\Lambda_c^2}{m_\phi^2}\right], \tag{1.94}$$

which was already discussed in the context of the CW potential and induces the hierarchy problem. The second contribution is a finite temperature dependent contribution of the form

$$\Pi_T = \lambda T^2. \tag{1.95}$$

This the *Thermal Mass*, or *Debye Mass*. At this point, an important comment is in order: we really can see that the thermal screening only matters for the soft modes with $n = 0$, since higher modes comes with at least a contribution $\sim \pi^2 T^2$, always much larger than $\Pi_T \sim \lambda T^2$. We conclude that for fermions, no screening enters, since they do not have soft modes. We can conclude that *only for the soft modes is the screening important.*

Of course realistic theories contain also fermions and gauge bosons, which also can receive or/and induce thermal masses. Here, after this first illustrative computation, we list the relevant results[6]. In the SM[16], the expressions of the thermal masses read

$$\text{Higgs scalar:} \qquad \Pi_h(T) = T^2\left(\frac{3g^2}{16} + \frac{g'^2}{16} + \frac{\lambda}{2} + \frac{y_t^2}{4}\right), \tag{1.96}$$

$$\text{Gauge bosons:} \qquad \Pi_g^L(T) = T^2 \text{diag}\left(\frac{11}{6}g^2, \frac{11}{6}(g^2 + g'^2)\right), \qquad \Pi_g^T(T) = 0\,, \tag{1.97}$$

$$\text{Fermions:} \qquad \Pi_f = 0\,, \tag{1.98}$$

where $\Pi_g^L(T)$ denote the thermal mass of the *longitudinal* mode of the gauge bosons, while transverse modes $\Pi_g^T(T)$ are protected by gauge invariance and thus do not receive a mass at leading order in perturbation theory, but only at next-to-leading order. We will encounter those thermal masses in the case of the standard model augmented of a singlet (which will only bring a mild corrections to Eq.(1.98)) in Chapter 5 where they play an important role.

To summarize: in the plasma there are then three different scales involved in the problem: i) a hard scale for the $n \neq 0$ scalars and all the fermions, πT, a soft scales, for the $n = 0$ scalars and longitudinal gauge bosons $(\text{coupling})T$ and finally a ultra-soft scale, which would occur for transverse gauge bosons $(\text{coupling})^2 T$. This last scale is dangerously non-perturbative.

1.4.3 Thermal corrections to the potential

In section 1.3, we have seen how to compute the zero temperature one-loop potential. In the section, with the purpose of describing a transition between two states - or two vacua - of a theory, we compute the potential - or, equivalently, the free-energy - in the hot thermal plasma. Those corrections to the potential induced by thermal correction have been introduced in Ref [17, 18].

As in section 1.3 we first focus on a pure scalar field, go through the computation explicitly and then quote the result for the other species. Applying the Feynman rules at finite-temperature in Eq.1.4.1 and using the same tricks than in section 1.3, we obtain

$$V_{\rm tot}(\phi) = \frac{T}{2} \sum_{n=-\infty}^{\infty} \int \frac{d^3p}{(2\pi)^3} \log(\omega_n^2 + \omega^2) \tag{1.99}$$

and

$$\omega^2 = \mathbf{p}^2 + m_\varphi^2(\phi). \tag{1.100}$$

The sum over the modes is divergent but does not depend on the VEV, so we can easily compute it by taking the derivative of the expression in Eq.(1.99). So

$$f(\omega) \equiv \sum_{n=-\infty}^{\infty} \log(\omega_n^2 + \omega^2) \qquad \Rightarrow \frac{df}{d\omega} = \sum_{n=-\infty}^{\infty} \frac{2\omega}{\omega_n^2 + \omega^2} \tag{1.101}$$

which has a known result

$$\frac{df}{d\omega} = \frac{2}{T}\left[\frac{1}{2} + \frac{e^{-\omega/T}}{1 - e^{-\omega/T}}\right]. \tag{1.102}$$

We can now integrate this result with respect to ω and discard the constant piece (which does not depend on ω). We obtain

$$f(\omega) = \frac{2}{T}\left[\frac{\omega}{2} + T\log(1 - e^{-\omega/T})\right]. \tag{1.103}$$

Plugging back into Eq.(1.99), we obtain

$$V_{\rm tot}(\varphi) = \int \frac{d^3p}{(2\pi)^3}\Big[\underbrace{\frac{\omega}{2}}_{\text{zero-T contribution}} + \underbrace{T\log(1 - e^{-\omega/T})}_{V_T}\Big]. \tag{1.104}$$

Using the residue theorem, it is easy to show that the first piece in the integral of Eq.(1.104) reduces to the zero-temperature potential of section 1.3. We can thus consider that we already treated this contribution.

The thermal part is usually written in the following way via defining a function J_B:

$$V_T(\phi) = \frac{T^4}{2\pi^2} J_B(m^2(\varphi)/T^2) \tag{1.105}$$

A similar computation can be made for the fermion case and wield and extra minus sign:

$$J_{B/F}(y^2) = \int_0^\infty dx\, x^2 \log\left[1 \mp \exp\left(-\sqrt{x^2+y^2}\right)\right] . \tag{1.106}$$

However, expressions in Eq.(1.106) are expensive to solve exactly numerically and to save computation time, we will use in the following chapters the approximate expansions of the function $J_{B/F}(y^2)$ as given in Ref. [16]:

$$\begin{aligned} J_B(y^2) &= \begin{cases} -\frac{\pi^4}{45} + \frac{\pi^2}{12}y^2 - \frac{\pi}{6}y^3 - \frac{y^4}{32}\log\left[\frac{y^2}{16\pi^2\exp[3/2-2\gamma]}\right], & y^2 \ll 1 , \\ -\sum_{n=1}^{m>3}\frac{1}{n^2}y^2 K_2(yn) , & y^2 \gg 1 , \end{cases} \\ J_F(y^2) &= \begin{cases} \frac{7\pi^4}{360} - \frac{\pi^2}{24}y^2 - \frac{y^4}{32}\log\left[\frac{y^2}{\pi^2\exp[3/2-2\gamma]}\right], & y^2 \ll 1 , \\ -\sum_{n=1}^{m>3}\frac{(-1)^n}{n^2}y^2 K_2(yn) , & y^2 \gg 1 . \end{cases} \end{aligned} \tag{1.107}$$

where $\gamma \approx 0.577$ is the *Euler constant*, and $K_2(z)$ are the second-kind Bessel function. Expressions in Eq.(1.107) are shown in very much detail in the book [15] and their convergence properties are studied. At this point we should also emphasize the appearance of a non-analytical term in the boson expansion, $\frac{\pi}{6}y^3$. This term is really what allows for *thermally-induced* FOPTs.

This suggests the following recipe to account for the thermal excitations due to the temperature and the density in the early universe plasma: we have to supplement the zero-temperature potential discussed in the previous sections with the thermal corrections of the form

$$\begin{aligned} V_T(M_i(\varphi)) &= \sum_{i\in B}\frac{n_i}{2\pi^2}T^4 J_B\left(\frac{M_i^2(\varphi)}{T^2}\right) - \sum_{i\in F}\frac{n_i}{2\pi^2}T^4 J_F\left(\frac{M_i^2(\varphi)}{T^2}\right) , \\ J_{B/F}(y^2) &= \int_0^\infty dx\, x^2 \log\left[1 \mp \exp\left(-\sqrt{x^2+y^2}\right)\right] , \end{aligned} \tag{1.108}$$

where V_T is usually called the *thermal potential*. At this point, we could also mention that the thermal correction to the mass that has been computed in subsection 1.4.2 could be now recovered by taking the high temperature expansion in Eq.(1.107) and taking two derivatives of the potential.

Though nice and simple to implement, this thermal potential suffers from IR issues coming from the diagrams displayed on Fig.1.3. The scaling of each of those diagrams can be evaluated using the Feynman rules for the finite-temperature case and the simple following rule: A diagram with a (zero-temperature) *superficial* divergence of $d > 0$ has a T^d scaling while a diagram with $d < 1$ has a scaling T. This trivially tells us that the diagram a) in Fig.1.3, the thermal mass, will scale as $\sim \lambda T^2$, which is verified.

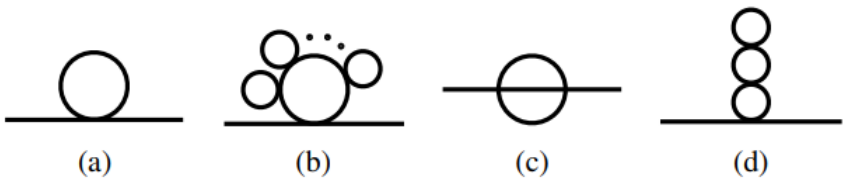

Figure 1.3: a) is the thermal correction to the mass, b) are the *daisy diagrams*, c) the *lollipop* and d) is the superdaisy contribution. Image borrowed from [16].

Using similar prescription, we can compute similar scaling for each of the diagrams in Fig.1.3, always assuming that the loop connecting to the external legs is *soft*, or $n = 0$ in terms of Matsubara modes. This gives

$$\begin{aligned} \text{b): Daisies with n petals :} \quad & \sim \frac{\lambda^n T^{2n-1}}{m_\varphi^{2n-3}} \\ \text{c): Two loops lollipops :} \quad & \sim \lambda^2 T^2 \\ \text{d): Three loops superdaisies :} \quad & \sim \lambda^3 \frac{T^4}{m_\varphi^2} \end{aligned} \tag{1.109}$$

Let us emphasize again that the m_φ appearing in the denominator of those expression comes *only* in the case of a soft boson in the first loop. A fermion loop would not produce this effect since even for $n = 0$, the denominator receives a πT and thus fermion loops are never soft.

At this point, it is good to remember that the phase transition is triggered by the competition between tree-level masses $-m_\varphi^2$ and the thermal correction λT^2. The transition will occur when they are of the same order of magnitude $m_\varphi^2 \sim \lambda T_{\rm PT}^2$. We can now evaluate the scaling of the diagrams in Eq.(1.110) at the moment of the phase transition: $T_{\rm PT}^2 = m_\phi^2/\lambda$: we obtain

$$\begin{aligned} \text{Daisies with n petals :} \quad & \sim \frac{\lambda^{1/2} m_\varphi^{2n-1}}{m_\varphi^{2n-3}} \sim \lambda^{1/2} m_\varphi^2 \\ \text{Two loops lollipops :} \quad & \sim \lambda m_\varphi^2 \\ \text{Three loops superdaisies :} \quad & \sim \lambda m_\varphi^2 \end{aligned} \tag{1.110}$$

and we observe that though two loops lollipops and three loops superdaisies are under perturbative control, the "daisy" diagrams have the same values at each order in the perturbation expansion n. This signals a serious breakdown of the perturbative expansion. In the next subsection, we will show how this issue can be solved for scalar and longitudinal modes of gauge bosons, but not for transverse modes.

1.4.4 Thermal potential and Daisy resummation

In the previous section, we saw the difficulties that the perturbative approach would encounter due to Daisy diagrams having the same parametric dependence at all orders in the perturbative series, endangering the perturbativity. In this section, to cure this issue and prove the Daisy resummation techniques, we follow the review [15]. The diagram with n petals (hard-loops) attached to the soft loop gives (after careful counting, see page 45 of [15])

$$\text{daisy n-loops} = \frac{6^n(-1)^{n+1}}{n!}\left(\frac{\lambda}{4!}\right)^n \underbrace{[2(n-1)][2(n-2)]...[2]}_{2^{n-1}(n-1)!} \underbrace{\left(\frac{T^2}{12}\right)^n}_{\text{hard petals}} \underbrace{T\int \frac{d^3p}{(2\pi)^3}\left(\frac{1}{p^2+m_\varphi^2}\right)^n}_{\text{soft part}}. \tag{1.111}$$

The difficult soft part of the integral can be solved by noticing a recursion law[8]:

$$\begin{aligned}\int \frac{d^3p}{(2\pi)^3}\left(\frac{1}{p^2+m^2}\right) &= -\frac{m}{4\pi} = -\frac{d}{dm^2}\left(\frac{m^3}{6\pi}\right)\\ \int \frac{d^3p}{(2\pi)^3}\left(\frac{1}{p^2+m^2}\right)^2 &= \frac{d}{dm^2}\left(\frac{m}{4\pi}\right) = \frac{d}{dm^2}\frac{d}{dm^2}\left(\frac{m^3}{6\pi}\right)\\ \int \frac{d^3p}{(2\pi)^3}\left(\frac{1}{p^2+m^2}\right)^n &= -\frac{1}{n-1}\frac{d}{dm^2}\int \frac{d^3p}{(2\pi)^3}\left(\frac{1}{p^2+m^2}\right)^{n-1}.\end{aligned} \tag{1.112}$$

At the end, we obtain

$$\int \frac{d^3p}{(2\pi)^3}\left(\frac{1}{p^2+m^2}\right)^n = \frac{(-1)^n}{(n-1)!}\left(\frac{d}{dm^2}\right)^n\left(\frac{m^3}{6\pi}\right). \tag{1.113}$$

And combining Eq.(1.111) and (1.113), we obtain that the contribution to the potential of the n-loop Daisy diagram is given by

$$\text{daisy n-loops} = -\frac{T}{2}\frac{1}{n!}\left(\frac{\lambda T^2}{4!}\right)^n\left(\frac{d}{dm_\varphi^2}\right)^n\left(\frac{m_\varphi^3}{6\pi}\right). \tag{1.114}$$

Armed with this result, we can now go to the sum over n and see the magic happen

$$\delta V_{\text{daisies}} = -\sum_{n=0}\frac{T}{2}\frac{1}{n!}\left(\frac{\lambda T^2}{4!}\right)^n\left(\frac{d}{dm_\varphi^2}\right)^n\left(\frac{m_\varphi^3}{6\pi}\right) = -\frac{T}{12\pi}\left(m_\varphi^2+\frac{\lambda T^2}{24}\right)^{3/2} = -\frac{T}{12\pi}\left(m_\varphi^2+\Pi(T)\right)^{3/2} \tag{1.115}$$

Going back to the expression for the thermal mass of the scalar field, we observe that resumming the Daysies amounts to *shift the mass of the scalar field by the thermal mass*.

$$m_\varphi^2 \to m_\varphi^2 + \Pi(T) \qquad \text{(Daisy resummation)}. \tag{1.116}$$

We can do so in the full thermal potential because, in the high T potential, the contribution at m_φ^2, when shifted, only brings a new field-independent that we can ignore and at m_φ^4 level, the contribution from the thermal potential cancels with the contribution from the CW potential at zero temperature, so it is irrelevant. On the other hand, at low T, this shift is irrelevant in any cases. However, we notice that thermal corrections are "slowing down" the convergence of the perturbation theory, since taking $m_\varphi \to 0$ in Eq.(1.115) produces at one loop $\lambda^{3/2}$, instead of the usual λ^2 at higher order.

A similar type of procedure can be performed for the longitudinal parts of the gauge bosons, since they receive a mass of the form $m_{L,g}^2 \sim g^2T^2$ (see page 79 section 5 of [15]). However, the transverse modes do not receive a mass at this order. If we speculate that transverse modes are screened at next order $m_{T,g}^2 \sim g^4T^2$ and using the gauge boson cousin of Eq.(1.115) and set the mass to zero, we obtain a term

$$\sim -\frac{T^4}{12\pi}g^6 \tag{1.117}$$

at all order in the perturbation series. This is the infamous "Linde Problem"[19] that plagues any thermal gauge theory and threatens the perturbation theory. Transverse modes cannot be screened and daisy resummation fails, so

[8]It takes a bit of courage to convince oneself of that result...

all the orders in perturbation theory are parametrically the same. This problem can be understood in an alternative way, if we notice that, in thermal field theory, the real expansion parameter is not g^2, but $g^2 f(\omega)$, where f is the distribution function. We can thus see again that for the soft modes $n = 0$, the effective coupling is

$$\text{(effective coupling)} = g^2 f(\omega_0) = \frac{g^2}{e^{\omega_0/T} - 1} \to \frac{g^2 T}{m_{T,g}} \to 1 \tag{1.118}$$

which is parametrically large. This is the source of the claim that *transverse gauge bosons in thermal field theory are strongly coupled*.

To summarize, to account for higher loops due to the Daisy diagrams at finite temperature, we can follow the so-called “Truncated-Full-Dressing" procedure [16]. Doing so, the full one-loop potential becomes

$$V_{\text{eff}}(\varphi, T) = V_{\text{tree}} + \sum_i V_{CW}(M_i(\varphi)^2 + \Pi_i) + V_T(M_i(\varphi)^2 + \Pi_i) \tag{1.119}$$

where Π_i are the so-called “thermal masses", dependent on the VEV φ and the temperature for each degree of freedom. This will be our way to build potentials in the models we will study later in this thesis. We, however, have to keep in mind the dangerous limitation of the Linde problem.

As a final comment, let us also mention the limitation of the Daisy resummation and 4D perturbative approach. In [20] it was shown that perturbative approach with daisy resummation was still very sensitive to the cut-off scale chosen and small changes in the cut-off could induce orders of magnitude changes in the GW signal (because of the strong dependence of the GW signal amplitude over the nucleation temperature). Alternative methods were advocated in[20, 21, 22].

Now that we have gathered all the theoretical tools to address the complicated problem of PT in the early universe, let us lay down the basics of nucleation and early dynamics of the FOPT.

1.5 Phase transitions in early universe and the fate of symmetries

A very interesting feature of QFT is that it allows, even for very simple setting, a theory to exist in different phases, and those phases will give very different phenomenologies in terms of particle physics. This comes from the fact that to extract predictions from a QFT, we need to expand the theory in terms of fluctuations around the minimum of the potential. A phase corresponds to one of the minima of the theory. As a consequence, we expect that expanding around two different minima provides us with very different phenomenologies.

Moreover, the concept of symmetries, and the possibility of breaking it, plays a crucial role in physics. In particular, the breaking of the EW symmetry via the introduction of four new scalar degrees of freedom, the Higgs field, permitted to obtain consistent mass terms for the fermions of the SM, if one of those degrees of freedom gets a non-vanishing VEV. This is the famous *Higgs-Brout-Englert* mechanism, which firmly established gauge theories as strong candidates for the description of nature.

If this pictures seems very neat at low energies, we might wonder what occurs to the EW symmetry (or any other broken symmetry) in the context of high energy. Even though, terrestrial experiments are naturally limited in energies that can be reached, the energy scale of primordial plasma, which follows the inflation and reheating, is naively expected to be several orders of magnitude larger, possibly reaching $T \sim 10^{14}$ GeV or above. In this context, the question of the fate of the EW symmetry (or other) becomes a pressing question, as naive thermal

field theory suggests the restoration of the symmetry. More quantitatively, the high temperature expansion of the thermal potential produces a $\propto +T^2\varphi^2$, where φ is the symmetry breaking field (for example the Higgs h). For high values of T, this term will stabilise the origin $\varphi = 0$ and restore the broken symmetry. If a symmetry is broken at low temperature and restored at high temperature, the thermal evolution of the universe needs to undergo a phase transition. In this section, we give an overview of the role that the phase transitions play in the early universe and the putative consequences of such a transition and we focus on the special case of *first order phase transition* (FOPT).

1.5.1 What characterizes an early universe phase transition ?

As an illustrative purpose, let us study the case of a scalar field with a Coleman-Weinberg (CW) potential, like in (1.43) and, on the top of it, we add the thermal corrections we have computed in Section 1.4. It is known that pure CW potentials display a unique symmetry-breaking minimum $v = \mu_R e^{1/4}$ as we discussed in section 1.3. This scalar field obtains a finite VEV at zero temperature and breaks a symmetry. The full potential (augmented by temperature corrections) of this very toy model is schematically given by

$$V_{\rm eff}(T,\varphi) = V_{\rm CW}(\varphi) + V_T(\varphi,T), \tag{1.120}$$

and we illustrate a typical potential of this type on Fig.1.4 for several values of the temperature T. Satisfactorily, we observe the suspected behaviour: the global minimum of the theory at large T is located at the origin, where the symmetry group is maximal, and at low temperature the global minimum is located away from the origin, as it becomes pure CW potential. This situation displays a very non-trivial coexistence of two minima at position $\varphi_{\rm sym} = 0$ and $\varphi_{\rm h} = v(T) \neq 0$, separated by a barrier of potential. The barrier between the two minima is a special feature coming from the non-analytic term in the thermal expansion $\sim -m^{3/2}$. This constitutes the special case of *first-order* phase transition (FOPT). The rest of this thesis will only consider this possibility and study some of its features. The Fig.1.4 shows two special values of the temperature: $T^\star$, where the minimum in $\varphi_{\rm h} = v(T) \neq 0$ forms for the first time and the *critical temperature* $T^{\rm crit}$, the temperature for which both minima have the same energy:

$$V(\varphi = 0, T = T^{\rm crit}) = V(\varphi = v(T^{\rm crit}), T = T^{\rm crit}). \tag{1.121}$$

For some range of lower temperatures, the symmetry breaking minimum will become energetically favorable but separated to the origin by a barrier of potential. This means that the transition initially needs some input of energy to proceed and to fall in the deeper minimum. It follows that the transition can be delayed and occur for $T < T^{\rm crit}$, allowing for the remarkable phenomena of *supercooling*. Supercooling is well-known of condensed matter physicists and also occurs in the everyday life, if we are bold enough to freeze pure water to below zero temperatures. However, supercooling in systems of everyday life can be terminated by the injection of external energy, which is not a possibility in the early universe. However, two types of effects can push the field above the barrier of potential: thermal fluctuations, related to the classical dynamics of finite temperature system, and quantum fluctuations, related to the intrinsic uncertainty in the position of the field (in field space). A fluctuation occurring in some region of the plasma converts the plasma “in the old phase" (that is to say, the phase with the scalar field located at the origin) into the “new phase" (the phase with the scalar close to the symmetry breaking value). Minimisation of energy, as we will further discuss later on, imposes that such a region takes a spherical shape: a *bubble*. Such bubble-nurturing fluctuations are both statistical in nature and thus the description of the phase transition requires the computation of the probability per unit of volume of the appearance, said *nucleation*, of such bubble. Before to go further and to engage in those computations, let us first say some few words on other types of phase transitions, as for example the case where always only one minimum exists and the field will be allowed to roll from the origin to the symmetry breaking minima. Such possibility is called a *second order* phase transition.

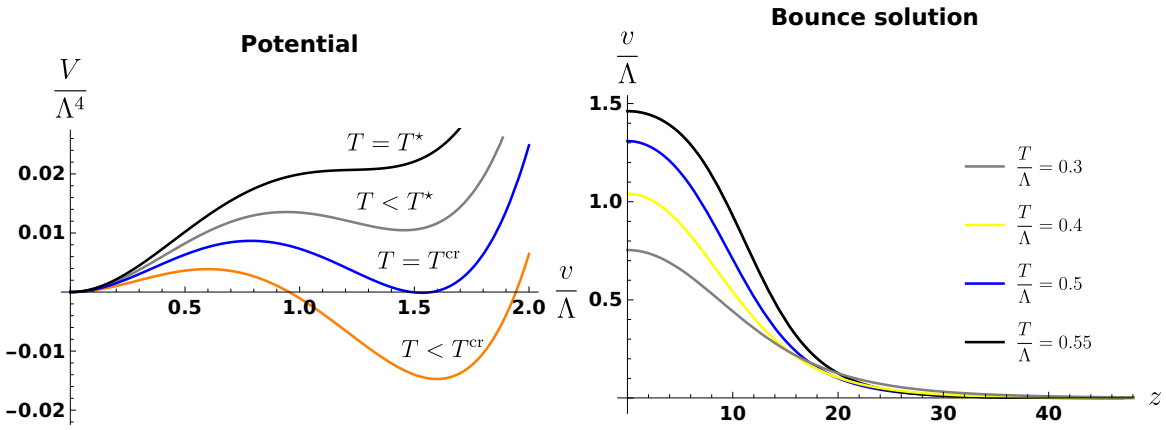

Figure 1.4: **Left**: Potential of the toy model with one scalar field as a function of the VEV for different values of the temperature. We display the temperature $T^\star$ where the symmetry breaking minimum appears and $T^{\rm crit}$ is the temperature where both minima have the same energy. **Right:** Typical *bounce solution* for different nucleation temperature. We can observe that lower nucleation temperature provides thicker walls.

1.5.2 Nucleation of O_3 and O_4 bubbles

The nucleation of a bubble of new phase surrounded by the old phase is a complicated QFT problem that is still not entirely solved. However, it was shown in [23, 24, 25] for the quantum[23] and the thermal[24, 25] fluctuations, that the probability is controlled by the exponential of the *bounce action*. This bounce action corresponds physically to an instanton solution of the path integral, *the bounce profile*, minimising the imaginary part of the action, which thus gives the “most probable escape path", as was first introduced in [26]. Fluctuations around this extremal solution provide the prefactor of the exponential and was estimated for the first time in [27]. A rough order of magnitude estimate of the probability is just obtained by matching the prefactor dimensionnally with the scale in the theory. The total probability per unit of volume of nucleation a bubble is thus given by

$$\Gamma(T) \simeq \Gamma_3(T) + \Gamma_4 = T^4 \left(\frac{S_3}{2\pi T}\right)^{3/2} e^{-S_3(T)/T} + \frac{1}{R_0^4}\left(\frac{S_4}{2\pi}\right) e^{-S_4} \,, \tag{1.122}$$

where S_3, S_4 are $O(3,4)$ bounce actions and R_0 is the bubble radius at nucleation. The solution for the bounce can be found numerically using the shooting method described for the 2D case in Appendix A.4 and some examples are displayed on the right of Fig.1.4. Most of the physical situation studied in the early universe showed dominance of the O_3 over O_4, though some very special cases might be dominated by quantum fluctuations.

1.5.3 Expansion of young bubbles

Now that the bubble has nucleated and that we know how to compute the probability of such an event, we would like to make progress and investigate the fate of this tiny bubble. A first important question is: will it expand ?

Critical Radius To be able to obtain analytic results, we assume *Thin wall*, that is to say, the thickness of the wall (*the region over which the VEV of the symmetry breaking field interpolates from zero to its true vacuum value*) is much smaller than the radius of the bubble. With this assumption, we can write the Lagrangian[28, 29]

$$\mathcal{L} = -4\pi\sigma R^2\sqrt{1-\dot{R}^2} + \frac{4\pi}{3}R^3 p \tag{1.123}$$

where R is the radius of the bubble and we clearly can observe the competition between the *pressure* $p \equiv \Delta V - \Delta\mathcal{P}_{\text{plasma}}$. We separated the pressure p into a driving force ΔV coming from the difference of vacuum energy of each minima and a slowing force $\Delta\mathcal{P}_{\text{plasma}}$ coming from the resistance of the plasma to the expansion of the wall, being proportional to the volume of the bubble and the *surface tension*, being proportional to the surface of the bubble. The surface tension is defined

$$\sigma \equiv \int_{\text{wall}} d\varphi \partial_{\perp}\varphi = \int_{\text{wall}} d\varphi \sqrt{2V(\varphi)} \tag{1.124}$$

which is a constant along the expansion. The derivation of (1.123) is reproduced in Appendix A.1 following the lines of [29]. At the onset of the bubble, the pressure from the plasma can be neglected, as it is vanishing in the limit of zero velocity, and we take for the moment $p \approx \Delta V_{\text{potential}} = \Delta V$. We will come back to the plasma pressure at length in Chapter 2.

The previous Lagrangian expression can be recasted into a Hamiltonian making the usual Legendre transform

$$\mathcal{H} = \dot{R}\frac{\partial\mathcal{L}}{\dot{R}} - \mathcal{L} = 4\pi\sigma R^2 \frac{1}{\sqrt{1-\dot{R}^2}} - \frac{4\pi}{3}R^3\Delta V. \tag{1.125}$$

This defines a *critical radius* R_c, that we can compute by extremizing the energy

$$\mathcal{E} = 4\pi\gamma_w\sigma R^2 - \frac{4\pi}{3}R^3\Delta V, \quad \gamma_w \equiv \frac{1}{\sqrt{1-\dot{R}^2}} \tag{1.126}$$

to obtain

$$R_c \equiv \frac{2\sigma}{\Delta V} \tag{1.127}$$

where we set the initial velocity to zero, and so $\gamma_{w,i} = 1$. A bubble nucleating with $R_0 < R_c$ would be unable to resist the pressure of the surface tension and would collapse. Only when bubbles have $R_0 > R_c$, they will be able to start to expand. But looking back at the Lagrangian in Eq.(1.123) teaches us that nucleating a bubble with $R_0 \gg R_c$ is highly improbable, since we are far away from extremizing the Lagrangian. So the most probable bubble that will eventually expand is the bubble with $R_0 = R_c$.

Let us make another comment on the energy budget of the bubble: In the plasma frame, it is apparent from Eq.(1.126) that the volumic release of energy is turned into increasing the velocity γ_w that we can already anticipate to behave like $\gamma_w \propto R/R_0$.

Early Expansion We have seen that bubbles nucleated with in initial radius of $R_0 \gtrsim R_c$ are energetically allowed to expand. The subsequent evolution can be obtained from the Lagrangian (1.123) and applying the Euler-Lagrange equations:

$$\ddot{R} + 2\frac{1-\dot{R}^2}{R} = \frac{\Delta V}{\sigma}(1-\dot{R}^2)^{3/2} \tag{1.128}$$

For a complete exposition of how to obtain those expressions in spherical coordinates, see [30]. The quantity $\dot{R}$ is the velocity of the wall, which is often written as well v_w. The equation in (1.128) can be rewritten in term of the Lorentz factor γ_w

$$\frac{d\gamma_w}{dR} + \frac{2\gamma_w}{R} = \frac{\Delta V}{\sigma}. \tag{1.129}$$

Again, this expression neglects the backreaction from the plasma, so it is expected to be valid at the very early stage of the expansion or when the release of energy from the transition is always stronger than the backreaction from the plasma: the *runaway regime*. We can now solve (1.129) and, taking the boundary condition $\gamma_w(R_0) = 1$, one finds the following solution

$$\gamma_w = \frac{\Delta V R}{3\sigma} + \frac{R_0^2}{R^2} - \frac{\Delta V R_0^3}{3\sigma R^2} \approx \frac{2R}{3R_0} + \frac{R_0^2}{3R^2} \tag{1.130}$$

where we used $R_0 \approx R_c \equiv \frac{2\sigma}{\Delta V}$. In the case where we can neglect the pressure from the plasma, we can approximate the energy stored in the wall by

$$E_{\text{wall}} = E_0 + \frac{4\pi}{3} R(t)^3 \Delta V(t) \tag{1.131}$$

with $E_0 = S_3(\varphi = \varphi_{in})$ the initial energy of the bubble. In this expression we took advantage of the fact that the energy which is released by the transition goes into the bubble wall and we avoid having to compute the tension. Here however, there is a subtlety: the value of the field at the center of the bubble at the moment of nucleation is not the value of the field in the minimum, but at the escape point $\varphi_r = \varphi_{in}$ which subsequently roll down with time $\varphi(t)$. Thus we define $\Delta V(t) = V(0) - V(\varphi(t, r = 0)$ and the initial radius is given by

$$R_0 = \left[\frac{3E_{0,V}}{4\pi\Delta(t=0)}\right]^{1/3} \tag{1.132}$$

To a rather good approximation, $\Delta V(t) = \Delta V$ and $E_{0,V}$ is the initial contribution to the energy of the bubble.

At the end of the day, very nicely, the pressure and the surface tension factor out of the evolution of the Lorentz factor and we can only keep in mind that

$$\boxed{\gamma_w(R) \approx \frac{2R}{3R_0}} \tag{1.133}$$

from which we can simply read that the evolution of the boost factor follows the grows of the bubble $\propto R$. The bubble accelerates very strongly.

1.5.4 Energy budget and parameters of the phase transition

As we have seen, the early stage of the bubble expansion reflects the competition between the surface tension scaling like the surface of the bubble and the injected energy, scaling like the volume of the bubble, leading to a simple law $\gamma_w \propto R$ of expansion. As a consequence, as soon as the bubble expands enough, the surface tension can be absolutely ignored with respect to the release of energy, and the dynamics is only controlled by the release of energy. The expansion of the bubble converts the plasma from the old phase into the new phase and large amount of energy is released in the plasma. At this point, if we want to be able to characterise the transition in terms of a possible signal, like a GW signal, it becomes important to describe the transition with some simple parameters. Presenting the parameters controlling the energy budget of the transition is the purpose of this section.

Energy budget of the phase transition

Bubble nucleation is characterised by a critical temperature T_{crit}, defined as the point when the two phases of the system have vacua with the same energy. Below T_{crit} phase transition becomes energetically possible. The probability to find a specific point of the Universe to be in the false vacuum is given by [31, 32]:

$$P_f[T] = \exp[-I(T)] \,, \qquad I(T) \equiv \frac{4\pi}{3}\int_T^{T_c} \frac{dT_1 \Gamma(T_1) v_w^3}{T_1^4 H(T_1)}\left[\int_T^{T_1} \frac{dT_2}{H(T_2)}\right]^3 . \tag{1.134}$$

In Eq.(1.122) the strongest dependence on the temperature comes from the $\Gamma(T) \propto \exp\left(-S_3/T\right)$, so that the quantity $I(T)$ is mostly controlled by the ratio $\Gamma\left(T\right)/H^4\left(T\right)$ and an order one fraction of the volume of the Universe will be in the true vacuum when $\Gamma[T] \sim H^4[T]$. The temperature that satisfy this condition is coined the *nucleation temperature* T_{nuc} or, to phrase differently, the nucleation temperature T_{nuc} corresponds to the appearance of roughly one bubble of true vacuum per Hubble volume. T_{nuc} can be obtained in the following way

$$\Gamma \sim H^4,$$

$$H(T)^2 = \frac{1}{3M_{\text{pl}}^2}(\rho_{\text{rad}} + \rho_{\text{vac}} + \rho_{\text{wall}}), \quad \rho_{\text{wall}} \approx 0, \quad \rho_{\text{rad}} = \frac{\pi^2 g_\star}{30}T^4, \qquad \rho_{\text{vac}} = \Delta V$$

$$\Rightarrow \quad \frac{S_3}{T_{\text{nuc}}} = \frac{3}{2}\log\left(\frac{S_3}{2\pi T_{\text{nuc}}}\right) + 4\log\left(\frac{T_{\text{nuc}}}{H(T_{\text{nuc}})}\right) . \tag{1.135}$$

More precisely the temperature of the phase transition can be found by following the procedure outlined in [33]

$$I(T_{\text{per}}) \gtrsim 0.34, \tag{1.136}$$

where the condition $I(T_{\text{per}}) \sim 0.34$ implies that the false vacuum occupies less than $\text{Exp}[-I(T_{\text{per}})] \sim 70\%$ of the total space of the universe. The reason of this choice comes from the following argument, due to [34], which shows that $\sim 34\%$ is the "minimal fraction of new phase such that bubbles can constitute an infinite connected cluster". T_{per} is dubbed the *percolation temperature* and this is the temperature at which the GW are typically emitted. If the condition in Eq.(1.136) is not fulfilled, $I(T) < 0.34$, then the bubbles do not percolate and the transition never completes.

The energy released during the PT is traditionally quantified by the ratio between the energy stored in the vacuum and in the plasma at the moment of the transition

$$\alpha(T) \equiv \frac{\Delta V(T) - \frac{T}{4}\frac{\partial \Delta V}{\partial T}}{\rho_{\text{rad}}} \approx \frac{\Delta V(T)}{\rho_{\text{rad}}} \qquad \text{(Strength parameter)}, \tag{1.137}$$

which has to be evaluated at the percolation temperature. This is one of the important parameters of the energy budget of the bubble. The α parameter, the latent heat of the transition normalized by the radiation energy of the universe, is related to the amount of supercooling in the following sense: as the temperature decreases below the critical temperature, the difference of depth between the true and the false vacua ΔV remains roughly constant, while the relativistic energy gets redshifted by the expansion of the universe $\rho_{\text{rad}} \propto T^4$ very fast. Then $\alpha \propto 1/T^4$ and a larger supercooling will induce a larger energy budget parameter α.

A second important parameter is the duration of the phase transition. The duration from the nucleation to the percolation can be approximated by expanded the rate of nucleation at first order. This leads to the definition:

$$\tilde{\beta} \equiv \frac{\beta}{H} = -\frac{d(S_3/T)}{Hdt} = T\frac{d}{dT}\left(\frac{S_3}{T}\right) \qquad \text{(Duration of the transition)} \tag{1.138}$$

Parameter	Symbol	Expression
Nucleation temperature	$T_{\rm nuc}$	$\Gamma \sim H^4$
Percolation temperature	$T_{\rm per}$	$I(T_{\rm per}) \gtrsim 0.34$
Reheating temperature	$T_{\rm reh}$	$T_{\rm reh} \approx (1+\alpha)^{1/4} T_{\rm per}$
Strength of the transition	α	$\frac{\Delta V - \frac{T}{4}\frac{\partial \Delta V}{\partial T}}{\rho_{\rm rad}}$
Duration of the transition	β	$T\frac{d}{dT}\left(\frac{S_3}{T}\right)$ or $\frac{(8\pi)^{1/3} v_w}{H(T_{\rm per}) R_\star}$
Velocity of the bubble wall	v_w	Chapter 2

Table 1.4: Summary of the energy budget of PT necessary for the computation of the GW signal as well as PT parameters.

The normalized speed of nucleation $\tilde{\beta} \sim \frac{t_{\rm expansion}}{t_{\rm transition}}$, with $t_{\rm transition}$ the typical time the transition takes to complete and $t_{\rm expansion}$ the Hubble time, measures how fast a bubble nucleates with respect to the expansion of the universe, giving an estimated of the speed of completion of the transition.

However, the derivative of the function S_3/T may be submitted to large uncertainties, due to the rapid change with T, as a consequence, it has been suggested to make the change [35, 33, 36]

$$\tilde{\beta} = T\frac{d}{dT}\left(\frac{S_3}{T}\right) \to \frac{(8\pi)^{1/3} v_w}{H(T_{\rm per}) R_\star}, \tag{1.139}$$

where the radius at collision $R_\star$ can be obtained from

$$R_\star \equiv \frac{(8\pi)^{1/3}}{\tilde{\beta}} \approx \left(\int_{T_{\rm per}}^{T_{\rm crit}} \frac{dT}{T} \frac{\Gamma(T)}{H(T)} \left(\frac{T_{\rm per}}{T}\right)^3 \right)^{-1/3}. \tag{1.140}$$

We will come back to this issue in the Chapter 5 where we will see that we need a more robust definition of the durations of the transition.

At last, the temperature at the end of the phase transition will control the redshift of the signal. Assuming that the transition occurs in less than an Hubble time, we can apply conservation of energy arguments to obtain the *reheating temperature* $T_{\rm reh}$:

$$(1-\Omega_{GW})(\Delta V + \rho_{\rm rad}\big|_{T=T_{\rm per}}) = \rho_{\rm rad}\big|_{T=T_{\rm reh}} \qquad \Rightarrow T_{\rm reh} \approx (1+\alpha)^{1/4} T_{\rm per}, \tag{1.141}$$

where we neglected the energy lost in the GW signal.

We will see that this quantity will play a very important role in the remainder of this thesis.

1.5.5 First encounter with the regimes of expansion

So far we have met three $(\alpha, \beta, T_{\rm reh})$ of the four parameters determining the GW signal emitted. The last one is the velocity of the bubble wall v_w. This parameter somehow splits into two different parameters: the absolute value of v_w and the *regime of expansion* at collision of the bubbles. Though it will be the main topic of the Chapter 2 let us introduce here the different *regimes of expansion* of the bubble[31, 36, 37, 5] that we can encounter. We will of

course abundantly come back on those issues later on, suffice it to say for now that the regime of expansion is fixed by the competition between the release of energy ΔV which pushes for the expansion of the bubble and the friction from the plasma $\mathcal{P}$: there are two possibilities

1. **Terminal velocity regime**: The pressure growing with the acceleration of the wall, the plasma finally balances the release of energy and the acceleration of the bubble terminates $\gamma_w \to \gamma_w^{\rm terminal}$. All the energy of the transition is then redirected to the plasma.
2. **Run-away regime**: The pressure from the plasma never manages to catch up with the release of energy and the bubble keeps accelerating until collision among the bubbles. In this case, the energy will be mainly stored into the shear-stress at the wall and in the sound waves in the plasma.

We will see now that those two cases are expected to produce very different GW signal.

1.6 GW signal from FOPTs

We have already emphasized the fact that strong enough FOPTs would produce copious GW signals, under the form of a homogeneous SGWB. This possible SGWB from FOPTs has been copiously studied in the past 10 years or so, and still come with large uncertainties. Let us present the state of the art here, the final purpose being to be able to constrain BSM physics from possible SGWB observers.

There are two crucial steps on constraining the BSM physics from gravitational observers. The first consists in mapping the thermal description of some theory in terms of energy budget parameters. Schematically, it is

$$\boxed{\text{BSM parameters} \Rightarrow (\alpha, \beta, T_{\rm reh}, v_w)}. \tag{1.142}$$

The second step consists in describing the power spectrum of the gravitational waves emitted in terms of the phase transition parameters:

$$\boxed{(\alpha, \beta, T_{\rm reh}, v_w) \Rightarrow \text{GW spectrum}}. \tag{1.143}$$

In this section, we review quickly the physics of the emission of gravitational waves during FOPT. We have however to keep in mind that the study of the spectrum and magnitude of the GW induced by PT remains a very active field and that none of the result we mention is definitive.

Our understanding of the GW signal from FOPT relies ultimately on scalar field and hydrodynamic simulations and combination of them[46, 47, 48, 49, 50, 51], see also the reviews in [52, 53] and the LISA working group [54]. Three main contributions to the GW signal have been determined so far: a *scalar field* contribution, originating from the collision of the bubbles, a *sound waves* contribution coming from sound waves propagating into the plasma, and a *turbulent* contribution due to turbulent motion of the plasma when non-linearities kick in. Each of those sources corresponds to a different stage in the phase transition. The *scalar field* contribution corresponds to the collision of bubbles among each other and the merging of the shells, which is typically of short duration. The second stage, which is much longer and possibly as long as an Hubble time, is the propagation of sound waves in the plasma and corresponds to the *sound waves* contribution. Finally, in the last stage, non-linearities in the plasma kicks in and the fluid shell develop shocks, this correspond to the turbulent contribution. Following the recommendations of [54], we will ignore the turbulence contribution due to the large uncertainties and, in our computation of the spectrum,

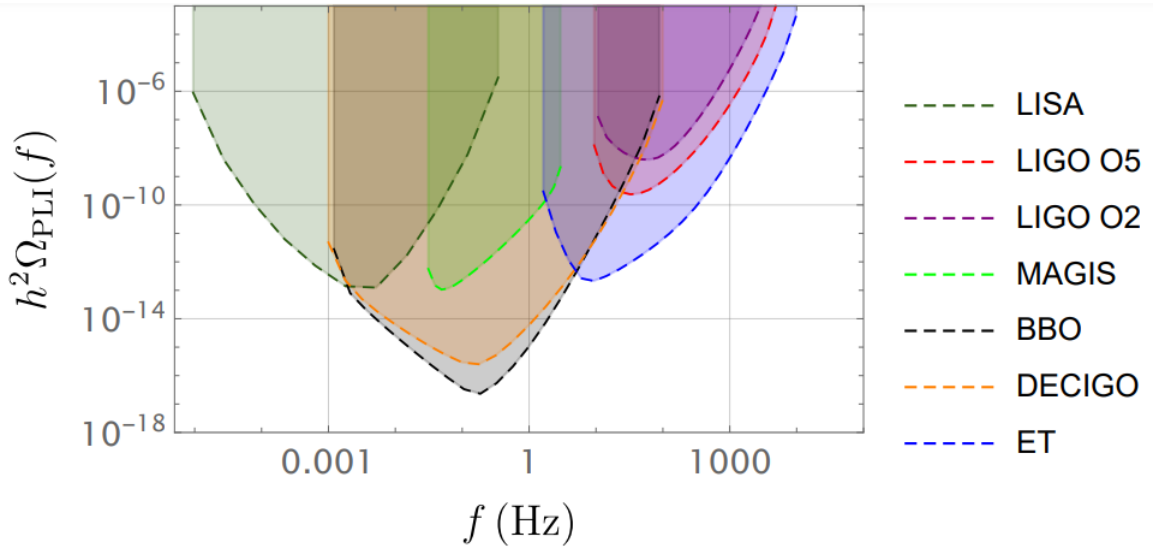

Figure 1.5: Prospect for observers in the near future. The signal-to-noise ratio and the sensitivity curves can be build following the recommendations of [38, 39, 40, 41, 42, 43, 44, 45] for the observe LISA, LIGO, MAGIS, Big Bang Observer, DECIGO, ET.

will focus only on the “sound waves" and “bubble collision" contributions. We already introduced the α parameter giving an estimate of the energy available to the transition and the β parameter providing its duration. Before to enter the physics of the different contributions, let us introduce a last important parameter controlling the signal: *the energy distribution between the motion of the wall and the excitation of the plasma*. As we will see, this quantity is inherently related to the regime of expansion of the bubble, that we introduced above.

From energy conservation consideration and to formalize this separation, we define two parameters

$$\kappa_{\rm wall}, \qquad \kappa_{\rm fluid} = 1 - \kappa_{\rm wall}, \tag{1.144}$$

where $\kappa_{\rm wall}$ is a measure of the ratio of energy going to the wall kinetic energy

$$\kappa_{\rm wall} \equiv \frac{E_{\rm wall}}{E_{\rm total}}. \tag{1.145}$$

Let us notice that even if the wall expands relativistically, $\kappa_{\rm wall}$ becomes vanishingly small as soon as the terminal velocity is reached. This is because the portion of the energy stored in the wall starts to decrease as inverse of the bubble radius. Then in the two regimes of expansion, the energy budget is distributed as a function of the bubble wall expansion regime:

1. **Terminal velocity**
   In this case only the sound waves are important and the energy will be distributed as follows:

$$\kappa_{\rm wall} = 0, \qquad \kappa_{\rm fluid} = 1. \tag{1.146}$$

2. **Runaway Regime**
   The release of energy is large enough to overcome all the source of friction and then the wall keeps accelerating

until the collision. We will formalise more quantitatively this condition in Chapter 2. For the moment, it is enough to say that the condition for runaway is that the release of energy overcome the pressure from the plasma

$$\Delta V > \Delta \mathcal{P}_{\rm LO}. \tag{1.147}$$

As a consequence, a fraction of the release of energy still goes to the plasma, via $\Delta\mathcal{P}_{\rm LO}$ and we quantify this fraction by introducing $\frac{\Delta\mathcal{P}_{\rm LO}}{\rho_{\rm rad}}$. In this case, the parameters introduced above become

$$\kappa_{\rm wall} = 1 - \frac{\alpha_\infty}{\alpha}, \qquad \kappa_{\rm fluid} = 1 - \kappa_{\rm wall} = \frac{\alpha_\infty}{\alpha}, \tag{1.148}$$

where

$$\alpha_\infty \equiv \frac{\mathcal{P}_{\rm LO}}{\rho_{\rm rad}} \tag{1.149}$$

In this situation, one can see that both sound waves as well as the bubble collisions are important for the generation of the gravitational waves.

With all those quantities in hands, we can now go to the computation of GW spectra.

- **Scalar field contribution**: The first contribution is the so-called *scalar field* contribution. During the phase transition, at the junction between the two phases, the VEV of the scalars involved in the transition smoothly interpolates between the two phases. The gradient in those background fields induces shear stresses. It was traditionally computed using the so-called "envelope approximation"[55, 49] in which the shear stresses are assumed to be concentrated in a thin shell at the boundary of the bubble, accumulating energy from the kinetic energy of the wall. This energy is then released when the bubbles collide under the form of gravitational waves and the shear stresses dissipate. For this reason, one also often calls this contribution the "Bubble Collision" contribution. The high frequency tail in the envelope approximation was found to be k^{-1} but in later simulation found a steeper dependence [49, 56].

  The scalar field contribution is expected to give a significant contribution, with respect to the sound waves only for very relativistic bubbles. The most recent numerical computation of the spectrum generated by this process can be approximated by [49]

$$\frac{d\Omega_\phi h^2}{d\ln(f)} = 4.7\times10^{-8}\left(\frac{100}{g_\star}\right)^{1/3}(H_{\rm reh}R_\star)^2\left(\frac{\kappa_{\rm wall}\alpha}{1+\alpha}\right)^2 S_{\rm wall}(f,\tilde{f}_\phi) \tag{1.150}$$

  where $g_\star$ is the number of relativistic degrees of freedom, $\kappa_{\rm wall}$ is the fraction of kinetic energy stored in the motion of the wall, $H_{\rm reh}$ is the Hubble constant evaluated at the reheating temperature and $R_\star$ is the size of the bubble at the collision (which is computed from the β parameter). The numerical fit to the spectral function reads

$$S_{\rm wall}(f,\tilde{f}) = \frac{(a+b)^c \tilde{f}^b f^a}{\left(b\tilde{f}^{\frac{a+b}{c}} + a f^{\frac{a+b}{c}}\right)^c} \qquad a=3, \quad b=1.51, \quad c=2.18, \tag{1.151}$$

  with peak frequency

$$\tilde{f}_\phi = 16.5\times10^{-5}\left(\frac{T_{\rm reh}}{100}\right)\left(\frac{g_\star}{100}\right)^{1/6}\left(\frac{3.2}{2\pi R_\star}\frac{1}{H_{\rm reh}}\right) \text{ Hz}. \tag{1.152}$$

and the typical bubble radius can be estimated to be

$$R_* = \frac{(8\pi)^{1/3} v_w}{\beta}. \tag{1.153}$$

as we already argued.

- **Sound waves contribution**: Another important mechanism of GW production comes from the sound waves in the plasma. In this case the spectrum of the stochastic gravitational wave background can be estimated following the recent recommendations in [48, 54]

$$\frac{d\Omega_{sw,0}h^2}{d\ln(f)} = \begin{cases} 0.678 h^2 F_{sw,0} K^2 (H_{\rm reh} R_\star / c_s) \tilde{\Omega}_{sw,0} C(f/f_{p,0}), & \text{if } \frac{H_{\rm reh} R_\star}{K^{1/2}} > 1 \\ 0.678 h^2 F_{sw,0} K^{3/2} (H_{\rm reh} R_\star / c_s)^2 \tilde{\Omega}_{sw,0} C(f/f_{p,0}), & \text{if } \frac{H_{\rm reh} R_\star}{K^{1/2}} < 1 \end{cases} \tag{1.154}$$

and the two regimes in the equation above correspond to the time scale of the shock formation being larger or smaller than the corresponding Hubble time, $\tau_{sh} >, < \frac{1}{H}$. The sound wave production efficiency is given by [57]

$$K \approx \frac{3}{4} \frac{k_{sw} \alpha}{(1+\alpha)}, \quad \kappa_{sw} = \kappa_{\rm fluid} \times \frac{\alpha}{0.73 + 0.083\sqrt{\alpha} + \alpha} \tag{1.155}$$

where for the case of the runaway bubbles we have to substitute $\alpha \to \alpha_\infty$. The factor $F_{sw,0} = \Omega_{\gamma,0} \left(\frac{g_{s0}}{g_{s\star}}\right)^{4/3} \frac{g_\star}{g_0} = 3.57 \times 10^{-5} \left(\frac{100}{g_\star}\right)^{1/3}$ converts the signal emitted at the percolation temperature to the signal we would observe today. $H_{\rm reh}$ and $R_\star$ are the Hubble constant and the size of the bubble at the collision (with reheating temperature correction for the Hubble constant) and the spectral shape $C(s)$ is a function determined numerically

$$C(s) = s^3 \left(\frac{7}{4 + 3s^2} \right)^{7/2} \tag{1.156}$$

with peak frequency

$$f_{p,0} \approx 26 \times 10^{-6} \left(\frac{1}{H_{\rm reh} R_\star} \right) \left(\frac{z_p}{10} \right) \left(\frac{T_{\rm reh}}{100 \text{ GeV}} \right) \left(\frac{g_\star}{100} \right)^{1/6} \text{Hz}, \tag{1.157}$$

$g_\star$ indicates the number of relativistic degrees of freedom. Numerical simulations give $z_p \approx 10$ and $\tilde{\Omega}_{sw,0} \approx 10^{-2}$.

Before to finish, we need to add a word of caution on the runaway regime: Simulations of sound waves have been only successfully performed for $\alpha \lesssim 1$, though the typical regime of runaway bubbles has $\alpha \gg 1$, as a consequence, we should consider any extrapolation of the previous expressions with great care.

Those are the expressions that we are going to use in the remainder of this thesis. We can also see the difference of behaviour between sound waves fuelled GW, fading as $\Omega_{sw} \sim f^{-4}$, much faster than the scalar field component, fading as $\Omega_\phi \sim f^{-3/2}$, and this raises the hope that the runaway and the terminal velocity regimes can be distinguished from the GW spectra. However, if all this story seemed grandiose and hopeful, a word of caution is in order at this point: *There is still huge uncertainties on the shape of the spectrum extracted from numerical simulations*, as we hope to illustrate in Table 1.5 where we gives the shape of the spectrum obtained by different groups. As a consequence, this is still not certain that we can exactly distinguish between bubble collision and sound waves GW signals. In the remainder of this thesis, though keeping in mind this funest caveat, we will bet that we will be able to do so in the future.

Reference and group	IR tail	UV tail
Envelope simulation[58] Ω_ϕ	3	1
Envelope simulation[59] Ω_ϕ	$2.9^r - 2.95$	$0.9 - 1$
Envelope analytic[60, 61] Ω_ϕ	3	1
Bulk flow[59] Ω_ϕ	$0.95 - 0.9^r$	$2.9 - 2.1^r$
Lattice Simulation[49] Ω_ϕ	3	~ 1.5
Lattice Simulation[62] Ω_ϕ	$0.68 - 1.56$	$1.35 - 2.25$
Sound Shell model[63, 64] Ω_ϕ	9	4
Analytic[61] Ω_{sw}	3	1
Hybrid simulation[65] Ω_{sw}	3	3
Lattice Simulation[48] Ω_{sw}	3	4

Table 1.5: Shape of the GW signals from some of the different groups working on WG from FOPT in the UV and the IR. Results are shown under the form of $(f/f_{p,0})^n$ for the IR and $(f/f_{p,0})^{-n}$ for the UV tail. The suffix r means that the result is specific to relativistic walls. The mismatch betweem numerical simulations and the current models available (Sound shell and Bulk flow) motivates us to investigate further the analytic understanding of GW from bubble collision.

Chapter 2

FOPT and Dynamics of the bubble wall

THE two earliest signals we have been able to thoroughly study today are the *Cosmic Microwave Background* (CMB) fluctuations, whose the precise understanding through early universe evolution models offered an impressive wealth of information, and *Big Bang Nucleosynthesis* (BBO) which provides very strong bounds on the post-1 second evolution and content of the universe.

However, the first second of the universe still did not provide any observable signal and thus remains a fertile playground for the model-builder. One of the few signals that we can expect to have escaped from the early hot plasma and to exist around us today are the *gravitational waves* (GW) (another obvious signal of the dynamics of the early universe, to be discussed in the next Chapters, are the over-abundance of matter over anti-matter and the presence of dark matter). Many events of the early universe have been proposed as copious sources of GW[1], namely the inflation, the preheating, the cosmic strings and domain walls, and the first order phase transitions (FOPT). A very important parameter in the computation of the GW signal emitted is the regime of expansion and the velocity of the bubble wall. In this chapter, we will focus on this last possibility and discuss at length the dynamics of the bubble wall.

As a strongly out-of-equilibrium process, the dynamics of the expansion and the computation of the velocity of the wall are very involved problems and demand a heavy mathematical treatment. After exposing the hydrodynamical description of the wall-plasma system and the different methods developed to deal with the problem of the velocity, we specialize to one specific regime, the ballistic regime of relativistic bubbles, and we go on to compute the different contributions to the pressure in this case. We discuss the numerous uncertainties.

Finally, in a last section, we will illustrate the usefulness of a precise computation of the pressure for the case of the prediction of the spectrum of GW emitted by the transition. This chapter relies strongly on the findings in [1].

Contents

[1] In comparison, second order phase transitions are expected to produce rather weak signals[66, 67, 68]

2.1 Hydrodynamic description of the transition

The first way to classify the types of FOPT is to study the behaviour of the plasma around the bubble wall. Let us clearly set the problem at hand. The bubble wall can be seen as an interface between two phases of the plasma that we describe as a perfect fluid. In turn the perfect fluid is characterized by three quantities 1) a bulk velocity v, 2) a temperature T and 3) pressure p. In principle, the bulk velocity is three-dimensional, but for the case of a large bubble, the only relevant direction is the one along the direction of the wall, that we denote z in the remainder of this thesis. As a consequence, v is to be understood as the velocity along this direction. The interface is a sharp discontinuity between two perfect fluids that, from the point of view of hydrodynamics, we can consider as infinitely thin. As a consequence, the set (T, v, p) does not need (and is not) to be the same on both sides of the interface. The goal of the hydrodynamical description is to relate $(T, v, p)_{\rm h}$ (h for higgsed, inside of the bubble) with $(T, v, p)_{\rm s}$ (s for symmetric, outside of the bubble) and the energy parameters of the transitions, that we have introduced in Chapter 1. The unknowns are 1) the shape of the scalar condensate 2) the temperature inside T_h, and outside T_s 3) the plasma velocity inside v_h and outside v_s, 4) the pressures inside p_h and outside p_s. In this section we will follow[69, 57]. Typically, the hydrodynamical approach leaves the velocity of the wall v_w as a free parameter, which has then to be obtained by other methods and approximations. We will treat the velocity issue in the second part of this chapter.

Thermodynamics quantities We reserve the notation v_w for the velocity of the wall and $\gamma_w \equiv \frac{1}{\sqrt{1-v_w^2}}$ for the boost from the plasma frame to the wall frame (Though we will often call γ_w the velocity of the wall). We define the thermodynamical quantities (w, s, ρ) in the following way

$$w \equiv T\frac{\partial p}{\partial T}, \qquad s \equiv \frac{\partial p}{\partial T} = Tw, \qquad \rho = w - p \qquad \mathcal{F} = -p = V_T(\phi, T) \tag{2.1}$$

respectively for the *enthalpy*, the *entropy density*, the *energy density* and the *Free Energy* or pressure.

Energy-momentum tensor of the bubble-plasma system Another important quantity in the description of the transition is the *energy-momentum* tensor, which permits to enforce the conservation of energy and momentum. The two ingredients of the system are, on the one hand, the **scalar field**, with the energy-momentum tensor taking the form

$$T^{\varphi}_{\mu\nu} \equiv \partial_\mu\varphi\partial_\nu\varphi - g_{\mu\nu}\left[\frac{1}{2}\partial_\mu\varphi\partial^\mu\varphi - V_0\right] \qquad \text{(Energy-momentum tensor of scalar field)} \tag{2.2}$$

where V_0 is the renormalised zero-temperature potential of the scalar field φ and, on the other hand, the **plasma**. A first grasp on the hydrodynamics of the expanding bubbles can be obtained by assuming that the fluid is in *Local Thermal Equilibrium* (LTE) and thus can be described as a perfect fluid:

$$T_{\mu\nu}^{\text{plasma}} = w u_\mu u_\nu - g_{\mu\nu} p, \qquad u_\mu = \frac{(1, \mathbf{v})}{\sqrt{1-\mathbf{v}^2}} = \gamma(1, \mathbf{v}) \tag{2.3}$$

where u_μ, $\mathbf{v}$ being the spatial component of the fluid velocity. In our one-dimensional case, $\mathbf{v}$ becomes only $v \equiv v_z$ along the bubble. $\gamma \equiv \frac{1}{\sqrt{1-v^2}}$ is the boost factor of the fluid motion frame and is not to be confused with the wall boost factor γ_w. In the end the full energy-momentum tensor of the system is given by the sum of contributions from the plasma and from the scalar field:

$$T_{\mu\nu}^{\text{tot}} = T_{\mu\nu}^{\text{plasma}} + T_{\mu\nu}^{\varphi}. \tag{2.4}$$

Imposing the conservation of the total energy-momentum tensor, we obtain

$$\nabla_\mu T_{\text{tot}}^{\mu\nu} \approx \partial_\mu T_{\text{tot}}^{\mu\nu} = 0 \qquad \Rightarrow \qquad \partial_z T_{\text{tot}}^{zz} - \partial_0 T_{\text{tot}}^{0z} = \partial_z T_{\text{tot}}^{z0} - \partial_0 T_{\text{tot}}^{00} = 0, \tag{2.5}$$

where we neglected the universe expansion in the first equality, as the time-scale of the transition is much shorter than the time-scale of the expansion. We can now *go the wall frame* and integrate the equations in (2.5) across the wall (z direction), obtaining the equations $\Delta T_{zz} = \Delta T_{z0} = 0$. Upon injecting the expressions of the energy-impulsion tensor, this gives the two following important relations between the pressures, the fluid velocities and the energy densities:[2]

$$w_s v_s^2 \gamma_s^2 + p_s = w_h v_h^2 \gamma_h^2 + p_h, \qquad w_s v_s \gamma_s^2 = w_h v_h \gamma_h^2. \tag{2.6}$$

We can now eliminate the enthalpy by substitution and factor out the velocities. We obtain

$$v_s v_h = \frac{p_s - p_h}{\rho_s - \rho_h}, \qquad \frac{v_s}{v_h} = \frac{\rho_h + p_s}{\rho_s + p_h}, \tag{2.7}$$

which relates pressure and energy density, with the bulk velocity. To make further progress, we need a relation between the pressure and the energy density, an equation of state. This is provided, in simple settings, by the *bag model*.

Equation of state in the bag model Obtaining a relation between the pressure and the energy density in the context of a PT, in general, is far from a trivial task. However, let us borrow some intuition from the case of the perfect gas, where the pressure and the energy density can be expressed in terms of the temperature via simple relations. Indeed, the free-energy can be expressed

$$\mathcal{F}(\varphi, T) = V_0(\varphi) + \frac{T^4}{2\pi^2} \sum_i g_i J_{B/F}(m_i/T) \tag{2.8}$$

where the second term is the thermal potential and the first is the vacuum energy and the $J_{B/F}$ have been defined in Eq.(1.107):

$$J_B(m_i/T) = \int_0^\infty dy y^2 \log[1 - \exp(-\sqrt{x^2+y^2})] \to \begin{cases} -\frac{\pi^4}{45} \text{ if } \frac{m_i}{T} \ll 1 \\ \exp[-m_i/T] \text{ if } \frac{m_i}{T} \gg 1 \end{cases} \tag{2.9}$$

$$J_F(m_i/T) = \int_0^\infty dy y^2 \log[1 + \exp(-\sqrt{x^2+y^2})] \to \begin{cases} -\frac{\pi^4}{45}\frac{7}{8} \text{ if } \frac{m_i}{T} \ll 1 \\ \exp[-m_i/T] \text{ if } \frac{m_i}{T} \gg 1 \end{cases} \tag{2.10}$$

[2]We also use the fact that the term $(\partial_z \phi)^2$ is zero when integrated across the wall and we hide ΔV inside of the pressure $p = p_{\text{plasma}} - V_0$. We also remind that we are using a mostly minus metric.

where we kept only the leading term, for the purpose of the explanation. Naively, this tells us that a state with low mass will contribute to the energy of the plasma by $\propto T^4$ and that a particle with a large mass will be suppressed from the plasma and would not enter into the description of the transition. This naive picture will have to be refined in the light of the further findings, but we can safely stick to it for the moment. Now recalling the definition of the thermodynamical quantities in Eq.(2.1) and the fact that the pressure is directly related to the free energy, this suggests to connect to the pressure and the energy to the temperature in the following way

$$p_s = \frac{1}{3}a_s T_s^4 - \Delta V, \qquad p_h = \frac{1}{3}a_h T_h^4 \tag{2.11}$$

$$\rho_s = a_s T_s^4 + \Delta V, \qquad \rho_h = a_h T_h^4 \tag{2.12}$$

$$a \equiv \frac{\pi^2}{30}\sum_{\text{light } i}\left[g_i^b + \frac{7}{8}g_i^f\right] \tag{2.13}$$

where ΔV is the difference of potential between the false and the true vacua at zero temperature, defined to zero in the higgsed vacuum, g_i are the number of degrees of freedom. The first two equations define the so-called *bag equations of states* and allow usually for unequal a_h, a_s free parameters. In this scheme, the density of heavy particles is Boltzmann suppressed and the species do not contribute in the potential and the pressure. To go beyond the bag equation of states, see for example the model-independent approach in[70].

It is clear that one of the limitation of the bag equation of states is that it does not allow for the number of degree of freedom to depend on the temperature, which might be the case in the realistic transitions. One of the approximation is that the light and the heavy species are clearly separated at all the temperature characterising the transition. This is typically the case of transition with barrier remaining in the zero temperature potential, leading to strong transition.

There is also another important word of caution at this point: The bag equation will not be able to describe the case of a runaway wall.

Velocity relation The relation between pressure, energy density, expressed in terms of the temperature, allows to eliminate both the pressure and the density in Eq.(2.7). Under the bag equation of states approximation, the relations in Eq.(2.7) become

$$v_s v_h = \frac{1-(1-\alpha)r}{3-3(1+\alpha)r}, \qquad \frac{v_s}{v_h} = \frac{3+(1-3\alpha)r}{1+3(1+\alpha)r}. \tag{2.14}$$

$$\alpha \equiv \frac{\Delta V}{a_s T_s^4}, \qquad r \equiv \frac{a_s T_s^4}{a_h T_h^4} \tag{2.15}$$

The parameters α, which was already defined in Eq.(1.137), and r admits simple interpretations as, the strength of the phase transition and the ratio of the radiative energy before and after the transition. The combination of those two relations gives

$$v_s(v_h,\alpha) = \frac{1}{1+\alpha}\left[\left(\frac{v_h}{2}+\frac{1}{6v_h}\right) \pm \sqrt{\left(\frac{v_h}{2}+\frac{1}{6v_h}\right)^2 + \alpha^2 + \frac{2}{3}\alpha - \frac{1}{3}}\right], \tag{2.16}$$

and reveals a rich phenomenology of the phase transitions, parametrized by the strength parameter α. This relation is very important and basically controls the types of FOPT that will occur. To see how it goes, we need now to study exactly the hydrodynamical equations, as we will do in the next subsection.

2.1.1 Hydrodynamic equations

In general, there is no guarantee that all the solutions that we can obtain from Eq.(2.16) indeed admit a hydrodynamical solution. To check this, we need to go back to the conservation equations and to study the profiles of the different physical quantities. Inserting the perfect fluid Ansatz inside of the conservation equation, and using again the conservation of momentum, we obtain

$$\partial_\mu T^{\mu\nu} = u^\nu \partial_\mu (u^\mu w) + w u^\mu \partial_\mu u^\nu - \partial^\nu p = 0. \tag{2.17}$$

Projecting this equation along the flow u^μ gives the continuity equation

$$\partial_\mu (u^\mu w) - u^\mu \partial_\mu p = 0, \tag{2.18}$$

and projecting perpendicularly to the flow $\bar{u}^\mu$, $\bar{u}^2 = -1$, $\bar{u}^\mu u_\mu = 0$, gives the Euler equation

$$\bar{u}^\nu u^\mu w \partial_\mu u^\nu - \bar{u}^\nu \partial_\nu p = 0. \tag{2.19}$$

As the problem does not contain intrinsic scale, the solution will only depend on the combination $\frac{z}{t}$. It then proves very convenient to introduce $\xi \equiv \frac{z}{t}$, inducing that $u_\mu \partial^\mu = -\frac{\gamma}{t}(\xi - v)\partial_\xi$ and $\bar{u}^\mu \partial_\mu = \frac{\gamma}{t}(1 - v\xi)\partial_\xi$. Introducing this variable, $u^\mu =$ and $\bar{u}^\mu = \gamma(v, \mathbf{v}/v)$ into Eq.(2.18) and (2.19) become

$$(\xi - v)\frac{\partial_\xi \rho}{w} = 2\frac{v}{\xi} + [1 - \gamma^2 v(\xi - v)]\partial_\xi v \tag{2.20}$$

$$(1 - v\xi)\frac{\partial_\xi p}{w} = \gamma^2 (\xi - v)\partial_\xi v \tag{2.21}$$

The speed of sound in a plasma is defined as $c_s^2 \equiv dp/d\rho = \frac{dp}{dT} \Big/ \frac{d\rho}{dT}$, thus $c_s^2 = \frac{\partial_\xi p}{\partial_\xi \rho}$, permits to relate the two equations (2.20) and (2.21) in

$$\frac{v}{\xi} = \frac{\gamma^2}{2}(1 - v\xi)\left[\frac{\mu^2}{c_s^2} - 1\right]\partial_\xi v, \qquad \mu = \frac{\xi - v}{1 - \xi v}. \tag{2.22}$$

To fix the solution of these equations, we need to impose proper boundary conditions, that is to say, i) vanishing of the fluid velocity far inside and far outside of the bubble and ii) recovering the nucleation temperature far away outside of the bubble.

2.1.2 The types of burning

Now we have all the elements needed to treat the problem of the type of burning. The topic of the type of burning of a *cosmological phase transition* is an exciting subject since it has been shown to differ strongly from chemical burning on earth[71] (against the previous suggestion[69]), where it can only be Jouguet type[3].

As we have seen, the conservation equations of the stress-energy tensor permits to relate the velocities $v_{h,s}$ to the pressures and the energy density on each sides of the wall. Then, imposing an equation of state relates the energy densities, the pressures and the temperatures, allowing us to eliminate the pressures and the energy densities. From Eq.(2.16), for some value of the velocity inside of the bubble v_h, we always find two solutions, however, only one of the two is physical (as often, when we solve a second order equation.) This leads to different types of bubble wall expansion, depending on the regime of expansion of the bubble.

[3]A Jouguet burning is characterised by the fact that the plasma *behind the wall moves at the speed of sound with respect to the wall.*

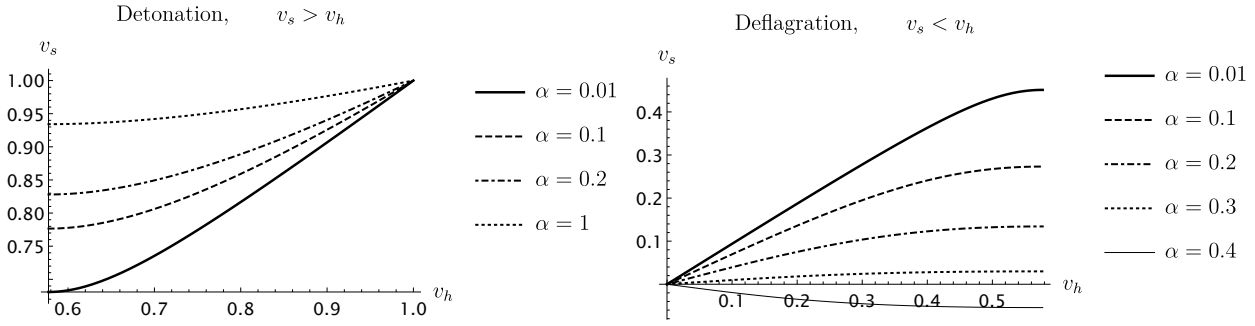

Figure 2.1: Example of detonation (Left Plot) and deflagration (Right Plot) from Eq.(2.16). We also observe on the deflagration plot that the value $\alpha = 0.4$ bring unphysical values. On general grounds, deflagration are only allowed if $\alpha < 1/3$.

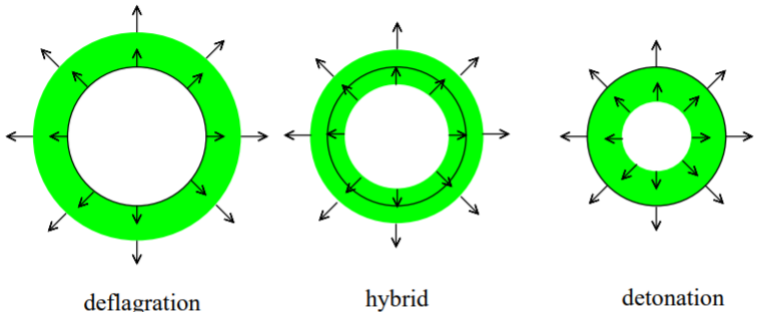

Figure 2.2: Cartoon of the plasma departure from equilibrium in the case of the deflagrations, hybrid and the detonations type of transition. Figure borrowed from [72].

Detonations: $v_w = v_s > v_h$**,** $v_w > c_s$ When the velocity of the plasma (*in the wall frame*) outside of the bubble is larger than the velocity inside, $v_s > v_h$, and the plasma hits the bubble wall at the wall velocity $v_s = v_w$, the expansion is of detonation type. We have also $r < \frac{1}{1+3\alpha}$ and the velocity relations are given on the Left of Fig.(2.1). Since the plasma "does not see the wall coming", the temperature on front of the bubble wall is the *nucleation temperature*.

In principle, there are three types of detonations parametrized by the velocity inside of the bubble: i) the weak detonations $v_h > c_s$, ii) the strong detonations $v_h < c_s$ and finally iii) the Jouguet detonations $v_h = c_s$. We observe that the transition has a limit of Jouguet detonation for all values of α. The limit $v_s = v_h \to 1$ also exists if $r = \frac{1}{1+3\alpha}$ for all the values of α. As already shown by [71], strong detonations are not possible for cosmological transitions. A pictorial representation of a detonation is provided on the right plot of Fig.2.2, borrowed from [72]. Solving the hydrodynamics equations for $v(\xi)$ shows that *inside* of the bubble a rarefaction front with bulk velocity forms.

An interesting question is: is it possible to have $v_h > v_s$ in the context of a detonation ? For example if the wall is runaway?

Deflagration: $v_s < v_h = v_w$ In the opposite case, when the wall expands slower than the speed of sound in the plasma $v_w < c_s$, then the velocity behind the wall will be equal to the wall speed $v_h = v_w$ and the velocity in the front of the wall will be slower. This signals the formation of a shockwave in front of the wall. This type of expansion is only allowed if $\alpha < 1/3$, as we can observe on the left of Fig.(2.1). A pictorial representation of a detonation is provided on the left plot of Fig.2.2, borrowed from [72]. Solving the hydrodynamics equations for $v(\xi)$ shows that *outside* of the bubble a shock front with bulk velocity forms. This shock is terminated in front of the bubble by a discontinuity.

In the context of a deflagration, it is also well known that the phase front may have an instability if the propagation is too slow[73, 74, 75, 76, 77].

Hybrid: $v_w > c_s$ In the hybrid type, the expansion is faster than the speed of sound, but the wall still present a shock front outside of the bubble. In this case, neither v_s or v_h can be identified with the wall velocity v_w and we have the coexistence of shock and a rarefaction wave behind the wall. This is illustrated on the middle panel of Fig 2.2.

Runaway So far, all what we discussed was valid for the steady state walls, where the release of energy due to the scalar field is compensated with the pressure coming from the plasma. Now we would like to treat the case where such a balance from the plasma does not occur and the wall accelerates until collision, we will come back to such situations in the next section. At this step we would like to mention that the thermodynamics of runaway wall has been studied in [78] and was found to be stable under very weak conditions.

In the case of runaway wall, the energy conservation takes a different form and going through the computation is instructive. We go to the frame of the plasma *in front of the wall*. The main difference now is that the gradients will not cancel as they did before.

We have to remind the definition of the surface tension $\sigma(t) \equiv \int d\varphi \partial_\perp \varphi(t)$. Now starting from the conservation of the energy-momentum tensor and integrating along the wall, we obtain

$$\Delta T^{00} - \Delta T^{z0} - \frac{d\sigma}{dt} = 0, \qquad \Delta T^{0z} - \Delta T^{zz} - \frac{d\sigma}{dt} = 0, \tag{2.23}$$

where as before we put the vacuum energy of the scalar field into the pressure and the energy density of the symmetric side, $p_s = p_{\rm plasma,s} - \Delta V, \rho_s = \rho_{\rm plasma,s} + \Delta V$, with ΔV positive. We can add the two equations in Eq.(2.23) to obtain

$$2\frac{d\sigma}{dt} = \Delta T^{00} - \Delta T^{zz} \tag{2.24}$$

We can observe that when the plasma is negligible $\Delta T^{00} - \Delta T^{zz} \to 2\Delta V$, all the release of energy goes into increasing the tension. Thus, we learn the following important statement: *when the release of energy is not balanced by the plasma friction, the release of energy goes into increasing the surface tension σ.*

2.2 Velocity: Friction on the wall

A crucial quantity necessary for the computation of the emission of GW and electroweak baryogenesis production is the velocity of the wall itself v_w. However, in full generality, determining the dynamics of the wall is a very involved problem, as we will see soon. This section deals with this important issue and draws a general picture of different methods and regimes that have been considered in the literature. After a quick explanation of the problem of the bubble velocity in Section 2.2.1 and the exposition of the methods assuming small perturbations of the plasma in Section 2.2.2, in Section 2.3 will give a thorough presentation on the case of the ballistic regime, which is the our main purpose.

2.2.1 The problem of the bubble wall velocity

As we have mentioned above velocity is the most difficult parameter to estimate. Initially thought to be fixed by [69] Chapman-Jouguet condition. This condition leads most of the time to very supersonic walls. The use of Chapman-Jouguet condition, in the case of cosmological phase transitions, was put in question in [71] where it was shown that a large class of cosmological phase transition do not satisfy the Jouguet condition. Later analysis[79, 80] proposed to apply the fluctuation-dissipation theorem to solve the problem. It was namely shown in [80] that the use of the fluctuation-dissipation theorem (where the equilibrium computation of a retarded correlator is related to the non-equilibrium response of a system to a perturbation) reduces to the simple picture of particles colliding on the wall, as presented in Appendix A.2 and [78]. As a consequence, we shall not present nor discuss the computation using the fluctuation-dissipation theorem in this thesis.

The system of equation Higgs-plasma The basic physics behind the friction of the plasma on the wall goes as follows: A plasma at equilibrium can be described by the distribution function $f_{\rm eq,i}$ of each component. However, the action of the scalar condensate hitting the plasma brings the system out-of-equilibrium and $f_i \neq f_{\rm eq,i}$. At the same time, the dynamics of the scalar condensate is itself coupled to the distribution function and is perturbed by it. This is this loop-reaction which makes the solution of the entire system very challenging. Let us start by laying down the equations in their most general form. The equation of motion respected by the Higgs VEV ϕ, computed in [81], at leading order, reads

$$\nabla^\mu\nabla_\mu\varphi + \frac{\partial V_0}{\partial\varphi} + \sum_i \frac{dm_i^2}{d\varphi}\int \frac{d^3p}{(2\pi)^3 2E_i} f_i(p,z) = 0 \qquad \text{(EoM scalar condensate)} \tag{2.25}$$

where the sum runs over all the *light* particles that couple to the wall and f_i are the *distribution function* of the species i. The last term on the LHS is actually the coupling between the condensate and the plasma particles. On the other hand, the Boltzmann equations controlling the plasma distributions reads

$$\partial_t f + \dot{z}\partial_z f + \underbrace{\dot{p}_z \partial_{p_z} f_i(p_z, z)}_{\text{forces}} = -\underbrace{\mathcal{C}[f, \varphi]}_{\text{collision}} \qquad \text{(Boltzmann equation)} \tag{2.26}$$

where the RHS term $\mathcal{C}[f, \varphi]$ designates the collision term, which describes the different interactions a particle can undergo inside the wall. The dot designates a derivative with respect to time and z is the direction of the wall, that we assume to be planar. It is common to rewrite the EoM of the condensate by separating the distribution function in an equilibrium part $f_{\rm eq}$ and a departure from equilibrium part δf:

$$\nabla^\mu \nabla_\mu \varphi + \frac{\partial V_0}{\partial \varphi} + \sum_i \frac{dm_i^2}{d\varphi} \int \frac{d^3p}{(2\pi)^3 2E_i} f_i^{\rm eq} = -\sum_i \frac{dm_i^2}{d\varphi} \int \frac{d^3p}{(2\pi)^3 2E_i} \delta f_i, \tag{2.27}$$

which can also be rewritten

$$\nabla^\mu \nabla_\mu \varphi + \underbrace{\frac{\partial V_{\rm eff}}{\partial \varphi}}_{\text{release of energy}} = \underbrace{-\sum_i \frac{dm_i^2}{d\varphi} \int \frac{d^3p}{(2\pi)^3 2E_i} \delta f_i}_{\text{friction}} \tag{2.28}$$

The combination of the zero temperature and the second term into the thermal potential is proven in [82, 6].[4]

The physics of the interaction between the wall and the plasma is contained in the system (2.26) and (2.28). The Boltzmann equations in Eq.(2.26) contains one force term (last term on the LHS) which is proportional to the change of momentum of the particle entering into the wall $\dot{p}_z$, which is controlled by the interaction with the wall. This term will feed departure from equilibrium in the distribution function. On the other hand, the collision term on the RHS contains the interactions of the plasma particles *within the wall*. Those interactions are a force pushing to restore the equilibrium. Those distribution functions have then to be fed into the scalar field equation (2.28).

The physics of the scalar equation of motion is also quite transparent in Eq. (2.28). The first term on the LHS contains the acceleration of the wall, the second term is the release of energy from the transition, which pushes the acceleration, and the term on the RHS contains the departure from equilibrium, which constitutes a friction on the wall. Thus naively, taking $\delta f_i \to 0$ should erase all the friction.

The coupled system of Eq.(2.26) and Eq.(2.28) is dauntingly difficult to solve in full generality. From this point of view, it is clear that the difficulty of the problem mostly lies in the collision term, because it requires to track a

[4] A nice and simple explanation is also provided in [83]: We start from the relation between the free-energy and the pressure of a plasma

$$\mathcal{F} = -\frac{1}{3} \int \frac{d^3p}{(2\pi)^3} \frac{p^2}{E} f^{\rm eq}(E) \tag{2.29}$$

Now simple derivative of this expression provides

$$\begin{aligned} \frac{dm^2}{d\varphi} \frac{d\mathcal{F}}{dm^2} &= -\frac{1}{3} \frac{dm^2}{d\varphi} \int \frac{d^3p}{(2\pi)^3} \frac{p^2}{E} \frac{d}{dE} \frac{f^{\rm eq}(E)}{2E} \\ &= -\frac{1}{3} \frac{dm^2}{d\varphi} \int \frac{d^3p}{(2\pi)^3} p \frac{d}{dp} \frac{f^{\rm eq}(E)}{2E} \\ &= \frac{dm^2}{d\varphi} \int \frac{d^3p}{(2\pi)^3} \frac{f^{\rm eq}(E)}{2E} \end{aligned} \tag{2.30}$$

where we used that $\frac{d}{dm^2} = \frac{1}{2E} \frac{d}{dE}$ and integrated by part in the last equality.

large number of interactions within the wall itself. At this point, two scales can be considered: 1) the length of the wall L_w and 2) the mean free path of a plasma particle entering the wall $\lambda_{\rm mfp}$. This suggests two limits in which our problem could largely simplify. If the wall is much longer than the mean free path of the particles, interactions inside the wall could tend to thermalise the particles entering, and their distribution function should remain close to equilibrium all along their way $f_i = f_{i,\rm eq} + \delta f_i$ with $\delta f_i \ll f_{i,\rm eq}$, and the plasma is never far from *Local Thermal Equilibrium*. In the opposite limit, when the mean free path is much longer than the wall, we can approximate the collision term to be zero $\mathcal{C}[f,\varphi] \to 0$, largely simplifying our problem. This is the so-called *semi-classical* approximation. Another attitude would be to give up on giving a microscopic description of the interactions and to forget about the Boltzmann equations Eq.(2.26). We thus only restart from EoM of the condensate in Eq.(2.38) and substitute $f = f_{\rm eq} + \delta f$,

$$\underbrace{-\sum_i \frac{dm_i^2}{d\phi}\int \frac{d^3p}{(2\pi)^3 2E_i}\delta f_i}_{\text{friction}} \equiv \mathcal{K}(\phi) \qquad \nabla^\mu\nabla_\mu\varphi + \underbrace{\frac{\partial V_{\rm eff}}{\partial\varphi}}_{\text{release of energy}} = \mathcal{K}(\phi) \quad \text{(Pheno parametrization)} \tag{2.31}$$

Then we need to provide a phenomenological way to parametrize the κ. We will not take this direction and will instead dig into the microscopic theory and extract some intuition for the velocity of the wall and the scaling of the friction.

2.2.2 In the limit of small departure from equilibrium

The first approach to solve the problem of the velocity of the wall is to assume small departure from equilibrium, which allows to expand into an *equilibrium* and a smaller perturbation part. In this context, we can approximation the plasma as a fluid (fluid approximation: each part of the fluid is in thermal equilibrium, and thus we can define a notion of temperature, entropy and chemical potential) We thus expect this description to hold for rather i) strong couplings, as strong interactions will manage to efficiently bring the components of the plasma to equilibrium, and ii) thick walls L_w, since we need the wall to be much longer than the mean free path and iii) slow walls, since fast walls would be Lorentz contracted from the point of view of the plasma and become thin. Formally, the condition writes:

$$\Gamma_{2\to2} \gg \frac{L_w}{\gamma_w v_w} \tag{2.32}$$

where $\Gamma_{2\to2}$ is the typical rate of $2 \to 2$ interactions of the particles inside the wall. That the wall is indeed slow will be an *a posteriori* check of the method. Those types of approaches can be separated in two families: 1) the *kinetic approach* and 2) the *exact LTE* approach.

- The kinetic approach has been widely applied in the 90‘ to compute the expected velocity of the wall of the EW transition (assuming some UV completion makes it FOPT). It was shown that solving Boltzmann equations in front of the wall[84, 81, 85, 71] leads to subsonic velocities for the wall in the case of the SM and MSSM, typically of order $v_{SM,w} \sim 0.4$ and $v_{MSSM,w} \sim 0.01$. This confirms a posteriori the assumption of slow walls necessary to the applicability of the method. However, the approach in [84, 81] relies strongly on the WKB approximation, which is valid if $p_z^2 \gg \frac{dp_z}{dz}$ and badly breaks for infrared gauge bosons. Taking analytically the infrared bosons into account provided the dominant contribution to the wall pressure [86] and reduced strongly the velocity to $v_w \lesssim 0.1$. The regime of subsonic walls allows for a microscopic approach in terms of particles diffusion. Despite being a rather hold topic, the kinetic approach remains a fertile ground of investigation and debates, see [87, 88, 89] and [90, 91].

- Another way is to assume exact *local thermal equilibrium* (LTE) all along the way. In this context, thermodynamical reasonings and conservation of entropy should be applicable. This permits to ignore the equation for the Higgs and to rely only on the conservations equations Eq.(2.5) for the fluid[92, 93, 94] and this will fix the velocity of the wall in the limit of very strong interactions. Let us give a taste on how it works. Taking the expectation value of the conservation equations, we obtain

$$-\partial_0\langle T^p_{00}\rangle + \partial_z\langle T^p_{z0}\rangle - \partial_0\langle T^\phi_{00}\rangle + \partial_z\langle T^\phi_{z0}\rangle = 0, \tag{2.33}$$

$$-\partial_0\langle T^p_{0z}\rangle + \partial_z\langle T^p_{zz}\rangle - \partial_0\langle T^\phi_{0z}\rangle + \partial_z\langle T^\phi_{zz}\rangle = 0. \tag{2.34}$$

  Recalling that in the wall frame the time derivative vanishes, this becomes

$$\partial_z\langle T^p_{z0}\rangle + \partial_z\langle T^\phi_{z0}\rangle = 0, \tag{2.35}$$

$$\partial_z\langle T^p_{zz}\rangle + \partial_z\langle T^\phi_{zz}\rangle = 0. \tag{2.36}$$

  Upon integration across the wall, the derivatives becomes the difference of the value on the symmetric and higgsed sides. Moreover, we have to note that in the *plasma frame* $\langle T^p_{zz}\rangle_p = p$ and $\langle T^p_{00}\rangle_p = \rho$, which, upon going to the wall frame, give $\langle T^p_{zz}\rangle_w = (1-\gamma_w^2)(p+\rho)+p = (1-\gamma_w^2)sT + p$ and $\langle T^\varphi_{zz}\rangle_w = V_{\min}$. Subtracting on each side of the wall tells us that the change in the pressure is compensated by a change in the quantity Ts,

$$\Delta\mathcal{P}_{\rm LTE} = -(\gamma_w^2 - 1)\Delta(Ts). \tag{2.37}$$

  This result is satisfactory in the sense that it contains a sensible limit in the case of low velocity, as $v_w \to 0, \Delta\mathcal{P}_{\rm LTE} \to 0$. However, in the literature, there is currently a debate about how to exactly compute the change in Ts across the wall, see [94, 30].

2.3 Semi-classical approximation

We have exposed the studies relying on LTE and explained that the applicability of such methods necessitates strong couplings and rather slow walls. Let us go now deeply in the opposite regime. In the case where the wall already accelerated, the thickness of the wall, in the plasma frame, becomes $\frac{L_w}{\gamma}$, and thus large enough velocities ensure that $\frac{L_w}{\gamma} < \lambda_{\rm mfp}$, allowing us to neglect the collision term in the Boltzmann equations. This regime is often dubbed the semi-classical approximation or "free-particle approximation" [81, 95], or again the "ballistic"[92] approximation. We will by using those terminologies interchangeably.

To see how this limit simplifies greatly the problem at hand, let us restart from the full equation of motion for the Higgs condensate

$$\nabla^\mu\nabla_\mu\varphi + \frac{\partial V_0}{\partial\varphi} + \sum_i \frac{dm_i^2}{d\varphi}\int\frac{d^3p}{(2\pi)^3 2E_i} f_i(p,z) = 0 \tag{2.38}$$

coupled with the collision free-Boltzmann equations

$$\partial_t f_i + \dot{\mathbf{x}}\partial_x f_i + \dot{\mathbf{p}}\partial_{\mathbf{p}} f_i = -\mathcal{C}[f_i] \to 0. \tag{2.39}$$

We can decide to work in the wall or in the plasma frame, but we pick the first possibility, inducing $\partial_t f \to 0$, $\dot{\mathbf{x}} = \frac{p_z}{E}$ and $\dot{\mathbf{p}} = -\frac{\partial_z m^2}{2E}$. With a planar wall along the z direction, the equation in (2.39) reduces to

$$\left(\frac{p_z}{E}\partial_z - \frac{1}{2E_i}\frac{dm_i^2}{dz}\partial_{p_z}\right) f_i(p,z) = 0 \tag{2.40}$$

which can be solved by knowing only the shape of the wall controlling $m_i^2(z)$. The term containing this mass acts as a classical force pushing the distribution functions far away from equilibrium. Upon inspection, it appears that the solution of this equation should depend on $\mathbf{p}_\perp$ and $\sqrt{p_z^2 + m^2(z)}$,

$$f_i(\mathbf{p}_\perp, \sqrt{p_z^2 + m^2(z)}). \tag{2.41}$$

The expression in Eq.(2.38) hides a very intuitive way to solve for the terminal velocity, that we will illustrate now and that will become our standard method for the rest of this section on semi-classical approximation. In section 1.5.3, we computed the evolution equation for the velocity γ_w but we neglected the plasma pressure. We can now follow the same steps but correct this approximation. If we integrate (2.38) over $d\varphi$, from the false to the true vacuum the first term on the LHS becomes, following a second time the steps of Appendix A.1, $-4\pi\sigma R^2\sqrt{1-\dot{R}^2}$ while the second and third terms combine to give

$$(\Delta V_0 - \Delta\mathcal{P}(R))\frac{4\pi R^3(t)}{3}. \tag{2.42}$$

Then going through the Legendre transform like in section 1.5.3, the energy is given by

$$\mathcal{E} = 4\pi\sigma R^2\gamma_w - (\Delta V_0 - \Delta\mathcal{P}(\gamma_w))\frac{4\pi R^3(t)}{3}, \tag{2.43}$$

which is turn permits to recover the equation for the velocity

$$\frac{d\gamma_w}{dR} + \frac{2\gamma_w}{R} = \frac{(\Delta V_0 - \Delta\mathcal{P}(\gamma_w))}{\sigma}. \tag{2.44}$$

We can see that when the plasma pressure is very subdominant, the expansion is mostly controlled by the release of energy, and the velocity γ_w basically scales like $\gamma_w \propto R$, as was explained in 1.5.3, however, a *terminal velocity* regime $\gamma_w^{\rm terminal}$ is reached when $(\Delta V_0 - \Delta\mathcal{P}(\gamma_w^{\rm terminal})) \to 0$ and the velocity saturates. In this context of the ballistic approximation, this provides us with a very simple criterion for finding the terminal velocity:

$$\Delta V_0 - \Delta\mathcal{P}(\gamma_w = \gamma_w^{\rm terminal}) = 0. \tag{2.45}$$

This leaves us with the task of searching for $\Delta\mathcal{P}(\gamma_w = \gamma_w^{\rm terminal})$ in a systematic way. In the following subsection, we will engage in the systematic study of the contributions to the pressure on the wall.

2.3.1 From particles involved in the transition

In this section, we sketch the computation of the pressure induced by particles involved in the transition, that is to say for particles with phase-dependent masses

$$m_s \to m_h > m_s \tag{2.46}$$

At this point, two limits would offer a simple solution: 1) the limit in which particles cannot enter the wall because the mass gain is too large. This is typically the case of particles with momentum $p_z \sim \gamma_w T_{\rm nuc}$ much smaller than the final mass m_s. In such context, all the particles are reflected and give a kick on the wall of order $\Delta p_z \sim 2\gamma_w T_{\rm nuc}$, inducing a final pressure scaling like $\mathcal{P} \sim \gamma_w^2 T_{\rm nuc}^4$. Though such situation can have very interesting phenomenological implications, we will focus on the 2) opposite regime, where $p_z \sim \gamma_w T_{\rm nuc}$ is much bigger than m_h and we can argue that all the incoming particles enter the wall. This is the limit of large γ_w and the transition regime between the two limits mentioned above is studied with more details in Appendix A.2.

A first, and likely the most satisfactory, way to solve for the friction on the wall is to go back to the Boltzmann and condensate equations and to solve them. The distribution function, in the wall frame will take the form

$$f(E,p,T) = f\left(\frac{p_\mu u^\mu}{T}\right) = f\left(\frac{\gamma_w(E+v_w p_z)}{T}\right), \tag{2.47}$$

where we have assumed like in Fig.2.3 that the wall moves along the positive z direction with velocity v_w and $u_\mu = \gamma_w(1,0,0,-v_w)$. We impose to recover the *equilibrium distribution function* deep inside and deep outside the bubble. The solution has to be of the type in Eq.(2.41). Shifting the integral $p_z^2 \to p_z^2 - m^2(z)$ in such a way that the z dependence disappears from the distribution function, the third term on the LHS of Eq.(2.38) becomes (for each species with phase-dependent mass and assuming $p_z \gg |p_\perp|$)

$$\begin{aligned}
\text{(Third term on LHS)} &\approx \frac{dm_i^2}{d\varphi}\int \frac{d^3p}{(2\pi)^3 2\sqrt{p_z^2+m^2(z)}} f_i^{F/B}(\mathbf{p}_\perp, \sqrt{p_z^2+m^2(z)}) \\
&= \frac{dm_i^2}{d\varphi}\int \frac{d^3p}{(2\pi)^3 2\sqrt{p_z^2}} f_i^{F/B}(\mathbf{p}_\perp, \sqrt{p_z^2}) \\
&= c_i \frac{dm_i^2}{d\varphi}\frac{T^2}{24}
\end{aligned} \tag{2.48}$$

where $c_i = 1(1/2)$ for bosons (fermions) and we used that $\frac{dp_z}{p_z}$ is invariant under the shift. In the second line, we have made the shift $p_z^2 \to p_z^2 - m^2$ and in the third we have performed the integral. After integration along the wall, the leading-order pressure (LO) on the wall is given by the simple velocity-independent expression

$$\boxed{\Delta\mathcal{P}_{\mathrm{LO},\gamma\to\infty}(T) = \sum_i c_i \frac{T^2 \Delta m_i^2}{24}} \tag{2.49}$$

where $\Delta m_i^2 \equiv m_{h,i}^2 - m_{s,i}^2$ denotes the difference of squared mass across the wall and we added the subscript $\mathcal{P}_{\gamma\to\infty}$ to emphasize that this result is strictly valid in the large γ_w regime, where all the particles enter the wall. This derivation was illuminating in the sense that it was directly solving the problem via the Boltzmann equations and the equation of motion. The index LO is here to indicate that this contribution to the pressure occurs at *leading order* in the couplings (hidden in the mass term).

Of course, the expression in Eq.(2.49) is only valid in the regime of very fast walls where all the particles enter into the bubble and becomes less precise for lower velocities. For lower velocities, we have the three following possibilities: a particle from outside can enter t_+, a particle from inside can escape the bubble t_- and a particle can be reflected t_r. Those three cases each bring a contribution to the pressure $\mathcal{P}_z^{t-}, \mathcal{P}_z^{tr}, \mathcal{P}_z^{t+}$. The transition regime in which a sizable amount of particles are reflected is exposed in A.2 and it is shown that

$$\mathcal{P}_z^{t-} \approx \mathcal{P}_z^{tr} \approx 0, \quad \mathcal{P}_z^{t+} \approx \frac{1}{2}\mathcal{P}_{\gamma_w\to\infty} \text{ for } \gamma_w T = m_h \tag{2.50}$$

$$\mathcal{P}_z^{t-} \approx \mathcal{P}_z^{tr} \approx 0, \quad \mathcal{P}_z^{t+} \approx 0.9 \times \mathcal{P}_{\gamma_w\to\infty} \text{ for } \gamma_w T = 10 m_h \tag{2.51}$$

Let us make a few comments about this result. For simplicity, let us first assume that $m_s = 0$ then it is obvious that the value in Eq. 2.49 will be reached only for the γ_w factors satisfying

$$\gamma_w \gtrsim \frac{m_h}{T}, \tag{2.52}$$

otherwise initial particles simply will not have enough momentum to pass through the wall (see more details in the Appendix A.2 as well as [92] for analytical results). Now let us look at the scenario when the initial mass as well is non-zero, $m_s \neq 0$. In this case the particle will contribute only if its mass is smaller than the temperature

$$m_s \lesssim T \tag{2.53}$$

otherwise the contribution of this particle to the pressure will be exponentially suppressed by a Boltzmann factor (see Appendix A.2).

Those consideration hints toward a nice interpretation for the pressure in Eq.(2.49): *at leading order in the couplings*, the simple expression in Eq.(2.49) is an upper bound on the friction (even if we will see that other contributions to the pressure can switch on for even larger values of γ_w). However, we can state the following statement, that will be crucial for the rest of this thesis: *if the release of energy is larger than the pressure in Eq.*(2.49)*, the wall will become eventually ultra-relativistic*

$$\boxed{\Delta V > \Delta\mathcal{P}_{\mathrm{LO},\gamma\to\infty} \qquad \text{relativistic wall condition)}}. \tag{2.54}$$

Though, the previous computation of the LO pressure for large velocities is probably the most satisfactory one, it remains intuitively obscure. We would like to provide a more intuitive picture, following the lines of [78]. The energy being conserved along the wall, we have

$$E = \sqrt{p_z^2 + p_\perp^2 + m^2(z)}, \qquad \frac{dE}{dz} = 0 \tag{2.55}$$

Thus to compensate for the change in the mass, the momentum p_z must be modified along the wall. Expanding for large p_z, the change of momentum of an incoming particle is given by

$$\Delta p_z \approx -\frac{\Delta m^2}{2E}, \tag{2.56}$$

for each of the incoming particles. We can interpret this change of momentum in the particle as a kick that is given to the wall: for each particle entering, the wall receive a momentum $-\Delta p_z$. Now, we have to sum over all the incoming particles to obtain the full pressure from the plasma:

$$\Delta\mathcal{P} \approx \int \frac{d^3p}{(2\pi)^3 2E} f_{\mathrm{incoming}}(E) \times (-\Delta p_z) \tag{2.57}$$

and upon performing the integral, we recover Eq.(2.49). Notice that this observation was already apparent when we emphasized that the solution of the Boltzmann equation should be of the form Eq.(2.41). This picture in terms of incoming particles imposing a kick on the wall is particularly interesting and we would like to generalize it. This is the task of the next subsection.

2.3.2 Master equation for friction

Suppose that we are looking at the effects coming from a particle A hitting the wall and producing a X final state (which can perfectly be a multiparticle state) (see Fig .2.3), then the pressure will be given by

$$\mathcal{P}_{A\to X} = \int \frac{p_z d^3p}{p_0(2\pi)^3} f_A(p) \times \sum_X \int dP_{A\to X}(p_A^z - \sum_X p_X^z), \tag{2.58}$$

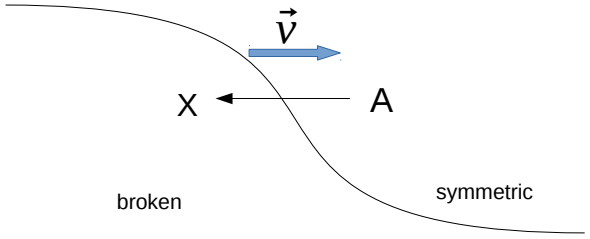

Figure 2.3: Cartoon of a bubble wall interpolating between the values of the VEV of the scalar field in the symmetric and in the broken phase. The domain wall hitting the plasma in the symmetric phase induces a $A \to X$ transition.

where the first factor is just a flux of incoming particles and the second includes the differential probability of the transition from A to X, $dP_{A\to X}$, as well as momentum transfer to the wall $(p_A^z - \sum_X p_X^z)$. The expression in Eq.(2.58) is the generalisation of the simple picture is terms of "kicks on the wall" from the previous section. The probability of transition can be calculated as follows

$$dP_{A\to X} = \prod_{i\in X} \frac{d^3k_i}{(2\pi)^3 2k_i^0} \langle\varphi|T|X\rangle\langle X|T|\varphi\rangle, \tag{2.59}$$

where φ is the wave-packet building the one-particle normalized state

$$\begin{aligned} |\varphi\rangle = \textstyle\int \frac{d^3k}{(2\pi)^3 2k_0}\varphi(k)|k\rangle, \;\; \langle p|k\rangle = 2p_0(2\pi)^3\delta^3(p-k) \\ \textstyle\int \frac{d^3p}{(2\pi)^3 2p_0}|\varphi(p)|^2 = 1. \end{aligned} \tag{2.60}$$

Combining all of this and using the energy and transverse momentum conservation we arrive at the following expression for the pressure from transition [96]

$$\mathcal{P}_{A\to X} = \int \frac{d^3p}{(2\pi)^3 2p_0} f_A(p) \prod_{i\in X} \int \frac{d^3k_i}{(2\pi)^3 2k_0^i} (2\pi)^3\delta^2(p_\perp - \sum_{i\in X} k_{i,\perp})\delta(p_0 - \sum_{i\in X} k_i^0)|\mathcal{M}|^2(p_A^z - \sum_{i\in X} k_i^z) \tag{2.61}$$

where we have ignored the high density effects for the final particles, $1 \pm f_X \to 1$ and $\mathcal{M}$ is defined as follows

$$\begin{aligned} \langle p|H_{\rm int}|k_1 ...\rangle &= (2\pi)^3\delta^2(p_\perp - \sum_{i\in X} k_{i,\perp})\delta(p_0 - \sum_{i\in X} k_i^0)\mathcal{M}, \\ \mathcal{M} &= \int dz \chi_p(z) \prod_{i\in X} \chi_i(z) V, \end{aligned} \tag{2.62}$$

where the χ's are the wave functions of (incoming and outgoing) particles. Armed with this expression we can proceed to the calculation of the friction effects.

Let us first review the Leading-Order (LO) effects i.e. when the initial and the final state contain one particle ($1 \to 1$ transition), that we already computed in the previous section. We will again be focusing on the very relativistic bubble expansions and, in particular, on regimes where the *WKB approximation* is valid, which is when

$$p_z L_w \gg 1, \tag{2.63}$$

where p_z is the momentum of the incident particle. The WKB approximation is explained in Appendix A.5. Let us suppose that the mass m_s, in the symmetric phase, changes when passing through the wall to m_h in the broken phase, $m_s \to m_h$. According to Eq.(2.60), the matrix element for this transition is equal to

$$\langle p|k\rangle = 2p_0(2\pi)^3\delta^3(p-k) \Rightarrow \mathcal{M}_{1\to 1} = 2p_0. \tag{2.64}$$

Then the pressure for the relativistic particles is equal to:

$$\mathcal{P}_{1\to 1} = \int \frac{d^3p}{(2\pi)^3} f(p)(p_s^z - p_h^z) \simeq \int \frac{d^3p}{(2\pi)^3} f(p) \times \frac{m_2^2 - m_1^2}{2p_0} = \int \frac{d^3p}{(2\pi)^3} f \times \frac{\Delta m^2}{2p_0} \tag{2.65}$$

where we have expanded the momenta in $m_{s,h}^2/p_0^2$ and defined $\Delta m^2 \equiv m_h^2 - m_s^2$ and where $p_s(p_h)$ denotes the momentum of the quasi-particle on the symmetric (broken) side of the bubble wall. Using that the quantity $\frac{d^3p}{p_0}$ is invariant under boost, this allows us to recover again Eq.(2.49). This is a confirmation that our expression in Eq.(2.58) is indeed a correct generalisation (at least within our approximations).

2.3.3 Friction from heavy particles

The usual lore for the computation of the velocity wall is that, concerning the EWPT and the extension of the Higgs sector, a strong friction can only occur from a rather light particle coupling strongly to the Higgs, which would be seen in the Higgs decay rates in the colliders[90] and not from a heavy physics sector. Here we would like to show that heavy d.o.f. that are normally decoupled from the Higgs at colliders energies can nonetheless contribute largely to the friction on the wall, if the wall is relativistic.

In the context of very relativistic bubble, in the rest frame of the wall, the particles colliding it can reach very high energies $\sim \gamma_w T_{\text{nuc}}$, much larger than the temperature of the transition $\sim T_{\text{nuc}}$ and symmetry breaking parameter $\sim \langle\varphi\rangle$. Then it becomes interesting whether new degrees of freedom absent in the low energy Lagrangian describing the phase transition can play a role in the dynamics of the bubble acceleration. The simplest example where this phenomena can occur is the following: let us consider the lagrangian of a *massless* fermion mixed with another *heavy* vectorlike fermion

$$\mathcal{L} = i\bar{\psi}\partial\psi + i\bar{N}\partial N + M\bar{N}N + Y\varphi\bar{\psi}N \tag{2.66}$$

ψ is the light fermion and N is the heavy fermion. In the regime $M \gg \langle\varphi\rangle \sim T_{\text{nuc}}$, then at the temperature of the transition, the species N can be ignored (they are Boltzmann suppressed and are not part of the plasma), so their contribution to pressure naively should be zero. However let us now consider a process of ψ hitting the wall.

We suppose that the energy of the incident ψ particles is much larger than the mass of the heavy species N; $E \gg M \Rightarrow \gamma_w T \gg M$. Note that the mass eigenstates inside and outside of the bubble are different due to the VEV of the $\langle\varphi\rangle$ and in particular there will be mixing between the ψ field and the heaviest mass eigenstate in the broken phase. The mixing angle inside the bubble $\theta_{\psi N}$ is approximately given

$$\sin\theta_{\psi N} \sim \frac{Y_{\text{mixing}}\langle\varphi\rangle}{M}. \tag{2.67}$$

From this mixing angle, we can deduce that, if the transition is satisfying the condition $\Delta p_z L_w \ll 1$, there will be a probability of transition $\psi \to N$ of the form

$$P(\psi \to N) \sim \sin\theta_{\psi N}^2 \sim \frac{Y_{\text{mixing}}^2\langle\varphi\rangle^2}{M^2}. \tag{2.68}$$

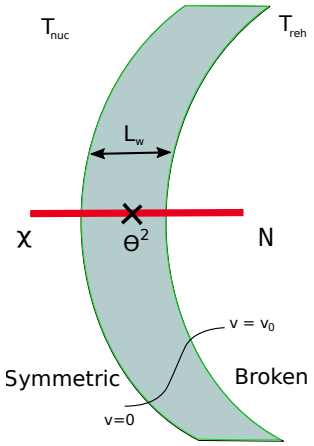

Figure 2.4: Cartoon of the transition $\chi \to N$, from light to heavy upon hitting a very relativistic wall.

Using the terminology of the neutrino oscillation in matter [97] (see for review[98]), to find an unsuppressed transition, we need to be in the regime of *non-adiabaticity*, $\Delta p_z L_w \ll 1$. In the opposite regime, $\Delta p_z L_w \gg 1$, the *adiabatic* regime, the incoming ψ remains in the lightest eigenstate, so that the transition $\psi \to N$ will be strongly suppressed[5]. Intuitively, we can understand that the change of the mixing parameter is slow enough for the system to instantaneously adapt. We can estimate the pressure due to this mixing using the results above. We obtain

$$\begin{aligned}
\mathcal{P}_{\rm mixing} &\sim \underbrace{\int \frac{d^3p}{(2\pi)^3} f_p}_{\text{Incident } \psi \text{ density}} \underbrace{P(\psi \to N)}_{\text{Probability of transition}} \times \underbrace{\frac{M^2}{2E}}_{\text{momentum transfer}} \\
&\approx Y^2_{\rm mixing} \langle\varphi\rangle^2 \int \frac{d^3p}{(2\pi)^3 2E} f_p \Theta(E-M)\Theta\left(E - M^2 L_w\right) \\
&\approx \frac{Y^2_{\rm mixing}}{48} \langle\varphi\rangle^2 T^2 \Theta(\gamma_w T - M)\Theta(\gamma_w T - M^2 L_w) \\
&= \frac{Y^2_{\rm mixing}}{48} \langle\varphi\rangle^2 T^2 \Theta(\gamma_w T - M^2 L),
\end{aligned} \tag{2.69}$$

where the Θ-functions have appeared in order to impose that the initial particle is energetic enough to produce the heavy state and that the process is non-adiabatic. In the next section, we will derive more accurately the condition of non-adiabaticity, by explicitly looking at the transitions with a finite wall width. Note that this new contribution to the pressure is not suppressed by the large M mass and can be present even if $M \gg \langle\varphi\rangle$.

Friction from mixing: more details

One can derive the expression for the friction force in Eq.(2.69) using the master equation (Eq.(2.62)) for the pressure from $\psi \to N$ transitions. Indeed, in the the WKB approximation, the solutions for the wave functions are given by

$$\chi(z) \simeq \sqrt{\frac{k_{z,s}}{k_z(z)}} \exp\left(i \int_0^z k_z(z')dz'\right), \tag{2.70}$$

[5]We thank the referee of JCAP for emphasizing this effect to us.

where $k_{z,s}$ is the z component of the momenta on the symmetric side of the wall. As we have seen above in the adiabaticity discussion, the wall width should play a role in the computation of the pressure effect. As an illustration, let us consider the model of a *linear* wall ansatz

$$\langle\varphi\rangle = \begin{cases} 0, & z<0 \\ v_\varphi \frac{z}{L_w}, & 0<z<L_w \\ v_\varphi, & z>L_w. \end{cases} \tag{2.71}$$

The consequences of different shapes of the wall is discussed in Appendix A.3 and lead to phenomenological similar conclusions. In the notations of [96], the $\mathcal{M}$ matrix takes the form

$$\mathcal{M} = \int_{-\infty}^{\infty} dz e^{i\int_0^z p_z^\psi(z')dz'} e^{-i\int_0^z p_z^N(z')dz'} V(z) \approx \int_{-\infty}^{\infty} dz e^{ip_z^\psi z} e^{-ip_z^N z} V(z) = \int_{-\infty}^{\infty} dz e^{i\Delta p_z z} V(z) \tag{2.72}$$

where we defined $\Delta p_z \equiv p_z^{\psi,in} - p_z^{N,out}$, the momentum exchange, and we safely neglected the change of momentum $\frac{m_\psi^2}{2E}$ induced by the phase-transition induced mass $m_\psi \propto \langle\varphi\rangle$, as it is largely subdominant with respect to the heavy mass M. *Energy* and *transverse momentum* conservation dictates that $p_z^{\psi,N}$ are different on the two sides of the wall, leading to an effective non-zero Δp_z. Performing the integral, the matrix element splits into three different pieces

$$\begin{aligned} \mathcal{M} &= \mathcal{M}_{\text{before wall}} + \mathcal{M}_{\text{inside wall}} + \mathcal{M}_{\text{after wall}} \\ &= V_h \frac{1-e^{i\Delta p_z L_w}}{iL_w \Delta p_z^2} + \frac{V_s}{i\Delta p_z}, \end{aligned} \tag{2.73}$$

where the h, s subscripts denote the interactions and momenta inside and outside of the bubble. The process under study is only possible on the broken side of the wall and thus $V_s = 0, \quad V_h \neq 0$. We obtain

$$|V_h|^2 = 2Y^2 \langle\varphi\rangle^2 p_z^\psi \Delta p_z. \tag{2.74}$$

On top of this there will be an effect due to the mass modification of ψ and N, however this effect will be subleading and suppressed by additional powers of $Y^2\langle\varphi\rangle^2/M^2$. Combining the expression for the matrix element Eq.(2.73) with the expression for the vertex Eq.(2.74), the matrix element squared becomes

$$|\mathcal{M}|^2 \approx \frac{V_h^2}{\Delta p_z^2}\left(\frac{\sin\alpha}{\alpha}\right)^2 = 2\frac{\langle\varphi\rangle^2 p_z^\psi}{\Delta p_z}\left(\frac{\sin\alpha}{\alpha}\right)^2 Y^2, \qquad \alpha = \frac{L_w \Delta p_z}{2} \approx \frac{M^2 L_w}{4E}, \tag{2.75}$$

with $\Delta p_z = p_z^\psi - \sqrt{(p_z^\psi)^2 - M^2}$. Plugging it in the master Eq.(2.62), we obtain the following estimate for the mixing pressure[6]

$$\mathcal{P}_{\text{mixing}} = \int \frac{d^3p}{(2\pi)^3} f_p \times \frac{Y_{\text{mixing}}^2 \langle\varphi\rangle^2}{2\sqrt{p_z^2 - M^2}} \times \left(\frac{\sin\alpha}{\alpha}\right)^2. \tag{2.76}$$

As $\left(\frac{\sin\alpha}{\alpha}\right)^2 \to 0$ for $\alpha \gg 1$, we can see that the pressure is suppressed for $\alpha \gg 1$, so that the suppression regime is given by

$$\frac{M^2 L_w}{E} \gg 1 \quad \Rightarrow \quad E \ll M^2 L_w \sim \frac{M^2}{\langle\varphi\rangle}, \tag{2.77}$$

[6]The integral below is assumed to be taken for the values of $p_z > M$, otherwise the process is forbidden.

where we have assumed that the width of the wall L_w, in the wall frame scales like the inverse of the VEV. At this point, it is good to make a comment on the estimate $L_w \sim 1/\langle\varphi\rangle$. Of course, estimating the length of the wall on general grounds is a difficult task, but here we would like to clarify some points. First we have to notice that the length of the wall cannot be possibly controlled by $1/T_{\rm nuc}$, as this is the case in the context of fluid approximation methods that have found $L_w \sim 30/T_{\rm nuc}$[81], otherwise the limit of infinite cooling would lead to infinitely thick walls, which is not physical. We can think of the thickness of the wall for long supercooling in the following way: the bubble nucleates with a thick wall in a very diluted plasma. As it accelerates the bubble wall still "does not feel" the plasma and so it is expanding virtually in vacuum. In this context, the wall relaxes to the shape controlled by the zero-temperature potential, with a length $L_w \sim 1/\langle\varphi\rangle$.

Using the fact that the energy of the incident particles is approximately equal to $\sim \gamma_w T$ we obtain a necessary constraint on the masses of the heavy particles which can be produced

$$\gamma_w T_{\rm nuc} \gtrsim \frac{M^2}{\langle\varphi\rangle}, \quad \boxed{M \lesssim \sqrt{\gamma_w T_{\rm nuc}\langle\varphi\rangle}} \tag{2.78}$$

which exactly corresponds to the regime where the passage of the particle through the wall cannot be treated adiabatically.

Finally, we would like to emphasize that the pressure from the mixing is not suppressed by the mass of the heavy particles and in general can be present even if we treat our theory as an effective field theory (EFT) with heavy degrees of freedom integrated out.

One can also ask what could be the maximal pressure from the mixing in this case. We can estimate it by using unitarity arguments on the maximal value of the mixing coupling $Y^{\rm max}_{\rm mixing} \sim 4\pi$. So that, the maximal pressure from mixing is

$$\mathcal{P}^{\rm max}_{\rm mixing} \simeq \frac{T^2}{24}(16\pi^2)\langle\varphi\rangle^2\theta(\gamma_w T_{\rm nuc} - M^2 L_w). \tag{2.79}$$

Importance of friction from heavy particles

One can wonder whether this friction from mixing can be phenomenologically important, since in any case we are looking at the very relativistic bubble expansion velocities $v_w \to 1$. However, we have discussed in section 1.6 that relativistic bubbles in runaway regime have a substantial fraction of their energy stored in the wall kinetic motion, while bubbles which have reached a terminal velocity have vanishingly small fraction of energy stored in the wall and most of the energy released in the phase transition is transferred to the sound waves (plasma motion) [33, 31, 57]. This different distribution of energy has important phenomenological consequences on the spectrum of stochastic gravitational wave background since the *bubble wall collisions* signal Ω_ϕ and *plasma motion* signal Ω_{sw} lead to different shape of the spectrum. Namely, the most obvious difference is the fall of the signal at high frequencies;

$$\Omega_{sw,f\to\infty} \propto f^{-4} \text{ (terminal velocity)}, \qquad \Omega_{\phi,f\to\infty} \propto f^{-3/2} \text{ (Runaway)}. \tag{2.80}$$

In order to understand whether the friction from mixing can indeed prevent the runaway bubble case, let us consider the following toy model ([99, 37]) described in the infrared region by the lagrangian

$$\mathcal{L}_{IR} = \frac{1}{2}(\partial_\mu\varphi)^2 + \frac{1}{2}(\partial_\mu\eta)^2 - \frac{m_\varphi^2\varphi^2}{2} - \frac{m_\eta^2\eta^2}{2} - \frac{\lambda_\varphi}{4}\varphi^4 - \frac{\lambda_\eta}{4}\eta^4 - \frac{\lambda_{\varphi\eta}}{2}\varphi^2\eta^2 + i\bar{\psi}\partial\psi. \tag{2.81}$$

We will assume that at high energies this lagrangian is UV completed to

$$\begin{aligned}\mathcal{L}_{UV} &= \frac{1}{2}(\partial_\mu\varphi)^2+\frac{1}{2}(\partial_\mu\eta)^2-\frac{\tilde{m}_\phi^2\varphi^2}{2}-\frac{\tilde{m}_\eta^2\eta^2}{2}-\frac{\tilde{\lambda}_\varphi}{4}\varphi^4-\frac{\tilde{\lambda}_\eta}{4}\eta^4-\frac{\tilde{\lambda}_{\varphi\eta}}{2}\phi^2\eta^2\\ &+i\bar{\psi}\partial\psi+i\bar{N}\partial N-M\bar{N}N-(Y_{\text{mixing}}\bar{\psi}\varphi N+h.c.),\end{aligned} \tag{2.82}$$

where all of the parameters $\tilde{m}^2_{\varphi,\eta}, \tilde{\lambda}_{\varphi,\eta,\varphi\eta}$ are the parameters of UV theory and m^2, λ in the Eq.(2.81) are the parameters of IR effective theory obtained by matching when integrating out the heavy fermion N. We also assume as before that M is much larger than the characteristic the scale of the symmetry breaking of the IR lagrangian $M \gg \langle\varphi\rangle, m_\varphi, m_\eta$. This introduces the usual tuning into the model which is analogous of the Higgs boson hierarchy problem in the presence of heavy new physics. However we will not bother about a solution to this hierarchy problem and take Eq.(2.81) as a toy, very fine-tuned example to illustrate the mixing from the friction effect.

Let us consider the potential for the scalar fields of the model, following the procedure already outlined in Chapter 1. On the top of the tree-level potential, at one loop, the usual Coleman-Weinberg potential is generated [8] for the fields φ, η (in $\overline{MS}$ scheme) (we are using the IR lagrangian of Eq.(2.81))

$$V_{CW}=\sum_{i=\eta,\varphi}\frac{m_i^4}{64\pi^2}\left[\log\frac{m_i^2}{\mu_R^2}-\frac{3}{2}\right], \tag{2.83}$$

since there is no gauge bosons in our model. The thermal corrections can be taken into account by adding the thermal potential V_T defined as follows

$$V_T=\sum_{i=\eta,\varphi}\frac{T^4}{2\pi^2}J_B\left(\frac{m_i^2}{T^2}\right),\quad J_B(y^2)\equiv\int_0^\infty dx x^2\log\left[1-\exp\left(-\sqrt{x^2+y^2}\right)\right]. \tag{2.84}$$

Higher loop corrections due to the daisy diagrams can be taken into account using the truncated full dressing procedure[16]

$$V(\varphi,\eta,T)=V_{\text{tree}}(\varphi,\eta)+\sum_{i=\eta,\varphi}V_{CW}(m_i^2+\Pi_i^2)+V_T(m_i^2+\Pi_i^2). \tag{2.85}$$

In the case of the model (2.81), the thermal mass corrections are given by

$$m_\varphi^2+\Pi_\varphi^2=m_\varphi^2+3\lambda_\varphi\varphi^2+\lambda_{\varphi\eta}\eta^2+T^2\left(\tfrac{\lambda_\varphi}{4}+\tfrac{\lambda_{\varphi\eta}}{12}\right), \tag{2.86}$$

$$m_\eta^2+\Pi_\eta^2=m_\eta^2+\lambda_{\varphi\eta}\varphi^2+3\lambda_\eta\eta^2+T^2\left(\tfrac{\lambda_\eta}{4}+\tfrac{\lambda_{\varphi\eta}}{12}\right). \tag{2.87}$$

Generically we have to analyze the phase transition in the (φ,η) field space, however the discussion simplifies if we put the coupling $\lambda_\varphi = m_\varphi = 0$. Indeed in this case, along the line $\eta = 0$, the tree-level potential is vanishing and only the one loop potential will be controlling the phase transition. The tree-level η^4-potential is stabilizing the η-direction, thus it is obvious that the tunnelling must happen along $\eta = 0$ direction. The calculation becomes even simpler if we set $m_\eta = 0$ then the only mass parameter in this construction is the renormalization scale $\mu_R \equiv \lambda_{\varphi\eta}w$ which fixes the value of the VEV of the field $\langle\varphi\rangle \sim w$.

The transition from the false to the true vacuum, separated by the potential barrier, can be calculated using the usual *bounce action* using the method outlined in section 1.5. We are prepared now to discuss the friction effects. The bubble will have runaway behaviour if the LO friction of Eq.(2.49), which in our model is equal to

$$\mathcal{P}_{\text{LO}}\simeq\frac{T_{\text{nuc}}^2}{24}\lambda_{\varphi\eta}\langle\varphi\rangle^2\Theta(\gamma_w T_{\text{nuc}}-\langle\varphi\rangle\sqrt{\lambda_{\varphi\eta}}) \tag{2.88}$$

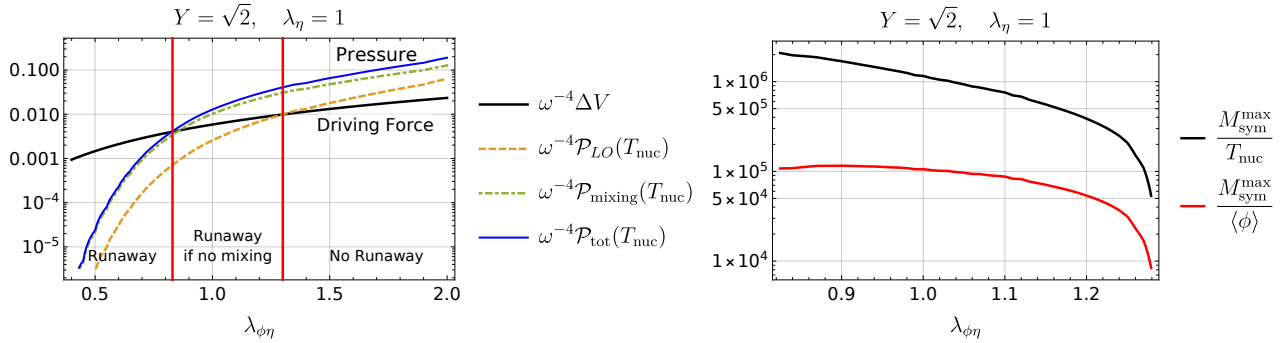

Figure 2.5: Left- the potential difference and various contributions to the pressure as a function of the coupling $\lambda_{\varphi\eta}$. The scale of the symmetry breaking was fixed to be $w = 10^5$ GeV so that $\langle\varphi\rangle \sim 10^5$ GeV. Right- The maximal mass of the heavy particle defined by the Eq.2.94 as a function of $\lambda_{\varphi\eta}$. As a typical width of the wall, we considered $L_w \sim 1/\langle\varphi\rangle$.

cannot overcome the potential difference, providing the driving force for the expansion of the bubble. In Eq.(2.88), the Θ function comes from the condition we outlined in Eq.(2.52). This amounts to the condition

$$\Delta V > \mathcal{P}_{\rm LO} \quad \text{(runaway condition)}. \tag{2.89}$$

At the same time, as we have seen, there can be an additional friction induced by the mixing effect

$$\mathcal{P}_{\rm mixing} \simeq \frac{T^2_{\rm nuc}}{48} Y^2_{\rm mixing} \langle\varphi\rangle^2 \Theta(\gamma_w T_{\rm nuc} - M^2 L_w), \tag{2.90}$$

which can prevent the runaway behaviour. Now if the condition

$$\mathcal{P}_{\rm LO} + \mathcal{P}_{\rm mixing} > \Delta V > \mathcal{P}_{\rm LO} \tag{2.91}$$

is satisfied we are in the situation when the mixing pressure is preventing the bubbles from the otherwise runaway motion. To analyse the $\mathcal{P}_{\rm mixing}$ effects in our model we have deferred from performing the full parameter scan and instead have fixed the symmetry breaking scale to be 10^5 GeV and the mixing coupling $Y_{\rm mixing} = \sqrt{2}$. Then the region of the parameter space where the mixing effect is important is displayed on the Fig.2.5.

In order to find the upper bound on the masses of the states which can be produced in mixing we need to estimate the maximum value of the Lorentz $\gamma_{\rm max}$ factor that would have been reached if the bubbles kept accelerating till the moment of the collision. It can be estimated from the ratio of initial and final radii of the bubble and is approximately equal to, using Eq.(1.133) of Section 1.5 that we corrected for the energy lost in the LO pressure,

$$\gamma_{\rm max} \simeq \frac{2R_*}{3R_0}\left(1 - \frac{\mathcal{P}_{\rm LO}}{\Delta V}\right). \tag{2.92}$$

The initial bubble radius and the bounce solution can be found numerically, while the final radius can be estimated according to Eq.(1.138) and (1.139) by the derivative of the bounce action:

$$R_* = \frac{(8\pi)^{1/3}}{\beta(T_{\rm nuc})}, \quad \beta(T) = HT\frac{d}{dT}\left(\frac{S_3}{T}\right), \tag{2.93}$$

where H is the Hubble constant.

Then the friction from mixing can be generated only by the states satisfying

$$M < M_{\max} = \min\left[\gamma_{\max} T_{\rm nuc}, \sqrt{\gamma_{\max} \frac{T_{\rm nuc}}{L_w}}\right]. \tag{2.94}$$

For a wall length $L_w \sim 1/\langle\varphi\rangle$, the condition simplifies to

$$M < M_{\max} = \sqrt{\gamma_{\max} T_{\rm nuc} \langle\varphi\rangle}. \tag{2.95}$$

We report the value $M_{\max}$ on the Fig.2.5. In our model, we can see that states as heavy as 10^{10} GeV, 10^5 times heavier than the scale of the transition, can lead to non-vanishing friction effects. Generically, one can also estimate $M_{\max}$ as follows

$$M_{\max} = \sqrt{\gamma_{\max} T_{\rm nuc} \langle\varphi\rangle} \sim \sqrt{\frac{R_*}{R_0} T_{\rm nuc} \langle\varphi\rangle}. \tag{2.96}$$

The values of the initial and the final radii are very roughly equal to:

$$R_0 \sim \frac{1}{T_{\rm nuc}}, \;\; R_* \sim (\tilde{\beta} H)^{-1} \sim \frac{M_{\rm pl}}{\tilde{\beta} \times \text{scale}^2}, \tag{2.97}$$

where "scale" refers to the energy scale of the potential $\sim \langle\varphi\rangle$. Combining all of this together we can find the estimate for the maximal mass to be

$$\boxed{M_{\max} \sim T_{\rm nuc} \left(\frac{M_{\rm pl}}{\tilde{\beta} \times \text{scale}}\right)^{1/2}}. \tag{2.98}$$

Of course this estimate is valid only for the theories where the bubbles are runaway without the friction from mixing. In the next section however we will review the NLO effects from the gauge field which generically prevent bubbles from infinite acceleration, so it was crucial for our point here that the model did not contain any gauge boson.

2.3.4 Next-to-leading order pressure from transition radiation effects

As we saw above, in the case of ultra-relativistic bubbles, the collisions of particles inside of the wall can be neglected. As a consequence, the particles involved in transition do not have the time to thermalise and we can approximate the distribution from the simple equation Eq.(2.39). This approximation becomes very precise as the wall reaches very relativistic velocities and becomes thin in the plasma frame. This permitted us to compute a simple formula for the pressure at leading order on relativistic walls in Eq.(2.49). We also noted that in this case the pressure is independent on the v_w. Initially, walls such that

$$\Delta V > \Delta \mathcal{P}_{\rm LO} \tag{2.99}$$

were believed to enter inevitably the *runaway* regime: Apparently, no pressure could prevent it from accelerating until the collision of different bubble walls. As a consequence, strong transition were expected to provide strong GW signal via bubble collision mechanism, as we have explained in Section 1.6. In the context of relativistic walls, we also discovered a new contribution which becomes important when the the wall becomes fast enough to produce heavy particles. We could think that this is all about the pressure on relativistic walls, up to negligible NLO effects.

Early computation: $1 \to 2$ **splittings[96]**

So now let us look deeper at $1 \to 2$ transitions, a cartoon of which is provided in Fig.2.6 (we closely follow the discussion in [96]) . Again we will assume that we are in the regime where WKB approximation is valid i.e. $p_z L_w \gg 1$, where L_w is the width of the wall. The calculation of the $A(p) \to B(k^{(1)})C(k^{(2)})$ splitting simplifies in the limit when $k_z \gg m_{B,C}, k_\perp$ and in this case it becomes easy to find the solution for the free wave functions

$$\chi_{A,B,C}(z) \simeq \sqrt{\frac{k_{z,s}}{k_z(z)}} \exp\left(i \int_0^z k_z(z')dz'\right). \tag{2.100}$$

Using the following notation for the initial and final momenta

$$\begin{aligned} p &= (p_0, 0, 0, \sqrt{p_0^2 - m_A^2(z)}) \\ k^B &= (p_0(1-x), 0, k_\perp, \sqrt{p_0^2(1-x)^2 - k_\perp^2 - m_B^2(z)}) \\ k^C &= (p_0 x, 0, -k_\perp, \sqrt{p_0^2 x^2 - k_\perp^2 - m_C^2(z)}), \end{aligned} \tag{2.101}$$

the product of three wave functions in $1 \to 2$ splitting is given by

$$\chi_A(z)\chi_B^*(z)\chi_C^*(z) \sim \exp\left[\int_0^z \left(\frac{m_A^2(z)}{2p_0} - \frac{m_B^2(z) + k_\perp^2}{2k_0^{(1)}} - \frac{m_C^2(z) + k_\perp^2}{2k_0^{(2)}}\right)\right]. \tag{2.102}$$

Then the matrix element is equal to

$$\begin{aligned} \mathcal{M} &= V_s \int_{-\infty}^0 \exp\left[iz\frac{A_s}{p_0}\right] + V_h \int_0^\infty \exp\left[iz\frac{A_h}{p_0}\right] = 2ip_0\left(\frac{V_h}{A_h} - \frac{V_s}{A_s}\right) \\ A &= -\frac{k_\perp^2}{x(1-x)} + m_A^2 - \frac{m_B^2}{1-x} - \frac{m_C^2}{x}, \end{aligned} \tag{2.103}$$

and at the end of the day we end up with

$$|\mathcal{M}|^2 = 4p_0^2 \left|\frac{V_h}{A_h} - \frac{V_s}{A_s}\right|^2. \tag{2.104}$$

The reference [96] has studied various splitting effects and it was shown that only the production of the vector particles gaining the mass during the phase transition can lead to the friction growing with the Lorentz factor γ_w. Let us apply this formalism for the case of the QED-like theory. In other words let us consider the process $\psi \to V\psi$, where the fermion ψ splits into a vector boson V and the fermion. This process, which is obviously forbidden by momentum conservation in the absence of the wall, can happen when the wall is present and the matrix element becomes equal to

$$\begin{aligned} V_h = V_s &= \tfrac{\sqrt{2}k_\perp}{x} \\ |\mathcal{M}_{\psi\to V\psi}|^2 &= \tfrac{8p_0^2k_\perp^2}{x^2}\left|\tfrac{A_h - A_s}{A_h A_s}\right|^2 = \tfrac{8p_0^2 m_V^4}{(k_\perp^2 + m_V^2)^2 k_\perp^2}. \end{aligned} \tag{2.105}$$

We are looking at $\psi \to \psi V^T$ at the production of the transversely polarized vector bosons and m_V is the mass of the gauge boson *in the higgsed phase*. In principle of course, a longitudinally polarized degree of freedom also exists in the broken phase, however, the matching with the goldstone boson in the symmetric phase in not obvious and is

still an open problem. We will thus ignore the possible pressure from emission of longitudinally polarized degree of freedom. Focusing on the limit $k_\perp \sim m_V \ll k_0 \sim k_z$ we recover the following expression for the pressure

$$\mathcal{P}_{\psi\to V\psi} = \int \frac{d^3p}{8p_0^2(2\pi)^6} f_\psi \int \frac{dk_0^{(2)}}{k_0^{(2)}} \int d^2k_\perp |\mathcal{M}_{\psi\to V\psi}|^2 \frac{k_\perp^2 + m_V^2}{2p_0 x}. \tag{2.106}$$

Plugging in our expression for the matrix element we will get:

$$\begin{aligned}
\mathcal{P}_{\psi\to V\psi} &= \int \frac{d^3p}{8p_0^2(2\pi)^6} f_\psi \int \frac{dk_0^{(2)}}{k_0^{(2)}} \int d^2k_\perp \frac{8p_0^2 m_V^4}{(k_\perp^2+m_V^2)^2 k_\perp^2} \frac{k_\perp^2+m_V^2}{p_0 x} \\
&= \int \frac{d^3p}{p_0(2\pi)^6} f_\psi \int \frac{dx}{x^2} \int_{\sqrt{\Pi_V}} \frac{d^2k_\perp}{k_\perp^2} \frac{m_V^4}{(k_\perp^2+m_V^2)} \\
&= \int \frac{d^3p}{p_0(2\pi)^3} f_\psi \pi m_V^2 \log(m_V^2/(eT)^2) \times \left[\int \frac{dx}{x^2} = \frac{p_0}{m_V}\right] \\
&= \int \frac{d^3p}{(2\pi)^3 p_0} f_\psi \left[\frac{m_V p_0}{8\pi^2} \log(m_V^2/(eT)^2)\right].
\end{aligned} \tag{2.107}$$

Let us make two important comments regarding this expression. First, we can see that in the wall frame the pressure is proportional to $\Delta\mathcal{P} \propto \int d^3p f_\chi$, however d^3p is not invariant under the boost and in the plasma frame it will lead to the additional γ_w factor found in [96]

$$\Delta\mathcal{P}_{\rm NLO} \propto \gamma_w T^3 m_V n_\psi \frac{\log(m_V^2/(eT)^2)}{8\pi^2}. \tag{2.108}$$

Second, the other important point we would like to stress is that the minimal value of the transverse momenta is cut in IR at the scale $k_\perp^{\rm min} \sim \sqrt{\Pi_V} \sim eT$, ($e$ is the gauge coupling). This might be a subtle point since we know that the transverse gauge boson do not receive a thermal mass from our discussion on the potentials. In this case, the effect is due to the screening of the long wavelength modes by the temperature effects which *indeed exists as well for transverse gauge bosons*. So we can see that the pressure from $1 \to 2$ radiation is dominated by the emission of the *soft* photons (gauge bosons), which provides the γ_w enhancement. The next subsections will be devoted to a discussion of this effect and the different results in the literature.

Multi-bosons emission

In the previous subsections, we have seen that, in the relativistic approximation, $1 \to 1$ transition were saturating at large γ_w but emission of soft gauge bosons in $1 \to 2$ actually produces a pressure scaling with the boost factor γ_w. This leads us naturally to wonder about the possible scaling of multi-bosons emission $1 \to N$, question that has been subject to some debates. This is the topic of this subsection.

Computation in [100]. Recently there has been a calculation of $1 \to N$ transition[100][7] of the friction which tried to take into account effects of the multiple soft emissions. In [100], the resulting friction pressure for the fermions emitting soft vector bosons was found to scale as

$$\mathcal{P}^{[100]} \sim \sum_i \alpha_i \gamma_w^2 T^4 \tag{2.109}$$

[7]We acknowledge J. Turner for discussion of the results of Ref. [100].

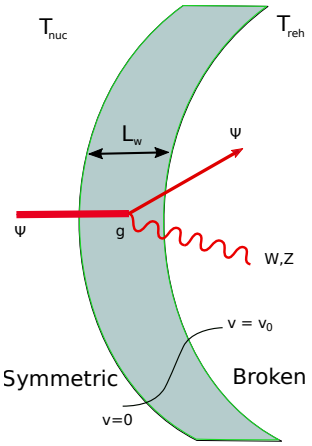

Figure 2.6: Cartoon of the radiation transition from $1 \to 2$ splittings with emission of a soft bosons.

and the sum runs over the gauge couplings of the theory, including those that are not broken in the transition. Thus, in the SM, there are the contributions from the electroweak sector and strong sector. The scaling γ_w^2 comes from the interplay between γ_w originating from the incoming density $n \propto \gamma_w T^3$ and the very large momentum exchange $\Delta p_z \propto \gamma_w T$ that is found in[100]. Intuitively, this results in surprising for several reasons:

- A first issue is that Eq.(2.109) does not have the correct $m_\psi, m_V \to 0$ limit (vanishing masses of the incoming fermion and the outgoing vector boson). Indeed in the case when both $m_\psi, m_V = 0$ the particles do not interact with the wall and it becomes completely transparent. However the particles which do not interact with the bubble wall cannot induce any friction so that on those grounds we would expect $\mathcal{P}^{\text{friction}}|_{m_\psi, m_V \to 0} \to 0$. This signals the inconsistency of the Eq.(2.109). On general grounds the inconsistency of Eq.(2.109) can be seen directly by noting that there is no dependence on the order parameter differentiating two phases separated by the bubble wall.

- A second issue is, as already mentioned, the resummation of [100] gives a γ_w^2 scaling pressure also for the gauge bosons that *do not* acquire a mass in the transition, e.g. the gluons. As a consequence, in the SM, the pressure on the electroweak wall would be dominated by the strong sector, that is to say, the emission of massless gluons:

$$\mathcal{P}^{[100]} \sim \alpha_s \gamma_w^2 T^4. \tag{2.110}$$

  where α_s is the strong coupling. This is highly counter-intuitive.

- A last issue that we would like to raise are the finite wall effect. Ref.[100] considered the case of the infinitely sharp wall with $L_w \to 0$. However, finite wall effect, within the WKB approximation are expected to limit the maximal unsuppressed momentum exchange. We have already shown that, using WKB phase, a exponentially strong suppression appears when

$$\Delta p_z L_w > 1. \tag{2.111}$$

  This sets an effective upper bound on the momentum exchange of order

$$\Delta p_z \lesssim \frac{1}{L_w} \ll \gamma_w T \tag{2.112}$$

  So the computation of Ref.[100] is explicitly deeply in the regime of suppression, the adiabatic regime.

However, to go beyond those rough intuitions, we need to provide an exact computation for the multi-bosons emission. This task was started in [1] by us, using the called *photon equivalent approximation*.

Equivalent photon approximation It is well-known that the effect of the soft and colinear photons can be taken into account using the equivalent photon approximation [101, 102, 103, 104] (see for review [105, 106, 107]). We believe that this picture offers an intuitive understanding of the pressure at NLO order and also makes quite easy to generalise it to $1 \to N$ by solving the DGLAP equations, as we will do. In other words, an initial fermion state can be thought as a state made of photons and fermions with the photons distributed with the *Weizsacker-Williams* parton distribution function

$$f_\gamma(x) = \frac{e^2}{8\pi^2} \log \frac{m_V^2}{(eT)^2} \left[\frac{1+(1-x)^2}{x} \right], \tag{2.113}$$

where the integral over the perpendicular momenta has already been performed and we are using the information from Eq. (2.107) that the pressure is dominated by the $k_\perp \lesssim m_V$ and the minimal value of transverse momenta is of the scale $\sim eT$[8]. We also know that a photon with a phase-dependent mass going through the wall will lose p_z component of momenta of the order $\sim \frac{m_V^2}{2E}$. Then the pressure can be trivially estimated to be

$$\begin{aligned} \mathcal{P}_{1\to 2}^{eq.\gamma} &= \underbrace{\int \frac{d^3p}{(2\pi)^3} f_p}_{\text{incident fermions}} \int_{m_V/p_0}^1 dx f_\gamma(x) \times \underbrace{\frac{m_V^2}{2p_0 x}}_{\text{momentum transfer}} \\ &= \int \frac{d^3p}{(2\pi)^3} f_p \times \left[\frac{e^2}{8\pi^2} m_V \right] \log \frac{m_V^2}{e^2T^2} \end{aligned} \tag{2.114}$$

which leads to the exactly same result as the expression in Eq.2.107. We have cut-off the integral in Eq.(2.114) at m_V/p_0 because from the considerations in Eq.(2.52), we do not expect the gauge bosons less energy to be able to enter the bubble, we will turn to those gauge bosons shortly. Intuitively the γ_w factor in the pressure comes from the two following effects: both the photon distribution function as well as momentum transfer to the wall are enhanced by the factor $1/x$, which together allows to enhance the pressure by the additional factor $p_0/m_V \sim \gamma_w$. One may wonder what will be the effect of the particles which do not have enough energy to pass through the wall, since for them the photon distribution function will be even larger, however, in that case the momentum transfer to the wall will scale as $p_0 x$ so that the pressure will scale as

$$\begin{aligned} \mathcal{P}_{1\to 2}^{\text{reflection}} &= \int \frac{d^3p}{(2\pi)^3} f_p \int_{x_{\text{min}}}^{x_{\text{max}}} dx f_\gamma(x) \times 2p_0 x \\ &= \int \frac{d^3p}{(2\pi)^3} f_p \times \left[\frac{e^2}{2\pi^2} (x_{\text{max}} - x_{\text{min}}) p_0 \right] \log \frac{m_V^2}{e^2T^2} \end{aligned} \tag{2.115}$$

$$x_{\text{min}} \sim k_\perp/p_0 \sim T/p_0, \quad x_{\text{max}} \sim m_V/p_0 \tag{2.116}$$

leading to the pressure from reflection

$$\mathcal{P}_{1\to 2}^{\text{reflection}} \simeq \int \frac{d^3p}{(2\pi)^3} f_p \left[\frac{e^2}{2\pi^2} m_V \log \frac{m_V^2}{e^2T^2} \right]. \tag{2.117}$$

[8]One can also argue that $k_\perp \lesssim m_V$ by noting that in the limit $p_0 x, k_\perp \gg m_V$ four momentum is approximately conserved, which should strongly suppress the splitting.

We have again the friction effect growing with the Lorentz factor γ_w, however, note that our calculation becomes questionable in this regime since we need $p_0 x L_w \gg 1$ in order to remain in the WKB validity range. Notice also the factor of 4 between the reflection contribution in (2.117) and the transmission contribution in (2.114).

We can generalize the Eq.(2.114) for arbitrary splitting and the resulting pressure will be

$$\mathcal{P}_{A\to BC} = \int \frac{d^3p}{(2\pi)^3} f_p \int_{m_B/p}^1 dx \frac{m_B^2}{2px}\frac{\alpha}{2\pi}\log\frac{m_B^2}{e^2T^2} P_{B\leftarrow A}(x) \tag{2.118}$$

where B is the soft particle and $P_{B\leftarrow A}(x)$ are Altarelli-Parisi [108] splitting functions. Then it is obvious that the friction proportional to $\propto \gamma_w$ can appear only from the splitting when the splitting functions scale as $1/x$ for small values of x. This is the case only when the soft final state is a vector boson, which confirms the results of [96].

The expression of the pressure in Eq.(2.118) was derived assuming single soft vector boson emission, and it corresponds to the solution of the DGLAP equations [108, 109, 110] (or for a pedagogical review [111])

$$\frac{df_B(x,Q)}{d\log Q} = \frac{\alpha}{\pi}\int_x^1 \frac{dz}{z} P_{B\leftarrow A}(z) f_A\left(\frac{x}{z}, Q\right) \tag{2.119}$$

up to the order $\mathcal{O}(\alpha^2)$ starting with initial conditions at the scale $Q = eT$

$$f_B(x, eT) = 0, \quad f_A(x, eT) = \delta(x-1) \tag{2.120}$$

The multiple emissions can be taken into account by solving the system of the DGLAP equations, however these will lead to only higher order in $\mathcal{O}(\alpha \log\frac{m_V}{eT})$ corrections. We observe that in absence of very strong log-enhancement $\log\frac{m_V}{eT} \sim \mathcal{O}(1)$, any multiple emission will be suppressed by powers of the coupling α with respect to the single-emission result.

Sudakov resummation A second step in the clarification of the controversy was taken in [112] where careful Sudakov resummation[113] was carried out. Such a careful computation confirmed our previous expectation that accounting for the multi-bosons emission should only bring a further mild $\log\frac{m_V}{gT}$ enhancement. The final result is given by[112]

$$\Delta\mathcal{P}_{\text{multi}-\text{NLO}} \approx \sum_C \left[\sum_{AB} \nu_A g_A C_{ABC}\right] \frac{\kappa\zeta(3)}{\pi^3}\alpha\gamma_w m_V(v_{EW}) \log\frac{m_V(v_{EW})}{eT_{\text{nuc}}} T_{\text{nuc}}^3 \tag{2.121}$$

where $\nu_A = 1(3/4)$ for A a boson (fermion), g_A is the number of degrees of freedom of A, M_V designates the mass of a gauge boson, C_{ABC} is relevant to the coupling appearing in the vertex. This is the expression we will be using in our future estimation of the pressure at NLO order.

Emission of massless vector bosons We have seen above that a very large pressure was predicted in [100], mainly due to the emission of massless gluons. We then argued that such a result was unphysical and proposed an alternative computation using the EPA[1] and Sudakov resummation in[112]. In this subsection, we would like to present a calculation that actually shows that the emission of particle that do not acquire a tree-level mass from the condensate actually contribute only a very small correction, following the lines of[112].

Let us consider the special case where the soft gauge boson remains massless but the particle that emits it has a mass which is however phase-dependent, $m_{A,h} \gg m_{A,s}$. In this context, considering a constant vertex, the WKB wave functions give

$$\left(\frac{1}{A_s} - \frac{1}{A_h}\right)^2 = \left(\frac{1}{-m_{A,h}^2 + \frac{k_\perp^2+m_{A,h}^2}{1-x} + \frac{k_\perp^2+m_{C,h}^2}{x}} - \frac{1}{\frac{k_\perp^2}{1-x} + \frac{k_\perp^2+m_{C,s}^2}{x}}\right)^2 \tag{2.122}$$

which gives the splitting probability after a simple computation

$$dP_{A\to BC} = \sum_{bc} \nu_A g_A C_{ABB} \frac{dk_\perp^2}{k_\perp^2} x dx \frac{k_\perp^4}{(k_\perp^2+\mu^2)} \frac{x^2 m_{A,h}^4}{(k_\perp^2+\mu^2+x^2 m_{A,h}^2)^2}. \tag{2.123}$$

where we introduced a cut-off μ that should be taken around eT. This result, because it does not contain any divergence when $x \to 0$ already hints that massless gluons cannot produce a γ_w scaling pressure. Applying Sudakov resummation techniques, Authors of [112] find that the exchange of momentum transferred to the wall is order

$$\Delta p_z \sim \frac{m_{A,h}^2}{2E_A}, \tag{2.124}$$

that is to say, of the same order of magnitude than the LO exchange of momentum. This is again to be contrasted with [100] which obtains, for the similar case, an exchange of momentum $\Delta p_z \propto E_A$.

Open questions about the NLO pressure

So far we have discussed the current state of the art of the NLO pressure in the semi-classical regime. In the subsection, we would like to draw attention to some of the unclear aspects of the computation and the physics associated. The purpose of this subsection is *not* to bring a final conclusion to those puzzles but to show that investigation is still lively in the field. Here is a non-exhaustive list:

- **The case of the longitudinal modes of the gauge bosons**

  We know that the point of the spontaneous symmetry breaking is to give a mass to the gauge bosons while maintaining gauge invariance. As a massive vector boson has one more degree of freedom than a massless one, the mechanism consists in assigning a degree of freedom, the longitudinal component, with polarisation along the direction of propagation, coming from a scalar introduced in the theory (the Higgs). This raises the question of the emission of those longitudinal modes during the bubble expansion.

  The role of longitudinal modes of the wall relativistic wall pressure constitutes an open problem and a work in progress. We will not comment on it anymore nor take them into account in our future estimates of the velocities. We however hope that including them should not change drastically the result.

- **Kadanoff-Baym formalism for the emission of gauge bosons** The previous estimates have always considered the emission of on-shell particles. It is however possible than plasma effects and off-shellness play an active role in the emission of soft-gauge bosons. The most honest formalism to take into account quantum and plasma effects is the Kadanoff-Baym formalism. This can become very relevant if off-shellness effects becomes large. However, at the current stage, a computation of the friction pressure using the KB formalism is still lacking in the literature, maybe due to the fact that such a computation is heavily involved.

- **Saturation of the soft bosons**

  It was emphasized in [96] and later in [112] that the strong emission of gauges bosons peaked around momentum of order $p \sim m_V$ could lead to the onset of collective effects for the soft modes of the bosons. Those collective effects are of concerns for two reasons: first they will lead to an effective mass for the low momentum modes and secondly, they could lead to the breakdown of the perturbativity of the plasma, as

large amount of particles with similar momentum are accumulating in the wall. Let us treat those two effects separately:

Using the Ward identities, and considering, as a toy model, a $SU(N)$ gauge theory we can estimate that high density effects lead to a mass gap, for the gauge bosons, in the dispersion equation of the form[114]

$$m^2_{V,\mathrm{HDE}} \sim 2Ng^2 \int \frac{d^3p}{(2\pi)^3 2|\mathbf{p}|} f_V(p) \tag{2.125}$$

where $f_V(p)$ is the density of soft bosons emitted, which is strongly peaked in the region $p_0 \in [0, m_V]$. It is roughly controlled by

$$f_V(p) = \sum_i g_A \int \frac{d^3p_A}{(2\pi)^2} f_A(p_A) \frac{dP_{A\to BC}(m_{V,HDE})}{d^2k_\perp dp^0} \sim \frac{\gamma_w T^3_{\mathrm{nuc}}}{k^2_\perp x p_0} \left(\frac{m^2_{V,h}}{k^2_\perp + m^2_{V,h}} \right)^2 \tag{2.126}$$

where g_A are the emitting degrees of freedom. We have already seen that the probability of emission of a gauge boson $dP_{A\to BC}(m_{V,\mathrm{HDE}})$ has a strong dependence on the screening mass because the emission is dominated by ultra-soft momentum. As noted by [96], this induces a cut-of in the integral over the emission

$$P_{A\to BC} \propto g^2 \int_{m^{\mathrm{tot}}_{V,s}} \tag{2.127}$$

where the total mass of the gluons of the broken $SU(N)$ *inside the wall*

$$m^{\mathrm{tot}}_{V,s} = \sqrt{m^2_{V,\mathrm{HDE}} + \underbrace{\Pi(T)}_{\text{Thermal mass}}} \approx m_{V,\mathrm{HDE}} \tag{2.128}$$

We now need to self-consistently solve for $m_{V,\mathrm{HDE}}$ using Eq.(2.125) and (2.126), reminding that Eq.(2.127). And we find that[112]

$$m^3_{V,\mathrm{HDE}} \approx \frac{2}{3\pi^5} \alpha^2 N \gamma_w T^3_{\mathrm{nuc}} \sum_{ABC} g_A \nu_A C_{ABC}, \tag{2.129}$$

from which we observe that $m_{V,\mathrm{HDE}}$ grows with $\gamma_w^{1/3}$, and could eventually catch up on the mass on the higgsed side $m_{V,h}$. When this occurs, we need to go back to our early expression for the computation of the probability of transition:

$$\begin{aligned} \mathcal{P}_{\psi\to V\psi} &= \int \frac{d^3p}{p_0(2\pi)^6} f_\psi \int_{m_{V,\mathrm{HDE}}/p_0} \frac{dx}{x^2} \int_{m_{V,\mathrm{HDE}}} \frac{d^2k_\perp}{k^2_\perp} \frac{m^4_{V,h}}{(k^2_\perp + m^2_{V,h})} \\ &\approx \int \frac{d^3p}{p_0(2\pi)^6} f_\psi \int_{m_{V,\mathrm{HDE}}/p_0} \frac{dx}{x^2} \int_{m_{V,\mathrm{HDE}}} \frac{d^2k_\perp}{k^4_\perp} m^4_{V,h}. \end{aligned} \tag{2.130}$$

However, the backreaction also concerns the HDE effect in Eq.(2.126)

$$f_V(p) = \sum_i g_A \int \frac{d^3p_A}{(2\pi)^2} f_A(p_A) \frac{dP_{A\to BC}(m_{V,\mathrm{HDE}})}{d^2k_\perp dp^0} \tag{2.131}$$

which changes behaviour as well and backreacts on $m_{V,\mathrm{HDE}}$. Doing a similar computation than before, we find $m^7_{V,\mathrm{HDE}} \propto \gamma_w$. Collecting the terms in a similar and computing the pressure on the bubble with cut-off given by $m_{V,\mathrm{HDE}}$, we obtain

$$m_{V,\mathrm{HDE}} > m_{V,h} \quad \Rightarrow \qquad \mathcal{P} \propto m_{V,\mathrm{HDE}} \gamma_w \left(\frac{m_{V,h}}{m_{V,\mathrm{HDE}}} \right)^4 T^3 \propto \gamma^{4/7}. \tag{2.132}$$

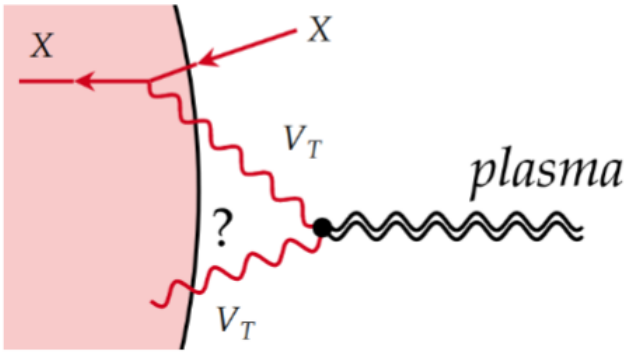

Figure 2.7: Cartoon of the possible reflection of soft gauge boson on thermal plasma entering the bubble. Thanks to *Giulio Barni* for sharing this nice cartoon!

since $m_{V,\mathrm{HDE}}\gamma_w\left(\frac{m_{V,h}}{m_{V,\mathrm{HDE}}}\right)^4 \propto \gamma_w^{3/7}$. It remains to determine when this saturation $m_{V,\mathrm{HDE}} > m_{V,h}$ becomes a possibility. Saturation occurs when (here v is the scale of symmetry breaking)

$$m_{V,h} \sim \alpha^{1/2} v < m_{V,\mathrm{HDE}} \sim \alpha^{2/3} T_{\mathrm{nuc}} \gamma_{w,\mathrm{terminal}}^{1/3} \sim \alpha^{2/3} T_{\mathrm{nuc}} \frac{\Delta V^{1/3}}{v^{1/3}\alpha^{1/2} T_{\mathrm{nuc}}}$$

$$\text{Saturation possible if:} \quad \Rightarrow \quad \boxed{v^4 < \frac{\Delta V}{\alpha}} \tag{2.133}$$

which is the case of very strong release of energy, or very weakly coupled theories. [96] already noted that even $\gamma_w^{4/7}$ is typically enough to prevent runaway walls. However, the arguments given here remain quite hand-waving and would deserve further investigation.

The previous discussion was mostly relying on a perturbative computation. In the case of *non-abelian gauge theories*, such a large density can induce the breaking of perturbative expansion, via the 3-bosons and 4-bosons vertices. Though this is also an issue which is plagued with uncertainties, let us give a flavor of it. The possible loss of perturbativity can be seen in the following way. In thermal field theory, the expansion parameter is typically

$$(\text{coupling})^2 f_C(p) \tag{2.134}$$

and perturbativity then requires that this quantity is much smaller than 1 for all p. This means that in the phase space of volume $m_{V,h}^{-3}$, a density of gauge bosons $T_{\mathrm{nuc}}^3 \gamma_w$ is accumulating. It is clear that

$$f_C(m_V) \sim \frac{n_V}{m_{V,h}^3} \propto \gamma_w \tag{2.135}$$

will become larger than the perturbativity bound $\frac{1}{(\text{coupling})^2}$. Despite the conclusions exposed here, the saturation regime remains mostly unexplored and we do not know what is going on there.

- **A thin surface of soft gauge bosons in front of the wall** Finally, let us come to a last comment about the dynamics of the emission of soft gauge bosons. We have seen that according to our previous results a substantial fraction

$$\sim \frac{\log m_{V,h}/gT}{\log \gamma_w T/gT} \tag{2.136}$$

of the soft gauge bosons will not be able to enter the wall, as their momentum is very soft, see Eq.(2.117). We could thus wonder what will happen to those *reflected* soft gauge bosons. The abundance of reflected gauge bosons is approximated by

$$n_{\rm ref} \sim n_A g^3 \log \frac{m_{V,h}}{g T_{\rm nuc}} \propto \gamma_w \tag{2.137}$$

After reflection, those gauge bosons will collide with the incoming dense plasma, as illustrated in Fig.(2.7). What will happen at this moment ? As a first simplifying assumption, let us consider that the gauge bosons are produced continuously by the wall, but are trapped by $2 \to 2$ scatterings in a layer of thickness $l_{\rm trapped}$. We can approximate the length of the trapped region $l_{\rm trapped}$ by :

$$l_{\rm trapped} \sim \frac{p_{z,c}^2}{\alpha^2 T_{\rm nuc}^3} \lesssim \frac{m_{V,h}^2}{\alpha^2 T_{\rm nuc}^3} \tag{2.138}$$

where R is the radius of the bubble. If those gauge bosons are not able to enter the bubble, the density will increase in a thin layer of thickness $l_{\rm trapped}$, as

$$n_{\rm soft}(R) \propto \frac{R}{l_{\rm trapped}} n_A g^3 \log \frac{m_{V,h}}{g T_{\rm nuc}}, \tag{2.139}$$

where R is the radius of the bubble. This will threaten again the perturbativity of the plasma. This regime as well has to be studied in more depth. Again, what occurs to this thin layer is mostly unknown.

2.4 The friction theory in the SM and in dark PT

In this final section of this chapter, we would like to present some few applications of the full theory of bubble friction in the relativistic regime that we developed above. We will also take the opportunity to summarize all the effects exposed above. As a consequence, we can see this section as a general guideline on how to compute the velocity in the semi-classical regime.

2.4.1 Dynamics of the bubble wall: Generic case

Let us now apply the theory developed above to the case of a dark transition triggered by the Higgs-like field φ acquiring a VEV v. We focus on the regime with ultra-relativistic bubble wall expansion with $\gamma_w \gg 1$. This regime is favoured when the transition is strong enough to develop at least some amount of supercooling. The dynamics of the bubble wall motion is controlled by the driving force due to the potential differences between the false and true vacuum

$$\Delta V \equiv V_{\rm false} - V_{\rm true} \ , \tag{2.140}$$

and the friction due to finite temperature effects. As we have seen, the calculation of the friction is generically a very complicated problem, however for the ultra-relativistic bubble motion at leading order (LO - tree level) very simple expressions have been obtained in section 2.3.1 for the pressure force from friction,

$$\Delta \mathcal{P}_{\rm LO} \simeq \sum_i g_i c_i \frac{\Delta M_i^2}{24} T_{\rm nuc}^2 \ , \tag{2.141}$$

where ΔM_i^2 is the change in the mass of the particle i during the PT, $c_i = 1\,(1/2)$ for bosons (fermions) and g_i is the number of d.o.f of the incoming particle. Eq.(2.141) assumes that the masses of the particles outside of the bubble are less than the temperature, otherwise the friction will have an additional Boltzmann suppression $\propto \exp[-M_{\rm false}/T]$. Secondly, the production of the heavy particles can also contribute to the friction at the same order as we have computed in section 2.3.3:

$$\Delta\mathcal{P}_{\rm LO}^{\rm mixing} \propto \sum_i g_i c_i \frac{v^2 T_{\rm nuc}^2}{24}\Theta(\gamma_w T_{\rm nuc} - M_{\rm heavy}^2/v)\ . \tag{2.142}$$

One can see that the friction (pressure from plasma on the bubble wall) becomes velocity independent so that permanent accelerating (runaway) behavior of the bubble expansion becomes possible. However for theories where the gauge bosons receive a mass during the phase transition, this is not the case and the effect with multiple gauge boson emissions, leads to the additional contribution (NLO- Next to Leading order) to the pressure which scales as we have discussed in section 2.3.4,

$$\Delta\mathcal{P}_{\rm NLO} \quad \propto \quad \frac{\sum_a g_a g_{\rm gauge}^3}{16\pi^2}\gamma_w T_{\rm nuc}^3 v\ . \tag{2.143}$$

At this point we can see that bubbles can end up in two different regimes :

1. **Runaway regime:** When the PT does not involve phase-dependent vectors, there is no NLO pressure and the wall keeps accelerating until collision. The γ_w at collision is [37, 1]

$$\gamma_{w,\rm MAX} \simeq \frac{2R_*}{3R_0}\left(1 - \frac{\mathcal{P}_{\rm LO} + \mathcal{P}_{\rm mixing}}{\Delta V}\right), \quad R_0 \sim 1/T_{\rm nuc}, \quad R_* \approx \frac{(8\pi)^{1/3} v_w}{\beta(T_{\rm nuc})},$$
$$\beta(T) = HT\frac{d}{dT}\left(\frac{S_3}{T}\right) \sim \tilde{\beta}H \sim \frac{\tilde{\beta}v^2}{M_{\rm pl}} \quad \Rightarrow \gamma_{w,\rm MAX} \sim \frac{M_{\rm pl}T_{\rm nuc}}{v^2\tilde{\beta}}, \tag{2.144}$$

   where $R_\star$ is an estimate for the bubble size at collision and R_0 is the bubble size at nucleation, β is the inverse duration parameter of the transition.

2. **Terminal velocity regime:** Terminal velocity regime can arise for two reasons: i) we hit some high scale physics with new states that induce a new pressure via mixing pressure. In this case, we have to search the contribution such that

$$\mathcal{P}_{\rm LO} + \mathcal{P}_{\rm mixing} = \Delta V \tag{2.145}$$

   and the terminal velocity is given by the velocity needed to activate the heavy states:

$$\gamma_{w,\rm terminal} \approx \frac{M_{\rm Heavy}^2}{vT_{\rm nuc}}. \tag{2.146}$$

   Or, ii) when the PT gives a mass to vectors, the pressure becomes dominated by the emission of ultra-soft bosons and quickly wield a terminal velocity of the form

$$\Delta\mathcal{P}_{\rm NLO} \simeq g_i g_{\rm gauge}\gamma_w T_{\rm nuc}^3\frac{v}{16\pi^2}, \qquad \Delta V \sim v^4 \tag{2.147}$$
$$\Delta V = \Delta\mathcal{P}_{\rm NLO} \qquad \Rightarrow \gamma_{w,\rm terminal} \approx \text{Min}\left[\frac{M_{\rm pl}T_{\rm nuc}}{v^2\tilde{\beta}}, \frac{16\pi^2}{g_i g_{\rm gauge}^3}\left(\frac{v}{T_{\rm nuc}}\right)^3\right],$$

   where in the last step we have to take the minimal of the two values, since the bubble collision can happen before the terminal velocity regime is reached.

2.4.2 Dynamics of the bubble wall: EWPT case

A particularly relevant special case is the EWPT case, as it is very likely that this transition must have occurred in the early universe. Though, lattice simulations of the pure SM indicates that the EWPT is a smooth cross-over, in Chap.5 we will provide a realisation of the transition which is strongly first order and we will focus on the region with relativistic walls. In this section, we would only like to lay down the formulas that will be later used.

Let us start with the LO friction. It is dominated by species gaining a large mass, the top, Z, and W and takes the form:

$$\Delta\mathcal{P}_{\rm LO}^{SM} \approx T_{\rm nuc}^2 v_{EW}^2 \left(\frac{y_t^2}{8} + \frac{g^2+g'^2}{32} + \frac{g^2}{16}\right) \approx 0.17 T_{\rm nuc}^2 v_{EW}^2. \tag{2.148}$$

There is also a contribution to the LO friction from the singlet and Higgs scalars, however it depends on the masses of these fields in the false vacuum and we find it subleading compared to the estimate in Eq. (2.148). These contributions are smaller due to the number of d.o.f and possible Boltzmann suppression factors $\propto \exp[-M_{\rm false}/T]$. This gives a rough condition on the nucleation temperature for the transition to become ultra-relativistic

$$\Delta V > 0.17 T_{\rm nuc}^2 v_{EW}^2 \qquad \text{(relativistic wall condition)}. \tag{2.149}$$

The computation of the NLO pressure from transitions $A \to BC$, with soft C, in the case of the SM has been carried out in [112] and in section 2.3.4, with the addition of higher order transitions, where the following approximate expression has been derived:

$$\Delta\mathcal{P}_{\rm NLO}^{SM} \approx \left[\sum_{ABC} \nu_A g_A \beta_C C_{ABC}\right] \frac{\kappa\zeta(3)}{\pi^3} \alpha M_Z(v_{EW}) \gamma_w \log\frac{M_Z(v_{EW})}{g T_{\rm nuc}} T_{\rm nuc}^3, \tag{2.150}$$

where $\nu_a = 1(3/4)$ for a a boson (fermion), g_a is the number of degrees of freedom of A, M_V designates the mass of a gauge boson, C_{ABC} is relevant to the coupling appearing in the vertex,$\beta_{c=Z^0} = 1$, and $\beta_{c=W^\pm} = \cos\theta_W = \frac{M_W}{M_Z}$, $\alpha = \frac{e^2(v_{EW})}{4\pi} \sim 1/128$ is the electromagnetic fine structure constant, $M_{V,i}(v_{EW})$ is the mass of the gauge boson inside the bubble. The κ factor is introduced to account for the contributions of the both reflected and transmitted bosons and is approximately equal to $\kappa \sim 4$. The sum in the square brackets will be computed in section below and is approximately equal to

$$\left[\sum_{ABC} \nu_A g_A \beta_C C_{ABC}\right] \approx 157, \tag{2.151}$$

Since, we do not know heavy particles in the SM that could contribute via the mixing pressure, we do not take it into account here. At this point we can compute the terminal wall velocity by balancing the pressure against the driving force

$$\begin{aligned} \Delta V - \Delta\mathcal{P}_{\rm LO}^{SM} &= \Delta\mathcal{P}_{\rm NLO}^{SM}(\gamma_w = \gamma_w^{\rm terminal}) \qquad \text{(Terminal velocity criterion)} \\ &\Rightarrow \gamma^{\rm terminal} \sim 3 \times \left(\frac{\Delta V - P_{\rm LO}}{(100\ {\rm GeV})^4}\right) \left(\frac{100{\rm GeV}}{T_{\rm nuc}}\right)^3 \frac{1}{\log\frac{M_Z}{gT}}. \end{aligned} \tag{2.152}$$

Taking into account that $\frac{\Delta V - P_{\rm LO}}{(100\ {\rm GeV})^4} \lesssim \mathcal{O}(1)$, we can see that the bubbles will become ultra-relativistic $\gamma^{\rm terminal} \gg 1$ if only $T_{\rm nuc}$ is significantly lower than the scale of the phase transition ~ 100 GeV. This is an interesting result!

The coefficient of NLO pressure Following closely[112], let us now report the value of the sum

$$\Big[\sum_{ABC} \nu_A g_A \beta_C C_{ABC}\Big] \tag{2.153}$$

where $\nu_a = 1(3/4)$ for A a boson (fermion), $\beta_C \equiv \frac{M_C}{M_Z}$and C_{ABC} stands for the couplings appearing in the vertex. Normalization of the C_{ABC} coefficient is the following:

for a chiral fermion coupled to the vector field the amplitude for the process $\psi \to \psi A_{soft}$ is equal to

$$g_\psi \bar{\psi}_L A_\mu \psi_L \Rightarrow \quad C_{\psi\psi A} = \frac{g_\psi^2}{4\pi\alpha_{em}}. \tag{2.154}$$

The relation Eq.2.154 is written only for one polarization of the vector field. Similarly for the scalar field

$$i g_\phi(\phi^* \partial_\mu \phi - \partial_\mu \phi^* \phi) A^\mu \Rightarrow \quad C_{\phi\phi A} = \frac{g_\psi^2}{4\pi\alpha_{em}}, \tag{2.155}$$

and the vector fields

$$g_{V^1V^2A^3}\left(V^1_{\mu\nu} V^2_\mu A_\nu + V^2_{\mu\nu} A_\mu V^1_\nu + A_{\mu\nu} V^1_\mu V^2_\nu\right) \Rightarrow C_{V_1V_2A} = \frac{g^2_{V^1V^2A}}{4\pi\alpha_{em}}, \tag{2.156}$$

where in all of these formulas C_{ABC} coefficients are reported only for one polarization vector fields both in the initial and the final states. Summing all of these contributions and taking care of the multiplicities of the initial and final states we find

$$\Big[\sum_{ABC} \nu_A g_A \beta_C C_{ABC}\Big] = 4\left(\frac{7 + 14 c_w}{s_w^2} - \frac{7 - 15 s_w^2}{c_w^2}\right) \simeq 157. \tag{2.157}$$

For the interested reader we refer various individual contributions in the Table 1. If in the false vacuum the Higgs doublet $\mathcal{H}$ is too heavy its contribution must be subtracted and the sum in Eq.2.157 reduces to

$$\Big[\sum_{ABC} \nu_A g_A \beta_C C_{ABC}\Big]_{\text{No Higgs}} \simeq 145. \tag{2.158}$$

At last we would like to emphasize that these results include only the transverse polarizations of the vector fields. As we discussed in section 2.3.4, NLO effects of the longitudinal polarizations are not fully established and we omit them here, however we believe that these cannot qualitatively modify the results.

Process	$\sum g_a C_{abc}$	β	ν	Result
$\psi \to W^{\pm}\psi$	$\frac{24}{s_w^2}$	c_w	$\frac{3}{4}$	$\frac{18c_w}{s_w^2}$
$\psi \to Z\psi$	$\frac{4(3-6s_w^2+8s_w^4)}{s_w^2 c_w^2}$	1	$\frac{3}{4}$	$\frac{3(3-6s_w^2+8s_w^4)}{s_w^2 c_w^2}$
$\mathcal{H} \to W\mathcal{H}$	$\frac{2}{s_w^2}$	c_w	1	$\frac{2c_w}{s_w^2}$
$\mathcal{H} \to Z\mathcal{H}$	$\frac{1-2s_W^2 c_W^2+c_W^4+s_W^4}{2s_W^2 c_W^2}$	1	1	$\frac{1-2s_W^2 c_W^2+c_W^4+s_W^4}{2s_W^2 c_W^2}$
$A \to W_{soft}W$ & $W \to W_{soft}A$	8	c_w	1	$8c_w$
$Z \to W_{soft}W$ & $W \to W_{soft}Z$	$\frac{8c_w^2}{s_w^2}$	c_w	1	$\frac{8c_w^3}{s_w^2}$
$W \to Z_{soft}W$	$\frac{4c_w^2}{s_w^2}$	1	1	$\frac{4c_w^2}{s_w^2}$
Total:				$2\left(\frac{7+14c_w}{s_w^2} - \frac{7-15s_w^2}{c_w^2}\right) \simeq 157$

Table 2.1: Different contributions to the sum in Eq.(2.150).

Chapter 3

Production of Dark Matter via relativistic bubble expansion

THE mystery of Dark Matter (DM) is one of the leading area of investigation in Cosmology and Particle physics and has many subdivisions and sub-questions, from the construction and conception of new detectors, to the non-linear evolution of DM in galactic halos. On the theoretical side, two of those sub-questions concern the *nature* and the *mechanism of production of DM* in the early universe. Obviously, those two problems are related and some specific mechanism is expected to work only with some specific sub-classes of DM candidates. Without trying to be exhaustive, in this chapter, we will present some potential DM candidates and discuss associated production mechanisms. We will see that thermal freeze-out with WIMPs is increasingly under pressure and so we will search for non thermal production mechanism. Phase transitions offer an intriguing prospect for the non-thermal production of DM and permits to broaden the range of masses of DM consistent with observation. In the previous chapter, we presented how heavy states can be produced during the expansion of relativistic bubbles, in this chapter, we study the exciting possibility that those produced states are stable and constitute the DM observed today. We find that super-heavy DM candidate can be copiously produced in that way.

Contents

3.1 The necessity of Dark Matter

Cosmological observations conspire to suggest the existence of a massive, undetected, dark component permeating the universe: this is the Dark Matter (DM) phenomenon. This phenomenon has a very long history and a monumental associated literature (see [115] for a condensed history of this adventure). In particular it is one of the very first bridge between particle physics and cosmology, two initially separated fields that got closer and closer and finally constituted the today called "astroparticle" field.

The implementation of more or less *ad hoc* hypothesis to explain a phenomenon that was not anticipated by the theory has a long history in physics. We can for example think of the involved modifications of the Ptolemy geocentric model or, much later, the bold hypothesis, proposed by *Urbain Le Verrier* and *John Couch Adams* in 1846, of the existence of a new planet, *Neptune*, to explain the anomalies in the trajectory of Uranus. Those solutions, which imply to postulate a new body, particle, or player of any sort, to explain the observation while keeping the theory intact, can be called a *ontological* solution.

On the other hand, reconciliation between observation and theory sometimes needed the drastic modification of the theory. Two examples for which spectacular departure from previous theories was indeed necessary are the *anomalous precession of the perihelion of Mercury* and the *Ultravioled catastrophy* of black bodies, leading respectively to the two pillars of contemporary physics, *General Relativity* and *Quantum Mechanics*[1]. Such a solution can be recast under the name of a *legislative* solution, since it requires a modification in the structure of the laws followed by the bodies.

Those two types of solutions often coexist when some field of physics encounters a crisis. Le Verrier, who himself discovered the anomalous precession of the Mercury perihelion and proposed the existence of Neptune, proposed for a second time an ontological solution to the problem; he postulated the existence of a dark planet, *Vulcan*. However, in did not go as well as with Neptune.

The hypothesis of non-observable matter in the sky is actually much older than the Zwicky's hypothesis. One early examples is the hypothesis by *Arthur Ranyard* in *Knowledge*, 1894, to explain the dark regions in the sky. He argued that "dark structures" were absorbing the light on the line-of-sight, inducing dark regions in the sky. The question was reassessed by *Lord Kelvin* in 1904[2], who, by modelling the distribution of stars as a gas of particles, predicted the presence of a large amount of dark bodies. *Poincaré* [3] pushed the analysis further and used for the first time the name of "dark matter".

But it is indeed the Swiss-American astronomer *Fritz Zwicky* who is known today as the most fervent promoter of DM. After the seminal work of *Edwin Hubble* and *Milton Humason*[4] on the scattering velocities of galaxies in the Coma clusters, he applied the *virial theorem* to determine the mass of the cluster and concluded, after several approximations, that "dark matter is present in much greater amount than luminous matter" [5]. Then [116] he

[1]The history is very famous and, to some extent I guess, mythical.
[2]https://archive.org/details/baltimorelecture00kelviala.
[3]Poincaré, H. (1906), L' Astronomie , 158
[4]Hubble, E., and M. L. Humason (1931), Astrophys. J. 74, 43.
[5]Zwicky, F. (1933), Helvetica Physica Acta 6, 110.

proposes some candidates for the excess of matter; "we must know how much dark matter is incorporated into nebulae in form of *cool and cold stars*, *macroscopic and microscopic solid bodies*, and *gases*."

On the side of galactic rotation curves, the discrepancies extend to much before the seminal publications by Vera Rubin and Kent Ford, however, it is the turn of the 1970' that brought all the material to the consensus. It is among the radio-astronomers Freeman[117] and Rogstad and Shostak [118], that claims of missing matter emerged with clarity. Some few years later, using optical rotation curves from 10 high luminosity galaxies, V.Rubin, Ford and Thonnard[119] established the issue of the missing mass the most famously. The observed galactic rotation curve of NGC 6503 is provided on the left panel of Fig.3.1, where we can observe the flat behaviour at large distance form the center, in contrast with the velocity that would be predicted by

$$v(r) = \sqrt{\frac{G_N M(r)}{r}} \tag{3.1}$$

where $M(r)$ is the mass enclosed in the radius r. A flat behaviour of v means that the mass increases with r linearly.

It was finally the understanding of the CMB and the Baryonic Acoustic Oscillations (BAO) that finished to convince most of the cosmologists of the existence and the necessity of Dark Matter under the form of microscopic particle (a fundamental excitation) or macroscopic object (for example primordial black holes). Indeed, observation of the CMB peaks requires the existence of a gravitational driving for the oscillations of the baryon and photon fluids. This gravitational driving is provided by the potential wells of clumped DM. Perhaps counterintuitively, during radiation domination, adding more DM density would actually reduce the gravitational driving and thus the height of the higher CMB peaks, which are resolved with a great accuracy, as seen in Fig.3.1. The reason goes as follows: higher peaks started to oscillate earlier in the universe history, when the radiation dominated the energy budget. However, the pressure of the photons tends to compensate the gravitational potential, which decay when the photons compress. The photons then bounce back due to pressure and see no gravitational potential. Then the peak is enhanced. This mechanism of suppression of the gravitational potential is however inefficient during matter domination, and the peaks are suppressed. This is the case of lowest order peaks. The density of photons being fixed by the thermal history and the average temperature of the CMB today, the density of DM can be extracted by measuring the height of the higher order peaks[6]. As a conclusion, if DM was absent, lowest order peaks (oscillation when DM domination) would be enhanced.

From CMB observation, the observed abundance of DM today is

$$\Omega_{\rm DM} \equiv \frac{\rho_{\rm DM}}{\rho_c} \approx 0.1 \qquad \text{(Density of DM today).} \tag{3.2}$$

This is our target value.

Many candidates for the nature of DM have been proposed, they are for example reviewed in [122]. In this thesis, and in the following, we will be focusing on the case of rather heavy (multi-TeV) fundamental DM candidate and will now review some of the usual mechanisms of early universe production of the observed abundance. Acknowledging the existence of DM around the recombination time, we are naturally lead to believe in its existence at much earlier time, in the first seconds of the universe. On the other hand, our strong belief in a very early period of inflation washing away any initial abundance forces us to build a mechanism for the production of this DM abundance that we observe today. Since injection of entropy is severely constrained by BBN we are lead to search this mechanism in the first second of the universe, prior to BBN.

[6]See http://background.uchicago.edu/ whu/intermediate/driving.html for nice animations of the physics involved

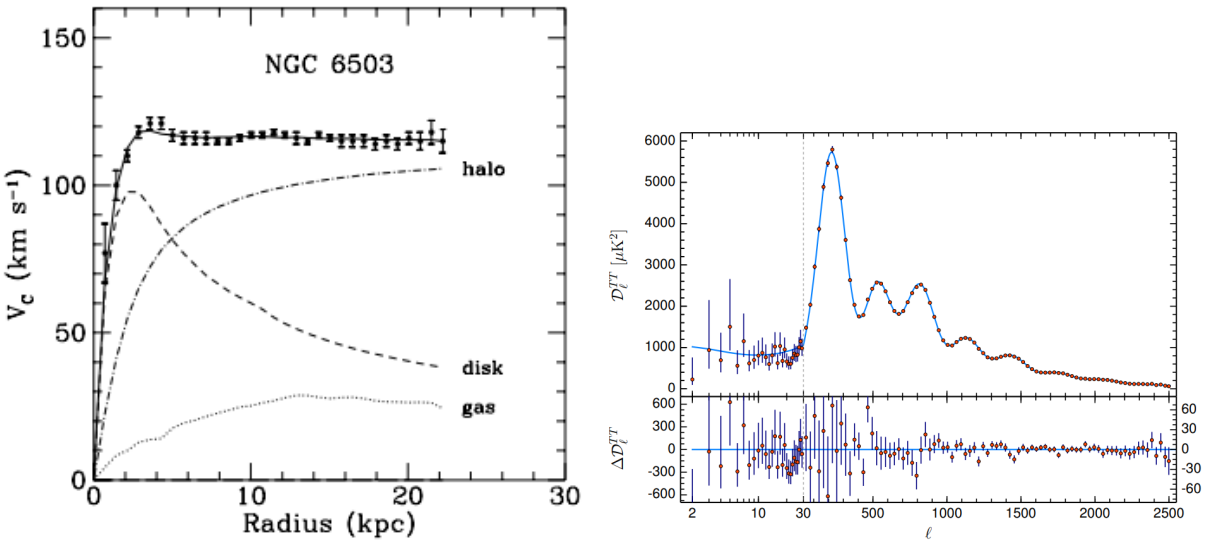

Figure 3.1: **Left**: Rotation curve of the galaxy NGC 6503 [120]. **Right**: CMB curve from [121]. CMB observation is probably the most solid argument in favor of the presence of DM, even at very early times.

3.2 Mechanism of DM production

So, as soon as we pick up a candidate for DM, with a nature, some interaction with the SM (possibly vanishing) and a typical mass scale, the question of its early universe production arises, accompanied by the requirement that the produced abundance should match the redshifted abundance of DM today in Eq.(3.2). Though most of those mechanisms rely on early universe dynamics, a great variety of possibilities already exists. In this section, we would like to discuss the freeze-out (FO) in some details, as the results will be useful in the next sections.

The Freeze-Out One of the early cosmological mechanism to produce dark matter is the well-known *freeze-out* mechanism[123, 124, 125, 126] (FO), which was put forward in the context of WIMP [127]. In a nutshell, this mechanism assumes that the DM candidate of mass M_ϕ, which can be fundamental or composite, is in thermal equilibrium in the early universe and couples to the SM via some portal, e.g. the Higgs portal.

As a warm-up exercise, let us go through the famous computation of the final relic abundance of FO. We want to compute the relic abundance

$$\Omega_\phi h^2 \equiv \frac{\rho_\phi}{\rho_c}, \qquad \rho_\phi = M_\phi n_\phi = M_\phi s Y_\phi \tag{3.3}$$

where we defined the usual $Y_\phi = \frac{n_\phi}{s}$.

For concreteness and for the purpose of future use, we consider a real scalar DM candidate ϕ. The first assumption that we need is that ϕ is firstly in thermal equilibrium with the SM via, for example, the *Higgs portal* $\propto \phi^2|\mathcal{H}|^2$, inducing $\phi\phi \leftrightarrow hh$ interactions. In this scenario, kinetic equilibrium is reached and the ϕ sector and the SM sector share the same temperature $T_{\rm SM}$, that we will simply call now T. At $T \gg M_\phi$, the abundance of DM follows the radiation abundance $n_\phi \propto T^3$. However, when $T \ll M_\phi$, $\phi\phi \to hh$ becomes favored with respect

to the opposite reaction and the ϕ abundance starts to be exponentially depleted, $n_\phi \propto (TM_\phi)^{3/2}e^{-M_\phi/T}$. At this point we need to remember that the expansion of the universe sets a scale that can compete with the rate of the interaction, and eventually overrules it. Thus, to precisely track the abundance of ϕ we need to solve the following BE

$$\dot{n}_\phi + 3Hn_\phi = \mathcal{C}, \qquad \mathcal{C} = -\langle\sigma v\rangle[n_\phi^2 - (n_\phi^{\rm eq})^2] \quad \Rightarrow \qquad \dot{Y}_\phi = -\langle\sigma v\rangle[Y_\phi^2 - (Y_\phi^{\rm eq})^2], \tag{3.4}$$

where the dot designates a derivative with respect to time and the brackets $\langle\rangle$ mean a thermal average of the form

$$\langle\sigma_{ij}v_{ij}\rangle = \frac{\int d^3\mathbf{p}_i d^3\mathbf{p}_j f_i f_j \sigma_{ij} v_{ij}}{\int d^3\mathbf{p}_i d^3\mathbf{p}_j f_i f_j} \tag{3.5}$$

and σ_{ij} is the cross-section of the collision and v_{ij} is the relative velocity of the two particles colliding

$$v_{ij} = \frac{\sqrt{(p_i \cdot p_j)^2 - M_i^2 M_j^2}}{E_i E_j}. \tag{3.6}$$

From the Eq.(3.4), we see that a strong rate of interaction $\propto \langle\sigma v\rangle n_\phi^{\rm eq}$ quickly suppresses any departure from the equilibrium abundance $n_\phi^{\rm eq}$, so we can conclude that as long as the expansion of the universe can be neglected, the interactions enforce chemical equilibrium. We can still further simplify it by introducing $z = \frac{M_\phi}{T}$, and assuming radiation domination, we obtain

$$\frac{dY_\phi}{dz} = -\frac{zs\langle\sigma v\rangle}{H(T=M_\phi)}[Y_\phi^2 - (Y_\phi^{\rm eq})^2]. \tag{3.7}$$

This equation is a *Riccati* equation, which cannot be solved in a closed form. Solving this equation exactly requires a numerical treatment. However, we can build a solid intuitive understanding by studying the *freeze-out epoch*, the moment when the rate of the interaction drops below the expansion rate of the universe:

$$\langle\sigma v\rangle n_\phi^{\rm eq}(z_{\rm FO}) \sim H(z_{\rm FO}) \qquad \text{(Freeze-out epoch)}. \tag{3.8}$$

Going back to Eq. (3.4), this is the epoch when the collision term becomes negligible with respect to the friction term coming from the expansion. This induces a departure from equilibrium distributions $n_\phi \neq n_\phi^{\rm eq}$. At this point, we should also mention that another possibility is that the interaction could freeze-out even before the temperature drops below the mass of the DM. This would be typically the case of neutrino, or neutrino-like particles. We thus end up with two possible regimes i) $z_{\rm FO} \ll 1$ and ii) $z_{\rm FO} \gg 1$. In the first case, the DM candidate abundance freezes-out when the distribution is still relativistic $n_\phi \propto T^3$. This is the so-called *Hot Dark Matter* (HDM) scenario, which is mostly ruled out by the formation of structures in the early universe[122]. In the second case, on the other hand, the FO occurs when DM particles are non-relativistic, and produces *Cold Dark Matter* (CDM)[7]. Solving (3.8) provides the following result

$$\begin{aligned} z_{\rm FO}^{1/2}e^{-z_{\rm FO}} &= \sqrt{\tfrac{\pi^2}{90}g_\star}\tfrac{(2\pi)^{3/2}}{M_{\rm pl}M_\phi g_\phi\langle\sigma v\rangle} \qquad \text{(FO epoch)} \\ Y_\phi(z_{\rm FO}) = \tfrac{g_\phi}{g_\star}\tfrac{45}{2\pi^2(2\pi)^{3/2}}z_{\rm FO}^{3/2}e^{-z_{\rm FO}} &\Rightarrow Y_\phi(z_{\rm FO}) = \sqrt{\tfrac{45}{8\pi^2 g_\star}}\tfrac{z_{\rm FO}}{M_{\rm pl}M_\phi\langle\sigma v\rangle} \simeq \tfrac{z_{\rm FO}}{4\pi M_{\rm pl}M_\phi\langle\sigma v\rangle} \end{aligned} \tag{3.9}$$

with $g_\star$ is the number of relativistic degrees of freedom in the plasma and g_ϕ is the number of degrees of freedom of the DM and we remind that $M_{\rm pl}$ is the reduced Planck mass. Solving the first equation typically gives $z_{\rm FO} \approx 20$.

[7]Notice also the possibility of a middle ground under the name of *Warm Dark Matter*, which would be gravitini or some WIMPs.

This is an important result and we call usually the freeze-out temperature $T_{\rm FO} \approx M_\phi/20$. If we can consider that $\langle \sigma v \rangle \sim \frac{\lambda^2}{4\pi M_\phi^2}$, we obtain

$$\boxed{\Omega^{\rm today}_{\rm CDM,\,FO} h^2 \approx 0.1 \left(\frac{0.03}{\lambda}\right)^2 \left(\frac{M_\phi}{100\ {\rm GeV}}\right)^2 .} \tag{3.10}$$

or more generically

$$\Omega^{\rm today}_{\rm CDM,\,FO} h^2 \approx 0.1 \left(\frac{\langle \sigma v \rangle_{FO}}{3 \times 10^{-26} {\rm cm}^3 s^{-1}}\right)^{-1} \tag{3.11}$$

This is the famous CDM abundance via FO. From this result we easily observe that a mass of order $\mathcal{O}(100)$ GeV with a weak coupling order $\mathcal{O}(0.03)$ would reproduction the observed abundance of $\Omega^{\rm today}_{\rm DM,\,FO} h^2 \approx 0.1$. This is the *WIMP miracle* and has lead to the strong conviction that the DM had to lie within the range of exploration of colliders, and maybe as a state of low energy supersymmetry.

However, today, many WIMP models have been excluded due to the bounds on the DM-nucleon scattering set by the direct detection experiments[128, 129, 130, 131, 132]. See also[133] for a review on the status of WIMPS and a good review on portal Higgs can be found in[134]. Moreover, vanilla FO mechanism comes with an embedded bound on the possible mass of DM, which originates from unitarity considerations on the coupling governing the scattering[135], the *Griest-Kamionkowski (GK) bound* of $O(100)$ TeV. Starting from Eq.(3.10) and pushing the coupling λ to its unitary limit $\lambda_{\rm MAX} \sim 4\pi$, the requirement to match the observed abundance imposes an upper bound on the DM mass

$$M_\phi \lesssim \mathcal{O}(100)\ \text{TeV} \qquad \text{(GK bound on thermally produced DM)} \tag{3.12}$$

Extrapolating the previous result in Eq.(3.12) means that any *stable* massive particle $M \gg 100$ TeV that reaches thermal equilibrium in the early universe would overclose the universe (assuming standard cosmology).

This bound as well as direct detection null results mentioned above seem to strongly constrain any *fundamental* particle coupling *via a* $2 \to 2$ *interaction*, that reached *thermal equilibrium* in the *standard early universe* history. A review of the domain of thermal DM is given in [136]. We will now see how relaxing each of those assumptions can enlarge the spectrum of possibilities.

3.2.1 Modifying the Freeze-Out case

As we said, relaxing any of the four above hypothesis above would enlarge the spectrum of possibilities. Let us go step by step:

- **Abundance controlled by standard $2 \to 2$ interaction**: we can first relax the form of the interaction of SM and the DM. Many models along those lines have been proposed recently, let us provides some few examples. We can introduce the possibility of catalyzed interaction via a catalyst[137]. In [138, 139] exponential enhancement of the annihilation in the early universe was also obtained by the introduction of a new field χ [8]. On the other hand, we can seclude the DM sector via the introduction of a mediator with a mass below the DM mass $m_{\rm med} \ll m_{\rm DM}$[140] such that the production via FO is maintained, but detection prospect today

[8] They showed us that no one was safe from a pandemic, not even DM.

is heavily suppressed, could also explain the null result at experiments. Another possibility is to have [126] two nearly degenerate states, boosting the annihilation rate in the early universe. By extension, the possibility of having many almost degenerate dark sector particles also permits to lift the mass of the DM[141] to a tantalizing mass of 10^{14} GeV without violating GK bound.

- **DM is a fundamental state**: The FO abundance is also largely modified in the case of technicolor-like theories, where we relax the assumption that DM is a fundamental state, and can relieve most of the bounds coming from direct detection. Before confinement, the technifermions degrees of freedom interact directly via renormalisable interactions with the SM degrees of freedom, fixing the relic abundance of DM. On the other hand, if after the confinement, the technibaryons are neutral under the weak SM interactions and thus only interact via non-renormalisable operators, the detectability today is very suppressed[142, 143]. In this condition, the interaction arises from form factors. If the strong dynamics plays a role in the EW symmetry breaking, then we are in the context of technicolor theories. In the case of technicolor models, the lightest technibaryon can be possibly identified, if stable enough, with DM. Those models provide natural models of decaying DM. However, the case of technicolor Dark Matter remains very difficult[144, 145]. On the other hand, if the strong dynamics does not play a role in the breaking of the weak symmetry, then we relieve most of the constraints from observation[146, 147].

- **DM reached thermal equilibrium**: Another possibility is to assume that DM never reached thermal equilibrium with the SM. This can be realised if the coupling between the SM and the DM is extremely small and DM abundance is created via slow out-of-equilibrium production: this is the *freeze-in*[148, 149] (FI) and *forbidden freeze-in*[150] production mechanisms. This proposal has the virtue and drawback (depending on personal tastes) that the dark matter candidate becomes very difficult to detect, since it is extremely feebly coupled. In a similar way, DM can be also produced via the out-of-equilibrium decay of super-heavy particles decay [151, 152]. This scenario permits to produce DM candidate that are much heavier than the one allowed by the GK bound. Black holes have been as well proposed as efficient emitters of DM[153], and those DM candidates could be very heavy[154].

- **Standard cosmology**: Finally, we could also relax the hypothesis of standard thermal history of the universe with simple radiation domination until equivalence time. In the following, we will be considering such a possibility, keeping in mind the exciting hope that discovery of DM could at the same time provide information on the early universe dynamics. A very simple case is to assume that the universe is not radiation dominated at the time of FO[155]. Another possibility is to consider the effect of phase transitions in the early universe on the final DM abundance. In the context of second order phase transition, phase transitions offer a way to fix the final relic abundance via the VEV flip-flop mechanism[156, 157, 158] and by modifying the stability of DM candidate[159]. The PT could also change the properties of the DM[160] and modify its abundance. Several proposals also take advantage of the possibility of an early First-Order Phase Transitions (FOPT) occurring in the universe, with many different consequences on DM abundance[161]. Thermal inflation after the end of FO due to a long supercooled FOPT would inevitable bring a dilution factor in the final abundance of the form[162, 163, 164, 165] $(T_{\rm nuc}/T_{\rm reh})^3$, allowing for a further suppression of the density and, according to the GK bound, to heavier DM masses. Very massive DM can be also directly produced by the bubbles colliding at very large velocities via non-thermal production mechanism[166, 167]. It was initially claimed that particles as massive as $M \sim \gamma_w T$ [166] could be produced in this mechanism. This was later shown to be too optimistic in [167] where only the vector and fermion DM candidates were considered as promising DM candidate, if the collision between the bubbles is close to being *elastic*, that is to say, proceeding via multiple bouncing of the bubble walls on each other. Since it is of importance for us, the production mechanism in [167] is touched upon in Appendix A.6. More recently, the mechanism dubbed *bubble filtering* (BF)[168,

169, 170] was proposed as another way to go around the GK bound and produce ultra-heavy DM candidate with the observed abundance. Taking the DM as a fermion field χ and considering that it receives via the transition a mass much larger than the nucleation temperature $m_\chi^{\rm inside} \gg T_{\rm nuc}$ ("inside" meaning the mass inside the bubble), then only an exponentially suppressed fraction of the thermal fermions χ will be able to enter the bubble. Outside, the remaining part will be annihilated by thermal interactions.

Interestingly enough, similar production of heavy DM seems to be occurring in long supercooled confining transition as well [171, 172, 173]. In this context, DM is a hadron of the strongly coupled Dark Sector and the final DM abundance has been studied thoroughly in [174].

In this chapter, in the context of *portal* DM, we also relax the assumption of standard cosmology and assume (model building for supercooled EWPT will be provided in Chapters 5) a FOPT with relativistic bubble walls. We thus present a new mechanism of DM production, occurring via very strong FOPT with ultra-relativistic walls. In[1] and in Chapter 2, we have showed that an ultra-relativistic wall, with Lorentz factor $\gamma_w \gg 1$, sweeping through the plasma can excite degrees of freedom of mass up to $M \sim \sqrt{\gamma_w v T_{\rm nuc}}$. We call this production mechanism *Bubble Expansion* (BE) production and study it in detail, for the purpose of DM in this chapter.

Bubble Expansion, Bubble Collision and Bubble Filtering production mechanisms share the common feature that they can proceed even with very massive DM candidate, thus possibly evading the direct detection experiments (XENON1T ...). However, an irreducible prediction of such mechanisms, which uses very strong FOPT, is the well-known large amount of gravitational waves emitted by the plasma motion and the bubble collision. As a consequence, such mechanisms could be tested in future GW detectors like LISA, BBO, LIGO, offering an alternative way to study DM production.

The remainder of this chapter is organised as follows: In Section 3.3 we discuss the set up we will use, the production mechanism and the amount of relic produced after the passage of the wall and in Section 3.4, we present first the maximal amount of DM abundance that can be produced via BE mechanism, and then discuss three ways of accommodating the parameter space; 3.4.1, we discuss how inverse annihilation can modify the early relics abundance, in Section 3.4.2 we discuss how some amount of supercooling modifies the relative FO and Bubble Produced abundances and, finally, in Section 3.4.3, we discuss the case of very massive DM candidate in the absence of FO relics. In Section 3.5, we specialize to the Electroweak Phase transition and discuss the allowed range of parameter providing the observed relic abundance. In section 3.6, we study an alternative model where the DM is not a scalar but a fermion. In Section 3.7, we expose the unavoidable signature expected by such mechanism. Finally, in Section 3.8 we conclude.

3.3 Production of scalar DM in bubble wall expansion

In this first section we present the set-up that we will specialize to and present the production mechanism via the bubble wall expansion.

3.3.1 Set-up with and Lagrangian

Let us introduce the Lagrangian for the minimal model which suffices for the illustration of the advertised effect

$$\mathcal{L}_h = \partial_\mu \varphi \partial^\mu \varphi^\dagger - V(\varphi), \tag{3.13}$$

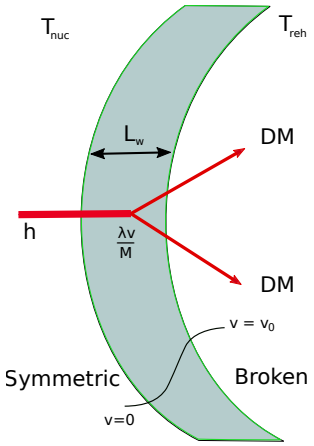

Figure 3.2: Cartoon of the production of DM mechanism in the wall frame for $h \to$ DM,DM in the case of the EWPT. The same can be extrapolate to a generic DS case upon making the following change $h \to \varphi$.

where φ is a complex scalar field obtaining a non-vanishing VEV via the phase transition and $V(\varphi)$ is its potential. We will not specify the form of $V(\varphi)$ in this paper, but will assume that it leads to the first order phase transition in the early universe. This field φ can be the physical Higgs $\varphi \to \mathcal{H}$, and thus the phase transition(PT) is the EWPT, or a new Dark Higgs, and then the transition happens only in the Dark Sector (DS). On the top of it, we introduce a DM candidate ϕ, that for simplicity we take to be only a single scalar field stabilized by a Z_2 symmetry, with Lagrangian of the form

$$\mathcal{L}_{\phi,\varphi} = \frac{1}{2}(\partial_\mu \phi)^2 - \frac{M_\phi^2}{2}\phi^2 - \frac{\lambda}{2}\phi^2|\varphi|^2. \tag{3.14}$$

We have assumed that DM candidate is coupled to the symmetry breaking sector via the portal coupling which is the simplest and most natural non-gravitational connection between the symmetry breaking sector and the DM candidate (for review on portal DM, see [175]). We will also assume $\lambda > 0$ in order to make sure the potential is bounded from below.

We will be mostly interested in masses of the DM candidate ϕ much larger than the mass scale in the φ potential, $M_\phi \gg m_\varphi$, for example $V(\varphi) = -\frac{m_\varphi^2}{2}|\varphi|^2 + \frac{\lambda_\varphi}{4}|\varphi|^2$[9]. As a consequence, the abundance of ϕ in the plasma at the moment of the transition is *Boltzmann-suppressed* and can be ignored in the dynamics of the transition. We thus neglect the quartic part of ϕ potential in the discussion as well as the change of M_ϕ due to the transition $\frac{\Delta M_\phi^2}{M_\phi^2} = \frac{\lambda v_\varphi^2}{M_\phi^2} \ll 1$, with v_φ the VEV of the φ field in the zero-temperature true vacuum, $v_\varphi \equiv \langle\varphi\rangle$. The hierarchy $M_\phi \gg m_\varphi, v_\varphi$ introduces the usual tuning of the scalar mass into the model if $\lambda M_\phi^2/(16\pi^2) \gg m_\varphi^2, v_\varphi^2$ (similar to the SM Higgs mass hierarchy problem), but in this paper we will not try to present a model where this hierarchy can be obtained naturally. The study of such a hierarchy and the tuning involved will be the topic of the Chapter 5.

3.3.2 $1 \to 2$ splittings

We now explicitly work out the expression for abundance produced, the probability of the $1 \to 2$ splitting, considering the simple model of Eq.(3.13). Usual Poincaré invariance would of course forbid the transition $1 \to 2$.

[9]Of course, other types of potentials are allowed.

However, in the presence of the bubble wall, Poincaré invariance is broken and this exotic transition can occur. We will consider the process $\varphi \to \phi\phi$, where φ is the field getting a VEV, the physical Higgs, and ϕ is the heavy field that will be our DM candidate. This is illustrated in Fig.3.2. Assuming a bubble wall along the z direction, we define the kinematics as

$$\begin{aligned} p^{\varphi} &= (p_0, 0, 0, \sqrt{p_0^2 - m_\varphi^2(z)}) \\ k^{\phi}_{(1)} &= (p_0(1-x), 0, k_\perp, \sqrt{p_0^2(1-x)^2 - k_\perp^2 - M_\phi^2(z)}) \\ k^{\phi}_{(2)} &= (p_0 x, 0, -k_\perp, \sqrt{p_0^2 x^2 - k_\perp^2 - M_\phi^2(z)}). \end{aligned} \tag{3.15}$$

In our set-up, M_ϕ is (almost) independent on z, and only $M_\varphi(z)$ is modified along the wall. Notice that now M_φ is not the parameter in the potential, but the physical mass of the field φ. In the toy potential we provided above: $M_\varphi(z) = -m_\varphi^2 + 3\lambda_\varphi v_\varphi^2(z)$. Here we will also assume that the thermal corrections, especially the thermal mass, can be neglected. This is the case for the Higgs boson with $T_{\rm nuc} \lesssim m_h$ even if the Higgs is interacting with the plasma, and is neglected for ϕ since ϕ is heavy.

To estimate the probability of transition, we use the WKB method, valid as long as the incoming momentum p_z^φ is much larger than the length of the wall L_w,

$$p_z^\varphi \sim p_0 \gg L_w^{-1} \qquad \text{(WKB condition)}. \tag{3.16}$$

In this limit, the wave function takes approximately the form

$$\phi(z) \simeq \sqrt{\frac{k_{z,s}}{k_z(z)}} \exp\left(i \int_0^z k_z(z')dz'\right), \tag{3.17}$$

and, using again the notations of [96], the $\mathcal{M}$ matrix writes

$$\begin{aligned} \mathcal{M} &= \int_{-\infty}^{\infty} dz e^{i\int_0^z p_z^\varphi(z')dz'} e^{-iq_z^\phi z} e^{-ik_z^\phi z} V(z) \\ &\approx \int_{-\infty}^{\infty} dz e^{ip_z^\varphi z} e^{-iq_z^\phi z} e^{-ik_z^\phi z} V(z) \equiv \int_{-\infty}^{\infty} dz e^{i\Delta p_z z} V(z), \end{aligned} \tag{3.18}$$

with $p_z^\varphi(z) = \sqrt{p_0^2 - k_\perp^2 - M_\varphi^2(z)} \approx p_0$ the momentum of the incoming φ particle and k_z^ϕ, q_z^ϕ the momentum of the two ϕ outgoing particles. In the second line, we neglected $M_\varphi^2(z)$, as it is much smaller than M_ϕ^2. We also defined $\Delta p_z \equiv p_z^\varphi - q_z^\phi - k_z^\phi \approx \frac{M_\phi^2 + k_\perp^2}{2x(1-x)p_0}$, the momentum exchange.

To approximate the integral, we need to use some estimation for the shape of the wall. For the purpose of the illustration, let us approximate it using a *linear* ansatz of the form

$$\langle\varphi\rangle = \begin{cases} 0, & z < 0 \\ v\frac{z}{L_w} & 0 \le z \le L_w \\ v & z > L_w \end{cases} \quad \Rightarrow \qquad V(z) = \begin{cases} V_s \equiv 0, & z < 0 \\ \lambda v \frac{z}{L_w} & 0 \le z \le L_w \\ V_h \equiv \lambda v & z > L_w \end{cases}. \tag{3.19}$$

Consequences and changes for different shapes of the wall have been discussed in Appendix A.3. The integral in Eq.(3.18) along the wall direction naturally splits into three parts

$$\begin{aligned}\mathcal{M} &= \int_{-\infty}^{0} dz e^{i\Delta p_z z} V(z) + \int_{0}^{L_w} dz e^{i\Delta p_z z} V(z) + \int_{L_w}^{\infty} dz e^{i\Delta p_z z} V(z) \\ &= 0 + (1 - e^{i\Delta p_z L_w} - i\Delta p_z L_w e^{i\Delta p_z L_w}) \frac{V_h}{\Delta p_z^2 L_w} + \frac{V_h}{i\Delta p_z}(-e^{i\Delta p_z L_w} + e^{i\infty}) \\ &= V_h \frac{1 - e^{i\Delta p_z L_w}}{L_w \Delta p_z^2}. \end{aligned} \tag{3.20}$$

Putting together the relevant pieces and dropping the unphysical wave functions at infinity, we see that the final matrix element squared is given by

$$|\mathcal{M}|^2 = \frac{V_h^2}{\Delta p_z^2}\left(\frac{\sin\alpha}{\alpha}\right)^2 = \frac{\lambda^2 v_\varphi^2}{\Delta p_z^2}\left(\frac{\sin\alpha}{\alpha}\right)^2, \qquad \alpha = \frac{L_w \Delta p_z}{2}. \tag{3.21}$$

We can observe the appearance of the function $\left(\frac{\sin\alpha}{\alpha}\right)^2$ that we already encountered and discussed in Chapter 2. This function goes to one for small α and is suppressed for large α. In Appendix A.3, we study this suppression for different shapes of the wall and find quantitative differences. However, the common result is the quick suppression for $\alpha > 1$, we will consider it as a sharp cut-off in what follows and introduce a Heaviside function. With those tools in hand, we can now compute the probability of 1 to 2 splitting. The expression for the probability of the transition generically takes the form

$$P_{\varphi\to\phi_1\phi_2} = \frac{1}{2p_0}\prod_{i\in 1,2}\int \frac{d^3k_i}{(2\pi)^3 2k_0^i}(2\pi)^3\delta^2(p_\perp - \sum_{i\in 1,2} k_\perp^i)\delta(p_0 - \sum_{i\in 1,2} k_0^i)|\mathcal{M}|^2 \tag{3.22}$$

and putting together Eq. (3.22), (3.21), using the kinematics (3.15) and the large velocity approximation $\Delta p_z \approx \frac{M_\phi^2 + k_\perp^2}{2x(1-x)p_0}$, we obtain

$$\begin{aligned} P_{\varphi\to\phi\phi} &\simeq \int_0^1 \frac{dx}{16p_0^2\pi^2 x(1-x)} \int dk_\perp^2 \frac{4p_0^2\lambda^2 v_\varphi^2 x^2(1-x)^2}{(k_\perp^2 + M_\phi^2)^2}\left(\frac{\sin\alpha}{\alpha}\right)^2 \Theta(p_0 - 2M_\phi) \\ &\simeq \frac{\lambda^2}{4\pi^2} v_\varphi^2 \int_0^1 dx x(1-x) \int \frac{dk_\perp^2}{(k_\perp^2 + M_\phi^2)^2} \times \left(\frac{\sin\alpha}{\alpha}\right)^2 \Theta(p_0 - 2M_\phi) \\ &\approx \frac{\lambda^2}{24\pi^2}\frac{v_\varphi^2}{M_\phi^2} \times \Theta(\gamma_w T_{\rm nuc} - m_\phi^2 L_w)\Theta(\gamma_w T_{\rm nuc} - 2M_\phi). \end{aligned} \tag{3.23}$$

where the $\Theta(\gamma_w T_{\rm nuc} - 2M_\phi)$ function appears from the trivial requirement that we need enough energy to produce the two heavy states and $\Theta(\gamma_w T_{\rm nuc} - M_\phi^2 L_w)$ comes from the behaviour of the function $\sin\alpha/\alpha$, as we already explained.

One can also estimate the typical energy of the produced ϕ in the bubble center frame:

$$\bar{E}_\phi \approx \frac{1}{2}\frac{\int dx x(1-x)\left[((k_1^\phi)_0 + (k_2^\phi)_0)\gamma_w - ((k_1^\phi)_z + (k_2^\phi)_z)v_w\gamma_w\right]}{\int dx x(1-x)} \sim \frac{3}{4}\frac{M_\phi^2}{T_{\rm nuc}}. \tag{3.24}$$

Here in the last approximation we have used that $p_0^\varphi \sim \gamma_w(1+v_w)T_{\rm nuc}$ and $v_w = \sqrt{1-\gamma_w^{-2}}$.

At the end of the day, the probability of the transition writes

$$\boxed{P(\varphi \to \phi\phi) \approx \left(\frac{\lambda v_\varphi}{M_\phi}\right)^2 \frac{1}{24\pi^2}\Theta(1-\Delta p_z L_w) \qquad \bar{E}_\phi \sim \frac{M_\phi^2}{T_{\rm nuc}}} \tag{3.25}$$

L_w is the width of the wall which is approximately $L_w \sim 1/v_\varphi$ (See again section 2.3.3 for a discussion of the width of the wall in the runaway regime) and $\Delta p_z \equiv p_z^\varphi - p_{z,1}^\phi - p_{z,2}^\phi \approx \frac{M_\phi^2}{2p_z^\varphi}$ is a difference of momenta between final and initial state particles in the direction orthogonal to the wall. $\bar{E}$ is the average energy immediately after the production.

3.3.3 Abundance inside of the bubble

As a consequence of the $\varphi \to \phi\phi$ transitions, inside of the bubble, a non-vanishing density of non-thermal ϕ accumulates. We expect them to quickly thermalise via $\phi\varphi \leftrightarrow \phi\varphi$ in the vast majority of the parameter space[10]. Thus, this "*Bubble Expansion* (BE)" produced density of ϕ, in the wall rest frame, takes the following form

$$\begin{aligned} n_\phi^{\rm BE} &\approx \frac{2}{\gamma_w v_w}\int \frac{d^3p}{(2\pi)^3}\frac{p_z}{p_0}P(\varphi\to\phi\phi)\times f_\varphi(p,T_{\rm nuc}) \\ &\approx \frac{2\lambda^2 v_\varphi^2}{24\pi^2 M_\phi^2 \gamma_w v_w}\int \frac{d^3p}{(2\pi)^3}\frac{p_z}{p_0}\times f_\varphi(p,T_{\rm nuc})\Theta(p_z - M_\phi^2/v_\varphi), \end{aligned} \tag{3.26}$$

$v_w = \sqrt{1-1/\gamma_w^2}$ is the velocity of the wall, and $f_\varphi(p)$ is the equilibrium thermal distribution of φ outside of the bubble. This writes $f_\varphi(p) = \frac{1}{e^{\frac{\gamma_w(E_h - v_w p_z^h)}{T_{\rm nuc}}}-1}$ if the mass of φ is negligible, as the Higgs-like field should be at equilibrium with SM. We will discuss the possibility a suppression if $m_\varphi > T$ in the next subsection.

Using Boltzmann distribution as a simplifying assumption, $f_\varphi(p) \approx e^{-\frac{\gamma_w(E_\varphi - v_w p_z^\varphi)}{T_{\rm nuc}}}$ and $E_\varphi = \sqrt{p_z^2 + \mathbf{p}_\perp^2}$, we can perform the integral in Eq. (3.26) and, in the limit of fast walls $p_z/p_0, v_w \to 1$, we obtain

$$n_\phi^{\rm BE} = \frac{\lambda^2}{48\pi^4\gamma_w^3}\times\frac{v_\varphi^2 T_{\rm nuc}^2}{M_\phi^2}\left(\frac{M_\phi^2/v_\varphi}{1-v_w} + \frac{T_{\rm nuc}(2-v_w)}{\gamma_w(v_w-1)^2}\right)\times e^{-\gamma_w\frac{M_\phi^2}{v_\varphi}\frac{1-v_w}{T_{\rm nuc}}}. \tag{3.27}$$

With $\gamma_w(1-v_w) = \gamma_w - \sqrt{\gamma_w^2-1} \to \frac{1}{2\gamma_w}$, the density in the plasma frame, the expression becomes

$$\boxed{n_\phi^{\rm BE} = \frac{T_{\rm nuc}^3}{12\pi^2}\frac{\lambda^2 v_\varphi^2}{\pi^2 M_\phi^2}e^{-\frac{M_\phi^2}{2v_\varphi T_{\rm nuc}\gamma_w}} + \mathcal{O}(1/\gamma_w)} \qquad \text{(density produced)} \tag{3.28}$$

The exponential factor is a consequence of $\Theta(p_z - M_\phi^2/v_\varphi)$ in the the Eq.(3.26). We thus have three different regimes.

[10]This might however not be always the case and this mechanism could thus produce heavy WDM. The author would like to thank Filippo Sala and Iason Baldes for enlightening discussions on this issue. I think we can thus consider the question of the production of WDM via this mechanism as an open issue

- **Non-adiabatic regime**:

  We can see that in the limit

$$\gamma_w > \frac{M_\phi^2}{2v_\varphi T_{\rm nuc}} \qquad \text{(Non-adiabatic production)} \tag{3.29}$$

  the exponential goes to one and the density becomes independent of the velocity of the wall v_w. The step function $\Theta(1-\Delta p_z L_w) \simeq \Theta(p_z - M_\phi^2/v_\varphi)$ is an approximation of the transition function which depends on the exact shape of the wall. It is important to note that in the regime $\Delta p_z L_w \lesssim 1$ the step function presents a good approximation and the results are independent of the wall shape as expected from the Heisenberg uncertainty principle.

- **Adiabatic regime**: However, if the inequality Eq.(3.29) is not satisfied and we are in the regime

$$\frac{M_\phi}{T_{\rm nuc}} < \gamma_w < \frac{M_\phi^2}{2v_\varphi T_{\rm nuc}} \qquad \text{(Adiabatic production)} \tag{3.30}$$

  then the wall shape effects start to become important. We discuss this wall suppression for the $\tanh$ and gaussian walls in the Appendix A.3. We find that generically the deviations from the naive step function are exponentially suppressed, so that expression in Eq.(3.27) can be used as an estimate in the transition regime Eq.(3.30).

- **No production regime:** At last, for

$$\gamma_w < \frac{M_\phi}{T_{\rm nuc}} \qquad \text{(No production)} \tag{3.31}$$

  the particle production gets additional suppression by the usual Boltzmann factor and makes it totally negligible.

From now we will keep working with expression Eq. (3.26), keeping in mind possible departure from pure exponential suppression behaviour.

The final number density of heavy non-thermal DM, in the unsuppressed (non-adiabatic) regime is of the form

$$n_\phi^{\rm BE} \approx \frac{\lambda^2 v_\varphi^2}{M_\phi^2}\frac{T_{\rm nuc}^3}{12\pi^4}\Theta(\gamma_w T_{\rm nuc} - M_\phi^2/v_\varphi). \tag{3.32}$$

Assuming no subsequent reprocessing (thermalisation, annihilation, dilution by inflation ...) of the relic abundance, the nowadays abundance of Bubble Expansion (BE) produced DM is given by

$$\Omega_{\phi,\rm BE}^{\rm today}h^2 = \frac{M_\phi n_\phi^{\rm BE}}{\rho_c/h^2}\frac{g_{\star S0}T_0^3}{g_{\star S}(T_{\rm reh})T_{\rm reh}^3} \approx 6.3\times 10^8 \frac{M_\phi n_\phi^{\rm BE}}{\rm GeV}\frac{1}{g_{\star S}(T_{\rm reh})T_{\rm reh}^3}. \tag{3.33}$$

where T_0 is the temperature today, ρ_c is the critical energy density and $g_{\star S0}(g_{\star S}(T_{\rm reh}))$ is the entropy number of d.o.f. today (at the reheating temperature). As a consequence, plugging the expression Eq.(3.32), the final relic abundance today writes

$$\Omega_{\phi,\rm BE}^{\rm today}h^2 \approx 5.4\times 10^5 \times \left(\frac{1}{g_{\star S}(T_{\rm reh})}\right)\left(\frac{\lambda^2 v_\varphi}{M_\phi}\right)\left(\frac{v_\varphi}{\rm GeV}\right)\left(\frac{T_{\rm nuc}}{T_{\rm reh}}\right)^3 e^{-\frac{M_\phi^2}{2v_\varphi T_{\rm nuc}\gamma_w}}, \tag{3.34}$$

and we see that, in the non-adiabatic regime, the produced relic abundance is controlled by the quantities

$$\frac{T_{\rm nuc}}{T_{\rm reh}}, \qquad \frac{v_\varphi}{\rm GeV}, \qquad \lambda^2 \frac{v_\varphi}{M_\phi}. \tag{3.35}$$

So far we have shown that a bubble with Lorentz factor γ_w sweeping through the plasma can produce massive states up to mass roughly $M_\phi^2 \lesssim \gamma_w T_{\rm nuc}/L_w$, where $L_w \sim 1/v_\varphi$ is the width of the wall. As we have already discussed at length in Chapter 2, the maximal value of the γ_w factor depends on the particle content of the theory (particularly the presence of the gauge fields) which influences the largest DM mass which can be produced. Using the simple criterion in Eq.(3.29), we can estimate this maximal mass by considering the two generic regimes of the bubble expansion:

1. **Runaway regime:** According to this maximal boost factor found in Section 2.4.1 in Eq.(2.144), the maximal mass $M_\phi^{\rm MAX}$ that can be produced, by the sweeping of the wall, scales like

$$M_\phi^{\rm MAX} \sim T_{\rm nuc} \left(\frac{M_{\rm pl}}{v_\varphi} \right)^{1/2}. \tag{3.36}$$

   We will study Dark Sectors of this type in Section 3.4.

2. **Terminal velocity regime:** Similar considerations from Eq.(2.147) give

$$M_\phi^{\rm MAX} \sim {\rm Min} \left[T_{\rm nuc} \left(\frac{M_{\rm pl}}{v_\varphi} \right)^{1/2}, 4\pi v_\varphi \left(\frac{v_\varphi}{T_{\rm nuc}} \right) \right], \tag{3.37}$$

   where we assumed, as in the remainder of this chapter, that $g_i g_{\rm gauge}^3 \sim \mathcal{O}(1)$. Above this maximal mass, the production of DM becomes exponentially suppressed according to $e^{-\frac{M_\phi^2}{2vT_{\rm nuc}\gamma_w}}$, as we have seen in Eq.(3.28). We will study a transition of this type in the context of EWPT in the Section 3.5 and later in Chapter 5.

The final relic abundance produced during BE has to compete with the relic abundance coming from FO, which provides a final relic abundance roughly of the form shown in Eq.(3.10). Notice that this component exists if the reheating temperature of the Universe after inflation is higher than $M_\phi/20$[11] and if ϕ couples to the thermal bath not too weakly so that ϕ is produced from the thermal scatterings. We will take into account the presence of FO abundance in the next part, except in section 3.4.3, where we will remove this assumption.

The ratio of the nucleation temperature $T_{\rm nuc}$ over the reheating temperature $T_{\rm reh}$ in Eq. (3.34), originates from the fact that the heavy particles are actually produced at the nucleation temperature, but that the release of energy reheat the plasma at $T_{\rm reh}$, providing the new initial condition for the evolution of the universe. Strong FOPT's are often accompanied by long supercooling and thermal inflation [176, 177], leading to the hierarchy between $T_{\rm nuc}$ and $T_{\rm reh}$ and strong suppression of the abundance. We will see that this new suppression factor can be useful in the range of parameters where the final relic abundance is overproduced, as illustrated on Fig 3.3: in the region II, where the BE abundance is dominant over FO, but both of them are too large to account for $\Omega_{\rm obs}^{\rm today}$ and I, where FO is not large enough. In this range, dilution related to thermal inflation can reduce the overproduced relic abundance to $\Omega_{\rm obs}^{\rm today}$.

[11] Here, there is a caveat to take into account[151], where it was shown that even in this case, some abundance of ϕ is produced. We will ignore this abundance in any case.

3.3.4 About the mass of the scalar in the false vacuum

In this section, we would like to draw attention on a possible issue of our production mechanism. We will see soon that for a successful DM production, a hierarchy between the reheating temperature and the nucleation temperature $(T_{\rm nuc}/T_{\rm reh}) \lesssim 0.1$ is typically needed. However, in Eq.(3.26) we have taken the distribution function of φ to be massless distribution, valid if the mass of the Higgs-like field is much smaller than the temperature. However, this is not necessarily the case.

The relevant parameter for the discussion is the ratio

$$\sqrt{\frac{d^2V}{d\varphi^2}\Big|_{\rm fv}}\frac{1}{T} \equiv \frac{m_\varphi^{\rm False}}{T}\ , \tag{3.38}$$

where fv denotes the position of the false vacuum and $\sqrt{d^2V/d\varphi^2|_{\rm fv}}$ is the mass of the φ $m_\varphi^{\rm False}$ in the false vacuum. As soon as this quantity becomes larger than 1, we expect exponential suppression of the φ abundance

$$C_{\rm eff}\frac{\zeta(3)T_{\rm nuc}^3}{\pi^2} \equiv \int \frac{d^3p}{(2\pi)^3} f_\varphi(p, T_{\rm nuc}) \approx \begin{cases} \frac{\zeta(3)T_{\rm nuc}^3}{\pi^2} & \text{if} \quad m_\varphi^{\rm False} < T\ , \\ \left(\frac{m_\varphi^{\rm False} T_{\rm nuc}}{2\pi}\right)^{3/2} e^{-m_\varphi^{\rm False}/T_{\rm nuc}} & \text{if} \quad m_\varphi^{\rm False} > T\ . \end{cases} \tag{3.39}$$

We defined $C_{\rm eff}$ to take into account the Boltzmann suppression. For the purpose of this chapter, we will set $C_{\rm eff} = 1$ and ignore this possible effect, but we have to keep in mind that $C_{\rm eff}$ should be computable if we have a model for the transition. This will be done in Chapter 5 in the context of the EWPT.

3.4 Dark Sector PT production of DM

In the previous section, we have presented a new mechanism of DM production. However it is important whether this mechanism can lead to the observed relic abundance. In order to consider the phenomenological relevance of our mechanism we will use the toy model presented in Eq.(3.13), which can perfectly constitute a viable model of DM. We consider the field φ as some scalar field experiencing the phase transition at some scale v_φ. Let us look at the nowadays relic abundance presented in Eq.(3.34). The results are presented on the Fig. 3.3 for $v_\varphi = 200$ and 2×10^4 GeV and importantly, we set the dilution factor $(T_{\rm nuc}/T_{\rm reh})^3$ to one, this factor will play an important role later on. Generically we can define four regions as follows: in region I, the abundance is under-produced via FO, but largely overproduced via BE. The region IV is the symmetric situation, where the BE is small but FO is very large. In region II(III), both FO and BE are overproduced, but BE (FO) production dominates over FO (BE):

$$\begin{aligned} I &: \Omega_{BE} > \Omega_{obs},\ \ \Omega_{FO} < \Omega_{obs} \\ II &: \Omega_{BE} > \Omega_{FO},\ \ \Omega_{FO} > \Omega_{obs} \\ III &: \Omega_{BE} < \Omega_{FO},\ \ \Omega_{BE} > \Omega_{obs} \\ IV &: \Omega_{BE} < \Omega_{obs},\ \ \Omega_{FO} > \Omega_{obs}. \end{aligned} \tag{3.40}$$

Very naively these equations indicate that none of the regions leads to a viable phenomenology and permit to match the observed abundance. However we have not yet taken into account few possibilities on the initial conditions as well as the evolution of ρ_ϕ/s which can make some parts of those regions viable.

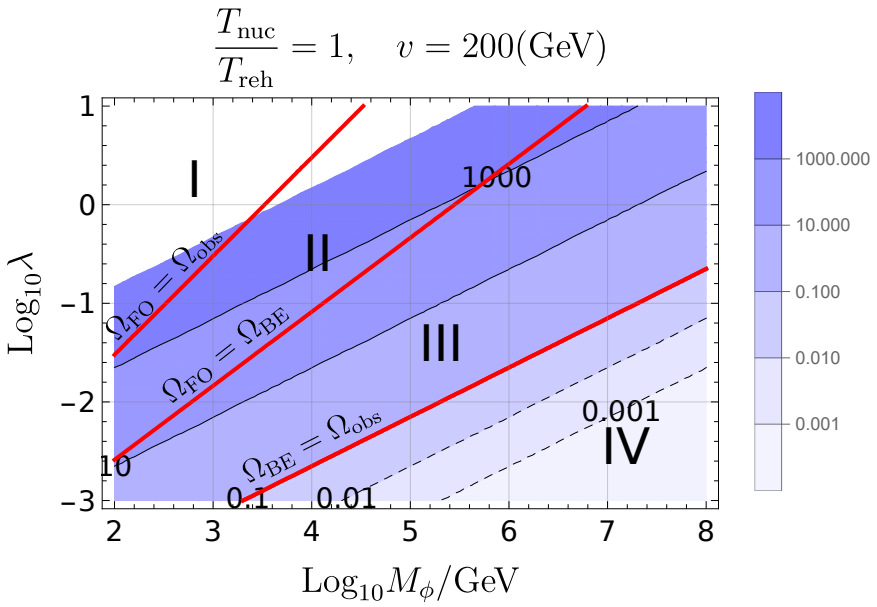

Figure 3.3: The *unprocessed* final relic abundance coming from FO and BE process with $T_{\rm nuc} = T_{\rm reh}$ and $v = 200$ GeV. The blue shading gives the value of $\Omega_{\rm BE}^{\rm today}$. The red lines $\Omega_{{\rm BE},\phi}^{\rm today} = \Omega_{{\rm FO},\phi}^{\rm today}$, $\Omega_{{\rm BE},\phi}^{\rm today} = \Omega_{\rm obs}^{\rm today}$ and $\Omega_{{\rm BE},\phi}^{\rm today} = \Omega_{\rm obs}^{\rm today}$ define 4 regions. In I, BE abundance is dominant and FO is not enough to account for the observation. In II, FO is too large, but BE is still dominant. In III, both BE and FO are too large, but FO is dominant. Finally, in IV, FO is dominant, and BE is not enough to account for $\Omega_{\rm obs}^{\rm today}$.

To be more precise, we will study three possibilities: i) in the regions where DM is overproduced via BE expansion, annihilation processes can reduce the DM density back to the observed relic abundance, as this can be for example the case in region I. We discuss this possibility in the Section 3.4.1. ii) as we already hinted above, another process which can reduce the DM density is a brief period of inflation during the FOPT, which happens if the nucleation temperature is significantly lower than the reheating temperature. This leads to the reduction of the overall DM density and as a result opens up some parameter space, typically inside of region I and II of Fig. 3.3. We discuss this effect in the section 3.4.2. iii) at last in the case that the thermal history begins with a reheating scale below the FO temperature[12], ϕ never reaches thermal equilibrium after the reheating and is (almost) not produced via FO. We discuss this possibility in the Section 3.4.3.

3.4.1 Late time annihilation

In the previous Section 5.4, we showed that if a relativistic bubble goes through the plasma, it can produce DM relics, possibly very over-abundant. On Fig. 3.3 we saw that, in region I, the FO contribution was not large enough to account for the observed DM abundance, but that on the contrary, BE production was extremely large. As a consequence we would like to track the evolution of the number of DM particles after the initial production. We will see that, as long as the DM density produced is very large, the final density does not depend on the initial density. Thus the physics of this part does not change even if ϕ is produced enormously from other dynamics e.g.

[12]This is the case that the inflaton coupling is so weak that the early produced ϕ is diluted due to the inflaton late-time decay, or the inflation scale itself is low. Inflation scale can be comparable or even smaller than the weak scale in ALP inflation models [178, 179].

inflaton/moduli decay.[13] Due to this reason, in the following, we make a general discussion which is not specific to the BE production unless otherwise stated. We assume for simplicity that the production happens instantaneously during the *radiation domination* epoch at $T[t_{\rm ini}] = T_{\rm reh}$, and assume that the density just after the production is much larger than that for the observed DM abundance (which is the case of the region I of Fig. 3.3).

The annihilation cross-section for the process $\phi\phi \to \varphi\varphi$ is well approximated as

$$\langle \sigma_{\phi\phi} v_{\rm rel} \rangle \sim \frac{g_4 \lambda^2}{16\pi M_\phi^2} \tag{3.41}$$

when ϕ is non-relativistic. Here $v_{\rm rel}$ is the relative velocity, and $\langle\rangle$ is the average over the distribution functions of ϕ and φ. g_4 counts the real degrees of freedom of φ normalized by the number of d.o.f. of the SM Higgs doublet, 4. For instance,

$$g_4 = 1 \text{ and } \frac{1}{4} \tag{3.42}$$

for φ being the SM Higgs and a real singlet Dark Higgs, respectively. (In the real singlet Dark Higgs case we should take $\mathcal{L}_{\rm scalar} \supset -\lambda\phi^2|\varphi|^2/4$.) In calculating the average, we have assumed that just after the production, the DM velocity v_ϕ (notice that dangerous confusion with notations, this is a velocity!) soon slows down due to the scattering with the ambient plasma, and we further assume φ soon decays into the SM plasma. When φ is the SM Higgs, the assumptions are easily satisfied. The mean-free path in the thermal environment is set by the inverse of $\Gamma_{\rm MFP} \sim y_q^2 \frac{\lambda^2 v^2}{E_\phi^2} T_{\rm reh}$ where y_q is the quark-Higgs Yukawa coupling (This expression is valid in the broken phase. In the case of symmetric phase, the scattering is with Higgs multiplet and the rate is larger.) Here $T_{\rm reh}$ is comparable or larger than the mass of the quark q. $\Gamma_{\rm MFP}$ is easily larger than the Hubble parameter unless E_ϕ is extremely large. When the dominant annihilation product is a dark Higgs boson, we can still have a sub-dominant portal coupling between the DM and the SM Higgs, via which the kinetic equilibrium can be easily reached. The typical velocity of ϕ in the kinetic equilibrium is

$$v_\phi \sim v_{\rm rel}/2 \sim \sqrt{2\frac{T_{\rm reh}}{M_\phi}}. \tag{3.43}$$

Thus a simple criterion to assess the stability of DM relics is the competition between the expansion rate of the universe,

$$H(T) \approx 1.66\sqrt{g_\star}\frac{T^2}{M_{\rm pl}},$$

and the rate of annihilation $\Gamma_{\rm ann}$. A rough *stability* condition thus writes

$$\Gamma_{\rm ann} \sim \langle \sigma_{\phi\phi} v_{\rm rel} \rangle n_\phi < H \qquad \text{(Stability condition)}.$$

If this condition is violated the annihilation gradually takes place even if $T_{\rm reh}$ is below the FO temperature $\sim M_\phi/20$, as discussed in the Wino and Higgsino DM cases [180, 181].

To evaluate the final abundance after the annihilation, we can solve the integrated Boltzmann equation (by assuming kinetic equilibrium as in the case of the WIMP):

$$\dot{n}_\phi[t] + 3{\rm H} n_\phi[t] = -\Gamma_{\rm ann}(n_\phi[t] - n_{\rm eq}[t]^2/n_\phi[t]) \tag{3.44}$$

$n_{\rm eq} \simeq (M_\phi T/(2\pi))^{3/2} \exp(-M_\phi/T)$ is the number density in the equilibrium, and the annihilation rate is given by

$$\Gamma_{\rm ann} \simeq \langle \sigma_{\phi\phi} v_{\rm rel} \rangle n_\phi S_{\rm eff} \tag{3.45}$$

[13] An extreme scenario may be even that ϕ is the inflaton which annihilates to reheat the Universe and becomes the DM. In this case, we should pay careful attention to the parametric resonance.

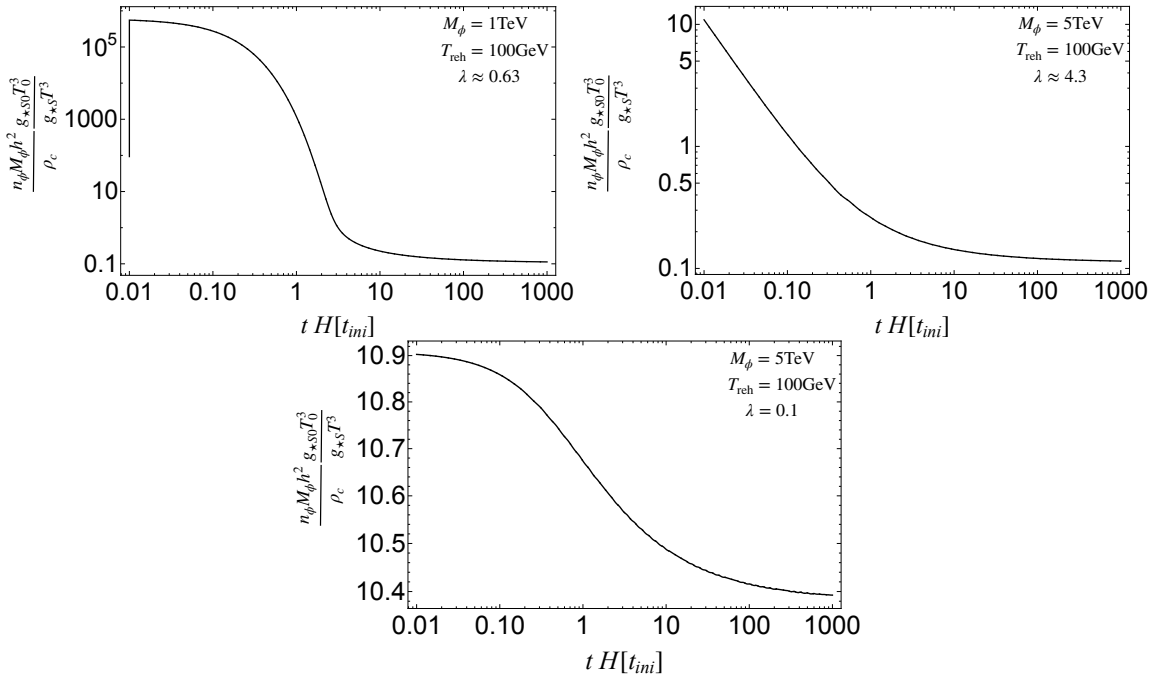

Figure 3.4: The evolution of the energy density of the Dark Higgs portal DM, with $v_\varphi = T_{\rm reh} = 100\,{\rm GeV}$, $M_\phi = 1\ {\rm TeV}(5\ {\rm TeV}, 5\ {\rm TeV})$, and $\lambda \simeq 0.63(4.3, 0.1)$ with large initial number density in the left top (right top, bottom) panel, which corresponds to late time FO (late time annihilation, satisfied stability condition).

$\langle\rangle$ being the thermal average and $S_{\rm eff}$ is the *Sommerfeld enhancement* factor, i.e. the boost factor from the interacting long-range force, as discussed in Appendix A.7. We assume the force potential between the ϕ pair distanced by r as

$$V(r) = -\frac{\alpha_{\rm med}}{r}\exp\left[-m_{\rm med}/r\right] \tag{3.46}$$

where $\alpha_{\rm med}$ ($m_{\rm med}$) is the messenger coupling (mass). For the Higgs-mediated force discussed in this section, we have

$$m_{\rm med} \simeq M_\varphi,\ \ \alpha_{\rm med} \simeq \frac{\lambda v_\varphi^2}{2\pi M_\phi^2}.$$

The analytic approximation of the enhancement factor is given by[182, 183] (See also Refs [184, 185, 186, 187])

$$S_{\rm eff} = \frac{\pi}{\epsilon_v}\frac{\sinh\left(\frac{2\pi\epsilon_v}{\pi^2\epsilon_{\rm med}/6}\right)}{\cosh\left(\frac{2\pi\epsilon_v}{\pi^2\epsilon_{\rm med}/6}\right)-\cos\left(2\pi\sqrt{\frac{1}{\pi^2\epsilon_{\rm med}/6}-\frac{{\epsilon_v}^2}{(\pi^2\epsilon_{\rm med}/6)^2}}\right)}, \tag{3.47}$$

where $\epsilon_v = v_\phi/(\alpha_{\rm med})$ and $\epsilon_{\rm med} = m_{\rm med}/(\alpha_{\rm med}M_\phi)$. Specifically, we have $S_{\rm eff} \to \frac{\pi\alpha_{\rm med}/v_\phi}{(1-e^{-\pi\alpha_{\rm med}/v_\phi})}$ with $M_\varphi \to 0$.

To solve numerically the Boltzmann equation, we set the initial condition of $n_\phi[t_{\rm ini}] \gg 0.2\,{\rm eV}\times s/M_\phi$, i.e. much larger than the corresponding value of the observed DM number density. Here s is the entropy density. The Boltzmann equation can be solved to give Fig.3.4 where we plot the time evolution of the number density with $n_\phi[t_{\rm ini}] \sim 40\,{\rm eV}\times s/M_\phi$. Indeed, we find that even when initially there is too large number density, with large enough coupling (and thus large annihilation rate), the number density decreases significantly within one Hubble time. We obtain suppressed abundance in the end (right top panel). On the bottom (left top) panel we can see that if the coupling is not very large this is not the case (if $M_\phi < T_{\rm reh}/20$, ϕ is thermalized soon and FO happens).

In Fig.3.5 with φ being the real singlet Dark Higgs-like, we represent the numerical result giving $\Omega_\phi h^2 = \Omega_{\rm DM}h^2 \approx 0.1$ [121] by taking $v_\varphi = T_{\rm reh} = 50, 100, 200, 400\,{\rm GeV}$ from top to bottom, with the initial condition set as $n_\phi[t_{\rm ini}] = 40\,{\rm eV}\times s/M$. We see that at lower mass range the predictions do not depend on $T_{\rm reh}$, which represents that the FO takes over since $T_{\rm reh} > T_{\rm FO} \sim M_\phi/20$. The FO prediction is displayed on Fig.3.5 (and 3.6) by the dotted orange line. On the larger mass range, the late time annihilation becomes important and reduces the abundance relevant to $T_{\rm reh}$.

In fact, we can explain the final number density, n_ϕ, in this region from the condition

$$\langle\sigma_{\phi\phi}v_{\rm rel}\rangle n_\phi S_{\rm eff}[T_{\rm reh}] = CH[T_{\rm reh}]. \tag{3.48}$$

This condition is similar to the freeze-out condition for the ordinary WIMP: the annihilation should end when the rate becomes comparable to the Hubble expansion rate. We obtain

$$\lambda = \lambda_{\rm ann} \sim 0.53(g_4 r S_{\rm eff})^{-1/2}\sqrt{C}\left(\frac{g_\star(T_{\rm reh})}{103.5}\right)^{-1/4}\left(\frac{M_\phi}{2\ {\rm TeV}}\right)^{3/2}\left(\frac{100\ {\rm GeV}}{T_{\rm reh}}\right)^{1/2} \tag{3.49}$$

from the condition that the ϕ abundance composes an r fraction of the observed dark matter abundance, $\Omega_\phi = r\Omega_{\rm DM}$ (and we are now focusing on $r = 1$.) Notice again that to use Eq.(3.49) we have assumed $T_{\rm FO} > T_{\rm reh}$, otherwise the DM is thermalized and then usual FO takes place after a certain redshift. From the numerical fit by solving the Boltzmann equations, we obtain $C = [0.1 - 1]$ depending on the initial condition. If the initial $n_\phi[t_{\rm ini}]$ is larger C becomes larger approaching to 1. In particular for our bubble wall scenario, we may have a very large $n_\phi(t_{\rm ini})$ and, in this peculiar case, C is almost 1.

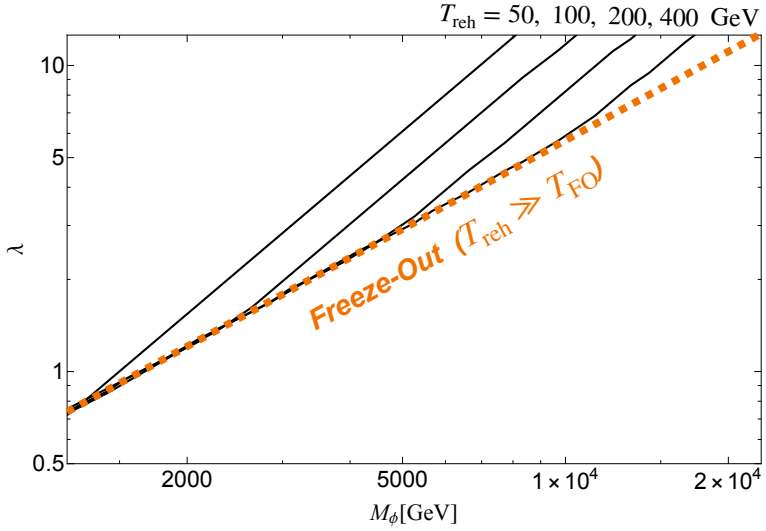

Figure 3.5: The parameter region of the Dark Higgs portal DM with non-thermal over-production at $v_\varphi = T_{\rm reh} = 50\ {\rm GeV}, 100\ {\rm GeV}, 200\ {\rm GeV}, 400\ {\rm GeV}$ from left to right [Black line]. $g_4 = 1/4$. We neglect the mass of the dark Higgs boson. The orange dashed line indicates the FO prediction.

So far we have been agnostic regarding the coupling of the DM to the SM sectors. We just have assumed that DM couples to the scalar field φ to which it annihilates into. However, to be in *kinetic equilibrium*, the DM should somehow couple to the SM plasma. This leads to the possibility of detecting DM with direct and indirect detection experiments. In particular, when φ is the SM Higgs boson, the coupling to nucleons is controlled by the coupling λ. The case where $\varphi \to \mathcal{H}$ is the SM Higgs multiplet is shown in Fig. 3.6, where the difference from Fig. 3.5 is that we fixed $v = 174$ GeV, $g_4 = 1$ and $m_h = 125$ GeV. We adopt the bound XENON1T experiment [188] from [175] (The Purple region above the purple solid line), which is extrapolated by us to multi-TeV range. The green dashed and blue dotted lines represent the future reaches of the XENONnT [189] and DARWIN [190], respectively, which are also adapted and extrapolated from [175]. The Cerenkov Telescope Array (CTA) reach (by assuming the NFW distribution of DM) is adopted from [191] and also extrapolated by us. Consequently, the predicted parameter region can be fully covered in the future direct detection and indirect detection experiments such as XENONnT, DARWIN and CTA. Interestingly, since the predicted black lines are parallel to the direct detection reaches in the late time annihilation region, $T_{\rm reh}$ corresponds to the DM-Nucleon interaction rate. If the DM is detected in the direct detection experiments, which implies the interaction rate is measured, we can tell the reheating temperature assuming late time annihilation.

Here we notice that the contribution of the Sommerfeld enhancement may be as large as $S_{\rm eff} - 1 = \mathcal{O}(10\%)$ when the mass is large. Usually in the (SM) Higgs portal dark matter model, the Sommerfeld enhancement is negligible due to the small Higgs-DM coupling, $\alpha_{\rm med} \propto (\frac{\lambda v_\varphi}{M_\phi})^2$ suppressed by the heavy DM mass. In the late annihilation scenario, since we need larger λ than conventional FO and smaller v_ϕ, we have larger $S_{\rm eff}$.

As a conclusion of this section, let us, finally, come back to the BE production. We have seen on Fig. 3.3 that in the region of parameter with large coupling and DM mass in the TeV range, the FO is subdominant and BE is largely over-produced, this was the region I of Fig. 3.3. This is exactly the setting we studied in this section and the result displayed on Fig. 3.5 can be used for the dark sector PT. Also Fig.3.6 can be straightforwardly extended to the EWPT, if we assume that some modification of the SM wield a strong enough EWPT. We will discuss this

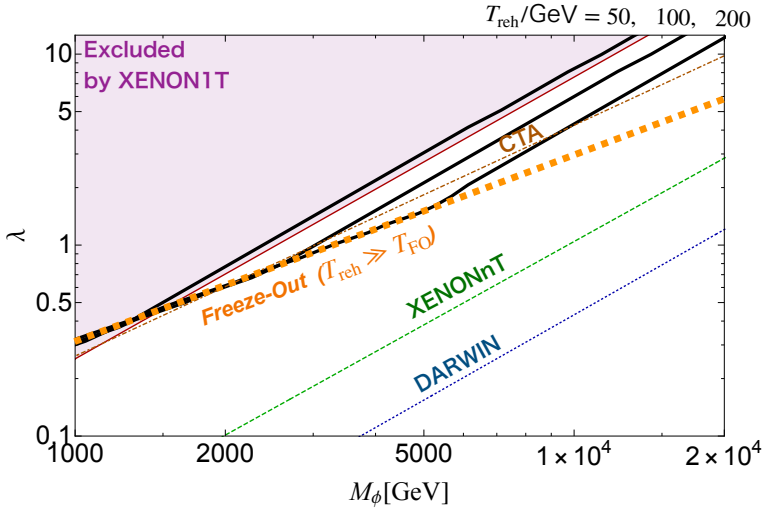

Figure 3.6: The parameter region of the SM Higgs portal dark matter with non-thermal over production for $T_{\rm reh} = 50\ {\rm GeV}, 100\ {\rm GeV}, 200\ {\rm GeV}$ from left to right [Black line]. $v_h = 174\,{\rm GeV}$, $m_{\rm med} = 125\,{\rm GeV}$, and $g_4 = 1$. The orange dashed line indicates the FO prediction. The purple region above the purple solid line may be excluded by XENON1T experiment [188]. The green dashed and blue dotted lines represent the future reaches of the XENONnT [189] and DARWIN [190], respectively. The lines are adopted from [175]. The Cerenkov Telescope Array (CTA) reach (by assuming the NFW distribution of DM) is adopted from [191].

possibility further in Section 3.5.

3.4.2 Dilution by supercooling

In Section 3.4.1 we saw that even if the DM is over-produced by the wall, the relic abundance can be reduced by the reaction $\phi\phi \to \varphi\varphi$. For the case of $v \approx 174$ GeV, this opened up the range of values $M_\phi \in [1, 10]$ TeV and $\lambda \in [0.3, 10]$, which is normally with too small abundance in usual FO. In this section, we would like to account for a second effect, which is the dilution induced by some amount of supercooling. Indeed, if some low-scale thermal inflation[176, 177] occurs due to the supercooling, a possibly large hierarchy between the reheating temperature and the nucleation temperature can occur.

During the thermal inflation[192], the expansion factor scales like $a \propto e^{Ht}$ and the temperature like $T_{\rm rad} \propto e^{-Ht}$, the FO abundance is a non-relativistic fluid scaling like $\Omega_{\rm FO} \propto T^3$. As a consequence, the FO abundance receives a further $\left(\frac{T_{\rm nuc}}{T_{\rm reh}}\right)^3$ suppression factor with respect to usual cosmology evolution. Summing both FO and BE contributions the total relic abundance will be approximately given by (we are assuming $M_\phi \gtrsim 20 T_{\rm reh}$)

$$\Omega^{\rm today}_{\phi,{\rm tot}} h^2 \approx \left(\frac{T_{\rm nuc}}{T_{\rm reh}}\right)^3 \times \Bigg[\underbrace{0.1 \times \left(\frac{0.03}{\lambda}\right)^2 \left(\frac{M_\phi}{100\ {\rm GeV}}\right)^2}_{\rm FO} + \underbrace{5 \times 10^3 \times \lambda^2 \frac{v_\varphi}{M_\phi}\left(\frac{v_\varphi}{\rm GeV}\right)}_{\rm BE}\Bigg]. \tag{3.50}$$

When BE contribution and FO contribution are small, the thermal production may become dominant, especially with $T_{\rm reh} \gtrsim 1/20 M_\phi$ (see Eq. (3.44)). Assuming an instantaneous reheating after bubble collision and negligible non-thermal production of ϕ via bubble collision [167], the additional contribution from thermal production takes

the form

$$\delta\Omega_{\phi,\mathrm{tot}}^{\mathrm{today}} \sim M_\phi \left.\frac{\langle\sigma_{\phi\phi}v_{\mathrm{rel}}\rangle n_{\mathrm{eq}}^2}{Hg_{\star S}(T)T^3}\right|_{T=C'T_{\mathrm{reh}}} \times \frac{g_{\star S0}T_0^3}{\rho_c}. \tag{3.51}$$

This formula agrees well with the numerical simulation by taking $C' \sim 0.9 - 1$. Since, around the T_{FO}, this contribution changes exponentially with temperature via n_{eq}, the range of C' may be slightly wider, which depends on the detailed process of the bubble collision.

Let us also mention that, insisting on dominant BE production (second term of Eq.(3.50) larger than first term and thermal production in Eq.(3.51)), perturbativity $\lambda < 4\pi$, maximal mass Eq.(3.36) and finally current bound on the relativistic species at BBN, impose the following constraints on the broken symmetry VEV of the (Dark-)Higgs:

$$\text{MeV} \lesssim v_\varphi \lesssim 10^8 \text{ GeV}, \quad \text{(scale range)}. \tag{3.52}$$

The upper bound is due to the quadratic dependence of the BE production on the VEV v_φ while the lower bound comes from stringent BBN bound on the number of relativistic species, which demands that our transition happens before $T \sim 1$ MeV.

On Fig. 3.7, we display the values of M_ϕ and λ providing the observed amount of DM relics for the various values of the reheating (T_{reh}) and nucleation (T_{nuc}) temperatures for the fixed scale $v_\varphi = 2000$ GeV. We have also assumed that the bubble wall could reach runaway regime due to suppressed plasma pressure (no phase dependent gauge fields), so that the upper bound for the DM mass in Eq.(3.36) becomes $\sim 10^8$ GeV. These curves were obtained by numerical solution of the Boltzmann equations but qualitatively we can understand the shape of the isocontours as follows:

- Let us start with the top left plot on the Figure 3.7. The orange dashed line corresponds to the usual DM *freeze-out*. As we can see, it is the case if the DM is lighter than roughly $20T_{\mathrm{reh}}$ and, in this case, the physics of the phase transition plays no role in the final DM relic abundance and the relic abundance is really fixed by a second freeze-out after the transition.

- For heavier masses the isocontours are given by the red dot-dashed triangles. The sides $\Omega_{\mathrm{BE,FO}}$ of the triangles are fixed by Eq.(3.50) and correspond to the cases when either Ω_{BE} or Ω_{FO} dominates the total relic abundance. The upper edge is controlled by the BE expansion and is more strongly coupled, the lower edge is controlled by FO. The almost vertical side at $M \sim 20T_{\mathrm{reh}}$ is given by Eq.(3.51) and corresponds to the thermal production of DM during reheating after bubble collision. Inside the triangle the DM is under-produced and outside, it is over-produced.

- Let us move on to the other plots on the Fig. 3.7. Multiple triangles correspond to the different values of supercooling. Finally the origin of the black line (continuation of the dashed orange line) can be traced back to the discussion in Section 3.4.1. In this case the DM is produced by BE mechanism, however the large coupling leads to an efficient annihilation and the final relic abundance is set by Eq.(3.49) .

3.4.3 Super-Heavy Dark Matter candidate

Another possibility to suppress the freeze-out (FO) density is to assume that the usual *inflation reheating temperature* T_R is too low and inflaton does not decay into the DM, so that ϕ is not produced by reheating and thermal scattering

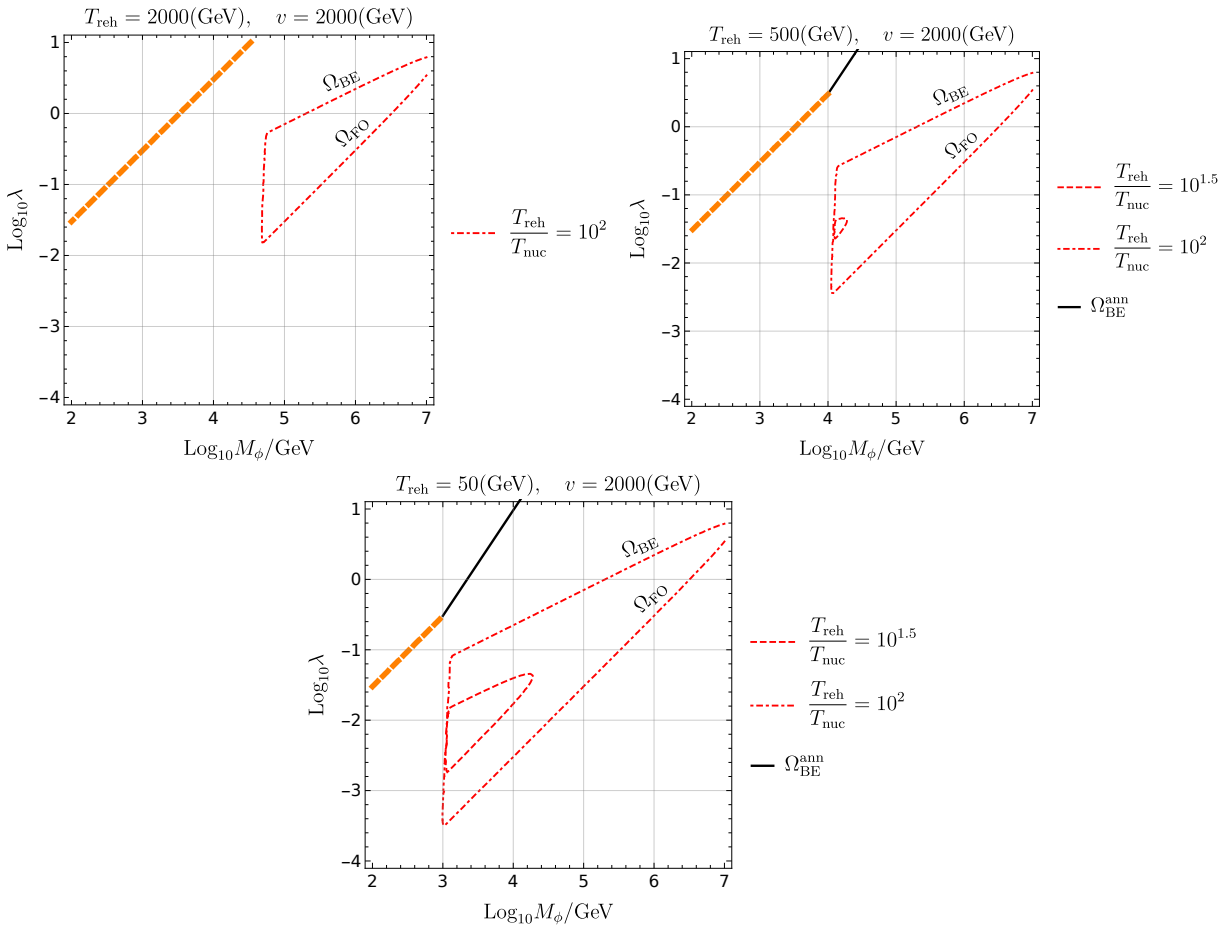

Figure 3.7: Values of M_ϕ and λ providing the observed DM relic abundance today in the Dark Higgs portal model, for values of supercooling $\frac{T_{\rm reh}}{T_{\rm nuc}} = (10^{1.5}, 10^2)$, $v_\varphi = 2000$ GeV, $g_4 = 1$. Each plot corresponds to a different value of the reheating temperature $T_{\rm reh} = 2000, 500, 50$ GeV. The Red lines correspond to contributions from FO and BE providing the observed DM abundance and that do not undergo annihilation after the transition. The black line is the result of DM annihilation, as in Section 3.4.1. Roughly when $M_\phi < 20 T_{\rm reh}$, the DM comes back to equilibrium after the transition and the final parameters compatible parameters are given by the orange dotted line. Let us also emphasize that we assumed runaway regime bubble, with the maximal DM mass given by Eq.(3.36)

process.[14] At this point, we can completely decouple FO contribution and we are left only with the BE production, so the region of parameter space with large masses M_ϕ or small coupling λ opens up. This condition writes

$$T_R \ll T_{\rm FO} \approx \frac{M_\phi}{20} \quad \text{(No FO condition)}. \tag{3.53}$$

where T_R is really the highest temperature at the end of inflation and is not the reheating temperature after the transition. There is again a word of caution about this interpretation of the reheating temperature as the highest temperature after the inflation, see [151], we will ignore it. Going back to Eq.(3.50) and assuming $T_{\rm reh} \approx v_\varphi$, we see that, in this scenario, the final relic abundance is now simply given by the BE contribution

$$\Omega^{\rm today}_{\phi,{\rm tot}} h^2 \approx 5 \times 10^3 \times \lambda^2 \left(\frac{v_\varphi}{M_\phi}\right)\left(\frac{v_\varphi}{\rm GeV}\right)\left(\frac{T_{\rm nuc}}{v_\varphi}\right)^3 \tag{3.54}$$

with four controlling parameters: $v_\varphi, T_{\rm nuc}, M_\phi$ and λ. Assuming vanishing supercooling in order to compute the maximal mass that can be produced, DM with mass as high as

$$\begin{aligned} M_\phi &\approx 5 \times 10^4 \lambda^2 \left(\frac{v_\varphi}{\rm GeV}\right)^2 \text{ GeV} \\ \lambda < 4\pi \quad &\Rightarrow M_\phi < M_\phi^{\rm MAX} \approx 5 \times 10^6 \left(\frac{v_\varphi}{\rm GeV}\right)^2 \text{ GeV} \end{aligned} \tag{3.55}$$

can provide the observed DM abundance, $\Omega_{\rm BE} = \Omega_{\rm obs}$. The second line was obtained by placing perturbativity bounds on the coupling, $\lambda < 4\pi$. Let us emphasize that this maximal mass has nothing to do with the previously computed maximal mass in Eqs.(3.36) and (3.37), where the production was suppressed by wall effects. In this case, the maximal mass originates from the fact that even in the unsuppressed region, the production scales as $\propto \frac{1}{M_\phi^2}$. Of course, those very large masses can only be activated by the transition if it does not contain gauge boson, according to (3.36). As a consequence, this possibility most probably can not be realised in the context of EWPT, as the wall quickly reaches a terminal velocity. Fixing $v_\varphi = 2 \times 10^2$ GeV, and considering vanishing supercooling, the observed relic abundance is displayed, in the space (M_ϕ, λ) on Fig.3.3 by the red line dubbed $\Omega_{\rm BE} = \Omega_{\rm obs}$.

3.5 BE production in EWPT

So far, with the exception of Fig.3.6, we have been general in our analysis and assumed that φ is a generic field undergoing a very strong FOPT. Let us now specialize to the case of EWPT $\varphi \to \mathcal{H}$ with $v_h \approx 200$ GeV and assume that the transition is strong enough to induce a relativistic wall. In Chapter 5 we will provide a model for realising such a EWPT, and revisit the DM production mechanism in this context. In this section, we would like to remain general. During the SM-Higgs transition, gauge bosons W and Z receive a mass and thus contribute to the pressure at NLO order. Thus the wall will inevitably reach a terminal velocity, which puts an upper bound on the maximal DM mass $M_\phi^{\rm MAX}$, above which the DM production starts to become exponentially suppressed. In Eq. (3.37), we have seen that this maximal mass increases with the supercooling :

$$M_\phi < M_\phi^{\rm MAX} \sim (\text{TeV}) \times \frac{T_{\rm reh}}{T_{\rm nuc}}. \tag{3.56}$$

[14] We may also consider that ϕ couples to the SM plasma via other couplings than that for the BE production. Then the FO component may be suppressed due to the large cross-section induced by the stronger couplings.

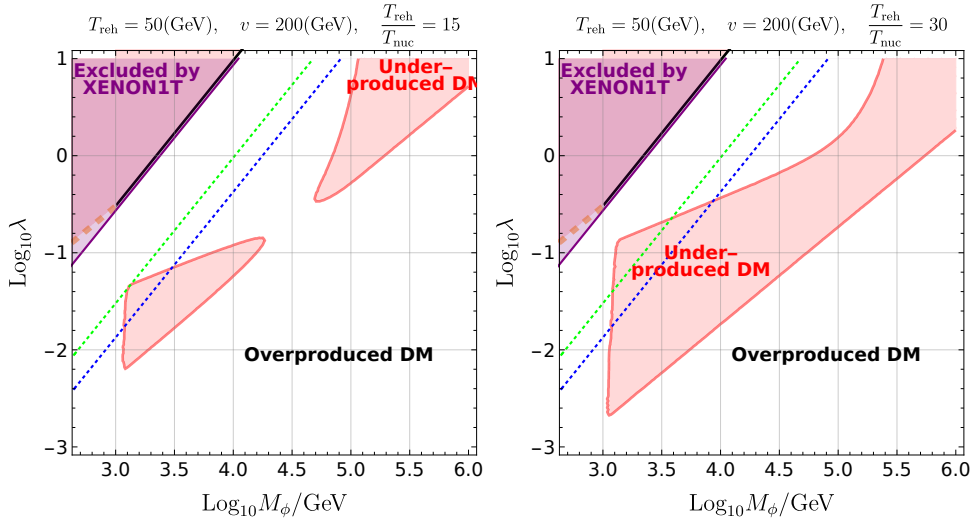

Figure 3.8: **Left**-Values of M_ϕ and λ providing the observed DM abundance in the SM Higgs portal model for $\frac{T_{\rm reh}}{T_{\rm nuc}} = 15$, $v = 200$ GeV, $T_{\rm reh} = 50$ GeV. The orange line gives the resulting FO prediction for thermal production in the case $M_\phi > 20T_{\rm reh}$ and the black line is the result of DM annihilation as computed in Section 3.4.1. The Dotted green and blue lines are defined like in Fig.3.6, as the future sensitivities of XENONnT and DARWIN and the violet region is already excluded by XENON1T. In the red-shaded region, DM is under-produced, outside, it is over-produced. **Right**-Same plot with $\frac{T_{\rm reh}}{T_{\rm nuc}} = 30$.

As a consequence, we will study the ϕ relic abundance in the range

$$[M_\phi^{\rm MIN}, M_\phi^{\rm MAX}] = [\text{TeV}, M_\phi^{\rm MAX}] \sim [\text{TeV}, \frac{T_{\rm reh}}{T_{\rm nuc}} \times \text{TeV}]. \tag{3.57}$$

We set the lower bound $M_\phi^{\rm MIN} \sim$ TeV, below which the usual FO takes over again after reheating if $T_{\rm reh} \sim 100$ GeV, and the sub-TeV WIMP Miracle is mostly excluded as mentioned in the introduction. We will also assume that $T_{\rm nuc} \gtrsim \Lambda_{\rm QCD}$, otherwise QCD effects can become important and may trigger themselves the phase transition (see for example [193, 194]). As a consequence, we will assume that the longest supercooling will be roughly $\sim \frac{T_{\rm reh}}{T_{\rm nuc}} \lesssim 10^3$. These assumptions confine the DM candidate mass to be in the range to TeV $\lesssim M_\phi^{\rm MAX} \lesssim 10^3$ TeV, thus leaving us with a generous range of exploration. However this setting renders the scenario of Section 3.4.3, with very massive DM, difficult, so we will not consider it. In this Section, we will only consider the two mechanisms of Section 3.4.1 and 3.4.2. The coupling λ in the Eq.(3.14) become the Higgs portal coupling and leads to the direct detection possibilities. Plotting the isocontours in the (λ, M_ϕ) space similarly to the Figure 3.7 we have checked the current bounds and future prospects for direct DM detection on the Fig.3.8. We can see that parts of the parameter space where the annihilation of DM (Black line of 3.8) plays a role is already probed by XENON1T experiment and parts of parameter space with BE production mechanism will be tested by the future DARWIN and XENONnT experiments, at least partially. The red-shaded region displays the regions of parameter space where the DM is under-produced, while outside of it, DM is over-produced and the observed DM abundance corresponds to the red line boundary. It is instructive to compare these results with the results of the Fig.3.7 where we have assumed that $\gamma_w \to \infty \Rightarrow M_\phi^{\rm MAX} \to \infty$. On left panel of Fig.3.8, for $\frac{T_{\rm reh}}{T_{\rm nuc}} = 15$ we can observe two islands of under-production: one at low mass and low coupling, which is exactly the same as on the Fig.3.7 and the one for the high masses and high couplings. In the later region the DM production from BE receives an additional suppression of the form $e^{-\frac{M_\phi^2}{2vT_{\rm nuc}\gamma_w}}$, according with the Eq.(3.28). On the right panel we present a similar plot for

$\frac{T_{\rm reh}}{T_{\rm nuc}} = 30$, however in this case two islands with and without exponentially suppressed DM production are joined.

Note that in our analysis we have included only the factor $e^{-\frac{M_\phi^2}{2vT_{\rm nuc}\gamma_w}}$, mentioned in Eq.(3.27) when we enter the regime of Eq. (3.30) and we have ignored further effects related to the exact wall shape see discussion in the in Appendix A.3 and Eq.(3.30).

To summarize we can see that a very strong EWPT can lead to the production of a DM candidate up to $10^2 - 10^3$ TeV with relatively large interaction couplings, while remaining consistent with observation. We will come back with more tools to this case in Chapter 5.

3.6 An alternative fermionic set-up

In this section, we would like to propose an alternative model, taking advantage of the production of fermions. We have already emphasized in section 3.3.4 the fact that the mass that the scalar would acquire in false vacuum could bring a crucial new factor $C_{\rm eff}$. Though we did not consider this factor explicitly, in this section we construct a model where the incoming particle is a massless fermion in the symmetric phase, so that $C_{\rm eff} \equiv 1$ by definition. The model consists of a vector-like neutral fermion N which is a singlet under SM and a couple of Z_2 odd scalar ϕ and fermion χ:

$$\mathcal{L} = \mathcal{L}_{SM} + Y_* \bar{L}\varphi N + M_N \bar{N} N + Y_{DM} \bar{N}\chi\varphi \ . \tag{3.58}$$

Here, L is a light fermion and N a heavy fermion coupling to φ undergoing the PT, respectively. The production mechanism works as follows: the heavy field N is produced during the phase transition of φ: $L \to N$ and it will subsequently decay into $N \to \chi\phi, N \to LH$.

In this model, heavy N are produced via $L \to N$ with a probability

$$\mathcal{P}^{\rm tree}(L \to N) \approx \frac{Y_\star^2 v_\varphi^2}{M_N^2} \Theta(\gamma_w T_{\rm nuc} - M_N^2 L_w) \ . \tag{3.59}$$

As a consequence, unstable heavy N accumulate behind the wall with initial density given by

$$\begin{aligned} n_N^{\rm BE} &\approx \frac{Y_\star^2 v_\varphi^2}{M_N^2 \gamma_w v_w} \int \frac{d^3p}{(2\pi)^3} \frac{p_z}{p_0} \times f_L(p, T_{\rm nuc}) \Theta(p_z - M_N^2/v_\varphi) \ , \\ &\approx \frac{Y_\star^2 v_\varphi^2 T_{\rm nuc}^3}{2\pi^2 M_N^2} e^{-\frac{M_N^2}{2v_\varphi T_{\rm nuc}\gamma_w}} + \mathcal{O}(1/\gamma_w) \ , \end{aligned} \tag{3.60}$$

where $v_w = \sqrt{1 - 1/\gamma_w^2}$, we expanded for large γ_w and approximated the Fermi-Dirac distribution as a Boltzmann distribution. Compared to the model with scalar fields, the density of the heavy fields inside the bubble will be additionally enhanced by $\sim 16\pi^2$ factor since $1 \to 1$ transitions are more effective than $1 \to 2$. Let us assume that $M_\phi < M_\chi$ so that ϕ is the DM candidate, then DM production will happen via the following chain of processes:

$$L \underset{\text{via PT}}{\to} N \underset{\text{via decay}}{\to} \phi\chi \to \phi\phi + \text{SM} \ . \tag{3.61}$$

However, the heavy N has two channels of decay: toward the heavy dark sector ϕ, χ and back to the light L. The abundance of ϕ, χ after the transition is thus suppressed and given by

$$n_\chi \approx n_\phi \approx \frac{Y_{DM}^2 Y_\star^2}{Y_{DM}^2 + Y_\star^2} \frac{v_\varphi^2 T_{\rm nuc}^3}{2\pi^2 M_N^2} e^{-\frac{M_N^2}{2v_\varphi T_{\rm nuc}\gamma_w}} + \mathcal{O}(1/\gamma_w) \ , \tag{3.62}$$

and the final relic abundance redshifted to today thus reads

$$\Omega^{\text{today}}_{\phi,\text{BE}}h^2 \;\approx\; 1.5\times10^8\times\frac{Y_\star^2Y_{DM}^2}{Y_\star^2+Y_{DM}^2}\frac{2M_\phi}{M_N}\left(\frac{v_{EW}}{M_N}\right)\left(\frac{v_{EW}}{246\text{GeV}}\right)\left(\frac{T_{\text{nuc}}}{T_{\text{reh}}}\right)^3 e^{-\frac{M_N^2}{2v_\varphi T_{\text{nuc}}\gamma_w}}\,. \tag{3.63}$$

For the freeze-out process in the symmetric phase, we have: $\phi\phi\to LHLH$ by neglecting co-annihilation. The cross-section is highly phase space suppressed (closing a loop for a 2 to 2 annihilation gives a similar scaling): $\sigma_{\phi\phi\to(L\varphi)^*L\varphi}\sim\frac{M_\chi^2(Y_{\text{DM}}Y_*)^2}{(16\pi^2)^2 4\pi M_N^4}$. The abundance by taking account the supercooling is

$$\Omega^{\text{today}}_{\phi,\text{FO}}h^2=10^3\left(\frac{T_{\text{nuc}}}{T_{\text{reh}}}\right)^3\frac{M_N^4/M_\chi^2}{(6\text{TeV})^2}\frac{10}{(Y_{\text{DM}}Y_*)^4}\,. \tag{3.64}$$

The total DM density today will be given by the sum of Eq.(3.63)-(3.64). Therefore, this scenario leads to the over-production of DM unless $M_\phi, M_\chi\lesssim 10$ GeV (assuming the EWPT case, as discussed above, making the scale of the transition higher could open some phase space). However, note that these equations are valid only for the heavy DM candidates which do not go back to equilibrium after the phase transition. Otherwise, the final density will be given by Eq.(3.64) only without $\left(T_{\text{nuc}}/T_{\text{reh}}\right)^3$ and we are going back to the normal freeze-out scenario.

Let us now investigate the regime $M_\phi\simeq M_\chi$, precisely $|M_\phi-M_\chi|\lesssim M_\phi/20$, where the co-annihilation takes place, which is concisely reviewed in Appendix A.7. In this case we have the channel $\phi\chi\to H\bar{L}$ to decrease the abundance of ϕ as well as χ. The cross-section is $\sigma_{\phi\chi\to H\bar{L}}\sim\frac{(Y_{\text{DM}}Y_*)^2}{4\pi M_N^2}$. Therefore, we have

$$\Omega^{\text{today}}_{\phi,\text{FO,Co}}h^2\sim 0.1\left(\frac{T_{\text{nuc}}}{T_{\text{reh}}}\right)^3\times\frac{M_N^2}{(10\text{TeV})^2}\frac{1}{(Y_{\text{DM}}Y_*)^2}\,. \tag{3.65}$$

Summing this estimate with the $\Omega^{\text{today}}_{\phi,\text{BE}}h^2$ in Eq.(3.63) we find that it becomes possible to reproduce the observed DM abundance. However we see that bubble expansion tends to overproduce the DM and the relic abundance in BE can be reproduced if only the factor $\exp[-M_N^2/(2v_\varphi T_{\text{nuc}}\gamma_w)]$ starts playing a role in suppressing DM relic density. We will check this fact numerically in Chapter 5 for the EWPT.

3.7 Observable signatures

As already presented in the Introduction 1.6, it is well known that an unavoidable signature of strong FOPT's, with very relativistic wall, is a significant Stochastic Gravitational Waves Background (SGWB) signal, with peak frequency controlled by the scale of the transition $f_{\text{peak}}\sim 10^{-3}\frac{T_{\text{reh}}}{\text{GeV}}$ mHz. As an example, the EWPT signal is expected to peak in the mHz range, which is the optimal range of sensitivity of the forthcoming LISA detector. Then the constraint Eq.(3.52) turns into a constraint on the frequency of the signal

$$10^{-6}\text{ mHz}\lesssim f_{\text{peak}}\lesssim 100\text{ Hz}\qquad\text{(Frequency range)} \tag{3.66}$$

We can also more or less constrain the model parameters for a given reheating temperature or peak frequency. In Fig. 3.9, we show T_{reh} (and thus f_{peak} by assuming $f_{\text{peak}}=10^{-3}\frac{T_{\text{reh}}}{\text{GeV}}$) vs the mass range. The parameter region satisfies the constraints of correct DM abundance Eq. (3.50)≈ 0.1, the dominant BE production (second term of (3.50) dominant, suppressed thermal production $T_{\text{reh}}<1/20M_\phi$), Eq. (3.36), perturbativity ($\lambda<4\pi$), and consistency conditions $T_{\text{reh}}\geq T_{\text{nuc}}, v_\varphi\geq T_{\text{reh}}$. For the late time annihilation, we can read the relation for mass, λ,

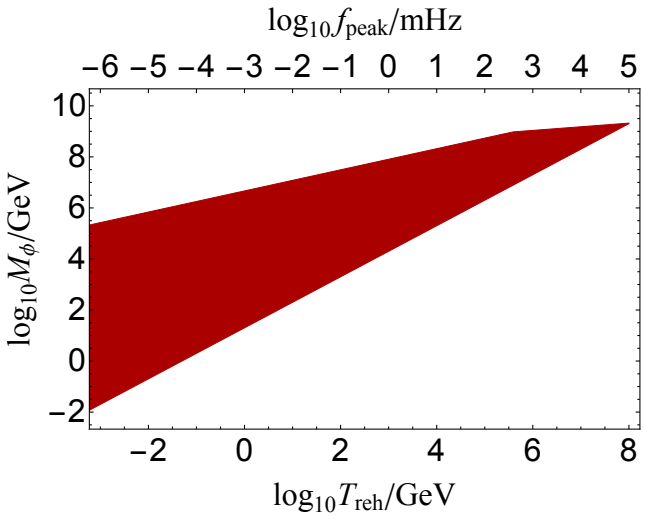

Figure 3.9: Reheating temperature vs the mass range of DM from BE production via a Dark PT. Also shown is an approximate peak frequency in the upper axis.

and $T_{\rm reh}$ from Figs. 3.5 and 3.6. These imply that the observation of the SGWB provides a probe of the parameter range.

Using the results presented in 1.6, we observe that strong GW signals are obtained for: 1) large α, which is the consequence of long supercooling and large latent heat, 2)small β, which are obtained for slow transitions and thus large bubbles at collision, and 3)relativistic walls $v_w \to 1$. Thus, the same conditions necessary for the BE production of Dark Matter will induce the strongest GW signal. In Fig.3.10, we present the signal induced by four benchmark point, each representative of a specific regime: P1 (runaway $\alpha = 1, \beta = 100$), P2 (runaway $\alpha = 0.1, \beta = 1000$), P3 (terminal velocity $\alpha = 1, \beta = 100$), P4 (terminal velocity $\alpha = 0.1, \beta = 1000$) with $T_{\rm reh} = v_\varphi = 200\,\text{GeV}$. We also represent the GW signal with several $T_{\rm reh}$ in the range corresponding to Fig. 3.9 by fixing $\alpha = 1$ and $\beta = 100$. As we expect the scaling $\frac{\alpha_\infty}{\alpha} \propto \left(\frac{T_{\rm nuc}}{v_\varphi}\right)^2$, we set a suppressed $\alpha_\infty = 0.001$, due to quite large supercooling that we considered in most of our scenarios.

We can see that generically BE mechanism for DM production leads to the stochastic gravitational wave signature in the frequency range Eq.(3.66), which is well in the reach of the current and future experimental studies.

Interestingly enough, it has been also recently noticed that this mechanism, in the context of a non-gauged transition could produce warm and hot dark matter with heavy mass[195] and several signatures were discussed.

3.8 Summary and outlook

In this chapter we have presented a novel mechanism of the DM production. We have shown that the ultra relativistic expansion of the bubbles during the first order phase transition in the early universe can produce a significant amount of the cold relics even if the mass of the DM candidate is much larger than the scale of the phase transition. This, as a consequence, "brings back to life" components that, due to Boltzmann suppression, did not belong to the plasma any more. We illustrate this mechanism on a simple renormalizable model where DM is a scalar coupled via portal coupling to the field experiencing the phase transition. When the bubble wall reaches velocities $\gamma_w > \frac{M_\phi^2}{v_\varphi^2}$ the exponential suppression of the heavy particle production disappears and BE mechanism can become very significant

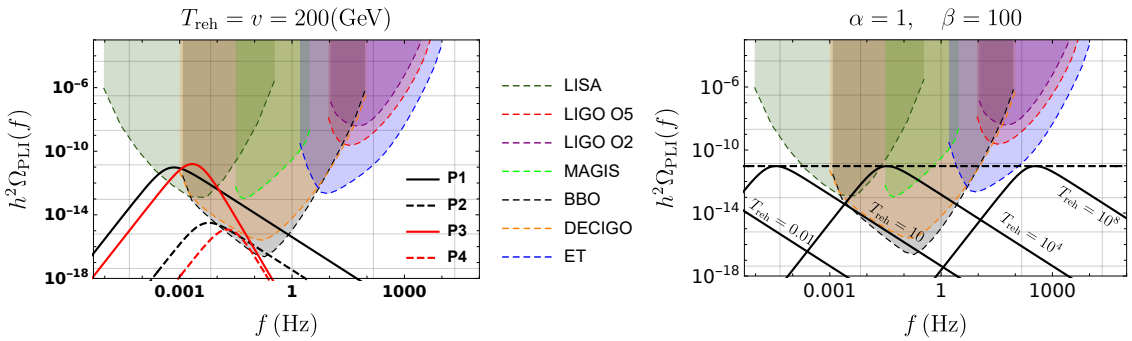

Figure 3.10: **Left**-GW signal with $v_\varphi = T_{\rm reh} = 200$ GeV for four benchmark points in four different regimes: P1 (runaway $\alpha = 1, \beta = 100$), P2 (runaway $\alpha = 0.1, \beta = 1000$), P3 (terminal velocity $\alpha = 1, \beta = 100$), P4 (terminal velocity $\alpha = 0.1, \beta = 1000$). We also took $\alpha_\infty = 0.001$. The signal-to-noise ratio and the sensitivity curves can be build following the recommendations of[38, 39, 40, 41, 42, 43, 44, 45]. **Right**- The runaway GW signal with fixed $\alpha = 1, \beta = 100$ are shown with $T_{\rm reh} = 10^{-2}, 10, 10^4, 10^8$ GeV corresponding to the parameter range given in Fig. 3.9.

in large ranges of parameter space. Thus the produced DM density can be easily dominant. In the simple model presented in the chapter both BE and FO contributions to the DM relic density were controlled by the same coupling, however this does not have to be the case for more complicated models, where additional interactions can suppress FO contribution further.

In the absence of FO produced relics, BE mechanism also provides the possibility of super-massive strongly coupled DM candidate, which is a scenario similar to the *baby-zillas* of [167]. We showed that there are parameter regions where the BE production dominates over the FO production and explains the observed amount of DM in the universe. This opened up the range of Multi-TeV DM with large coupling, thus being more detectable at direct detection (like forthcoming XENONnT and DARWIN) experiments and indirect detection (like the CTA) experiments than the usual FO mechanism.

Our mechanism is also characterized by an unavoidable and possibly observable imprint in the SGWB, with peak frequency controlled by the scale of the transition. The shape of the spectrum can then discriminate between runaway or terminal velocity bubble wall behaviour. Let us also emphasize that if the DM belong to a totally decoupled DS, SGWB signal is the only unavoidable imprint.

An interesting question is how to embed our production mechanism into a theoretically motivated model of DM.

Chapter 4

Relativistic bubble wall Baryogenesis

In the previous two chapters, we have seen that phase transition, when the wall becomes ultra-relativistic, could activate heavy states in the plasma. In Chapter 2, we saw that those states, when produced, induce a new contribution to the pressure on the wall and in Chapter 3, we saw that the heavy states produced could also fix the DM abundance. In this chapter, we would like to go one step further and compute the production mechanism at one-loop and prove that it can transform a imaginary phase in the Yukawa into a CP-violation in the production abundances. With this in mind, we then embed the model with a L or B violation and build a mechanism of baryogenesis with *relativistic walls*.

Contents

4.1 Matter anti-matter asymmetry

The existence of anti-matter famously originates from the relativistic formulation of Quantum Mechanics by *P.A.M Dirac* in 1928. In this framework, the description of the electron immediately induces the existence of a new degree of freedom with same spin and mass but opposite charge: this is the *positron* or *anti-electron*. Only some few years later, in 1932, *Carl Andersen* observed in a cloud chamber, tracks from cosmic rays of a particle with same mass than the electron but opposite charge. He interpreted it as being the previously theorised positron.

Today, the existence of anti-matter is not a source of discussions anymore and it is known that all the fermions of the SM (with maybe the exception of the neutrinos) come with an anti-matter partner. At this point, we could believe that the existence of this symmetric partner would be absolutely unproblematic from a theoretical and a observational point of view. However, let us consider the origin of the universe and, for the concreteness (and also naturalness), let us initially set an equal amount of matter and anti-matter. Then a channel of the form $f\bar{f} \to \gamma\gamma$ exists for all the fermions.

The intuition from freeze-out exposed in the previous chapter can be carried out in the same way to this channel. When some fermion f become non-relativistic, $M_f \gtrsim T$, its equilibrium abundance starts to become suppressed according to $\propto e^{-M_f/T}$ until the reactions controlling the annihilation $f\bar{f} \to \gamma\gamma$ cannot compete with the expansion of the universe and go out-of-equilibrium. The abundance is then frozen-out. For the case of protons, we can plug in $M_f = m_p$ and a typical cross-section $\sigma_{p\bar{p}\to\gamma\gamma} \sim 1/m_p^2$ and we obtain a relic abundance of the order $n_p/n_\gamma \sim 10^{-20}$. So there would be very small amount of matter and anti-matter (in equal amounts) left with respect to the photons. Is it realistic ?

First of all, the absence of high-energy gamma rays from distant galaxies and that no “anti-galaxy" has ever been observed[196] indicates that most likely, all the galaxies in the observable universe are made of matter, and not anti-matter. Moreover, the ratio of protons over photons strongly controls the features of two of the very important early universe processes: Big Bang nucleosynthesis (BBN) and Cosmic Microwave Background (CMB). The BBN predictions are strongly dependent on the ratio n_B/n_γ at the time of BBN. If there are more photons, the photo-dissociation is enhanced and the neutrons have more time to decay. The CMB also depends on this ratio: as the the early universe photon fluid comes with an internal pressure while the fluid of baryons is essentially pressureless, the relative abundance of baryons and photons controls the efficiency of baryon acoustic oscillations and thus the high of the CMB peaks. Matching with observation totally rules out the naive possibility of frozen-out matter and anti-matter, by roughly 10 orders of magnitude.

We thus have to change attitude. Let us now assume that in the initial conditions of the universe, there was a slight mismatch between the amount of baryon and anti-baryon. The very efficient interactions would thus totally annihilate the common part of matter and anti-matter, and leave only the initial difference. The over-abundance of matter is commonly parametrized via the difference of matter and anti-matter densities, normalised by the entropy

$$Y_B \equiv \left.\frac{n_B - n_{\bar{B}}}{s}\right|_0 \tag{4.1}$$

with $n_B, n_{\bar{B}}$ and s respectively the number density of baryons, anti-baryons and the entropy density. The subscript 0 means “at present time”. As already mentioned, Planck data and evolution models of the early universe permit to compute this ratio with high accuracy[197]

$$Y_B = (8.75 \pm 0.23) \times 10^{-11}. \tag{4.2}$$

Remarkably, the BBN data, though a bit less precise, points toward the same ballpark of values. This means roughly that in the initial conditions of the universe there was $10^{10} + 1$ baryons for 10^{10} anti-baryons.

In the standard picture of cosmology, this remains highly unsatisfactory. Indeed, it is believed that the first phase of the universe history was a dramatic exponential expansion, the *inflation*, which should have diluted away any initial conditions. This blindness to the initial conditions is at the same time a blessing and a curse: everything can be explained in terms of dynamics, but we cannot rely on an initial over-abundance of matter. In the context of the inflationary paradigm, we thus need a mechanism for the creation of an over-abundance of matter over anti-matter, a mechanism of *Baryogenesis*, which has to occur *before* BBN, at around $T \sim 1$ MeV.

4.1.1 Sakharov conditions

The conditions for a successful over-abundance of matter over anti-matter were realised already more than 50 years ago in the seminal paper by Sakharov [198]. For a successful baryogenesis scenario, the well-known Sakharov requirements should be satisfied [198]; namely the violation of the baryon number, violation of C and CP symmetries, and an out-of-equilibrium process. Let us go through those conditions and explain them more in detail.

- **B violation**: This condition is rather obvious since no baryon can be created in a reaction if $i \to f$ does not change the baryon number of the initial and final states.
- C **and** CP **violation**: Let us now assume a B-violating interaction $f_i \to f_j$. If C was conserved, the interaction rates of $f_i \to f_j$ and $\bar{f}_i \to \bar{f}_j$ would be equal. Now the baryon number of f_j is *opposite* to the one of $\bar{f}_j$, and if the two reactions occur with the same rate, they would cancel each other. In a similar way, if CP was conserved, then, due to the renowed CPT theorem, T would be conserved as well. This would enforce the equality of the rates of

  $$\Gamma[f_i(\mathbf{r},\mathbf{p},\mathbf{s}) \to f_j(\mathbf{r},\mathbf{p},\mathbf{s})] = \Gamma[f_i(\mathbf{r},-\mathbf{p},-\mathbf{s}) \to f_j(\mathbf{r},-\mathbf{p},-\mathbf{s})] \tag{4.3}$$

  We thus observe that after averaging over the phase space and the spin, the baryon number vanishes.
- **Departure from the thermal equilibrium**: This is maybe the less intuitive of the three Sakharov conditions. The standard argument is to say that a perfectly equilibrated situation does not offer a direction to the time, which makes the reversal with respect to time irrelevant, and by extension the CP-flipping as well irrelevant. An elegant proof of this statement is given in the TASI lecture [199]. In this mathematical form, if the equilibrium condition is enforced, the following is valid

  $$\begin{aligned}\langle B\rangle_T = \text{Tr}[e^{-H/T}B] &= \text{Tr}[(CPT)(CPT)^{-1}e^{-H/T}B] \\ &= \text{Tr}[e^{-H/T}(CPT)^{-1}B(CPT)]\end{aligned} \tag{4.4}$$

  where the last step is valid because of the CPT theorem. On the other hand, B receives a minus sign upon conjugation, so this is equal to $-\langle B\rangle_T$. So overall $\langle B\rangle_T = 0$ and baryogenesis is impossible.

  Let us however try to make this condition more precise. At this point, an important clarification is in order. For concreteness, let us take a particle ψ: for this particle ψ, two types of equilibrium can be defined in a plasma: the *kinetic* equilibrium and the *chemical* equilibrium: the former is related to the thermal distribution of the gas of ψ and is enforced if the rate of elastic collision of ψ with the bath is in equilibrium (faster than the Hubble expansion). In this case, the distribution function of the ψ particle is given by the standard result of statistical physics, Fermi-Dirac if ψ is a fermion, Bose-Einstein of ψ is a boson, f_{eq}, possibly suppressed by an overall constant. The second, the chemical equilibrium is related to the number of the χ particles in the plasma, which is controlled by ψ number changing interactions. If the rates of ψ number changing interactions are in equilibrium, the chemical equilibrium is enforced and the sum of the chemical potentials of the particles in the initial state is equal to the sum of the chemical potential in the final state,

  $$\Gamma(A + B \leftrightarrow C + D) \gg H \Rightarrow \mu_A + \mu_B = \mu_C + \mu_D. \tag{4.5}$$

  It is typically easier to reach kinetic than chemical equilibrium. To be perfectly clear: baryogenesis requires a departure from *chemical* equilibrium.

Though those conditions are not an absolute necessity for baryogenesis (mechanisms avoiding one of those conditions can be manufactured, see[200] for a review), they provide a powerful guidance for model building. Those three conditions set the game for the play: *we need to imagine an early universe event that is out-of-equilibrium, violate C and CP and B number, and finally occurs for temperature higher than* ~ 1 *MeV.*

4.1.2 Sphalerons

Though conserved at the classical level, the baryon and lepton number conservations are violated at quantum level by the anomalies[201].

$$\partial_\mu J^\mu_B = \frac{g^2 n_f}{32\pi^2} F\tilde{F}, \qquad \partial_\mu J^\mu_L = \frac{g^2 n_f}{32\pi^2} F\tilde{F} \tag{4.6}$$

where $J^\mu_B(J^\mu_L)$ is the baryon (Lepton) current, $n_f = 3$ is the number of families and F ($\tilde{F}$) is the $SU(2)$ weak force strength (its dual). We thus immediately see that $B - L$ should be conserved, but it will not be the case of $B + L$.

Integrating the equation in Eq.(4.6), we see that the baryon number is connected to

$$B(t) - B(0) = n_f Q(t), \qquad Q(t) = \int d^3x \int_0^t dt_1 \frac{g^2}{32\pi^2} F\tilde{F} \tag{4.7}$$

Moreover, it can be shown that the so-called *Chern-Simons* number

$$N_{CS} \equiv \int d^3x \frac{g^2}{32\pi^2} F\tilde{F} \tag{4.8}$$

is a topological number and has to be an integer, and, via non-perturbative interactions, can have jumps of one unit. Though exponentially suppressed by the mass of the gauge bosons and the small couplings at zero temperature and then totally negligible, sphaleron rates are strongly enhanced by thermal effects. In a thermal environment [202]

$$\Gamma_{\rm spha} \sim 25\alpha_W^5 T^4 \tag{4.9}$$

Sphalerons are active, in thermal equilibrium for temperature in the crude range

$$T_{\rm EWPT} < T_{\rm spha} \lesssim 10^{12}\ \text{GeV} \tag{4.10}$$

Also, in the case of leptogenesis, the asymmetry is first produced in the lepton sector, and is then transferred to the baryon section via the sphalerons themselves, upon a multiplicative factor (see for example [203]). If we start with some asymmetry Δn_L, we produce

$$\Delta n_B = -\frac{28}{79}\Delta n_L \tag{4.11}$$

4.1.3 Theories

Based on those general requirements various models have been constructed (for reviews see for example [204, 205]) based on the different realizations of the Sakharov's conditions. To see how broad is the landscape of baryogenesis, let us present of some of the baryogenesis scenarios that have already been proposed.

As we already said, the inflation itself imposes the need for a baryogenesis mechanism, but as well could be at the origin of it. This is the case in the context of a rotating condensate[206, 207, 208, 209] with baryon violating interactions through the famous *Affleck-Dine*(AD) mechanism. More recent proposals use the QCD axion as the rotating field[210, 211] and as been dubbed *axiogenesis*. Baryogenesis could also occur during the strongly out-of-equilibrium first phase of reheating, the preheating[212]. Though they have been connected to the emission

of GW[213], AD baryogenesis and baryogenesis in preheating would have likely occurred at very high energy and would have left very elusive signals.

One of the leading candidate for baryogenesis is the out-of-equilibrium decay of heavy particles, that materializes itself in the mechanisms of *GUT baryogenesis*[214] if we consider Grand-Unified theories and *baryogenesis via leptogenesis*[215] (and [216] for a nice review), where the CP violation occurs in the leptonic sector and is transmitted to the baryons via the sphalerons. Usually the Heavy neutrino is required to be Majorana, for the violation of the lepton number to be present, however, models with Dirac neutrinos also exist, the Neutrino-genesis scenario[217, 218], where the lepton number is *not* violated. In the previous models, the decaying particles are produced thermally. A third class of out-of-equilibrium decay is when the decaying particle is produced non thermally: the production can happen during inflation [219, 220] or during preheating [221, 222].

A class of baryogenesis models that does not require departure from equilibrium is *Spontaneous baryogenesis*[223, 224], which can also be realised with the collapse of axion domain walls[225]: the main idea is that the Sakharov conditions are needed only as long as we enforce the CPT theorem, which can be effectively violated in the early universe.

Baryogenesis can also occur through neutrino oscillations[226, 227, 228], from black hole evaporation[229, 230, 231], or via asymmetric Freeze-out, where particle and anti-particle decouple at a slightly different temperature and create baryon number[232].

An exciting possibility is that baryogenesis occurs at the same time than DM production, as in the scenarios of *cogenesis*[233, 234, 235, 236] and *Darkgenesis*[237]. Those scenarios have the nice feature of addressing the "coincidence problem", of why the density of baryonic matter and dark matter are so similar $5\Omega_b \sim \Omega_{\rm DM}$.

One of the most interesting possibility for the fulfillment of the out-of-equilibrium process requirement is a scenario in which a phase transition occurs in the early history of the universe. Many baryogenesis mechanisms using PT have been studied, here are some: Darkogenesis[238] where the PT occurs in a dark sector, baryogenesis via the collision of runaway bubbles[239], liberating heavy states, EWBG with Yukawas varying during the EWPT[240, 241] which makes the transition strong and permits to strongly violate CP in the symmetric phase, baryogenesis from confining EW phase transition[242], baryogenesis with ultra-relativistic walls[243], baryogenesis using a Composite Higgs[244]. A very studied other possibility is the Cold Baryogenesis[245, 246], [247, 248, 249, 250, 251, 252] where the transition is again the EWPT but the mechanism is very different. In this case, the EWPT is triggered by a fast tachyonic instability in the Higgs potential, coming from the coupling with another scalar potential, for example a dilaton. This case, in which the Higgs mass squared turns negative abruptly due to the rolling of the other field is called *Higgs quenching*. For example, we can have

$$\Delta\mathcal{L} = \frac{\Lambda^2 - \sigma^2}{2}\mathcal{H}^\dagger\mathcal{H} \tag{4.12}$$

where σ is some rolling scalar field and Λ is some scale. When $\sigma \to \Lambda$, two things occur: there is an explosive production of Higgses, and there is a production of EW gauge *textures*. Those textures being unstable, they decay via Chern-Simons number transitions. If CP violation comes only from the SM, it has been claimed that the baryon asymmetry is strongly underproduced[253]. Another source of CP-violation often introduced is

$$\Delta\mathcal{L} = \frac{\mathcal{H}^\dagger\mathcal{H}}{M^2}\mathrm{Tr}F\tilde{F}. \tag{4.13}$$

During the decay of textures, $\mathcal{H}^\dagger\mathcal{H}$ will be time dependent, which will act as an effective chemical potential (because effectively, in the lagrangian, there is a $\mu_B N_{CS}$ term) for baryons and will feed baryon number.

But, by far the most studied case is the *Electroweak Baryogenesis* (EWBG)[254, 255] (for reviews see e.g.[256] and references therein). The usual tale for EWBG is: the universe starts, possibly after a period of inflation, with an early hot, radiation-dominated, plasma where EW symmetry $SU(2)_L \times U(1)_Y$ is restored. During this evolution, the relevant mass scale is the temperature of the plasma, which controls most of the dynamics and stabilizes the electroweak interactions in the symmetric minimum. The universe expanding, the cooling of the plasma suppresses the temperature corrections, until the symmetric vacuum becomes unstable. Assuming that the EWPT is first order, the discontinuity between the symmetric and higgsed phases induces an out-of-equilibrium region in front of the discontinuity, thus fulfilling one necessary Sakharov conditions.

As the bubble of new higgsed phase expand in the symmetric phase, plasma particles can enter or scatter back on the wall. If the underlying theory contains CP violation, then the scattering off the wall happens in a CP violating way, inducing a chiral asymmetry in front of the wall. As in the symmetric phase, sphalerons are very efficient, they convert this chiral violating abundance in baryon asymmetry. The plasma is then swallowed by the expanding bubble. The last condition for the successful baryogenesis is then that the sphalerons are inefficient inside of the bubble, which imposes a condition on the strength of the transition. Thus, the condition for the sphalerons to decouple after the EWPT is given by [257, 258]

$$\frac{v_h(T_{\rm crit})}{T_{\rm crit}} \gtrsim 1.1. \tag{4.14}$$

where it has been assumed that $T_{\rm nuc} \approx T_{\rm reh} \approx T_{\rm crit}$.

However in the standard model, lattice simulations have suggested that the EWPT *is not* of the first order[259]. As such the SM faces two major difficulties for EWBG: the lack of FOPT, due to heavy Higgs and the lack of CP violation in the SM[260, 261, 262].

Various physically motivated extensions of the standard model could provide room for EWBG via a first order EWPT [263, 264, 265, 266, 267] (see [256] for review) or via some other dark phase transitions, typically a $U_L(1)$ breaking transition [268, 269] in the early universe. MSSM, providing many new source of CP-violation and making the EWPT strongly first order via the light stop, was arguably the most attractive case. However, the window allowing for EWBG requires a stop mass $m_{\tilde{t}} \lesssim 120$ GeV[270]. Unfortunately *Light Stop Scenario* is now excluded by the LHC searches[271]. On the other hand, EWBG maybe still has some allowed parameter space in NMSSM[272] and in Split NMSSM [273]. However, strong constraints from EDM [274]

$$\frac{d_e}{e} < 1.1 \times 10^{-29}\text{cm} \tag{4.15}$$

[205] seems to definitively rule out those scenarios. According to the words of [196], EWBG is *sleeping beauty mode, waiting to be awaken* by positive experimental data.

On the top of all the previous mechanisms, news proposals are reviewed in [275].

In this chapter we propose a new mechanism for the production of the baryon asymmetry during a FOPT, which is only effective in the opposite regime than EWBG i.e. *for the ultra-relativistic bubble wall expansions.* The idea will be based on the recent observation already presented in the previous chapters that, in the presence of a very relativistic bubble expansion with Lorentz factor $\gamma_w \gg 1$, particles with mass up to $M \lesssim \sqrt{\gamma_w T_{\rm nuc} \times v}$ can be produced. The parameters $T_{\rm nuc}$ and v are the temperature of FOPT and the scale of the symmetry breaking respectively. The process of the heavy states production during the FOPT is obviously out-of-equilibrium, so that if it proceeds through a CP-violating process and baryon number is not preserved we can have a successful baryogenesis scenarios[1]. We confirm the statements above by analyzing the CP-violating effects in the interference

[1]For other baryogenesis models with new heavy fields production during FOPT see [239].

of tree and one-loop level processes. Then we construct explicit models where the baryogenesis is realized during the strong FOPT, which can be either the EWPT itself, if it comes with the necessary new physics, or related to some other symmetry breaking in the early universe.

We finally note that, interestingly, this class of models contrary to the "traditional" baryogenesis presented just above needs ultra-relativistic bubble wall velocities and is generically accompanied with strong gravitational waves signal.

4.2 Mechanism of CP-violation via bubble wall

In this section we go beyond the two previous chapters 2 and 3 where we presented the computation of the production at tree-level. To compute the possible CP violation, we need to provide a one-loop computation of the production. To do so, in a first subsection, we present a new formalism, then we revisit the tree-level computation. Finally, we are in position of computing the one-loop production.

Method of calculation of the light $\to$ heavy transition

Before we proceed to the one loop calculation, let us present a generic method to compute the transition amplitudes[2]. We will then apply it to recover Eq.(3.59) and later for the computations of the one loop corrections. In this section we will omit the flavour indices which we will easily recover once the loop functions will be derived. We restart from a Lagrangian like in Eq.(2.66):

$$\mathcal{L}_{\text{fermion}} = i\bar{\chi}\partial\chi + i\bar{N}\partial N + M\bar{N}N + Y\varphi\bar{\chi}N. \tag{4.16}$$

Let us look at the correlation function $\langle 0|T\{\bar{\chi}(x_1)N(x_2)\}|0\rangle$ and calculate it to first order in $\mathcal{O}\left(\frac{\langle\varphi\rangle}{M}\right)$ which will be our expansion parameter. We assume that the wall is located in $x-y$ plane at $z=0$. The correlation function writes

$$\langle 0|T\{\bar{\chi}(x_1)N(x_2)\}|0\rangle = \int d^4x Y\langle\varphi(x)\rangle S_\chi(x_1-x)S_N(x-x_2) + \mathcal{O}\left(\frac{Y\langle\varphi\rangle}{M}\right)^2 \tag{4.17}$$

where we are expanding the correlation functions of the theory with $\langle\varphi\rangle \neq 0$ in terms of the correlation functions $S_{\chi,N}$ of the unbroken $\langle\varphi\rangle = 0$ theory. Then performing the Fourier transformation we will obtain

$$\begin{aligned}
&\int d^4x d^4k d^4q e^{ik(x_1-x)+iq(x-x_2)} S_\chi(k)S_N(q)Y\langle\varphi(x)\rangle \\
&= \int d^4k d^4q e^{ikx_1-iqx_2} S_\chi(k)S_N(q) \times \left[(2\pi)^3\delta^{(3)}(k-q)\int dz e^{iz(k_z-q_z)}Y\langle\varphi(z)\rangle\right], \\
&\delta^{(3)}(k-q) \equiv \delta^{(1)}(k_0-q_0)\delta^{(1)}(k_x-q_x)\delta^{(1)}(k_y-q_y).
\end{aligned} \tag{4.18}$$

Let us make a few comments regarding this expression. The propagators $S_{\chi,N}$ have poles at, respectively $p^2 = 0, M^2$ and this, together with energy and $(x-y)$-momentum conservation, fixes the exchange of momentum Δp_z from the plasma to the wall;

$$\Delta p_z = q_z - k_z = -k_z + \sqrt{k_z^2 - M^2} \approx -\frac{M^2}{2k_z}. \tag{4.19}$$

[2]We are using slightly different derivation compared to the previous chapters

Now we can use the LSZ reduction formula to relate the correlation function to the matrix element of the $\chi \to N$ transition and we find that

$$\langle N, q|\chi, k\rangle = \left[(2\pi)^3\delta^{(3)}(k-q)\int dz e^{-iz\Delta p_z}\langle\phi(z)\rangle\right] \times \bar{u}_N(q)u_\chi(k)Y \tag{4.20}$$

which coincides with the result found in previous chapters. Note that the last factor is exactly equal to the amplitude of the transition $\chi(k) \to N(q)\varphi(\Delta p_z)$, $\mathcal{M}_{\chi(k)\to N(q)\varphi(\Delta p_z)}$. Thus we can write

$$\langle N, q|\chi, k\rangle = \left[(2\pi)^3\delta^{(3)}(k-q)\int dz e^{-iz\Delta p_z}\langle\varphi(z)\rangle\right] \mathcal{M}_{\chi(k)\to N(q)\varphi(\Delta p_z)}, \tag{4.21}$$

where the piece between brackets is dependent on the exact shape of the wall and has been computed in Eq.A.3. Of course on-shell φ cannot have the space-like momentum Δp_z but since it is a scalar we can still formally define such an "amplitude". These relations are the consequence of the following *Ward identity* which is satisfied if we are looking at the effects with just one VEV $\langle\varphi\rangle$ insertion:

$$\langle O_1(x_1)...O_n(x_n)\varphi(x_{n+1})\rangle|_{\langle\varphi\rangle=0} = \int dz \left[\frac{\delta}{\delta\langle\varphi(z)\rangle}\langle O_1(x_1)...O_n(x_n)\rangle|_{\langle\varphi\rangle\neq 0}\right] D_\varphi(x_{n+1}-z), \tag{4.22}$$

where D_φ is the propagator of the φ field. Then the application of the LSZ reduction together with energy and transverse momentum conservation leads to the Eq.(4.21).

After this warm-up exercise we can proceed to the calculation of the one loop effects. We will focus again only on the terms with just one VEV $\langle\varphi\rangle$ insertion and proceed in the same way as we have done for the tree-level calculation in the previous chapters. Note that the Eq. (4.21) will remain true also at loop level if we are focusing only on the effects with one VEV insertion. Indeed the momentum is not conserved only in the vertex with the $\langle\varphi\rangle$ insertion, however the energy and $x-y$ momentum conservation still fixes the value of the loss of the z component of momentum. At this point since φ is a scalar (no polarization vectors are needed) the matrix element is exactly the same as for the process $\chi(k) \to N(q)\varphi(\Delta p_z)$ and can be calculated using the usual Lorentz invariant Feynman diagram techniques.

4.2.1 CP-violation in production

So far we have been looking at $\chi \to N$ transition. However if there are more than one species of χ, N then the couplings Y become in general complex matrices, and, if it contains a physical phase, this can lead to CP-violating processes. We also couple the heavy states N_i to the SM. In this context, the Lagrangian in Eq.(4.16) generalises to

$$\mathcal{L} = i\bar{\chi}_i P_R \partial\chi_i + i\bar{N}_I\partial N_I - M_I\bar{N}_I N_I - Y_{iI}\varphi\bar{N}_I P_R\chi_i - y_{I\alpha}(\mathcal{H}\bar{L}_\alpha)P_R N_I + \text{h.c.} \tag{4.23}$$

where $\mathcal{H}$ and L_α are the usual SM Higgs and fermions that we couple to the heavy N_I, P_R, P_L are the chiral projectors. We choose this assignment of chirality in agreement with our further toy models. In particular the rates $\Gamma(\chi_i \to N_I) \neq \Gamma(\bar{\chi}_i \to \bar{N}_I)$ and after the phase transition there could be an asymmetry in $N, \bar{N}$ and $\chi, \bar{\chi}$ populations. Let us calculate these asymmetries. It is known that at tree level no asymmetries can be generated since both processes will be proportional to $|Y_{iI}|^2$, so we need to consider one loop corrections to it, in particular it is known that the imaginary part of the loop is the crucial ingredient for asymmetry generation. In general performing such calculation in the presence of the bubble wall background is quite involved, however things simplify if the bubble expansion is ultra-relativistic.

Calculation of the light → heavy transition *at 1-loop level*

Let us now compute the asymmetries in the populations of the various particle immediately after the PT in the case of the model in Eq.(4.23). First of all we need to know the CP violating effects in the $\chi_i \to N_I$ transition, which will appear in the interference between the loop and tree level diagrams.

$$\begin{aligned} &A(\chi_i \to N_I)_{\rm tree} \propto Y_{iI} \qquad \text{(tree level)} \\ &A(\chi_i \to N_I)_{1-\rm loop} \propto \sum_{k,J} Y_{iJ}Y^*_{kJ}Y_{kI} \times f^{(\chi\varphi)}_{IJ} + \sum_{\alpha,J} Y_{iJ}y^*_{\alpha J}y_{\alpha I} \times f^{(\mathcal{H}L)}_{IJ} \qquad \text{(one loop level)} \end{aligned} \tag{4.24}$$

where the functions $f^{(\mathcal{H}L)}$ and $f^{(\chi\phi)}$ refer to the loop diagrams with virtual χ, ϕ and $\mathcal{H}L$ respectively. As a consequence, there will be the following asymmetries in N_I populations immediately after the PT

$$\epsilon_{Ii} \equiv \frac{|\mathcal{M}_{i\to I}|^2 - |\mathcal{M}_{\bar{i}\to\bar{I}}|^2}{\sum_i |\mathcal{M}_{i\to I}|^2 + |\mathcal{M}_{\bar{i}\to\bar{I}}|^2} \tag{4.25}$$

$$= \frac{2\sum_{k,J}{\rm Im}(Y_{iI}Y^*_{iJ}Y_{kJ}Y^*_{kI}){\rm Im}f^{(\chi\varphi)}_{IJ}}{\sum_i |Y_{iI}|^2} + \frac{2\sum_{\alpha,J}{\rm Im}(Y_{iI}Y^*_{iJ}y_{\alpha J}y^*_{\alpha I}){\rm Im}f^{(\mathcal{H}L)}_{IJ}}{\sum_i |Y_{iI}|^2}, \tag{4.26}$$

where ϵ_{Ii} refers to asymmetry in N_I particle population which are produced from the i initial flavour of χ_i. The loop functions take the form

$$f^{(\mathcal{H}L)}_{IJ}(x) \equiv 2\int \frac{d^4p}{(2\pi)^4} \frac{P_R \not{p} P_L (\not{p}_{out} + M_J) P_L}{(p^2 + i\epsilon)((p - p_{out})^2 + i\epsilon)(p^2_{out} - M^2_J + i\epsilon)} \tag{4.27}$$

$$f^{(\chi\varphi)}_{IJ}(x) \equiv \int \frac{d^4p}{(2\pi)^4} \frac{P_L \not{p} P_R (\not{p}_{out} + M_J) P_L}{(p^2 + i\epsilon)((p - p_{out})^2 + i\epsilon)(p^2_{out} - M^2_J + i\epsilon)}, \tag{4.28}$$

where p_{in}, p_{out} are the initial (particle i) and final (particle I) state four momenta. p is the momentum running into the loop. The factor of two in front of the $f^{(\mathcal{H}L)}_{IJ}(x)$ function comes from the two contributions with a loop of $\nu_L, \mathcal{H}^0$ and $e^-_L, \mathcal{H}^+$ (one loop involves the leptons and the charged Higgs, and one loop involve the neutrinos and the neutral Higgs). This factor is absent in the case of $f^{(\chi\varphi)}_{IJ}(x)$ because we have only the loop of χ and φ. The imaginary part of those loop functions take the form

$${\rm Im}[f^{(\mathcal{H}L)}_{IJ}(x)] = \frac{1}{16\pi}\frac{\sqrt{x}}{1-x}, \qquad x = \frac{M^2_J}{M^2_I} \tag{4.29}$$

$${\rm Im}[f^{(\chi\varphi)}_{IJ}(x)] = \frac{1}{32\pi}\frac{1}{1-x}. \tag{4.30}$$

Summing over the flavours of χ_i we arrive at the following asymmetry in N_I abundance[3]

$$\epsilon_I \equiv \sum_i \epsilon_{Ii} = \frac{2\sum_{\alpha,J,i}{\rm Im}(Y_{iI}Y^*_{iJ}y_{\alpha J}y^*_{\alpha I}){\rm Im}f^{(\mathcal{H}L)}_{IJ}}{\sum_i |Y_{iI}|^2}. \tag{4.31}$$

Note that the only diagrams contributing to the asymmetry are shown on the Fig.4.1 and these have virtual $\mathcal{H}L$, we observed that the net asymmetry from the loop involving χ and φ cancelled upon summation.

[3]The asymmetry can be equivalently obtained from the "tree-level" graph of the 1PI effective action by integrating out the fermions.

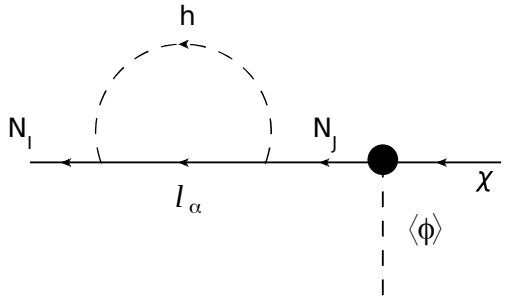

Figure 4.1: The diagram contributing to the function $f^{(\mathcal{H}L)}$. Only this diagram gives non zero asymmetry after summing over the flavors.

So far we have shown that during the production we can create a difference in the abundances of N_I and $\bar{N}_I$ inside the bubble. However since it was produced by $1 \to 1$ transitions exactly the same difference will be present inside the bubble also for the abundances of $\bar{\chi}_i$ and χ_i. Using the "$\langle\varphi\rangle \neq 0$" and "$\langle\varphi\rangle = 0$" subscribes for the particle densities inside and outside the bubbles and taking into account that the number density of some particle entering inside the bubble is $n = \frac{\Delta N}{\Delta A \Delta t}\frac{\Delta t}{\Delta z} = \frac{J}{v_w}$ with entering flux $J = \int \frac{p_z d^3p}{p_0(2\pi)^3} f_\chi(p, T_{\rm nuc})$ we can conclude that, in the plasma frame,

$$n_{N_I}^{\langle\varphi\rangle=0}(T_{\rm nuc}) \simeq 0, \quad \text{(Boltzmann suppressed)} \tag{4.32}$$

the initial abundance of the heavy states outside of the bubble is very suppressed, but inside the bubble a abundance is building up

$$\begin{aligned}
n_{N_I}^{\langle\varphi\rangle\neq 0} &\simeq \frac{1}{\gamma_w v_w}\int \frac{d^3p}{(2\pi)^3}\frac{p_z}{p_0} P_{\chi\to N}(p) \times f_\chi(p, T_{\rm nuc}) \\
&\simeq \sum_i \frac{|Y_{iI}|^2\langle\varphi\rangle^2}{M_I^2\gamma_w v_w}\int \frac{d^3p}{(2\pi)^3}\frac{p_z}{p_0} \times f_\chi^{\rm eq}(p, T_{\rm nuc})\Theta(p_z - M_I^2/\langle\varphi\rangle) \\
&\simeq \sum_i \frac{|Y_{iI}|^2}{\pi^2\gamma_w^3} \times \frac{\langle\varphi\rangle^2 T_{\rm nuc}^2}{M_I^2}\left(\frac{M_I^2/\langle\varphi\rangle}{1-v_w} + \frac{T_{\rm nuc}(2-v_w)}{\gamma_w(v_w-1)^2}\right) \times e^{-\gamma_w \frac{M_I^2}{\langle\varphi\rangle}\frac{1-v_w}{T_{\rm nuc}}} \\
&= \sum_i \frac{|Y_{iI}|^2 T_{\rm nuc}^3\langle\varphi\rangle^2}{\pi^2 M_I^2} e^{-\frac{M_I^2}{2\langle\varphi\rangle T_{\rm nuc}\gamma_w}} + \mathcal{O}(1/\gamma_w) \\
&\simeq \sum_i \theta_{iI}^2 n_{\chi^i}^{\langle\varphi\rangle=0}(T_{\rm nuc}).
\end{aligned} \tag{4.33}$$

where $v_w = \sqrt{1 - 1/\gamma_w^2} \approx 1 - \frac{1}{2\gamma_w^2}$ is the velocity of the wall. The integral is performed in the wall frame and the γ_w^{-1} factor in front takes care of the conversion to the plasma frame. In the second line we introduced the expression for the probability of production obtained in Chapter 2 and assumed that, the transition being a detonation, the density distribution of χ is the equilibrium distribution $f_\chi^{\rm eq} \approx e^{-\frac{\gamma_w(E_\chi - v_w p_z^\chi)}{T_{\rm nuc}}}$ (using Boltzmann distribution as a simplifying assumption) and $E_\chi = \sqrt{p_z^2 + \mathbf{p}_\perp^2}$. In the third line we performed the phase space integral. In the last approximation, we have taken the exponential to be unity since the wall is relativistic and $\gamma_w T_{\rm nuc} \gg M_I$, and defined

$$\theta_{iI} \equiv \frac{|Y_{iI}|\langle\varphi\rangle}{M_I}. \tag{4.34}$$

	N_I	N_I^c	χ_i	χ_i^c	Δn_{N^I}
$\epsilon = 0$, without CP-violation					
Out	0	0	n_{χ^i}	n_{χ^i}	0
In	$\theta_{Ii}^2 n_{\chi^i}$	$\theta_{Ii}^2 n_{\chi^i}$	$(1-\theta_{Ii}^2) n_{\chi^i}$	$(1-\theta_{Ii}^2) n_{\chi^i}$	0
$\epsilon \neq 0$, with CP-violation					
Out	0	0	n_{χ^i}	n_{χ^i}	0
In	$\theta_{Ii}^2(1-\epsilon_{Ii}) n_{\chi^i}$	$\theta_{Ii}^2(1+\epsilon_{Ii}) n_{\chi^i}$	$(1-\theta_{Ii}^2(1-\epsilon_{Ii})) n_{\chi^i}$	$(1-\theta_{Ii}^2(1+\epsilon_{Ii})) n_{\chi^i}$	$2\epsilon_{Ii}\theta_{Ii}^2 n_{\chi^i}$

Table 4.1: Densities and asymmetry, with and without CP-violation, inside and outside of the bubble. For clarity we got rid of the temperature dependence, assuming that the density have to be evaluated at the nucleation temperature.

This means that some of the abundance of χ_i has been removed from the plasma and since we are focusing on $1 \to 1$ transitions, this gives :

$$\begin{aligned} &\sum_I \Delta n_{N^I} = -\sum_i \Delta n_{\chi^i} \Rightarrow \\ &\sum_I \left(\Delta n_{N^I} - \Delta n_{\bar{N}^I}\right) = -\sum_i \left(\Delta n_{\chi^i} - \Delta n_{\bar{\chi}^i}\right), \end{aligned} \tag{4.35}$$

where $\Delta n_{N,\chi}$ are the differences in abundances of the particles in the broken and unbroken phases. As a consequence, there will be also an asymmetry in the abundances of the light fields. Note that the asymmetry in the χ field will be further diluted by the factor $\sim \frac{y^2\langle\varphi\rangle^2}{M^2}$ due to the large symmetric thermal densities of the light fields during and after the phase transition.

Resonant effects in production

It is known that the CP violation in Leptogenesis can be greatly enhanced in the case of nearly degenerate heavy neutrinos, since the CP-violation is proportional to

$$\epsilon \propto \frac{1}{M_i - M_j} \tag{4.36}$$

which grows without boundaries as $M_i \to M_j$. It was however showed that such an enhancement is bounded by the decay width of the heavy neutrinos[276, 277], controlled by $\sim y^2 \frac{M_N}{4\pi}$. For small couplings and very degenerate spectrum this effect can induce an enhancement of the CP violation by many orders of magnitude, and bring the scale of thermal leptogenesis as low as TeV scale.

Looking back at Eq. (4.64) which contains a similar degeneracy singularity, we could naively expect the same type of mechanism for the enhancement of the CP violation. We have not studied further this possibility, as the field-theoretic formalism becomes quickly involved. However, we can argue on dimensional level, that the enhancement should not be as dramatic than in the thermal leptogenesis case, for the following reason: thermal leptogenesis takes advantage of very small couplings, and thus on small decay width, allowing for large enhancement. As we have seen, our mechanism favors strong coupling $Y \sim \mathcal{O}(1)$, and thus large decay width $\Gamma_N \sim \frac{M_N}{4\pi}$, thus mitigating the maximal enhancement that we can hope for to around one order of magnitude, which would not dramatically modify our conclusions. As a consequence, we do not proceed further in this direction.

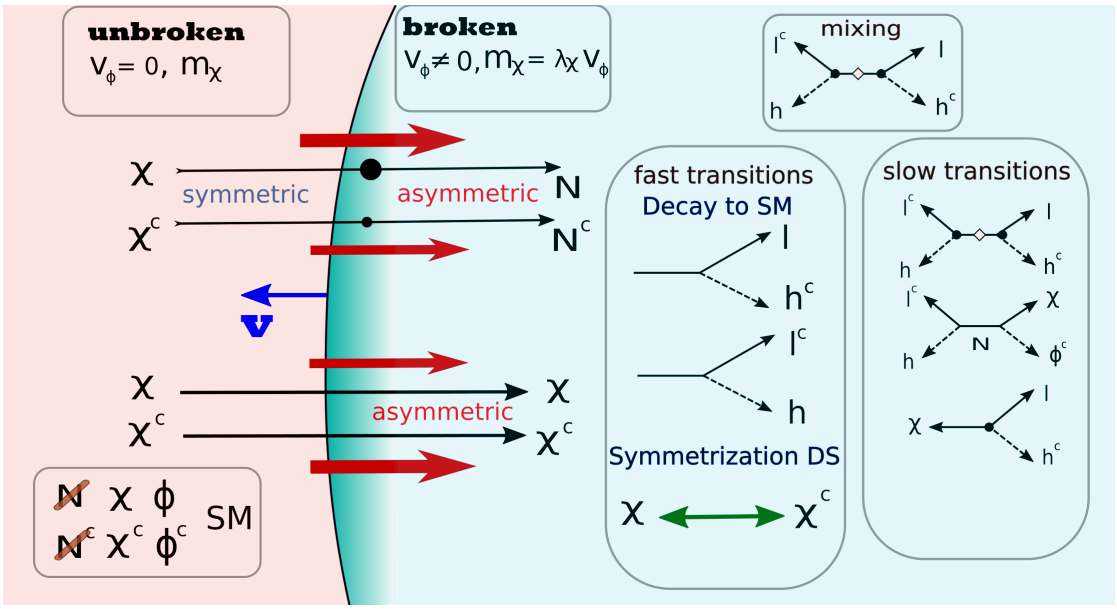

Figure 4.2: Mechanism at play in the phase transition-induced leptogenesis. In the diagrams the black dot denotes a mixing between χ and N and so the insertion of a factor of θ, the white diamond is a χ mixing insertion. A thicker arrow designates a larger flux (though it is exaggerated on the figure.)

4.3 Application of the mechanism for Baryogenesis

In the previous section we have shown that the wall, if it becomes relativistic enough, can produce states much heavier than the reheating temperature and also that this production process can induce CP-violation via the interference of tree-level and loop-level diagrams.

Now we will present some examples of applications of this new CP-violating source for the explanation of the observed matter asymmetry. Of course, many other examples could take advantage of the configuration presented in the previous section, so what we will present now serve as a proof of existence.[4] For this reason, in the following we will present two classes of models that take advantage of the mechanism presented above.

4.3.1 Phase-transition induced leptogenesis

Let us consider the following extension of the Lagrangian in Eq.4.23, where we have introduced φ -dependent Majorana mass for the field χ and kept the rest of the interactions the same. We restrict to only one specie of the Majorana fermion χ, since it is sufficient for the generation of CP phase. In this model, only two Dirac neutrinos

[4]It is also clear that the baryogenesis model can be built from CP-violating decay of the produced heavy particle due to the bubble expansion. This is nothing but the non-thermal baryogenesis [219, 220, 278, 279, 280, 281, 282, 283, 284, 285, 286, 287, 288].

$I = 1, 2$ are sufficient to have CP phases.

$$\begin{aligned}\mathcal{L}_{\text{int}} &= \underbrace{\sum_I \Big(Y_I(\varphi^\dagger \bar{\chi}) P_L N_I + Y_I^\star \bar{N}_I P_R(\varphi\chi)\Big) - V(\varphi) + \frac{1}{2}\lambda_\chi \varphi \bar{\chi}^c \chi + \sum_I M_I \bar{N}_I N_I}_{\text{Toy model of Dark Sector}} \\ &+ \underbrace{\sum_{\alpha I} y_{\alpha I}(\mathcal{H}\bar{L}_{\alpha,SM}) P_R N_I + \text{h.c.},}_{\text{Connection to SM}}\end{aligned} \tag{4.37}$$

The interactions in Eq.(4.37) respect $U_L(1)$ lepton number with the following charge assignments $L(\chi) = -1, L(N) = 1$ and $L(\varphi) = 2$. This symmetry is obviously broken after the phase transition by the VEV of $\langle\varphi\rangle$ field and the Majorana mass of the χ field $m_\chi = \lambda_\chi\langle\varphi\rangle$. Perturbativity bound imposes that $\lambda_\chi \lesssim \sqrt{4\pi}$. The generation of the baryon asymmetry proceeds as follows: during the bubble expansion we generate asymmetry in N and χ, as they have been estimated in the section 4.2.1. Immediately after the transition, the asymmetry in χ is washed out due to the lepton-number violating Majorana mass term, which constitutes the first source of asymmetry for the system. Part of this asymmetry in N is passed to the SM lepton sector during the decay $N \to L\mathcal{H}$, which constitutes a second source of asymmetry for the system, via the usual CP-violating decay. We will see that the dominant contribution depends on the different couplings of the systems This asymmetry in return is passed to the baryons by sphalerons, similarly to the original leptogenesis models [289]. The scheme of the construction is shown on the Fig.4.2.

Estimating the baryon asymmetry

So far we have generated the asymmetry in N particle population, however we need to find what part of it will be passed to SM lepton sector. This can be done by comparing the branching ratios of $N \to \mathcal{H}L$ and $N \to \chi\varphi$ decays

$$\begin{aligned}\frac{n_L - n_{L^c}}{s} &\simeq \frac{1}{s(T_{\text{reh}})}\sum_{iI}\epsilon_{Ii}\frac{3\zeta(3)|Y_{iI}|^2 T_{\text{nuc}}^3\langle\varphi\rangle^2}{4\pi^2 M_I^2} \times \frac{Br(N_I \to \mathcal{H}L)}{Br(N_I \to \mathcal{H}L) + Br(N_I \to \chi\varphi)} \\ &\simeq \frac{135\zeta(3)g_\chi}{8\pi^4 g_\star}\sum_I \theta_I^2 \frac{2\sum_{\alpha,J}\text{Im}(Y_I Y_J^* y_{\alpha J} y_{\alpha I}^*)\text{Im} f_{IJ}^{(\mathcal{H}L)}}{|Y_I|^2}\left(\frac{T_{\text{nuc}}}{T_{\text{reh}}}\right)^3 \times \frac{\sum_\alpha |y_{\alpha I}|^2}{\sum_\alpha |y_{\alpha I}|^2 + |Y_I|^2}\end{aligned} \tag{4.38}$$

where g_χ is the number of degrees of freedom of χ particle. By assuming $O(1)$ parameters in the potential and dominant latent heat, $T_{\text{reh}} \sim \langle\varphi\rangle$. The factor θ_I^2 is the suppression due to the heavy field production and $(T_{\text{nuc}}/T_{\text{reh}})^3$ factor comes from the fact that n_N is fixed by the nucleation temperature (see Eq.(4.33)) and s is at the reheating temperature after the PT. The factor $\frac{\sum_\alpha |y_{\alpha I}|^2}{\sum_\alpha |y_{\alpha I}|^2 + |Y_I|^2}$ appears since a part of the asymmetry in N is decaying back to $\varphi\chi$, thus washing out a part of the asymmetry.

Lepton asymmetry generation in decay Note that there is an additional effect contributing to the baryon asymmetry generation. The decays of the heavy fields N are out of equilibrium and there is a CP phase in the Yukawa interactions. Thus the rates

$$\Gamma(N \to \bar{\mathcal{H}}L) \neq \Gamma(\bar{N} \to \mathcal{H}\bar{L}) \tag{4.39}$$

induce a non-vanishing CP-violation in decay

$$\epsilon_{\text{decay}}^I \equiv \frac{\Gamma(N^I \to \bar{\mathcal{H}}L) - \Gamma(\bar{N}^I \to \mathcal{H}\bar{L})}{\Gamma(N^I \to \bar{\mathcal{H}}L) + \Gamma(\bar{N}^I \to \mathcal{H}\bar{L})}. \tag{4.40}$$

As a consequence, after the asymmetry induced by the production of heavy states, there will be an additional asymmetry due to the decay. This will scale as :

$$\frac{n_L - n_{L^c}}{s}\Big|_{\rm decay} \sim \sum_I \frac{\theta_I^2}{g_\star}\epsilon^I_{\rm decay}\left(\frac{T_{\rm nuc}}{T_{\rm reh}}\right)^3 \times \frac{\sum_\alpha |y_{\alpha I}|^2}{\sum_\alpha |y_{\alpha I}|^2 + |Y_I|^2} \tag{4.41}$$

where the asymmetry in decay ϵ^I will be generated by the diagram similar to the one in Fig.4.1 with $\mathcal{H}, L$ in the final state and φ, χ inside the loop. In the limit $m_\chi, m_\varphi \ll M_I$ (which is exactly where one VEV insertion approximation used in the section 4.2 is motivated) the loop function for both production and decay will be exactly the same up to the factor of 2 (particles running in the loop are EW singlets) compared to Eq.(4.31). However the couplings will be complex conjugates so that

$$\epsilon^I_{\rm decay} = -\frac{{\rm Im}[Y_I Y_J^* y_{\alpha_J} y^*_{\alpha_I}]{\rm Im}[f_{IJ}^{(\mathcal{H}L)}]}{\sum_\alpha |y_{\alpha I}|^2}. \tag{4.42}$$

Combining both effects and taking into account sphaleron rates converting the lepton asymmetry to the baryon, we obtain the following baryon asymmetry:

$$\begin{aligned}\frac{\Delta n_B}{s} \equiv \frac{n_B - n_{\bar B}}{s} \simeq \quad & -\frac{28}{79} \times \frac{135\zeta(3) g_\chi}{8\pi^4 g_*} \times \sum_I \theta_I^2 \sum_{\alpha,J} {\rm Im}(Y_I Y_J^* y_{\alpha J} y^*_{\alpha I}) {\rm Im} f_{IJ}^{(\mathcal{H}L)} \\ & \times \left(\frac{2}{|Y_I|^2} - \frac{1}{\sum_\alpha |y_{\alpha I}|^2}\right)\left(\frac{T_{\rm nuc}}{T_{\rm reh}}\right)^3 \frac{\sum_\alpha |y_{\alpha I}|^2}{\sum_\alpha |y_{\alpha I}|^2 + |Y_I|^2}\end{aligned} \tag{4.43}$$

The prefactor $-\frac{28}{79}$ comes from the sphalerons rates (see [203]). The observed asymmetry is given by $\frac{\Delta n_B}{s} \sim 8.8 \times 10^{-11}$. The quantities in Eq.(4.43) can be estimated in the following way; outside of the resonance regime but for mild hierarchy between the masses of the heavy neutrinos $M_1 \lesssim M_2 \lesssim M_3$, with order one couplings, $2{\rm Im} f_{IJ}^{(\mathcal{H}L)} \to \frac{1}{8\pi}$, $g_\star \sim 100$ and $\sum_\alpha |y_{\alpha I}|^2 \gtrsim |Y_I|^2$ induces $\frac{\sum_\alpha |y_{\alpha I}|^2}{\sum_\alpha |y_{\alpha I}|^2 + |Y_I|^2} \sim 1$. As a consequence, the production of the observed asymmetry demands, in order of magnitude,

$${\rm Max}[\theta^2 y^2]\left(\frac{T_{\rm nuc}}{T_{\rm reh}}\right)^3 \sim 10^{-6}. \tag{4.44}$$

with an $O(1)$ CP phase and $|Y_I| \sim |Y_J|$.

Constraints on the model

Let us examine various bounds on the construction proposed. Let us start from neutrino masses. Indeed after the PT, the Lagrangian (4.37) generates a dimension 5 operator of the see-saw form [290, 291, 292, 293, 294]

$$\sum_{I,\alpha,\beta} \theta_I^2 \frac{y_{\alpha I} y^*_{\beta I} (\bar L^c_\alpha \mathcal{H})(L_\beta \mathcal{H})}{m_\chi} \tag{4.45}$$

which induces a mass for the active neutrinos (for the heaviest light neutrino)

$${\rm Max}[m_\nu] \sim {\rm Max}\left[\sum_I |y_{\alpha I}|^2 \theta_I^2\right] \frac{v_{EW}^2}{m_\chi}. \tag{4.46}$$

Combining Eqs. (4.43), (4.46) with observed neutrino mass scale and the constraints Max$[\theta_I^2] \gtrsim 10^{-5}, y \sim \mathcal{O}(1)$, we obtain the following constraints

$$\Rightarrow \qquad m_\chi \gtrsim 5 \times 10^9 \text{GeV} \qquad \Rightarrow \qquad \langle\varphi\rangle \gtrsim 10^9 \text{GeV}. \tag{4.47}$$

Let us list additional conditions on this baryogenesis scenario which must be satisfied. First of all, the decay processes of $\chi \to \mathcal{H}L$, and $\chi \to (\mathcal{H}L)^*$ have the same probability since χ is a Majorana fermion. Then we need to make sure that, immediately after the reheating, processes involving χ do not erase the asymmetry stored in the SM sector. Let us list these processes and their rates:

- χ production in $\mathcal{H}L$ collisions: Ideally we have to solve the Boltzmann equation for the density evolution, which focusing only on this process will be given by:

$$szH(z)\frac{dY_{L,L^c}}{dz} = -\frac{Y_{L,L^c}Y_{\mathcal{H}}}{Y^{\rm eq}_{L,L^c}Y^{\rm eq}_{\mathcal{H}}}\gamma(\mathcal{H}L \to \chi) + \frac{Y_\chi}{Y^{\rm eq}_\chi}\gamma(\chi \to L\mathcal{H}, (L^c\mathcal{H})), \tag{4.48}$$

  where $z \equiv m_\chi/T$ (not to be confused with the spatial direction z along the wall) and $Y_i \equiv n_i/s$ and $\gamma(\mathcal{H}L \to \chi)$ is the rate of the reaction $\mathcal{H}L \to \chi$. However note that χ, χ^c decay quickly with the rate $\sim \frac{y^2\theta^2 m_\chi}{4\pi} \gg H$ unless we consider the scales close to the Planck mass, this process induces that the density Y_χ is always kept close to equilibrium. Introducing the asymmetry density $Y_{\Delta_\alpha} \equiv Y_{L_\alpha} - Y_{L^c_\alpha}$ and subtracting for the matter anti-matter densities, we obtain

$$szH(z)\frac{dY_{\Delta_\alpha}}{dz} = -\frac{Y_{\Delta_\alpha}}{Y_{L_\alpha}}\gamma(\mathcal{H}L_\alpha \to \chi) \tag{4.49}$$

  where $\gamma_\alpha[z] \equiv \gamma(\mathcal{H}L_\alpha \to \chi)$ is given by[295]

$$\gamma_\alpha[z] = \frac{g_\chi T^3}{2\pi^2} z^2 K_1(z)\Gamma_\alpha \tag{4.50}$$

  where the Bessel functions $K_1(z)$ satisfy the two limiting behaviours

$$zK_1(z) = \begin{cases} 1 & z \ll 1, \\ \sqrt{\frac{\pi z}{2}}e^{-z} & z \gg 1. \end{cases} \tag{4.51}$$

  So, for large values of z, we get

$$\frac{dY_{\Delta_\alpha}}{dz} \simeq -\frac{0.42 e^{-z} z^{5/2}}{g_*^{1/2} g_\alpha}\left(\frac{M_{\rm pl}}{m_\chi}\right)\left(\frac{g_\chi \Gamma_\alpha}{m_\chi}\right) Y_{\Delta_\alpha}, \qquad \Gamma_\alpha \approx \left|\sum_I y_{\alpha I}\theta_I\right|^2 \frac{m_\chi}{8\pi g_\chi}. \tag{4.52}$$

  Solving this equation numerically we can find that Y_{Δ_α} remains invariant for $m_\chi/T_{\rm reh} \gtrsim 15$ (for the scale $m_\chi \sim 10^9$ GeV), so that the wash out process can be safely ignored. The following approximate relation for the minimal $m_\chi/T_{\rm reh}$ to avoid wash out is valid

$$\frac{m_\chi}{T_{\rm reh}} \gtrsim \log\frac{M_{\rm pl}}{m_\chi} - 9 \tag{4.53}$$

  where we took $\theta_I \sim 10^{-2}$ as a typical value. Similarly to the process above there will be additional effects which can lead to the wash-out of the lepton asymmetry like; $\mathcal{H}L \to \varphi\chi$. However the rate of this reaction will be further suppressed by the phase space and it will be subleading compared to the $\mathcal{H}L \to \chi$.

- On top of these wash out effects there will be the "usual" processes from the $LL\mathcal{H}\mathcal{H}$ operator $\mathcal{H}^c L \to \mathcal{H} L^c$, $LL \to \mathcal{H}\mathcal{H}$ and $\mathcal{H}\mathcal{H} \to LL$ which will violate the lepton number with rates

$$\Gamma(\mathcal{H}^c L_\alpha \to \mathcal{H} L^c_\beta)(T) = \frac{2 g_\beta}{\pi^4} \sum_{iI} \frac{\theta^4_{iI}}{m^2_\chi} y^2_{i\alpha} y^2_{i\beta} \frac{n_{\mathcal{H}}}{n^{\rm eq}_{\mathcal{H}}} \frac{1}{n^{\rm eq}_\alpha} T^6 \approx \frac{4}{1.2\pi^2 g_\alpha} \sum_{iI} \frac{\theta^4_{iI}}{m^2_\chi} y^2_{i\alpha} y^2_{i\beta} T^3.$$
$$\Rightarrow \Gamma(\mathcal{H}^c L \to \mathcal{H} L^c) \approx \frac{2}{1.2\pi^2} \left(\frac{m_\nu}{v^2_{EW}} \right)^2 T^3, \tag{4.54}$$

  (where we consider the heaviest light neutrino m_ν in our estimates) and may wash out the asymmetry created. Requiring these processes to be slow, we arrive at the condition

$$\Gamma(\mathcal{H}^c L \to \mathcal{H} L^c) < H(T_{\rm reh}) \quad \Rightarrow \quad T_{\rm reh} \lesssim 5\sqrt{g_\star} \frac{v^4_{EW}}{M_{\rm pl} m^2_\nu} \sim 5 \times 10^{12}\ \text{GeV}. \tag{4.55}$$

  where we took $m^2_\nu \sim 0.0025\ \text{eV}^2$.

- During the symmetry breaking topological defects may be formed. For the cosmic strings $\langle \varphi \rangle \lesssim 10^{14}$ GeV is needed to evade the CMB bound [296]. If the $U_L(1)$ is explicitly broken by the potential of ϕ, domain walls will form. Depending on the explicit breaking the domain wall or string network would be unstable and decay. In this case the CMB bound is absent. Instead, the string-wall network emits gravitational waves and may be tested in the future with VEV $\gtrsim 10^{14}$ GeV and the axion mass range of $10^{-28} - 10^{-18}$ eV [297, 298].

- (Pseudo) Nambu-goldstone boson which may be identified as $\arg \phi$, exists in this scenario. If it acquires mass via the explicit breaking of the $U_L(1)$ symmetry, the late-time coherent oscillation should not over-close the Universe. This requirement sets an upper bound on the explicit breaking-term or the decay should happen early enough. In the former case, we have a prediction on dark radiation corresponding to the effective neutrino number of $\Delta N_{\rm eff} \sim 0.03$, since the light boson is easily thermalized around and after the PT. This can be tested in the future. The consequences of such a majoron are discussed in [269].

In conclusion we can see that this construction can lead to the viable baryogenesis if there is a mild hierarchy between the scales; $M_I > \langle \varphi \rangle$ and $m_\chi, M_I > T_{\rm reh}$. In particular we need $M_I / \langle \varphi \rangle \gtrsim 10$ in order to remain in the range of validity for our calculation from perturbation theory point of view and we need $(m_\chi, M_I)/T_{\rm reh} \gtrsim 15$ to suppress the wash-out. Correct reproduction of neutrino masses makes this mechanism operative in the range of scales $10^9 < \langle \varphi \rangle < 5 \times 10^{12}$ GeV. We would like to emphasize that the discussion above assumed one mass scale for all M_I, and similarly all of the couplings Y, y are of the same scale. However this is not the case in general and the discussion of such "flavour" effects can significantly modify the allowed scale of the transition.

Before going to the next model let us mention that there is no lepton number violation in the symmetric phase, and in the broken phase χ is heavier than the plasma temperature. Thus the thermal leptogenesis does not happen in the parameter range for this scenario.

For this model to work, we need the wall to become relativistic, so *a minima*, we need to fulfill the relativistic condition $\Delta V > \Delta \mathcal{P}$, which will be favored in the case of supercooling. In the other hand, the mild hierarchy in Eq.(4.53) between m_χ and the reheating temperature is easily achievable in the case of long and flat potentials where the difference of energies between false and true vacua is smaller than the VEV: $T_{\rm reh} \sim (\Delta V / g_*)^{1/4} \lesssim \mathcal{O}(10^{-1}) \langle \varphi \rangle \sim \mathcal{O}(10^{-1}) m_\chi$, which can be achieved for example by simply taking small quartic coupling in the φ potential.

Fortunately, both those situations, supercooling and suppressed reheating temperature, occur together typically in models with approximate conformal symmetry [299, 242, 192, 5], and in the case of models containing heavy fermions[300, 301]. As a consequence, from the model building point of view, there is no difficulty in writing a potential realising our scenario.

To conclude this section, let us give a word on the reach of the mechanism. We have already seen in the previous chapters that the rough maximal mass that we can produce the the BE mechanism is

$$M^{MAX} \sim \text{Min}\left[\frac{4\pi}{g_{\text{gauge}}^{3/2}}\frac{\langle\varphi\rangle^2}{T_{\text{nuc}}}, \frac{M_{\text{pl}}^{1/2}T_{\text{nuc}}}{\langle\varphi\rangle^{1/2}}\right] \tag{4.56}$$

(where an non-gauged theory amount to take $g_{\text{gauge}} \to 0$). If we assume $T_{\text{nuc}} \sim (0.1-0.01)\langle\varphi\rangle$, then (for ungauged transition)

$$M^{MAX} \sim (0.3-0.1)\sqrt{M_{\text{pl}}\langle\varphi\rangle} \tag{4.57}$$

which is really enough. Indeed, for an efficient production of heavy states we saw that we needed only $10^{-(2-3)} \lesssim \theta \sim \frac{\langle\varphi\rangle}{M}$.

New hierarchy problem ?

In this very short section, we would like to address a possible problem that seems to occur in our model of PT induced leptogenesis: the possibility of a new hierarchy problem. Indeed, in principle, no symmetry prevents us from writing a portal between the Higgs and the new scalar field φ

$$\lambda_{\varphi\mathcal{H}}|\mathcal{H}|^2\varphi^2. \tag{4.58}$$

As our mechanism is confined to high scales $v_\varphi > 10^9$ GeV, we could be worried that φ transition could induce a large mass term in the Higgs sector $\sim \lambda_{\varphi\mathcal{H}}v_\varphi^2$. This requires that $\lambda_{\varphi\mathcal{H}}$ is tuned to be very small. This is indeed a new hierarchy problem (though not of quantum origin).

We however believe that this new hierarchy problem remains a ill-defined issue as long as the usual hierarchy problem of the Higgs (of quantum origin) has not found a proper solution.

Gravitational waves

In the scenario we presented in this section, GW signal can be produced via two mechanisms: i) the GW coming from the dynamics of bubbles and their expansion in the plasma. This production mechanism is expected to be very efficient since we require a strong PT. However, the frequency of the signal is controlled by the reheating temperature, which will be bounded by $T_{\text{reh}} \gtrsim 10^8 - 10^9$ GeV. This would produced a signal at frequencies too high to be observable by fore-coming observers (Though maybe at the limit of ET range). ii) GW will also be strongly emitted by the cosmic strings produced during the breaking of $U_L(1)$. This was studied in the case of non-thermal leptogenesis in [302], where it was shown that if $v_\varphi \gtrsim 10^{10}$ GeV, signal could be observable at DECIGO, BBO, and possibly LISA.

4.3.2 Alternative Phase-transition induced leptogenesis

So far, we presented one specific model of PT induced leptogenesis. Let us quickly mention some possible variations.

- The simplest modification we can take of the Eq.(4.37) is the consider the opposite chiralities;

$$\begin{aligned}\mathcal{L}_{\text{int}} &= \underbrace{\sum_{iI}\left(Y_{iI}(\varphi\bar{\chi}_i)P_R N_I + Y_{iI}^{\star}\bar{N}_I P_L(\varphi^{\dagger}\chi_i)\right) - V(\phi) + \sum_i \lambda_\chi \varphi\bar{\chi}_i^c\chi_i + \sum_I M_I\bar{N}_I N_I}_{\text{Toy model of Dark Sector}} \\ &+ \underbrace{\sum_{\alpha I} y_{\alpha I}(\mathcal{H}\bar{L}_{\alpha,SM})P_R N_I + h.c.}_{\text{Connection to SM}}\end{aligned} \tag{4.59}$$

  In this case the generation of CP asymmetry proceeds in the similar way to the discussion above but neutrino masses are generated at one loop level. As a result parameter space with lower masses m_χ by around two orders of magnitude becomes accessible. We leave the thorough study of this case to further studies.

- So far, we only considered, for our baryogenesis mechanism, the production of fermions. Other variations takes advantage of the production of *heavy scalars*[303] via the interaction

$$\Delta\mathcal{L} = -\frac{\lambda}{2}\varphi^2|\phi|^2 \tag{4.60}$$

  which is very similar to the DM production mechanism introduced in Chapter 3. Here ϕ is charged under QCD, such that they can decay to the quarks and produced baryon asymmetry via an usual out-of-equilibrium decay. Also in this case, the scale of the mechanism is pushed to $T_{\text{reh}} \gtrsim 10^{10}$ GeV by wash-outs.

4.3.3 Low-energy baryogenesis via EW phase transition

In the previous section we have presented a model generating the baryon asymmetry during the phase transition at the high scale. However we can wonder whether the mechanism proposed (in section 4.3.1) can be effective for generation of the baryon asymmetry during the EWPT. The necessary ingredient for the mechanism is a strong first order electroweak phase transition and various studies indicate that even a singlet scalar (see ref.[304, 305, 306, 307, 308, 309, 33]) or dimension six operator (see ref. [310, 311, 312, 9, 33]) extensions of SM can do the job. In this chapter however we take an agnostic approach about the origin of such EW FOPT and just assume that it has happened with nucleation and reheating temperature as an input parameters and present the detailed analysis of such a model (the case of a singlet scalar) to Chapter 5. Below we present a prototype example for baryogenesis:

$$\begin{aligned}\mathcal{L} = &\quad \mathcal{L}_{SM} + m_\eta^2|\eta|^2 + \sum_{I=1,2} M_I\bar{B}_I B_I \\ &+ \left(\sum_{I=1,2} Y_I(\bar{B}_I\mathcal{H})P_L Q + y_I\eta^*\bar{B}_I P_R\chi + \kappa\eta^c du + \frac{1}{2}m_\chi\bar{\chi^c}\chi + h.c.\right).\end{aligned} \tag{4.61}$$

As before we do not write kinetic terms. The model contains a Majorana field χ and two vector-like B quarks with the masses $M_{1,2} \sim m_\chi$[5]. Notice here an important caveat with respect to our usual notations: χ is *not* light outside

[5]This is because we have a total of $2n+1$ complex phases and $n+2$ fields, where n is the number of B_I. So one B is not enough, but two is.

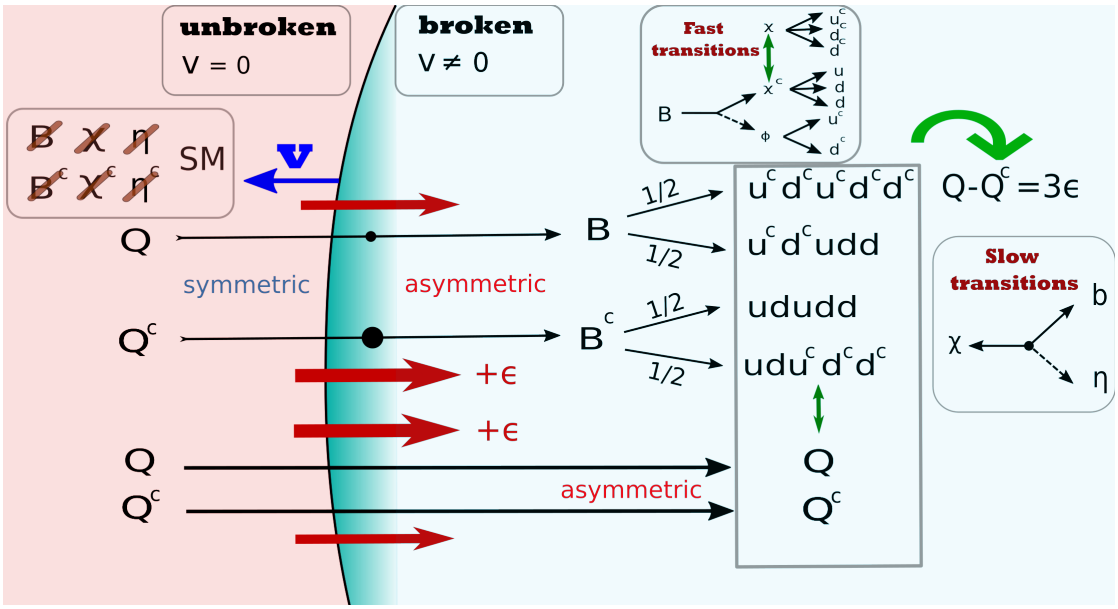

Figure 4.3: Mechanism at play in the low energy baryogenesis.

of the bubble, we should keep this point in mind. Here η is a scalar field which is in the fundamental representation of QCD with electric charge $Q(\eta) = 1/3$, Q, u, d are the SM quark doublet and singlets respectively, we ignore the flavour indices for now, $\mathcal{H}$ is the SM Higgs and we assume that the EW phase transition is of the first order with relativistic enough bubbles. Note that the interaction $L\mathcal{H}\chi^c$ is consistent with all the gauge symmetries of the model, however we set it to zero in order to avoid proton decay. This can be attributed to some accidental discrete symmetry. Let us also assume that only the third generations couples to the heavy vector like B quark, $Q = (t, b)$ in Eq.(4.61), then unlike the previous leptogenesis model, the asymmetry will be generated when the relativistic SM b quarks are hitting the wall.

Let us look at the baryon number assignments of the various fields in our lagrangian: $B(\eta) = 2/3, B(\chi) = 1$, so that the m_χ violates the baryon symmetry by two units. In this case, the story goes as follows: the sweeping of the relativistic wall, via the collision of the b-quarks with bubbles, produces B_I, B_I^c. Thus inside the bubble

$$\begin{aligned} n_{B_I} - n_{B_I^c} &= -\theta_I^2 \epsilon_I n_b^0 \\ n_b - n_{b^c} &= \sum_I \theta_I^2 \epsilon_I n_b^0 \end{aligned} \tag{4.62}$$

where n_b is the number density of the bottom-type quark, $\theta_I \approx \frac{Y_I v_{EW}}{M_I}$ is the mixing angle and ϵ_I is defined like in Eq. (4.26) (in this case there is no i index since we coupled it only to the third generation of quarks). CP asymmetry will be generated by the diagram represented on the Fig. 4.4 with χ, η fields running inside the loop. The loop function generated by the diagram of Fig. 4.4 becomes

$$f_B^{IJ}(x) = \int \frac{d^4p}{(2\pi)^4} \frac{P_R(\not{p} + m_\chi)P_L(\not{p}_{out} + M_J)P_L}{(p^2 - m_\chi^2 + i\epsilon)((p - p_{out})^2 - m_\phi^2 + i\epsilon)(p_{out}^2 - M_J^2 + i\epsilon)} \tag{4.63}$$

after taking the imaginary part, we obtain

$$\mathrm{Im}[f_B^{IJ}(x)] = \frac{1}{32\pi} \frac{M_I M_J}{M_I^2 - M_J^2} \frac{\sqrt{(M_J^2 - m_\eta^2 + m_\chi^2)^2 - 4m_\chi^2 M_J^2}}{M_J^4} \left(M_J^2 + m_\chi^2 - m_\eta^2\right) \tag{4.64}$$

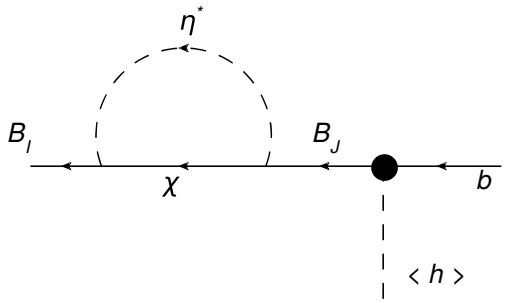

Figure 4.4: One loop diagram contributing to the $b \to B$ transition

Compared to Eq. (4.29) we have an additional $1/2$ factor (at the massless limit of η, χ) because η, χ are $SU(2)_L$ singlet now.

Similarly to our general discussion after the passage through the wall the following asymmetric abundances will be generated

$$\sum_I \left(n_{B_I} - n_{B_I^c}\right) = -(n_b - n_{b^c}). \tag{4.65}$$

Let us see what will happen after B_I decays. There are two decay channels that lead back to b quarks and thus can erase the asymmetry, one which is direct back-decay to SM $B_I \to bh$ (h is the CP even neutral component of the Higgs doublet) and the other through χ, η, $B_I \to \chi\eta^c$ if kinematically allowed. The last channel will lead to the following decay chain

$$B_I \to \chi\eta^c \to \chi d^c u^c. \tag{4.66}$$

Let us look at the decays of the χ field. For concreteness we will assume the following ordering of the masses

$$M_I > m_\chi > M_\eta. \tag{4.67}$$

Then the Majorana fermion χ is not stable and decays

$$\chi \to b\eta, \tag{4.68}$$

where $\chi^c b\eta$ interaction is generated after EWSB due to the mixing between vectorlike quarks and SM fields once the Higgs boson develops the VEV. The η field later decays to two quarks. However the Majorana nature of the field χ makes the decay to the CP conjugate final state open as well so that

$$\begin{aligned} &\chi \to b\eta \to bdu \\ &\chi \to b^c\eta^c \to b^c d^c u^c, \end{aligned} \tag{4.69}$$

decays are allowed and both final states have the same probabilities. As a result there will be two decay chains of B one leading to the generation of the baryon asymmetry and another to the wash-out

$$\begin{aligned} &(i)\ \text{wash-out}: \quad B_I \to \chi d^c u^c \to (bdud^c u^c) \qquad B_I^c \to \chi^c du \to (b^c d^c u^c du) \\ &(ii)\ \text{asymm. generation}: \quad B_I \to \chi^c d^c u^c \to (b^c d^c u^c d^c u^c) \qquad B_I^c \to \chi du \to (bdudu) \end{aligned} \tag{4.70}$$

As a result the asymmetry between SM quarks and antiquarks will be given by

$$(n_q - n_{q^c}) = \sum_I (n_{B_I} - n_{B_I^c}) \left[\left(-\frac{5}{2} + \frac{1}{2} \right) Br(B_I \to \chi \eta^c) + Br(B_I \to bh) \right] + (n_b - n_{b^c})$$
$$, = -3 \sum_I (n_{B_I} - n_{B_I^c}) Br(B_I \to \chi \eta^c), \tag{4.71}$$

where we have used $Br(B_I \to \chi\eta^c) + Br(B_I \to bh) = 1$ and Eq.(4.65) to derive the last relation. At last we have to take into account CP violating decays of the B particles similarly to the discussion in Eq.(4.40):

$$\epsilon^I_{\rm decay} = \frac{\Gamma(B^I \to \chi\eta^c) - \Gamma(B^{I,c} \to \chi^c \eta)}{\Gamma(B^{I,c} \to \chi\eta^c) + \Gamma(B^{I,c} \to \chi^c\eta)} = -\frac{4{\rm Im}(Y_I Y_J^* y_I^* y_J){\rm Im}[f_B^{IJ}]|_{m_{\eta,\chi}\to 0}}{|y_I|^2} \tag{4.72}$$

where the loop function is exactly equal to the one in Eq. (4.64) with zero masses of the particles inside the loop and an extra factor of 2, since inside the loop will now circulate the EW doublet. Thus for the total baryon asymmetry we obtain

$$\frac{\Delta n_B}{s} \approx \quad \frac{135\zeta(3)}{8\pi^4} \sum_{I,J} \theta_I^2 \frac{|y_I|^2}{|y_I|^2 + |Y_I|^2} \times \frac{g_b}{g_\star} \left(\frac{T_{\rm nuc}}{T_{\rm reh}} \right)^3$$
$$\times {\rm Im}(Y_I Y_J^* y_I^* y_J) \left(-\frac{2{\rm Im}[f_B^{IJ}]}{|Y_I|^2} + \frac{4{\rm Im}[f_B^{IJ}]|_{m_{\chi,\eta}\to 0}}{|y_I|^2} \right). \tag{4.73}$$

With $\frac{135\zeta(3)}{8\pi^4} \times \frac{|y_I|^2}{|y_I|^2+|Y_I|^2} \times \frac{g_b}{g_\star} \frac{{\rm Im}[Y_2 Y_1^* y_2^* y_1]}{16\pi |Y_I|^2} \sim 10^{-(3-4)}$ and $g_b = 6$ being the degrees of freedom of b quark and assuming $y_I = O(1)$ and $|y_I| \gg |Y_I| \sim |Y_J|$, recovering the observed baryon abundance $\frac{\Delta n_{\rm B}}{s} \sim 8.8 \times 10^{-11}$ requires, in order of magnitude,

$$\Rightarrow \boxed{\theta_I^2 \left(\frac{T_{\rm nuc}}{T_{\rm reh}} \right)^3 \sim 10^{-(6-7)}}. \tag{4.74}$$

The decay chains described above are very fast compared to the Hubble scale so that we can treat them as instantaneous. Indeed the

$$\Gamma(\chi \to \eta b) \approx \left| \sum_I y_I \theta_I \right|^2 \frac{m_\chi (1 - m_\eta^2/m_\chi^2)}{8\pi g_\chi} \qquad \Rightarrow \qquad \frac{\Gamma(\chi \to \eta b)}{H(v_{EW})} \simeq 10^{-3} \frac{M_{\rm pl}}{m_\chi} \gg 1, \tag{4.75}$$

since in the range of interest $\theta \lesssim 10^{-2}$. We conclude that decays are very fast. Thus, after this first phase of very fast decays, that produces the baryon asymmetry in the quark sector, slow transitions mediated by the heavy states can still wash out the asymmetry. Now, we check for which region of the parameter space it is not the case. The various wash-out transitions include

- $b\eta \to \chi$
  The decoupling of this transition provides the following condition, reminiscent of Eq.(4.52):

$$szH(z) \frac{d(Y_b - Y_{b^c})}{dz} \simeq -\gamma_{\chi \to \eta b} \left(\frac{Y_b Y_\eta - Y_{b^c} Y_{\eta^c}}{Y_b^{\rm eq} Y_\eta^{\rm eq}} \right) \tag{4.76}$$

and assuming that the asymmetries in B and η are related as follows

$$Y_{b,b^c} = (1 \pm \epsilon_q) Y^b_{\rm eq}, \quad Y_{\eta,\eta^c} \simeq Y^\eta_{\rm eq} \tag{4.77}$$

then, we arrive at the following equation

$$\begin{aligned} szH(z)\frac{d(\epsilon_q Y_{\rm eq})}{dz} &\simeq -\gamma_{\chi\to\eta b}\epsilon_q, \quad \gamma_{\chi\to\eta b} = \frac{g_\chi T^3}{2\pi^2} z^2 K_1(z)\Gamma(\chi\to\eta b) \\ \frac{d\epsilon_q}{dz} &= -\frac{0.42 e^{-z} z^{5/2}}{g_*^{1/2} g_q}\left(\frac{M_{\rm pl}}{m_\chi}\right)\left(\frac{g_\chi \Gamma(\chi\to\eta b)}{m_\chi}\right)\epsilon_q \end{aligned} \tag{4.78}$$

where

$$\Gamma(\chi\to\eta b) \approx \left|\sum_I y_I \theta_I\right|^2 \frac{m_\chi(1-m_\eta^2/m_\chi^2)}{8\pi g_\chi}. \tag{4.79}$$

Then the process is decoupled for the temperatures of EW scale if $m_\chi/T_{\rm reh} \gtrsim 30$, which pushes us to the limits of the maximal asymmetry which we can achieve in the mechanism. Indeed assuming $T_{\rm reh} \sim 100$ GeV, we are required to have $m_\chi \gtrsim 3$ TeV and $m_B \gtrsim 3$ TeV. Note that on top of the process above there will be reactions $\eta b \to \eta^c b^c$ which will also lead to the wash out of the asymmetry. This process is suppressed by the Boltzmann factor for η field abundance so that the condition to not erase the asymmetry becomes

$$\frac{m_{B,\chi,\eta}}{T_{\rm reh}} \gtrsim 30. \tag{4.80}$$

- $ddu \leftrightarrow d^c d^c u^c$
  After integrating out all the new heavy fields the following baryon violating number operator, which violates baryon number by two units, is obtained:

$$\frac{ddu\overline{d^c d^c u^c}}{M_\eta^4} \times \frac{1}{m_\chi} \times \theta^2 \qquad \Rightarrow \qquad \frac{1}{4\pi^5}\left(\frac{1}{16\pi^2}\right)^2 \frac{T_{\rm reh}^{11}}{M_\eta^8 m_\chi^2}\theta^4 \lesssim \frac{T_{\rm reh}^2}{M_{\rm pl}}. \tag{4.81}$$

  However, it can easily be seen that the rate of the baryon number violating processes mediated by it are much slower than the Hubble expansion as well.

- **Sufficient velocity for production of B_I**

  In the case of the EWPT, the gauge bosons play a role, so the maximal mass that we can produce will roughly scale like

$$M_\phi^{\rm MAX} \sim {\rm Min}\left[T_{\rm nuc}\left(\frac{M_{\rm pl}}{v_\varphi}\right)^{1/2}, \frac{4\pi v_\varphi}{g^3 n_{\rm transition}}\left(\frac{v_\varphi}{T_{\rm nuc}}\right)\right] = \frac{4\pi v_\varphi}{g^3 n_{\rm transition}}\left(\frac{v_\varphi}{T_{\rm nuc}}\right), \tag{4.82}$$

  where g is the typical gauge coupling and $n_{\rm transition}$ is the number of transitions emitting soft gauge bosons and which is order $\mathcal{O}(100)$. This is a rough estimate however, that we will strongly improve upon in Chapter 5. However, we will take Eq.(4.82) as indicative for now.

Experimental signatures

This low-energy model has the interesting consequence that it induces potential low-energy signatures. In this section, we enumerate those possible signatures without assuming that $Q, u,$ and d are the third generation quarks.

Neutron oscillations The baryon number violating processes in the model will violate the baryon number only by 2 units, so proton decay is not allowed but $n-\bar{n}$ oscillations can be present[313]. Integrating out the heavy states, we obtain the following operator

$$\frac{1}{\Lambda_{n\bar{n}}^5}\overline{u^c d^c d^c} udd \equiv \frac{(\sum \kappa\theta_I y_I)^2}{M_\eta^4 m_\chi}\overline{u^c d^c d^c} udd \tag{4.83}$$

thus inducing a neutron mixing mass of the form

$$\delta m_{\bar{n}-n} \sim \frac{\Lambda_{QCD}^6}{M_\eta^4 m_\chi}(\sum \kappa\theta_I y_I)^2. \tag{4.84}$$

Current bounds on this mixing mass are of order $\delta m_{\bar{n}-n} \lesssim 10^{-33}$ GeV [314, 315, 316, 317, 318]. This is extremely significant if the SM quarks in the Lagrangian are in first or second generation. If we take order 1 couplings and $\theta^2 \sim 10^{-5}$, it places a bound on the typical mass scale of

$$\Lambda_{n\bar{n}} \gtrsim 10^6 \text{GeV} \quad (M_\eta, m_\chi) \gtrsim 10^5 \text{GeV} \tag{4.85}$$

This bound becomes weaker if the new particles couple only to the third generation. Then we have an additional suppression factor $(V_{td}^4 V_{bu}^2)^{1/5} \sim 10^{-2}$. As a consequence, depending on the flavor of Q, u, d our scenario can be tested in the future experiment [319, 320, 321, 322].

Flavor violation The model predicts new particles in the $1-10^3$ TeV range coupled to the SM light quarks-η field. So the question about low energy bounds naturally rises. However the FCNC are absent at tree level for the η-diquark field [323]. The loop level effects can lead to strong constraints if ηdu coupling contains the light generation quarks [323], but if du are only the third generation fields t_R, b_R the bounds are practically absent.

Bounds from EDMs If there is CP violation in the mixing between bottom quark and heavy bottom partners then we expect an operator of the form

$$-i\frac{g_3\tilde{d}_q}{2}\bar{Q}\sigma^{\mu\nu}T^A\gamma_5 Q G_{\mu\nu}^A \tag{4.86}$$

which is the chromo-electric dipole moment (see [324] for a review), where $G_{\mu\nu}^A$ is the QCD field strength, with coefficient scaling like

$$\tilde{d}_q \sim \text{Im}[y_I^2]\frac{\theta_I^2 m_b}{16\pi^2}\frac{1}{\Lambda_{\text{EDM}}^2} \tag{4.87}$$

where $\Lambda_{\text{EDM}} \sim M_\eta \sim m_\chi \sim (1-100)$ TeV is the scale of the new physics that we are considering. Up-to-date bounds [325, 326] are $\tilde{d}_b < 1.2\times 10^{-20}\text{cm} \sim 10^{-6}\text{GeV}^{-1}$, which include the nucleon EDM bound via the RG effect. Taking typical values of the mixing angle $\theta^2 \sim 10^{-4}$, it can be seen that those bounds are not stringent.

Electron EDM is known to be one of the important test of the EW baryogenesis theories. In our model the leading contribution appears at three loop level due to the Barr-Zee type [327] of diagram with $b-B$ mixing. The estimate of the dipole operator goes like

$$\frac{d_e}{e} \sim \frac{m_e(yYe)^2}{(4\pi)^6}\left(\frac{1}{\Lambda_{EDM}^2}\right) \sim 3\times 10^{-33}\times\left(\frac{10\text{TeV}}{\Lambda_{\text{EDM}}}\right)^2 \text{cm} \tag{4.88}$$

which is several orders of magnitude below the current experimental bound [274] $|d_e| < 1.1\times 10^{-29}\text{cm}\cdot e$ if $\Lambda_{\text{EDM}} > 1$ TeV.

Gravitational waves One very robust prediction of such a scenario is the large amount of GW emitted at the transition, with peak frequency fixed by the scale of the transition $f_{\rm peak} \sim 10^{-3} \frac{T_{\rm reh}}{\rm GeV}$ mHz (see [52] for review). Such SGWB signal could be detected in future GW detectors such as LISA[328, 54], eLISA[329], LIGO[330, 331], BBO[332, 333], DECIGO[334, 335, 336], ET[337, 45, 338], AION[339], AEDGE[340]. This array of observers will be able to probe GW with frequencies in the window of mHz to kHz, which is the optimal scale for our mechanism to take place.

Direct production in colliders An almost coupling- and flavor-independent bound is the LHC one. The heavy quark can be produced via the strong or electro-magnetic interaction. From the recent squark or gluino bounds in the LHC e.g.[341, 342], we expect a mass bound of ~ 2 TeV on the lightest colored particle.

Parameter region

By combining all the previous bounds and by numerically solving the washout condition Eq.(4.79) we show the parameter region of this scenario in Fig.4.5. Here the horizontal axis is the $T_{\rm nuc}$ which, in order to produce a relativistic bubble wall, is favored to be smaller than $T_{\rm reh}$, which we took equal to 100 GeV. The vertical axis denotes $m_\eta (< M_I)$, which is the lightest diquark in this scenario. All the data points give the correct baryon asymmetry $\Delta n_B/s = 8.8 \times 10^{-11}$, with all the couplings smaller than $\sqrt{2\pi}$. The green points satisfy the bound on $n - \bar{n}$ oscillation in Eq.(4.85). The red and blue points do not satisfy it, which implies a special flavor structure for example that only b is coupled to the BSM particles. For both red and green points, both M_1 and M_2 satisfy the relativistic wall in Eq.(4.82), which is denoted by the black solid line. For the blue points, the lighter of M_1 and M_2 satisfies the condition. The horizontal dotted at 2 TeV is the typical bound on new colored particles. Therefore our mechanism predicts light quarks, which may be searched for in the LHC and future colliders. Moreover, since our data points include parameter space both consistent and inconsistent with the neutron-anti-neutron oscillation bound, some points with BSM particles that also couple to the first two generation quarks can be tested in the future. Note again that $T_{\rm nuc} \sim O(0.1) T_{\rm reh}$ may be the consistent range for our scenario to work.

Alternative baryogenesis models

Let us here enumerate the possible change that we can make in the Lagrangian of Eq.(4.61)

- We can couple η instead of the right-handed to the left-handed ones via $\eta^c QQ$.
- We can also couple the opposite chirality to the the diquark with the coupling $y\eta\chi P_R B$. In the case of the coupling $y\eta\chi P_R B$, on the top of the previous estimates, there will be an additional m_b/M_B suppression in the χ decay and a similar m_b^2/M_B^2 is the $n - \bar{n}$ oscillations.
- We may also replace B_i by an up-type-like quark, and assume that it mainly couples to the top quarks, this effect is suppressed by a further Boltzmann factor. Then the Lagrangian is given as

$$\sum_{i=1,2} Y_i (\bar{U}_i H^*) Q + M_{Bi} \bar{U}_i U_i + \lambda_i U_i \chi^c \eta + \kappa \eta^c dd + \frac{m_\chi}{2} \bar{\chi}^c \chi + m_\eta |\eta|^2. \tag{4.89}$$

  Here dd denotes ($d_2 d_3$ or $d_1 d_2$). The FCNC constraint is stringent but there is a viable parameter region.

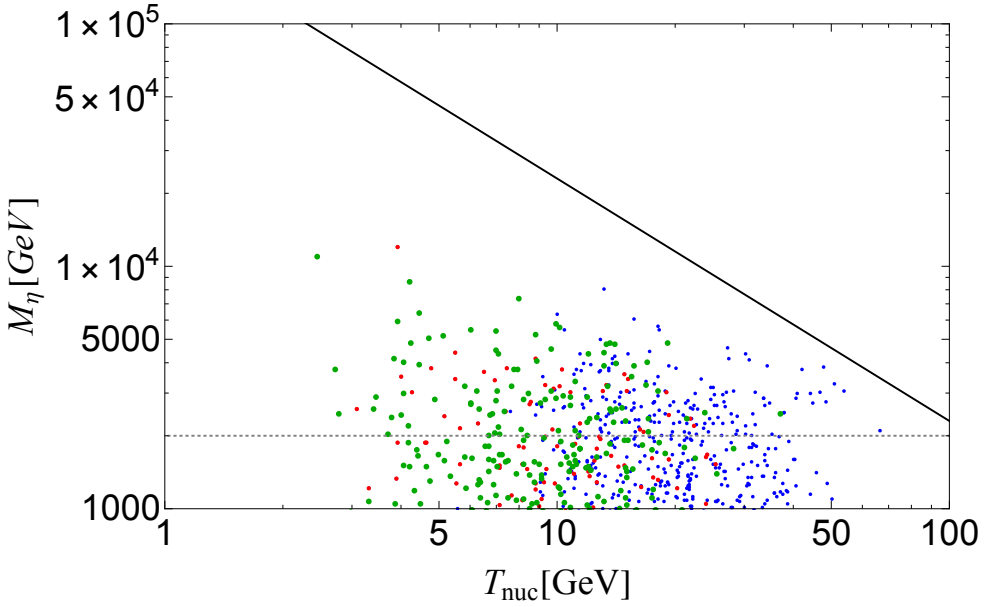

Figure 4.5: m_η (which is the lightest colored particle mass) vs $T_{\rm nuc}$ in the low energy baryogenesis. The green points satisfy (4.85), while the red and blue points do not satisfy it and thus require a special flavor-structure. Both (the lighter of) M_1 and M_2 are taken to satisfy the conditions from maximal wall velocity (4.82), which is shown by the black solid line, in the appendix for green and red (blue) points. Here we fix $\langle \mathcal{H} \rangle = T_{\rm reh} = 100\,\text{GeV}$ to consider the electroweak phase transition and fix $\Delta n_B/s = 8.8 \times 10^{-11}$. Other parameters are randomly chosen within the perturbative unitarity range. Below the 2TeV (dotted line) may be disfavored by the null detection of new colored particle in the LHC.

Baryogenesis from non-EW FOPT

At last we note that, with a simple modification of the model in Eq.(4.61), the mechanism can be operative for an arbitrary phase transition. Indeed let us assume that φ is the field experiencing the FOPT then the following lagrangian :

$$\mathcal{L}_\phi = \mathcal{L}_{SM} + \sum_{I=1,2} \tilde{Y}_I(\bar{B}_I\varphi)b_R + M_I\bar{B}_I B_I + \lambda_I B_I \chi^c \eta + \kappa \eta^c du + \frac{m_\chi}{2}\bar{\chi}^c\chi \tag{4.90}$$

can induce the required baryon asymmetry. The phenomenology remains similar to the model of Eq.(4.61) however the experimental constraints from $n-\bar{n}$ oscillations and other low energy searches become even weaker. At the limit, the only robust experimental signature of such a scenario is the GW background emitted if the VEV is not extremely larger than the EW scale.[6]

4.4 Summary and outlook

In this chapter we have presented a novel mechanism for the generation of the baryon asymmetry during the early universe evolution. We have first shown that the mechanism of production of the heavy particles from the relativistic bubble expansion during the FOPT can lead to CP violating effects. This mechanism of particle production is out of equilibrium, so that if baryon number violating interactions are present a baryon asymmetry can be generated. We have constructed two viable baryogenesis models implementing this idea. The first scenario is the phase-transition-induced leptogenesis, where the bubble wall should be composed by some new Higgs field charged under the lepton number, and after the phase transition we are still in the symmetric phase of the EW interactions but in the broken phase of the lepton number. Later EW spharelons transfer the lepton asymmetry to the baryon sector. In this scenario, a net $B-L$ asymmetry is generated since the Majorana term of the right-handed neutrino after the PT violates the $B-L$ symmetry. Neutrino mass observations make the mechanism viable if the scale of the phase transition is between $[10^9, 10^{13}]$ GeV, which makes it borderline detectable for the future gravitational wave experiments such as ET[337, 45, 338] if the signal comes from the phase transition. GW signal from the possible cosmic strings accompanying the transition could improve this situation and induce detection at LIGO, DECIGO and maybe LISA. The second scenario can happen during EW phase transition. In this case, new fields charged under QCD with $\lesssim 100$ TeV scale masses are needed to have enough baryon number production. In both cases the baryon/lepton number violating interactions are coming from the Majorana masses of new heavy particles. This leads to the Majorana neutrino masses in the first class of models and $n-\bar{n}$ oscillations in the second class of models. Another feature of this mechanism is that baryogenesis happens for the ultra-fast bubble expansions thus generically strong stochastic gravitational wave signatures are expected. Moreover, in the case of the second scenario, the frequency range is well within the reach of the current and future experiments. However, in our survey, we did not study the possibility of flavor effects. A natural question is: can the flavor effects strongly modify our picture ?

[6]For the values the VEV $\langle\varphi\rangle \gtrsim 10^{12}$ GeV, there is no need to suppress the interaction $HL\chi$ since the bounds from proton decay become compatible with experiment.

Chapter 5

Relativistic bubble walls in the Electroweak Phase Transition

The previous chapters were dedicated to an exposition of a mechanism of production of heavy states during the expansion of very relativistic bubbles and to the cosmological consequences: pressure on the wall, production of heavy Dark Matter and Baryogenesis. In those settings we always left the transition scalar sector physics unspecified. Now, in this last chapter, we come back to this issue and we use our experience from Chapter 2 to search for the relativistic bubble walls in the context of long supercooling. We focus on the simple case of a real singlet extension of the electroweak sector and specialize to 2-steps PT, where we see that very strong supercooling is indeed realisable. We quantify the region of parameter space where the EW bubble becomes ultra-relativistic and deduce the maximal mass that can be produced via the bubble wall expansion mechanism. We then revisit our previous models of Baryogenesis and DM production in this special context.

Contents

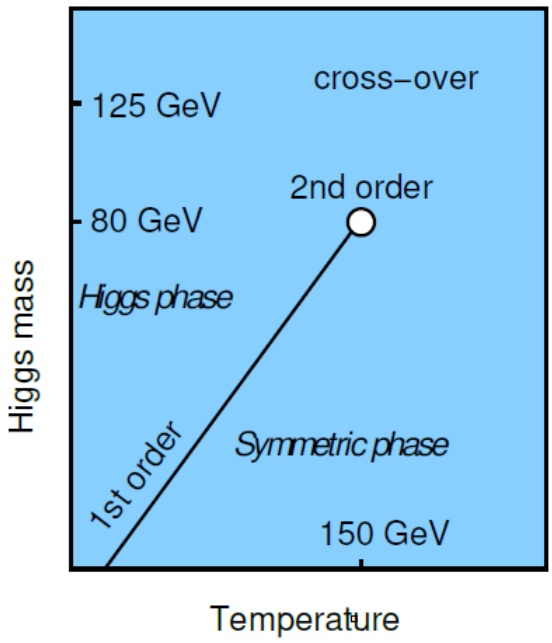

Figure 5.1: As we increase the mass of the Higgs boson m_h, the temperature of the FOPT increases, until the correlation length diverges and the latent heat goes to zero at a critical mass around $m_h \approx 80$ GeV. From [53].

The origin of Dark Matter (DM) and matter-antimatter asymmetry are one of the most important unresolved puzzles of the early Universe cosmology. In the previous chapters 3 and 4, we have presented and investigated in detail the novel mechanisms proposed in [3, 2, 303] for DM production[1] and baryon asymmetry generation during the first order phase transitions (FOPT) that were efficient for relativistic bubble walls. We each time studied this mechanism in the context of a generic PT and for the EWPT, however, we delayed the study of the model allowing for relativistic walls in EWPT. In this chapter, we fill this gap and we study in detail the ultra-relativistic regime of EWPT. The main question is thus: can we even build a simple extension of the SM that features a FOPT with long supercooling and then relativistic bubble walls? Long supercooling is known to occur typically for long, flat and shallow potentials, as studied in [193, 11, 348, 31, 5], and it was shown that the bubble wall was typically ultra-relativistic. However in the case of electroweak phase transition, the requirement of long supercooling leads to very non-trivial constraints on the effective potential.

It is well-known that the description of the dynamics of the EW phase transition necessitates non-perturbative tools[259, 349, 350, 351]. The transition is non-perturbative due to soft modes having momentum $p \sim g^2 T$ and thus being non-perturbative, as explained for the Linde problem.

From those non-perturbative studies, it was found that: if the mass of the Higgs is larger than about ~ 80 GeV, then the transition is expected to be a smooth cross-over. Around this critical point, the phases becomes

[1]Recently, there have been many classes of models where DM production and FOPT in the early universe have been related (see for example Ref[343, 156, 157, 344, 160, 159, 162, 163, 164, 165, 173, 238, 345, 346, 347, 167, 168, 169, 170]).

indistinguishable. This is analog to the case of water at the tri-critical point where the vapor and the liquid phase cannot be distinguished anymore. Conversely, if we keep the same matter content, we can argue that the EWPT becomes a strong FOPT if $m_h \lesssim 35$ Gev[352, 353]. This is however far below the measured mass of the Higgs boson ~ 125 GeV and it is considered today as settled that the EWPT in the SM is a cross-over, which rules out the SM baryogenesis.

However, this is not the case for various Beyond Standard Model (BSM) frameworks where successful scenarios of FOPT in EWPT and thus electroweak baryogenesis can be built (see for a recent review [256]). Many ideas have been put forward in order to make naturally the EWPT first order, among other proposals: varying Yukawas during the EWPT, raised in[354] and then studied in [355] was shown to produced FOPT for low scale flavons, non-linearly realised EWPT can be FOPT [356, 357] in a tuned region due to a tree-level cubic term, and in the 2HDM[358] large room is still left for FOPT. More generic studies using a EFT for the $SM + \mathcal{H}^6$ have studied the EWPT and shown that the transition would become FOPT in a significant part of the parameter space[359, 9, 33, 31] (specially if the cut-off is not too high $\Lambda \sim 500 - 800$ GeV). In the MSSM, in the *Light Stop Scenario* the EWPT can become FOPT[270], however, it is now excluded by the LHC searches[271] of stops. The EWPT can also become strongly first order if it occurs at the same time than the confinement transition of the strong dynamics of a composite Higgs, when the dynamics is nearly conformal[267, 360] and when it is controlled by nearly conformal dynamics[361]. Finally, a particularly simple way to make the EWPT first order is to couple the Higgs to a new scalar transforming as a singlet under the SM gauge groups. There have been numerous studies of phase transition in this type of scenario [362, 363, 364, 365, 366, 367, 368, 369, 308, 370, 371]. The Lagrangian can be restricted further by considering Z_2 [372] or Z_3 symmetries[373, 374]. Interestingly such a real singlet scalar field can appear in composite Higgs models [375] (see also [244, 376] for studies pertaining to phase transition). However, most of the above mentioned works did not analyze in detail the region of parameter space with *relativistic bubbles* since slow bubble wall velocities are required [254, 255] for the usual electroweak baryogenesis.

In this chapter we analyze in detail the simplest extension of the SM that can lead to a FOPT: the real singlet extension of SM with an approximate Z_2 discrete symmetry and we focus on the parameter space which results in very fast bubble expansions. if there is no mixing in the true vacuum and the singlet is heavy enough to forbid exotic Higgs decay, this is the "nightmare scenario" of [377]. Anticipating the results of this paper we found that the most promising scenario for relativistic bubbles is the case where the phase transition occurs in two steps: the first transition is related to the Z_2 symmetry breaking while keeping EW symmetry unbroken and in the second one the Higgs field acquires its vacuum expectation value (vev) which comes together with Z_2 symmetry restoration.

This will permit us to evaluate the region of parameter space where Baryogenesis via relativistic bubble walls of Chapter 4 is viable and to put constraints on the mass scale of the dark sector responsible for CP and B violation. Implications for non-thermal DM production from bubble wall plasma particle collisions of Chapter 3 will also be considered. Our purpose is to show that even in this minimal setting, the ultra-relativistic region exists, and thus we hope that it should exist as well in most of the possible models.

This chapter is organised as follows: in section 5.1, we review the singlet extension of the SM and write the two field potential with thermal corrections. In section 5.2, we qualitatively discuss the different patterns of phase transitions and argue that only a two-steps PT can yield ultra relativistic bubble wall motion. In section 5.3 we present a numerical study of the two-step PT analyzing in detail the region with fast bubble motion. In section 5.4, we draw the consequences of our previous results for the production of heavy DM and Baryogenesis and in section 5.5, we comment on the GW signal induced by such strong transitions. Finally, in section 5.6, we summarize and conclude.

5.1 Review of the singlet extension of the SM

Let us start by reviewing the effective potential of the SM with a real scalar field s.

5.1.1 Tree-level scalar potential

The tree-level scalar potential will be given by

$$V(\mathcal{H},s) = -\frac{m_h^2}{2}(\mathcal{H}^\dagger\mathcal{H}) + \lambda(\mathcal{H}^\dagger\mathcal{H})^2 - \frac{m_s^2}{4}s^2 + \frac{\lambda_{hs}}{2}s^2(\mathcal{H}^\dagger\mathcal{H}) + \frac{\lambda_s}{4}s^4 \,, \tag{5.1}$$

where $\mathcal{H}$ is the SM Higgs doublet and $m_h \approx 125$ GeV is the physical mass of the Higgs. For simplicity, we will impose Z_2 symmetry on the potential to avoid the terms with odd powers of s field. As a result, when $\langle s\rangle = 0$, we avoid any scalar mixing terms which are constrained by the recent Higgs signal strength measurements [378]. The Higgs doublet can be decomposed as usual

$$\mathcal{H}^T = \left(G^+, \frac{h+iG^0}{\sqrt{2}}\right) , \tag{5.2}$$

where h is the usual physical Higgs boson getting a vev which in the true minimum is given by $v_{EW} = \sqrt{m_h^2/2\lambda} \approx 246$ GeV if $\langle s\rangle \equiv v_s = 0$.

5.1.2 Coleman-Weinberg potential

For taking into account the loop-corrections, we will use the very handy on-shell renormalisation scheme presented in sec 1.3.2, where

$$V_{CW}(h,s) = \sum_{i=Z,h,W,t} \frac{g_i(-1)^F}{64\pi^2}\left[M_i^4(h,s)\left(\log\frac{M_i^2(h,s)}{M_{i0}^2} - \frac{3}{2}\right) + 2M_i^2(h,s)M_{i0}^2\right] . \tag{5.3}$$

In this expression, $M_i(h,s)$ stands for the masses depending on the Higgs and singlet fields values, $M_i \equiv M_i(h,s)$, and M_{i0} are the field values from the tree-level VEV in the true minimum. The number of d.o.f, masses of various particles and the scalar mass matrix as a functions of h, s are given by:

$$\begin{gathered} g_{W^\pm} = 6, \qquad g_Z = 3, \qquad g_{G^{\pm,0}} = 3, \qquad g_t = -12 \,, \\ M_{W^\pm}^2(h) = \frac{g^2h^2}{4}, \quad M_Z^2(h) = \frac{g^2+g'^2}{4}h^2, \quad M_{G^{\pm,0}}^2(h) = -\frac{m_h^2}{2} + \lambda h^2, \quad M_t^2(h) = \frac{y_t^2h^2}{2} \\ M^2(h,s) = \begin{pmatrix} 3\lambda h^2 + \frac{\lambda_{hs}}{2}s^2 - \frac{m_h^2}{2} & \lambda_{hs}sh \\ \lambda_{hs}sh & 3\lambda_s s^2 + \frac{\lambda_{hs}}{2}h^2 - \frac{m_s^2}{2} \end{pmatrix} . \end{gathered} \tag{5.4}$$

As a side remark, in the region where the Higgs $h \to 0$ and $s \sim \mathcal{O}(v_{EW})$, there will be two scales involved in the problem: the value of the singlet field s and the masses of the SM particles $M_{W,Z,t}(h \to 0, s) \to 0 \ll s$. This type of two scale potential has been studied in the past [379], by using two different renormalisation scales. It was concluded that resummation is needed when the $\log\left(M_i(0,s)/s\right)$[2] is large enough to cancel the loop suppression. Although we have two largely separated scales, we have checked that for our region of the parameter space, such a resummation is not necessary.

[2]We will see soon that, in a thermal context, $M_i(0,s)$ is controlled by the scale of the temperature, creating a hierarchy $\log\frac{T}{v_{EW}}$.

5.1.3 Finite temperature potential

We now need to take into account the thermal effects in the early universe. We presented in section 1.4.3 how to do so. On the top of it, to account for dangerously divergent higher loops due to the Daisy diagrams at finite temperature, we rely again on the "Truncated-Full-Dressing" procedure [16] of section 1.4.4. Doing so, the full one-loop potential becomes

$$V(h,s,T) = V_{\rm tree}(h,s) + \sum_i \left[V_{CW}\Big(M_i^2(h,s) + \Pi_i(h,T)\Big) + V_T\Big(M_i^2(h,s) + \Pi_i(h,T)\Big)\right], \quad (5.5)$$

where $\Pi_i(T)$ are the thermal masses of various degrees of freedom. In the real singlet extension of the SM we only need to add the contribution of the singlet on the top of the expressions already presented in Eq.(1.98). This gives

$$\text{Scalar:} \qquad \Pi_h(T) = T^2\Big(\frac{3g^2}{16} + \frac{g'^2}{16} + \frac{\lambda}{2} + \frac{y_t^2}{4} + \frac{\lambda_{hs}}{24}\Big)\,, \qquad \Pi_s(T) = T^2\Big(\frac{\lambda_{hs}}{6} + \frac{\lambda_s}{4}\Big)\,, \quad (5.6)$$

$$\text{Gauge:} \qquad \Pi_g^L(T) = T^2 \text{diag}\Big(\frac{11}{6}g^2, \frac{11}{6}(g^2+g'^2)\Big)\,, \qquad \Pi_g^T(T) = 0\,, \quad (5.7)$$

where $\Pi_g^L(T)$ denotes the thermal mass of the *longitudinal* mode of the gauge bosons, while transverse modes $\Pi_g^T(T)$ are protected by gauge invariance and thus do not receive a mass at leading order in perturbation theory.

5.2 Phase transition in the singlet extension

After the preparatory discussion in the previous sections 5.1, we can proceed to the analysis of the phase transition in the model with the singlet field, Eq.(5.1). Our analysis will be focused on the region of parameter space with relativistic bubble expansion, for other studies of phase transition in SM plus Z_2 real singlet scalar, see for other studies Refs. [380, 372, 377, 381].

In the Chapter 2, we have seen that the velocity of the bubble expansion is fixed by the balance between the friction from the plasma and the driving force. At low temperatures the friction is suppressed (see Eq.(2.148) and (2.150)) so that we expect the bubbles to become relativistic (large Lorentz $\gamma_w^{\rm terminal}$ factor).

Let us check whether low nucleation temperatures are feasible in the singlet extension. We will assume that Z_2 remains unbroken in the true vacuum in order to avoid the constraints from the Higgs-scalar mixing (see for example [382]). Then in the model with Z_2 odd singlet, the phase transition can occur in two ways: one-step $(\langle h\rangle = 0, \langle s\rangle = 0) \to (v_{EW}, 0)$ and two-steps[3] $(\langle h\rangle = 0, \langle s\rangle = 0) \to (0, \langle s\rangle \neq 0) \to (v_{EW}, 0)$ [308, 377, 372], and each of these phase transitions can be first or second order. We review both of these scenarios of phase transitions in order to understand in which case it is possible to obtain relativistic bubbles.

5.2.1 One-step phase transition:

This case has been largely studied in the literature [377, 372] and we will not provide a complete description of it. In this scenario the singlet never gets a VEV, and all of its effect reduces to the additional contributions to the Higgs potential from Coleman-Weinberg terms and thermal corrections. However it turns out that relativistic bubbles are

[3]We will see later that at temperatures $T \ll T_c$ the Coleman-Weinberg potential can shift a little bit the false vacuum position to $(\delta v_h, v_s)$ where $\delta v_h \ll v_s, v_h$.

very unlikely for such phase transitions (see also results in [372]). In the limit when $|m_s| \ll T_c$ we can show analytically that this is indeed the case. Near the origin $h \to 0$, the potential in h direction is dominated by the $\propto h^2$ terms

$$V_{\text{dominant}}(h \to 0, s = 0, T) \quad = \quad \frac{m^2_{\text{eff}}(T)}{2} h^2 + \dots \tag{5.8}$$

The effective mass m^2_{eff} include the tree-level terms and the leading thermal contributions and is approximately equal to

$$m^2_{\text{eff}}(T) \simeq -m_h^2 + T^2 \left(\frac{m_h^2}{4v_{EW}^2} + \frac{y_t^2}{4} + \frac{g^2 + g'^2}{16} + \frac{g^2}{8} + \frac{\lambda_{hs}}{24} \right) . \tag{5.9}$$

The FOPT can happen only if $m^2_{\text{eff}}(T) > 0$ at the moment of the PT. Then assuming perturbative values of the coupling λ_{hs} we can estimate the lowest temperature where the FOPT can occur to be $T^{\min}_{\text{nuc}} \gtrsim 100$ GeV. Comparing this value with the discussion in the Chapter 2, section 2.4.2, and more specifically the expression

$$\gamma^{\text{terminal}} \sim 3 \times \left(\frac{\Delta V - P_{\text{LO}}}{(100 \text{ GeV})^4} \right) \left(\frac{100\text{GeV}}{T_{\text{nuc}}} \right)^3 \frac{1}{\log \frac{M_Z}{gT}}, \tag{5.10}$$

we can see that the bubble wall velocities will always satisfy $\gamma_w \lesssim \mathcal{O}(1)$. As mentioned before, we are interested in the expansions with much larger γ_w factors, so that we do not discuss one step phase transition further.

5.2.2 Two step FOPT with relativistic bubbles

Two-steps realisations of the EWPT have already been studied in many works, see for example[307, 308, 383, 377, 384, 385, 372, 386]. The novelty of our study is that we will be focusing on the parameter space with relativistic bubbles which was previously ignored. We organize the discussion as follows: In section 5.2.2, we show qualitative results based on approximate treatment of the potential and then in the section 5.3 we present the exact numerical results obtained with our code. The two step phase transition

$$(0, 0) \to (0, \langle s \rangle) \to (v_{EW}, 0) \, , \tag{5.11}$$

can happen if the m_s^2 parameter of Eq.(5.1) is positive. In this case it is convenient to parameterize the Lagrangian in the following way

$$V_{\text{tree}}(h, s) = -\frac{m_h^2}{4} h^2 + \frac{m_h^2}{8v_{EW}^2} h^4 - \frac{m_s^2}{4} s^2 + \frac{\lambda_{hs}}{4} s^2 h^2 + \frac{m_s^2}{8v_s^2} s^4 \, . \tag{5.12}$$

where $v_{EW} = \sqrt{m_h^2/2\lambda}$ GeV and $v_s = \sqrt{m_s^2/2\lambda_s}$ correspond to the local minima at $(\langle h \rangle = v_{EW}, \langle s \rangle = 0)$ and $(\langle h \rangle = 0, \langle s \rangle = v_s)$ respectively. The origin of two-step PT can be intuitively understood from the following considerations. For simplicity let us ignore the Coleman-Weinberg potential and restrict the discussion by considering only the thermal masses. Then the potential will be given by

$$\begin{aligned} V(\mathcal{H}, s) \quad &\approx \quad V_{\text{tree}}(\mathcal{H}, s) + \frac{T^2}{24} \left[\sum_{bosons} n_i M_i^2(\mathcal{H}, s) + \frac{1}{2} \sum_{fermions} n_F M_F^2(\mathcal{H}, s) \right] \, , \\ &= \quad V_{\text{tree}}(\mathcal{H}, s) \\ &+ \quad T^2 \left[h^2 \left(\frac{g'^2}{32} + \frac{3g^2}{32} + \frac{m_h^2}{8v_{EW}^2} + \frac{y_t^2}{8} + \frac{\lambda_{hs}}{48} \right) + s^2 \left(\frac{m_s^2}{16v_s^2} + \frac{\lambda_{hs}}{12} \right) \right] . \end{aligned} \tag{5.13}$$

From this expression we can clearly see that the temperatures when the minima with non zero vevs appear for the Higgs and singlet fields can be different. Then it can happen that the Z_2 breaking phase transition occurs before the EW one. This means that there will be first a phase transition from $(0,0) \to (0, v_s)$. After this phase transition the Universe keeps cooling down and the minimum with $\langle h \rangle \neq 0$ will be generated. Choosing the appropriate values of masses and couplings we can make sure that the minimum with $(v_{EW}, 0)$ is the true minimum of the system. The transition $(0, v_s) \to (v_{EW}, 0)$ will be of the first order if there is a potential barrier between the two minima. One of the necessary condition in this case will be $\partial^2 V/\partial h^2|_{s=v_s, h\to 0} > 0$, which using Eq.(5.13) we get

$$\frac{-m_h^2}{4} + \frac{\lambda_{hs} v_s^2}{4} + T^2 \left(\frac{g'^2}{32} + \frac{3g^2}{32} + \frac{m_h^2}{8v^2} + \frac{y_t^2}{8} + \frac{\lambda_{hs}}{48} \right) > 0 \, . \tag{5.14}$$

From this discussion we can see that there are qualitatively two different cases depending on whether the potential barrier between two minima remains or disappears at zero temperature, *i.e.* when $m_h^2 \gtrless \lambda_{hs} v_s^2$. In the first case the phase transition will necessarily happen before the "No Barrier"(NB) temperature

$$T^{\rm NB} = \sqrt{\frac{m_h^2 - \lambda_{hs} v_s^2}{\frac{g'^2}{8} + \frac{3g^2}{8} + \frac{m_h^2}{2v^2} + \frac{y_t^2}{2} + \frac{\lambda_{hs}}{12}}} \sim \frac{v_s \sqrt{-\lambda_{hs} + \left(\frac{m_h}{v_s}\right)^2}}{0.8} \, , \tag{5.15}$$

which we define as the temperature when the barrier disappears. This is because the bounce action drops once the potential barrier between two minima reduces.

From Eq.(5.14) we can see that the size of the potential barrier between the two minima is controlled by the coupling λ_{hs}. Increasing this parameter will enhance the potential barrier and will lead to the reduction of $T^{\rm NB}$ so that $(v_s, 0)$ remains a local minimum even at zero temperature. At some point we expect the potential barrier to become so large that the system will remain trapped in the false vacuum forever. From this discussion we can expect that the lowest temperatures will be achieved at the boundary of the region where no PT can occur. The lowest temperature will correspond to the (global) minimum of S_3/T controlling the tunneling rate, as explained later in section 5.3. If this minimum happens at temperatures much lower than $T_{\rm crit}$, then there will be super-cooling ($T_{\rm nuc} \ll T_{\rm crit}$). Even though this discussion was made by considering only the thermal masses in the potential, numerically we find that for the effective potential with truncated full dressing [16] the qualitative behaviour does not change, and only explicit conditions for m_h^2 and $T_{\rm min}^{\rm nuc}$ are modified.

At last we always check whether the condition for the EWSB minimum to be the global minimum at zero temperature is satisfied:

$$m_s^2 v_s^2 < m_h^2 v_{EW}^2 \qquad \text{(EWSB is global minimum)} \, , \tag{5.16}$$

where the above equation is valid up to small loop-level corrections.

5.3 Numerical results

After the qualitative discussion, let us proceed to the numerical calculations. The bounce action for $(0, v_s) \to (v_{EW}, 0)$ was computed using our own dedicated code (cross checked against `FindBounce`[387]) and we relegate the details and methods of this calculation to Appendix A.4. We parameterize our model in terms of (m_s, λ_{hs}, v_s) parameters (see Eq.(5.12)). Instead of analyzing all the possible values of m_s, in this section we report the results by fixing $m_s = 125$ GeV on Fig 5.2 and $m_s = 150$ GeV on Fig.5.8, that we report in section 5.3.3 (there is no

particular reason for those values of m_s). In the plane (see Fig.5.2) $v_s - \lambda_{hs}$, we identify four regions with different behaviours under the phase transition. The blue region shows a second order transition[4] when there is no barrier between the two separated vacuum. Next to it there is a light red region where the transition is of the first order. We indicate separately (dark red) the region, where the transition is of the first order and the bubbles are relativistic. In particular the boundary between the regions with relativistic and non-relativistic bubbles is defined by the criteria of Eq.(2.149), *i.e.* when the LO pressure for relativistically expanding bubbles is less than the driving force. At last, there is the "NO PT" region, where the system remains stuck in the false vacuum since the tunnelling rate is too small.

The structure of the diagram (on the Fig.5.2 top−left panel) can be easily understood from the qualitative discussion in the previous section. Indeed, keeping v_s fixed, the size of the potential barrier is controlled by the coupling λ_{hs}. Moving from left to right the size of the potential barrier increases and we are gradually moving from the region of second order phase transition → FOPT → FOPT with relativistic bubbles → no PT region. Similarly moving up (increasing v_s for fixed values of λ_{hs}) also corresponds to the increase of the potential barrier as we pass though the regions with different PT in the same order. On the upper axis we report the physical mass of the singlet in the true vacuum $M_s(v_{EW}, 0)$ and exclude the constrained region where $h \to ss$ is kinematically allowed (the gray meshed region).

Next we plot the values of $T_{\rm nuc}$ and $\gamma_w^{\rm terminal}$ as a function of (λ_{hs}, v_s) (Fig.5.2). As discussed in the previous section, the region with the smallest values of the nucleation temperature (thus the fastest bubbles) is located near the "NO PT" region, *i.e.* where the system remains trapped in the false vacuum. The blue dot on the $T_{\rm nuc}$ plot indicates the last point (up to 6 decimals of precision in λ_{hs}) we have found before the system enters the regime of no phase transition (NO PT). In the bottom right we plot the $M_{\rm max} = \sqrt{\gamma_w T_{\rm nuc} v_{EW}}$ quantity which indicates the maximal energy in the c.o.m frame for the plasma particle−bubble wall collision, which corresponds to the largest mass of the heavy particles we can produce (see discussion in sec 5.4.1).

In order to better understand the dependencies of $T_{\rm nuc}$ and γ_w on the parameters of the model, it is useful to separate further the parameter space depending on whether the potential barrier disappears at zero temperature or not. This is important since the bounce action in such cases has very different dependencies on the temperature. See for example Fig.5.3, where we have plotted the S_3/T for $v_s = 170, m_s = 125$ GeV for the various couplings λ_{hs}. In the case when the potential barrier disappears at some temperature $T^{\rm NB}$ the function S_3/T drops to zero, but if the barrier remains even at zero temperature S_3/T has a global minimum for $T \neq 0$ which will be controlling the lowest nucleation temperature possible.

5.3.1 No potential barrier at zero temperature

Let us start by defining the region where there is no potential barrier at zero temperature. On Fig.5.2, we display the curves where the barrier disappears for various values of the temperatures ($T^{\rm NB}$). For $T^{\rm NB} = 0$ case, approximate curve can be obtained analytically by looking at the leading terms in the zero temperature CW potential

$$\lambda_{hs} \lesssim \frac{m_h^2}{v_s^2} - \frac{n_t y_t^4}{32\pi^2} \frac{v_{EW}^2}{v_s^2} \ . \tag{5.17}$$

The agreement between this equation and exact $T^{\rm NB} = 0$ curve is at the level of a few permille discrepancies. To the right of $T^{\rm NB} = 0$ curve, the potential barrier between the two minima remains even at zero temperatures. For the values $v_s \gtrsim 200$ GeV, we find that the line $T^{\rm NB} = 0$ approximately coincides with the boundary of no

[4]More exactly it shows the region where out perturbative analysis should be inconclusive about the order of the transition.

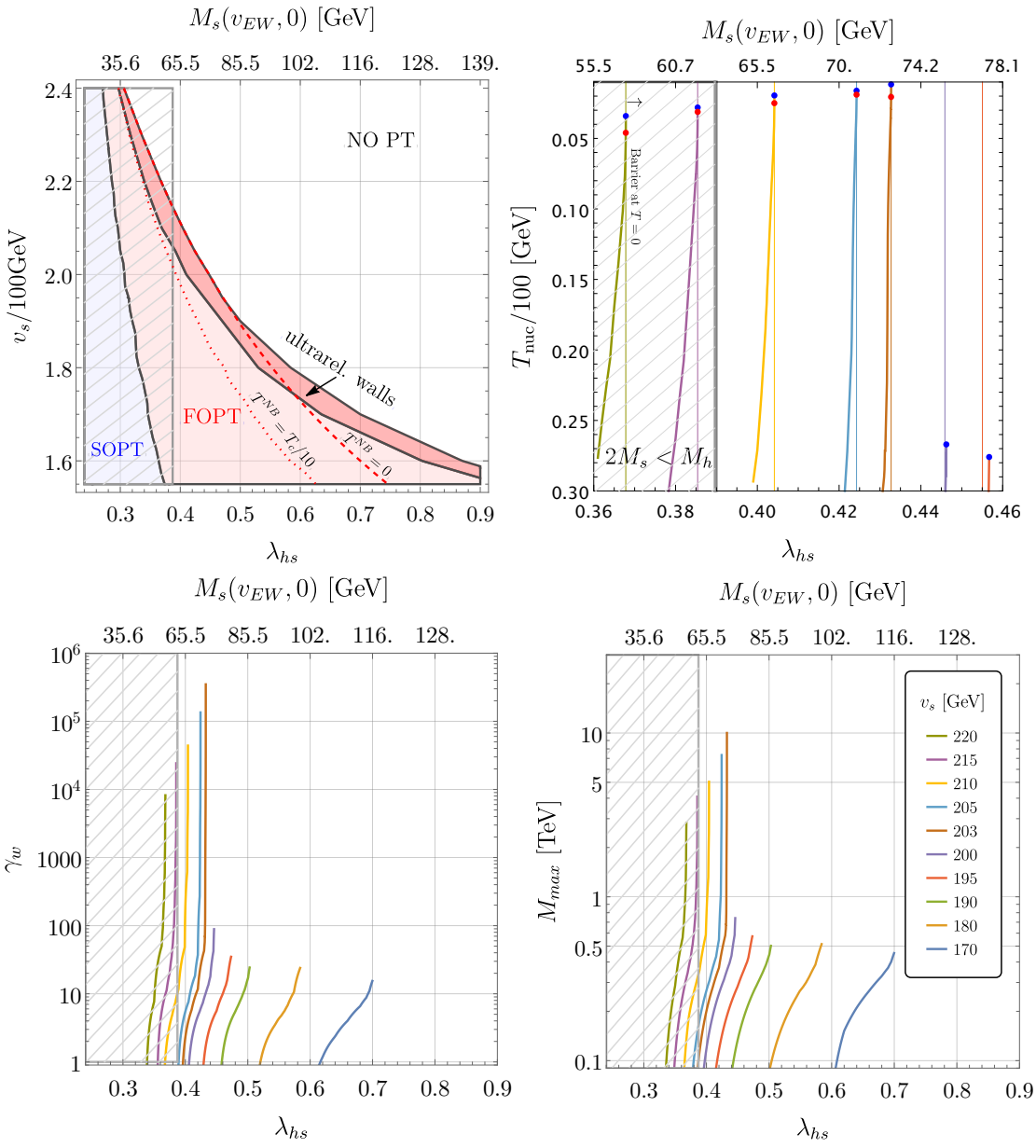

Figure 5.2: **Top-Left**: Scan of the parameter space in the plane $\lambda_{hs} - v_s$ for $m_s = 125$ GeV. The four regions are as follows: i) white - "NO PT", the region where the transition never completes because the barrier remains at zero temperature and the function S_3/T never passes below the nucleation condition, ii) light and dark red are the regions where the FOPT happens. Dark (light) red corresponds to the region with relativistic (non-relativistic) bubble expansion. The boundary between two regions is given by Eq.(2.149) iv) blue - the phase transition is of the second order. The gray meshed region is the one in which $M_s(v_{EW},0) < m_h/2$, that is constrained from collider experiments. **Top-Right and Bottom**: the dependencies of $T_{\rm nuc}, \gamma_w,\ M_{max}$ on the λ_{hs} coupling for $m_s = 125$ GeV. The blue dot on the Top-Right plot designates the end of the curve, when the tuning becomes 10^{-6} and the red dot signals the appearance of a barrier at zero temperature (all the points above the red dot have a barrier at $T = 0$). For the last three plots we varied the λ_{hs} parameter with the steps of 10^{-6}. The value of v_s is encoded in color according to the bottom-right plot.

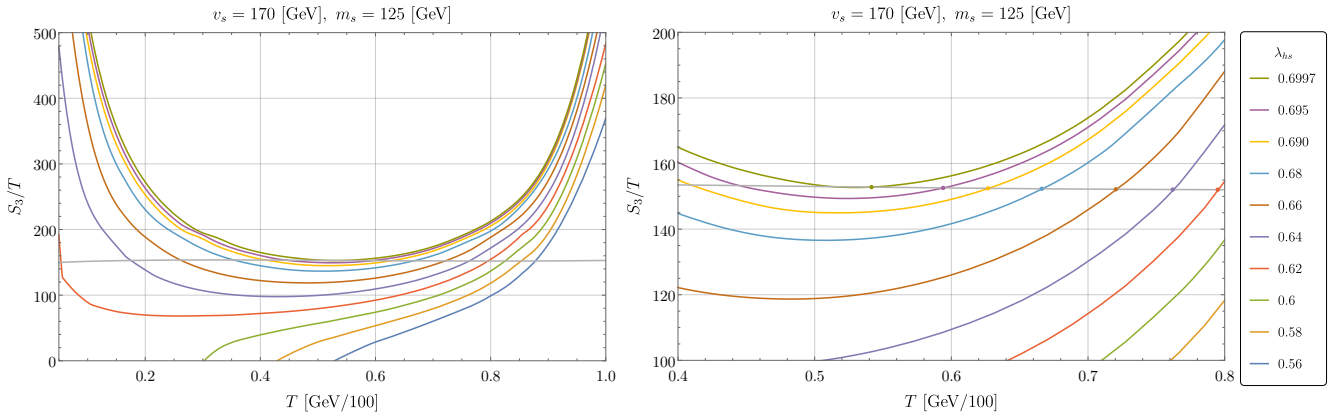

Figure 5.3: **Left**: S_3/T function with $v_s = 170$ GeV and $m_s = 125$ GeV. We observe that the nucleation temperature saturates around $T_{\rm nuc} \approx 52$ GeV. The horizontal gray line satisfy the nucleation condition $S_3/T_{\rm nuc} = \frac{3}{2}\log\left(S_3/2\pi T_{\rm nuc}\right) + 4\log\left(T_{\rm nuc}/H\right)$. **Right**: Zooming in on the region with lower nucleation temperatures.

phase transition region (where system remains stuck in the false vacuum) but obviously the boundary of "NO PT" is always to the right of $T^{\rm NB} = 0$ curve. The size of the narrow strip between the two boundaries "NO PT" and $T^{\rm NB} = 0$ is of the order 10^{-4} in λ_{hs} values. One can see it from the $T_{\rm nuc}$ panel of Fig.5.2 where we have indicated the value of λ_{hs} when $T_{\rm NB} = 0$ by vertical thin line and red dot (for intersection) and the position of the blue dot which is the last point where the transition is of the first order before we enter NO PT region. The boundaries of this region were obtained by numerical calculations where we have scanned λ_{hs} parameter with a step 10^{-6}. We postpone the discussion of the FOPT in this narrow region to the next section 5.3.2.

In this section we restrict our discussion only to the region to the left of $T^{\rm NB} = 0$ curve. Then the phase transition will be always completed before the universe cools down to $T^{\rm NB}$, *i.e.* $T^{\rm NB} < T_{\rm nuc}$, which provides a lower bound for the nucleation temperature. At the same time the velocity of the bubbles become largest for the smallest possible values of the nucleation temperature. So that the fastest bubbles will be near the $T^{\rm NB} = 0$ curve. Looking at Fig.5.2 we can see that the largest γ_w (Lorentz boost factor) and lowest nucleation temperatures happen for $v_s \gtrsim 200$ GeV, where the $T^{\rm NB} = 0$ curve passes very close to the NO PT boundary. The shape of the lines in Fig.5.2 clearly indicates the necessity of tuning in order to obtain low nucleation temperatures (large γ_w). In particular for the values of $v_s \gtrsim 200$ GeV we can see that the nucleation temperature drops by choosing λ_{hs} close to the NB value (similarly γ_w becomes maximal see Fig.5.2). We can estimate this tuning by looking at $\partial \log \lambda_{hs}/\partial \log T_{\rm nuc}$ quantity (analogue of Giudice-Barbieri [388] measure of the tuning) as a function of $T_{\rm nuc}$. This result agrees with our expectation from the steepness of the curves in the Fig.5.4 and with the naive tuning expectation which scales as $\sim \left(T_{\rm nuc}/m_h\right)^2$[5].

At last we would like to remind that the discussion in this section always assumed that the phase transition completes before the potential barrier disappears. We have checked numerically that this is always the case. Indeed the time of the phase transition is given approximately by the bubble radius at the moment of percolation [33, 389]

$$R_\star \simeq \left(\int_{T_{\rm per}}^{T_{\rm crit}} \frac{dT}{T} \frac{\Gamma(T)}{H(T)} \left(\frac{T_{\rm per}}{T}\right)^3 \right)^{-1/3} . \tag{5.18}$$

[5]This expression follows Eq.(5.14) if we require the cancellation between the terms independent of temperature.

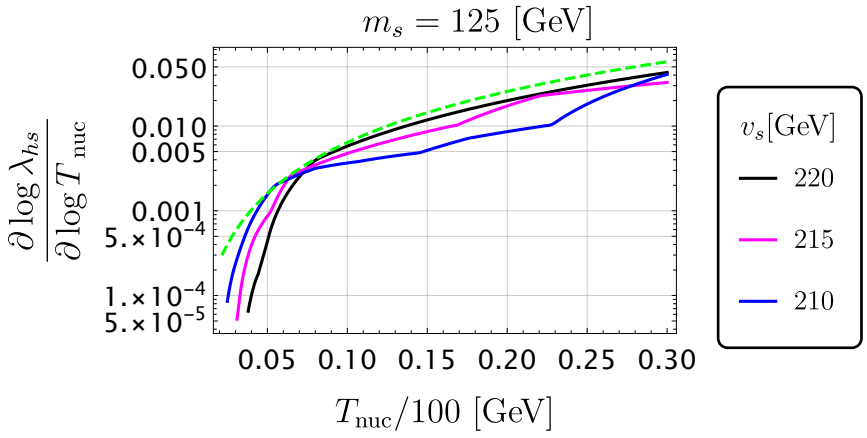

Figure 5.4: Tuning of the coupling λ_{hs} as a function of the nucleation temperature. The dashed green line represents the naive tuning $\sim (T_{\rm nuc}/m_h)^2$. We observe that this naive estimation for the tuning is rather precise at large nucleation temperature but can underestimate the tuning by one order of magnitude for very low nucleation temperature.

This radius is related to the $\beta \equiv -\frac{d}{dt}\frac{S_3}{T} = HT\frac{d}{dT}\frac{S_3}{T}$ parameter by an approximate relation [389]

$$\left.\frac{\beta}{H}\right|_{T_{\rm per}} \simeq \frac{(8\pi)^{1/3}}{R_\star H} \ , \tag{5.19}$$

where we find $R_\star^{-1} \sim \beta_{\rm typical} \sim (10 - 10^4)H$. At this point the temperature drop during the bubble expansion will scale as

$$\Delta T \sim T_{\rm nuc}(H\Delta t) \sim \frac{T_{\rm nuc}H}{\beta} \ . \tag{5.20}$$

Due to the large value of β/H we find numerically that this drop of the temperature is not enough for the barrier to disappear or in other words

$$T_{\rm nuc} - \Delta T > T^{\rm NB} \ . \tag{5.21}$$

Such behaviour can be understood from the following consideration: near $T_{\rm NB}$ the bounce action drops very quickly and as a consequence the tunneling becomes very efficient and typical bubble radiuses are much smaller than the Hubble scale. This would lead to another prediction: the GW signal will be suppressed as well since it is controlled by the (β/H) quantity Eq.(5.19). However, As we will see, even with this suppression the GW signal is efficient enough to be detected in the future.

5.3.2 Tunneling with potential barrier at zero temperature

Let us proceed to the analysis of the case when the potential barrier does not disappear at zero temperature. The parameter space with the lowest nucleation temperatures (fastest bubbles) will be located again near the "NO PT" boundary. However in this case the nucleation temperature will be controlled by the local minima of the S_3/T function, see Fig.5.3. At least a minimum is expected since the potential at low temperature becomes fully temperature independent and $S_3(T \to 0) \to$ const., so that S_3/T necessarily starts to grow for $T \to 0$.

Numerically (see Fig.5.2) for the value of $m_s = 125$ GeV we find that for $v_s \lesssim 180$ GeV, the entire region with the fast bubbles has a potential barrier at zero temperature. On Fig.5.3, we present the euclidean action for $v_s = 170$ GeV and $m_s = 125$ GeV. Going back to Fig.5.2, we see that for those values the "NO PT" curve and the "$T_{\rm NB} = 0$" curve are largely separated. This is not a surprise since in this region of parameter space the bounce action $S_3/T \sim \mathcal{O}(10^2)$ is small enough to guarantee the successful tunneling even when the barrier remains at zero temperature. In the range of λ_{hs} from 0.5 to 0.7, numerically we find that nucleation temperatures are $\gtrsim 30$ GeV, and the corresponding maximal Lorentz factors for the velocities of the bubble expansion in the ranges of $\lesssim 30$, see Table 5.1. Interestingly we find that in this case the bubble radius $R_\star \sim \frac{(8\pi)^{1/3} v_w}{\beta}$ are a little bit larger than the ones discussed in the section 5.3.1, corresponding to a bit smaller values of β/H parameter.

Moreover, on Fig.5.5, we display the transition regime between transitions controlled by the global minimum which is typical of cases with zero temperature barrier, but which still displays a disappearance of the barrier: see the blue curve of Fig.5.5.

Finally, we could also wonder what happens at the *upper* boundary of the deep supercooling region, as we have observed on Fig.5.2 a sharp decrease in the supercooling allowed around $v_s \lesssim 200$ GeV (for $m_s = 125$ GeV). This transition regime can be understood if we plot the explicit S_3/T functions on Fig.5.5. Comparing the plot in Fig.5.5 with the one in Fig.5.6, we see that as we decrease v_s, the full pattern of S_3/T is shifted toward smaller values. At some critical point around $v_s \approx 200$ GeV, the nucleation becomes controlled by the first minimum in the function S_3/T and not by the disappearance of the barrier. This largely suppresses the possibility for large supercooling.

Super fine-tuned region We finally comment on the parameter space with $v_s \gtrsim 200$ GeV (again we are fixing $m_s = 125$ GeV), where the curves "NO PT" and "$T_{\rm NB} = 0$" almost superimpose (the region between red and blue dots on the $T_{\rm nuc}$ panel of the Fig.5.2). There will be a very narrow strip between the curves "NO PT" and "$T_{\rm NB} = 0$" regions, where the tunnelling will happen even though the barrier remains at zero temperature. We find (see Fig.5.6) that the region corresponds to the variations of the λ_{hs} parameter of the order $\delta\lambda_{hs} \sim O(10^{-4})$, *i.e.* two order of magnitude smaller than the full region with relativistic bubbles. In this very small region various additional effects can start playing a role. For example let us look at the Fig.5.6 we can see that the bounce action S_3/T has a local maximum and a deeper (global) minimum with respect to the standard scenario. Such a behaviour of the action is coming from the cancellations of various terms in the effective potential. For simplicity let us look at $T = 0$ case. Then there is a region of parameter space where the potential has no local minimum at $(0, v_s)$, but the effects of the $\frac{-3M_t^4(h)}{8\pi^2} \log \frac{M_t(h)}{M_t(v_{EW})}$ terms in Coleman-Weinberg contribution lead to the appearance of the local minimum at $(\delta v_h, v_s)$. On Fig.5.7 we plot the contributions of the various terms in the effective potential leading to the appearance of this local minimum and the trajectory of the typical bounce solution in this case. As a result the distance in the fields space between the two minima decreases and the tunneling becomes faster, which leads to the appearance of the second (global) minimum in S_3/T. This induces the possibility of very long supercooling.

Benchmark points

In Table 5.1 and 5.2, we give typical values of the nucleation temperature, the Lorentz factor γ_w, the β/H factor for the three benchmarks values that we discussed $v_s = 170, m_s = 125$, $v_s = 205, m_s = 125$, and we indicate if the barrier remains at zero temperature, applying the criterion in Eq.(5.21). We can see that the largest bubble radius at the collision (smallest β) correspond to the case when S_3/T is monotonic and very flat near the tunneling temperature (c.f. the right panel of Fig. 5.6).

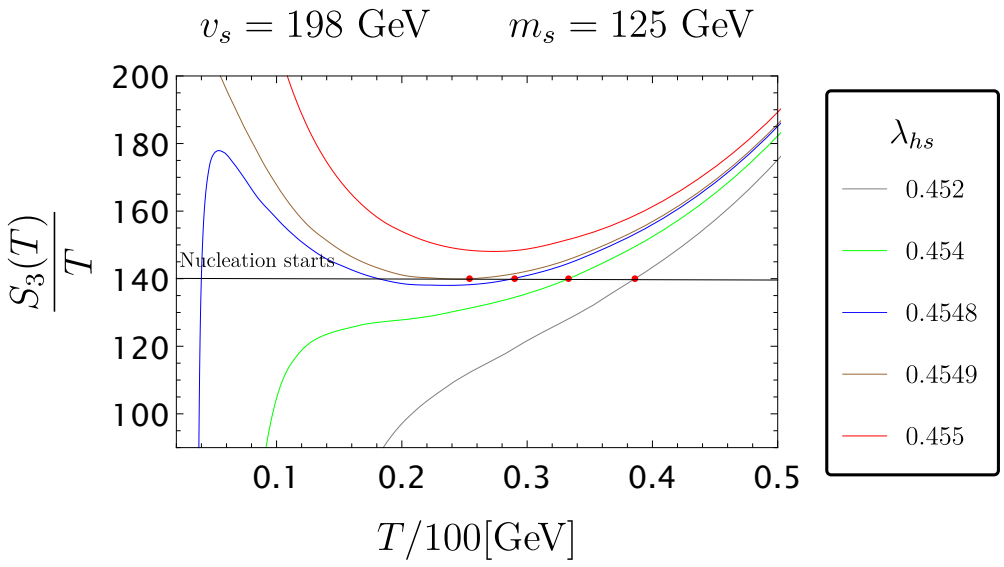

Figure 5.5: On this plot we show the regime of transition. We observe that several points display a disappearance of the barrier which is typical of the regime of no barrier at $T = 0$. However, the nucleation temperature is controlled by the first minimum of S_3/T, which is typical of the regime with a barrier at $T = 0$.

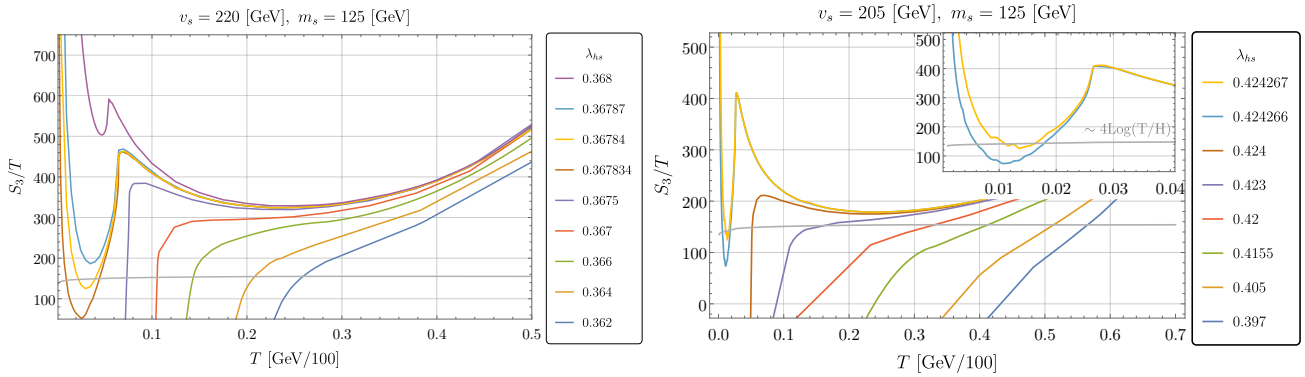

Figure 5.6: **Left**: Plot of $S_3(T)/T$ as a function of the temperature, for different values of λ_{hs} in the case where $m_s = 125$ GeV and $v_s = 220$ GeV. As we increase the value of the coupling λ_{hs}, the disappearance of the potential barrier happens later, allowing for longer supercooling, until it is large enough to remain even at zero temperature. For the first four curves from the top, we observe a second drop in the function at very low temperature. This second drop corresponds to the displacement on the false minimum that we describe in this section. **Right**: Same plot as in the left panel, but with a lower value for v_s. The pattern we found is the same, but lowering v_s causes a lowering of the curves and the displacement of the false minimum is less pronounced.

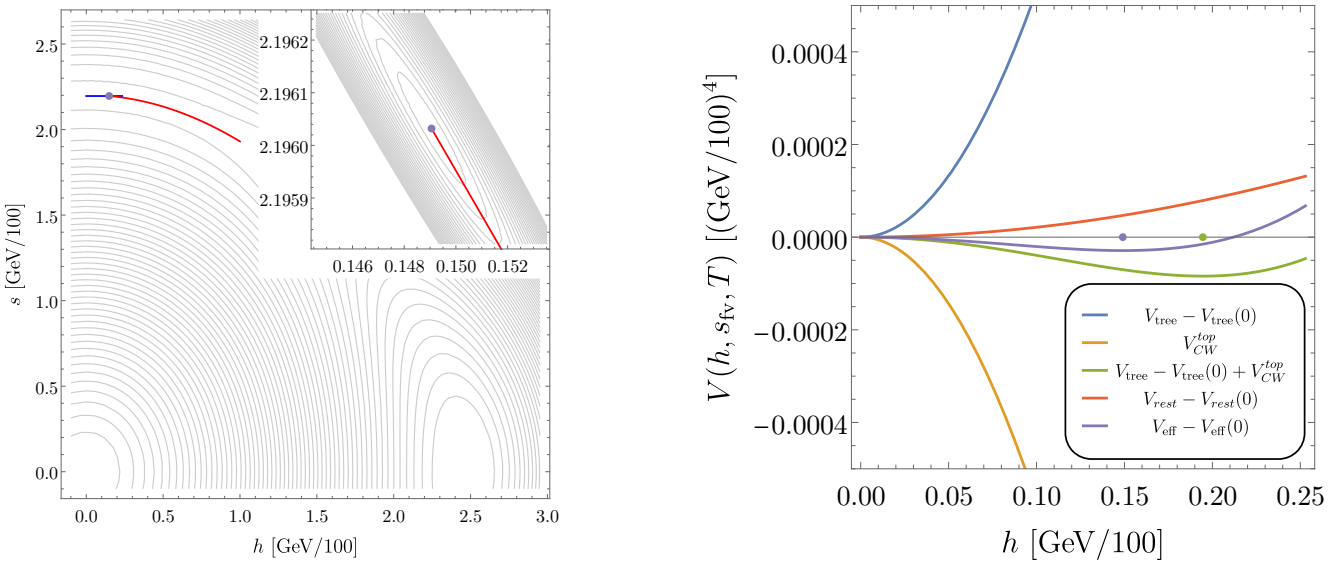

Figure 5.7: Here is presented an explicit example of displacement of the false vacuum for $\{\lambda_{hs}, v_s, T\} = \{0.36784, 220\ \text{GeV}, 3\ \text{GeV}\}$. **Left**: we show the 2D potential where the blue line corresponds to the part of the potential plotted in the right panel and the (purple) dot is the position of the displaced false minimum, in both the plots. Red line indicates the bounce trajectory. **Right**: plot of the different contributions to the potential. We see that a displaced minimum can be generated balancing the tree level and the CW potential of the top quark, for low enough temperature, in such a way all the other particles, that are massless in the false vacuum, have a negligible contribution. It can be shown that they cause, as the temperature increases, the shift of the local minimum towards $h = 0$.

$m_s = 125$ GeV, $v_s = 170$ GeV							
λ_{hs}	$\frac{T_{\rm reh}}{100\text{GeV}}$	$\frac{T_{\rm nuc}}{100\text{GeV}}$	$\frac{T_{\rm per}}{100\text{GeV}}$	γ_w	$\frac{\tilde{\beta}}{H} = \frac{(8\pi)^{1/3}}{R_\star H}$	$m_H^{\rm False}$/GeV	FM_0
0.56	0.880	0.877	0.850	–	434	35.4	No
0.58	0.855	0.851	0.822	–	355	37.3	No
0.6	0.829	0.824	0.790	–	296	39.2	No
0.62	0.800	0.795	0.762	1.2	209	40.1	No
0.64	0.769	0.762	0.714	2.4	158	42.5	No
0.66	0.729	0.720	0.661	4	108	43.4	No
0.68	0.678	0.666	0.582	6.6	51	44.8	No
0.69	0.642	0.627	0.506	8.8	18	45.0	No
0.695	0.612	0.594	0.412	11	5	44.7	No
0.6997	0.566	0.542	0.237	15	1.4	43.8	No

Table 5.1: We report for Fig.5.3, $m_s = 125$ GeV and $v_s = 170$ GeV, reheating, nucleation and percolation temperatures, respectively, for different values of λ_{hs} and γ_w reached by the expanding walls as well as the parameter $\tilde{\beta}/H$ computed using Eq.(5.19). We also show the effective Higgs mass in the false vacuum at the nucleation temperature defined as $(m_H^{\rm False})^2 = \frac{\partial^2 V}{\partial h^2}\big|_{T=T_{\rm nuc}}$, relevant for DM production explained in section 5.4.2. In the last column, FM_0 concerns the displacement of the false minimum. No if it is at the (Higgs) origin, yes if it moved. In this case, the minimum is always at the origin.

$m_s = 125$ GeV, $v_s = 205$ GeV							
λ_{hs}	$\frac{T_{\rm reh}}{100\rm GeV}$	$\frac{T_{\rm nuc}}{100\rm GeV}$	$\frac{T_{\rm per}}{100\rm GeV}$	γ_w	$\frac{\tilde{\beta}}{H} = \frac{(8\pi)^{1/3}}{R_\star H}$	$m_H^{\rm False}$/GeV	$\rm FM_0$
0.397	0.577	0.564	0.544	4	371	19.1	No
0.405	0.530	0.512	0.488	8	268	19.1	No
0.4155	0.448	0.412	0.379	18	130	17.7	No
0.42	0.393	0.330	0.290	37	72	15.2	No
0.423	0.339	0.161	0.124	270	66	7.1	No
0.4234	0.335	0.107	0.095	805	109	3.9	No
0.424	0.335	0.051	0.051	$5.7 \cdot 10^3$	$3.3 \cdot 10^3$	0.7	No
0.4242	0.335	0.0337	0.0337	$1.8 \cdot 10^4$	$3.2 \cdot 10^4$	0.25	No
0.42424	0.335	0.028	0.0279	$3.0 \cdot 10^4$	$1.8 \cdot 10^3$	4.4	No
0.424266	0.335	0.018	0.017	$1.0 \cdot 10^5$	99	6.2	Yes
0.424267	0.335	0.016	0.014	$1.3 \cdot 10^5$	44	6.3	Yes

Table 5.2: Same as Table 5.1, but for Fig.5.6 and with $v_s = 205$ GeV. We observe that the last two points display a displacement of the false minimum.

$m_s = 150$ GeV, $v_s = 175$ GeV							
λ_{hs}	$\frac{T_{\rm reh}}{100\rm GeV}$	$\frac{T_{\rm nuc}}{100\rm GeV}$	$\frac{T_{\rm per}}{100\rm GeV}$	γ_w	$\frac{\tilde{\beta}}{H} = \frac{(8\pi)^{1/3}}{R_\star H}$	$m_H^{\rm False}$/GeV	$\rm FM_0$
0.53	0.616	0.608	0.592	–	580	17.4	No
0.54	0.581	0.570	0.552	3	420	17.8	No
0.56	0.492	0.470	0.444	9	228	17.7	No
0.58	0.329	0.141	0.130	348	160	4.7	No
0.582	0.327	0.051	0.0508	$5.3 \cdot 10^3$	$9.5 \cdot 10^3$	0.4	No
0.582262	0.327	0.025	0.0236	$3.7 \cdot 10^4$	194	8.2	Yes
0.582264	0.327	0.024	0.0219	$4.3 \cdot 10^4$	130	8.3	Yes
0.582266	0.327	0.021	0.017	$5.7 \cdot 10^4$	24	8.5	Yes

Table 5.3: Same as Tables. 5.1 and 5.2, but with $m_s = 150$ GeV and $v_s = 175$ GeV.

5.3.3 $m_s = 150$ GeV

Previously, we studied specifically the case where the parameter $m_s = 125$ GeV and we observed that for this value, the region of deep supercooling displayed small masses of the singlet in the real vacuum, being on the verge of detection due to exotic Higgs decays: $h \to ss$ at $M_s \lesssim 62$ GeV. We also concluded in section 5.3 that this region was closing around $M_s \approx 75$ GeV. We could wonder if this conclusion would change if we modify the value of the parameter m_s, and if so in which direction. On Fig.5.8 we show similar plots than in Fig.5.2 and 5.4 for the case of $m_s = 150$ GeV. Thus, increase the value of m_s pushes the deep supercooling region to $M_s \approx 90$ GeV, at the price of increasing the portal coupling λ_{hs}. However, we can observe on the last plot of Fig.5.8 that the typical tuning remains roughly the same and that we can still trust our naive $(T_{\rm nuc}/m_h)^2$ for an order-of-magnitude estimate of the tuning.

On the other hand, we also observed that decreasing the parameter m_s to ≈ 100 GeV was pushing all the deep supercooling region inside $M_s \lesssim 62$ GeV, which is thus strongly disfavored by colliders. *We hope that this trend can be extrapolated to larger values of m_s, until we hit perturbativity bounds for λ_{hs}.*

Finally, in Table 5.3, we provide the value of the velocity, reheating and nucleation temperature for $m_s = 150$ GeV and $v_s = 175$ GeV that will be used in Fig.5.10.

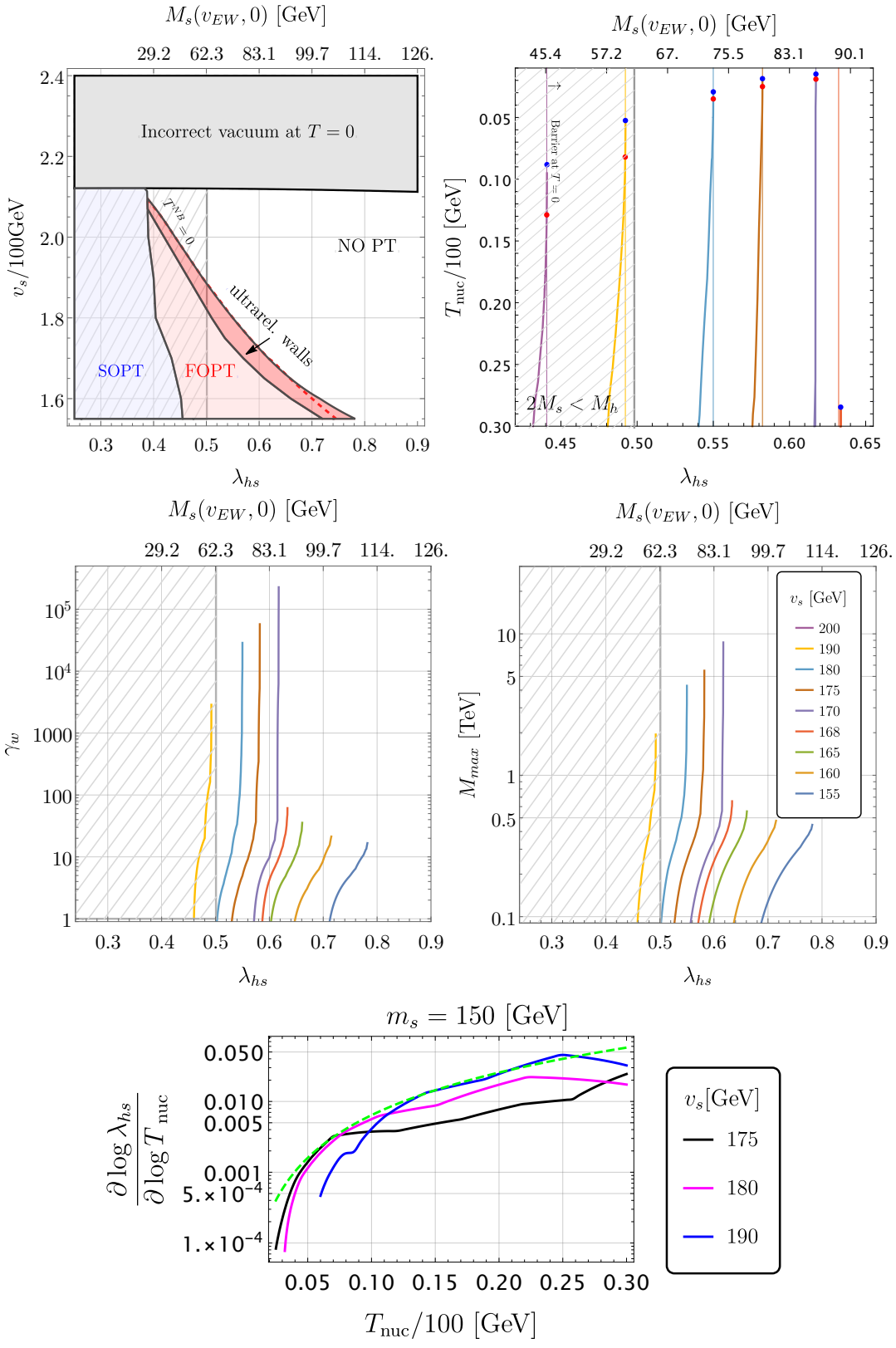

Figure 5.8: Similar plots than in Fig.5.2 and Fig.5.4 for the value of $m_s = 150$ GeV.

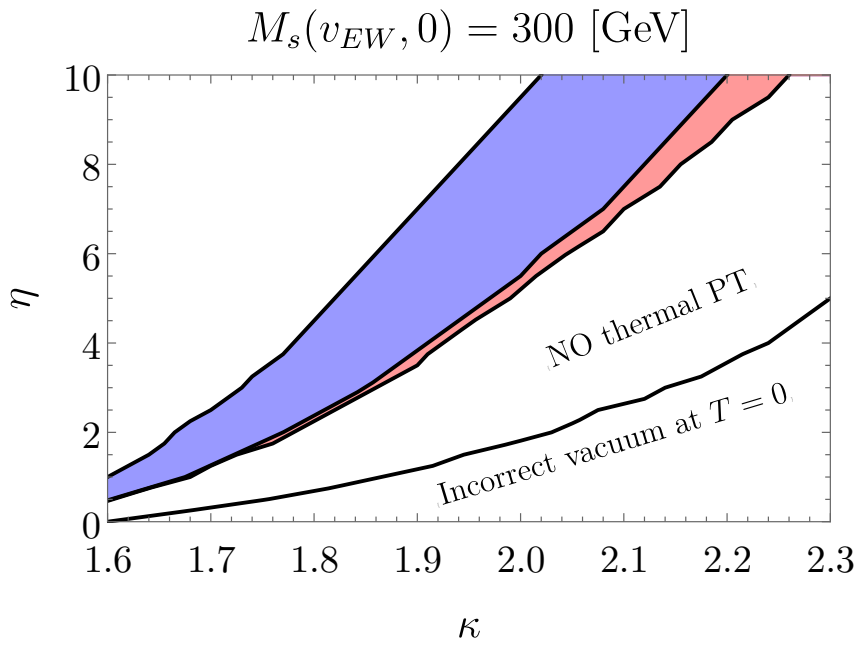

Figure 5.9: Here is presented the same results found in Fig. 6 of Ref. [372]. It has to be noted that these results are obtained with only the thermal potential and without Daisy resummation, *i.e.* without thermal masses. The relation with our parameters is $(\lambda_s,\ \lambda_{hs}) = (\eta, 2\kappa)$ and $M_s(v_{EW}, 0) = 300$ GeV.

5.3.4 Matching with former results

We would also like to compare our result with previous studies. Though we focused mostly on a more weakly coupled part of the parameter space, we would like to compare our findings with the ones in the Ref.[372] and argue that we observed only small changes, due to the inclusion of loop-corrections and Daisy resummation. On Fig.5.9 we make a reproduction of the scan of the Fig.6 of [372] using our potential and emphasize the close similarities. The relations between the parameters κ, η and the couplings in the Eq.(5.1) is as follows

$$\kappa_{[372]} = \frac{\lambda_{hs}}{2}, \quad \eta_{[372]} = \lambda_s. \tag{5.22}$$

5.3.5 Z_2-Domain wall collapse

Our main discussion was focused on the two step phase transition $(0,0) \to (0, v_s) \to (v_{EW}, 0)$ where the first phase transition is Z_2 breaking. Obviously during such a phase transition domain walls will be formed which can drastically modify the cosmology of the system. We can avoid the stable domain walls if we assume some small Z_2 breaking, however in this case the question rises about the timescale for the stability of the domain walls. This is particularly important since recently it was shown [390] that for singlet extension of the SM the domain walls (if still present) will become seeds for the secondary phase transition $(0, v_s) \to (v_{EW}, 0)$ and will dominate the probability of tunneling of the phase transition. We will follow closely the discussion in the section 5.2.2 using only the tree level potential and the thermal corrections to the masses. Then the Z_2 breaking phase transition will occur

at the temperatures

$$T_{Z_2} \simeq v_s \left(\frac{12}{3 + 4\lambda_{hs} \frac{v_s^2}{m_s^2}} \right)^{1/2} \simeq 200 - 300 \ \text{GeV}, \tag{5.23}$$

which is the temperature of the domain wall formation. The domain wall mediated transition will happen at the temperature T_w which is found to be order one different from T_{Z_2}. The exact mechanism of the transition depends on the values of the couplings and can proceed either with the classical rolling or 2D bounces localized on the domain wall. The temperature when the classical rolling can start is reported in Ref.[390] and is equal to

$$T_w^{\text{rolling}} \simeq T_{Z_2} \left[\frac{4m_h^2 + m_s^2 \left(1 - \sqrt{1 + \frac{8v_s^2 \lambda_{hs}}{m_s^2}} \right)}{8\Pi_h(T_{Z_2}) + m_s^2 \left(1 - \sqrt{1 + \frac{8v_s^2 \lambda_{hs}}{m_s^2}} \right)} \right]^{1/2} . \tag{5.24}$$

The nucleation temperature (T_w^{2D}) of $2D$ bounces should be found numerically (Ref.[390]) however it will be obviously smaller than T_{crit} (of $(0, v_s) \to (v_{EW}, 0)$ phase transition). At this point we can safely ignore the seeded phase transition effects if all of the domain walls annihilate in the interval of temperatures

$$[T_w, T_{Z_2}], \quad T_w < T_{\text{crit}}, \tag{5.25}$$

where T_* is the temperature when the seeded phase transition will be completed and it is obviously less than T_{crit} of EW phase transition. Let us estimate how strong should be the bias ΔV between the potential energies of the two minima of Z_2 potential so that all of the walls can disappear. For these estimates it is sufficient to assume that there is order one difference between T_w and T_{Z_2}, which is generically the case. We define a little bias between the two Z_2 related minima along the s direction: ϵ. The critical radius (above which) areas with true vacuum will start to expand is roughly

$$R_c \sim \frac{\sigma_{DW}}{\epsilon}, \tag{5.26}$$

where σ is surface energy density of the domain wall, not to be confused with the tension of the bubble wall that we already discussed. So the domain walls will exist on the time scale of

$$\Delta t_w \sim \frac{R_c}{u} \sim \frac{\sigma_{DW}}{u\epsilon}, \tag{5.27}$$

where u is velocity of the domain wall motion. The change of the temperature before the domain wall annihilation will be roughly

$$\Delta T \sim TH\Delta t_w. \tag{5.28}$$

So that if $\Delta t_w H \ll 1 \Rightarrow \Delta T \ll T$ the wall annihilation happens almost instantaneously. Assuming $\sigma_{DW} \sim T_{\text{crit}}^3$ and $H \sim \frac{T_{\text{crit}}^2}{M_p}$ we get

$$\frac{\epsilon}{T_{\text{crit}}^4} \gg \frac{T_{\text{crit}}}{uM_{\text{pl}}}. \tag{5.29}$$

Balancing the pressure against the friction forces $\epsilon \sim uT_{\text{crit}}^4$ we can estimate the velocity and then the condition for the quick wall annihilation becomes

$$\frac{\epsilon}{T_{\text{crit}}^4} \gg \sqrt{\frac{T_{\text{crit}}}{M_{\text{pl}}}} \sim 10^{-8}, \tag{5.30}$$

which is not restrictive at all.

5.4 Revisiting the production of DM and Baryogenesis

One of the motivation for the study of a model of EWPT with relativistic bubbles is the relation between relativistic expansion and the out-of-equilibrium production of heavy states presented in the previous chapters, when the field undergoing the PT (here the Higgs) is coupled to some heavy dark sector at typical mass M_N. In this section, we remind the principle of the production mechanism and we study the scenario of the production of Dark Matter[2] and Baryogenesis[3], that were previously agnostic about the EWPT realisation.

First of all, the strong FOPT involves a supercooling represented by a dilution factor,

$$D \equiv \frac{g_{\star s}^{\rm sym}(T_{\rm nuc})}{g_{\star s}(T_{\rm reh})} \left(\frac{T_{\rm nuc}}{T_{\rm reh}}\right)^3, \tag{5.31}$$

with $g_{\star s}(T)$ ($g_{\star s}^{\rm sym}(T)$) being the number of relativistic degrees of freedom of the entropy in the broken (symmetric) phase. This means that with $D \ll 1$, any type of dark matter production or Baryogenesis mechanism that happens much earlier than the PT should provide values denser than the conventional estimation by a factor of $1/D$ (see for example [165, 174]). For instance, the WIMP cross section should be $\sigma \sim \frac{D}{10^{-3}} 10^{-29} {\rm cm}^3/{\rm s}$ to produce a correct dark matter abundance. This is the case when freeze-out happens at temperatures much higher than the reheating.

5.4.1 Production of heavy states during ultra-relativistic expansion

The results in Sec. (2.150) on the terminal velocity in the SM allow us to compute the maximal mass of the particles which can be produced during the electroweak FOPT in the singlet extension. Indeed saturating the step function in the above equation and assuming the $L_w \sim 1/v_{EW}$ we get approximately:

$$M^{MAX} \approx \frac{400 \text{ GeV}}{\log^{1/2} \frac{M_Z}{g T_{\rm nuc}}} \left(\frac{\Delta V - \Delta P_{\rm LO}}{(100 \text{ GeV})^4}\right)^{1/2} \left(\frac{100 {\rm GeV}}{T_{\rm nuc}}\right). \tag{5.32}$$

Numerical results for the maximal mass $M^{\rm MAX}$ are reported in Fig.5.2. We can see that the maximal mass we can produce is roughly ~ 10 TeV scale.

We would like to note that our results can be easily applied for the mass gain mechanism of the heavy state production [303], where a particle which is massless outside of the bubble, acquires a mass $M \sim y v_{EW}$. Indeed in this case the maximal mass will be $M_{\text{mass gain}} \simeq \gamma_w T$ (This is the condition for the particle to enter the bubble), and can be read off from the bottom right plot of the Fig.5.2 by noting that it will scale as $M_{\text{mass gain}} \sim M_{\rm MAX}^2/v_{EW}$. Since the mass of the heavy field comes from the vev of the Higgs, it will additionally be bounded by the unitarity considerations, $y \lesssim \sqrt{4\pi}$ to be below $\lesssim 2$ TeV.

5.4.2 Dark Matter production

In this section we will apply the results for the velocity of the bubble expansion for DM model building and to the several models that we already presented in Chapter 3: we will start by presented the vanilla model of 3, then we will propose a new case specific to the singlet model, where it is the singlet itself which is coupled to DM and produces it, finally, we will also discuss the case of fermionic DM, like presented in section 3.6.

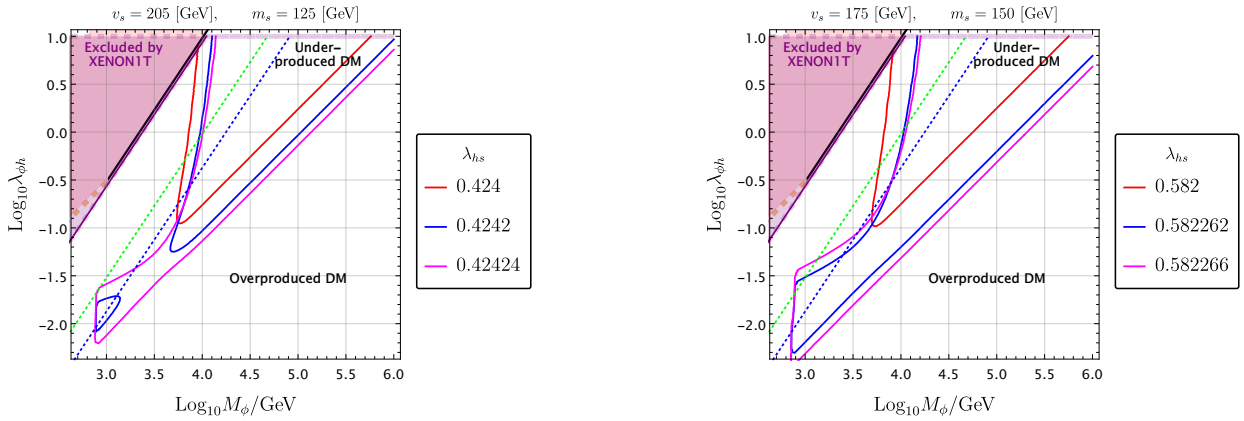

Figure 5.10: **Left**: DM abundance in the parameter space $\lambda_{\phi h} - M_\phi$ for different values of λ_{hs} by fixing $v_s = 205$ GeV and $m_s = 125$ GeV (that fixes the values of $T_{\rm nuc}, T_{\rm reh}$ and $\gamma_w^{\rm terminal}$). The solid lines represent correct DM abundance, while underproduced inside and overproduced outside. The lower part of each contour is dominated by freeze-out and the upper part via bubble expansion. The connecting vertical line (independent of the portal) comes from thermal production after the reheating of the transition. The magenta shaded region is excluded by XENON1T while the dotted green and blue lines are projected limits from XENONnT and DARWIN respectively. **Right**: same plot for $v_s = 175$ GeV and $m_s = 150$ GeV. As expected, increasing the tuning from red to magenta increases the amplitude of the curve. The values used are extracted from Table 5.3.

Scalar DM coupled via the Higgs portal

In this first section, we present the DM abundance produced in the vanilla model with DM-Higgs portal presented in Chapter 3 Eq.(3.14). In this context, the $C_{\rm eff}$ discussed in section 3.3.4 is always one, as we have checked. Instead of making a scan of the parameter space, we will just focus on a few representative benchmark points.

For $m_s = 125, v_s = 205$ GeV, we show in Fig.5.10 the isocontours reproducing the correct relic density for three reference values of λ_{hs} (corresponding nucleation temperatures can be found in the Table 5.1). Firstly, $C_{\rm eff} \simeq 1$ for all three reference points. For $\lambda_{hs} = 0.424$ the upper red curve corresponds to the case when DM production is dominated by the BE (bubble expansion) and the lower curve by FO. The steepness of the upper red curve (BE) comes from the fact that we are in the region of parameter space where $\exp\left[-M_\phi^2/(2\gamma_w v_{EW} T_{\rm nuc})\right] \ll 1$, leading to a very strong sensitivity on M_ϕ mass. Physically this means that the model generically predicts large overproduction of DM in BE process unless the Boltzmann suppression $\exp\left[-M_\phi^2/(2\gamma_w v_{EW} T_{\rm nuc})\right]$ is playing a role. For the other two reference points $\lambda_{hs} = 0.4242, 0.42424$ we can see that there is an additional part of parameter space for the DM masses $M_\phi \sim 1 - 4$ TeV, which corresponds to the region without the Boltzmann suppression $\exp\left[-M_\phi^2/(2\gamma_w v_{EW} T_{\rm nuc})\right] \sim 1$. This is related to larger values of $M^{\rm MAX} \sim \sqrt{\gamma_w v_{EW} T_{\rm nuc}}$ and smaller values of the nucleation temperature, reducing the excess of the DM abundance. On the right panel of Fig.5.10, we report similar plots for $v_s = 175, m_s = 150$ GeV.

Singlet portal DM

In this section we mention an alternative possibility of coupling the DM (ϕ) to the singlet field s via "singlet portal"

$$\Delta\mathcal{L} \supset \frac{\lambda_{s\phi}}{2}\phi^2 s^2 + \frac{1}{2}M_\phi^2\phi^2 \ , \quad P(s \to \phi^2) \approx \left(\frac{\lambda_{s\phi} v_s}{M_\phi}\right)^2 \frac{1}{24\pi^2}\Theta(\gamma_w T_{\rm nuc} - M_\phi^2 L_w^s) \ , \tag{5.33}$$

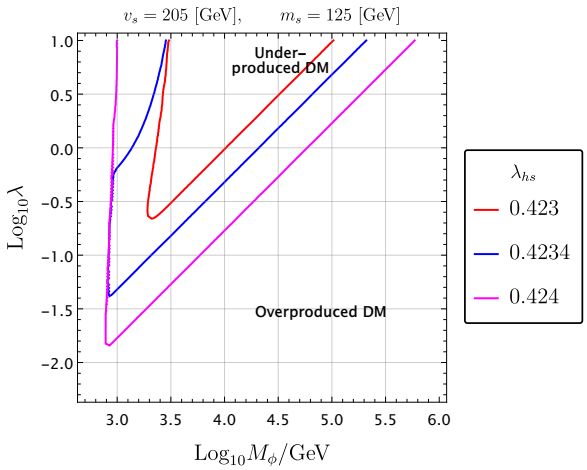

Figure 5.11: DM production for the singlet portal model. In this context, the Boltzmann suppression $\sim e^{-m_s/T_{\rm nuc}}$ plays a strong role and allows for bubble expansion produced DM with much higher nucleation temperature $T_{\rm nuc} \sim 15$ GeV.

where the width of the singlet wall is similar to the length of the Higgs wall L_w. Interestingly even though FOPT is from $(0, v_s) \to (v_{EW}, 0)$, the singlet scattering of the wall can lead to the production of the ϕ field. Phenomenology of DM production is very similar to the Higgs portal case discussed in the previous section, with one main difference: in the false vacuum, the mass of the singlet is not small and the factor $C_{\rm eff}$ introduced in the Eq.(3.39) plays an important role. The results are shown in Fig.5.11. For example, if we compare the curves for $\lambda_{hs} = 0.424, m_s = 125, v_s = 205$ in Fig.5.11 and in Fig.5.10, we can see that, for the Higgs portal DM, the isocontour has the same shape, but with the larger values of DM M_ϕ masses. As shown in Eq.(3.33), this is due to the proportionality between the DM relic abundance produced during the bubble expansion with $\propto C_{\rm eff}/M_\phi$.

Singlet portal with additional field A slight modification of this scenario is to further introduce a light scalar $\tilde{s}$. Then we can have,

$$\mathcal{L} = \mathcal{L}_{SM} - \tilde{\lambda}\tilde{s}s\phi^2 - \frac{M_\phi^2}{2}\phi^2, \tag{5.34}$$

where again ϕ is the DM. We assume that $\tilde{s}$ is in the thermal bath before the PT. Then due to the field change of s in the bubble wall, the momentum conservation violating process $\tilde{s} \to \phi\phi$ can occur ($h \to \phi\phi$ may also occur if there is the $h^2\phi^2$ term.) In this model $s \to \tilde{s} + SM$ particles happen via the DM loop.

Fermion-mediated Dark Matter

In this subsection, we take back the model presented in section 3.6 and study it in the context of the singlet extension. We already argued that it seems very difficult to reproduce the observed DM abundance if we are not in the co-annihilation regime, because otherwise the DM would be largely overproduced, so we will not consider this case any more.

However, in the co-annihilation regime, where the interaction rate is boosted, we find that it becomes possible to reproduce the observed DM abundance. Results are displayed on the Fig. 5.12 for $v_s = 205, m_s = 125$ GeV and

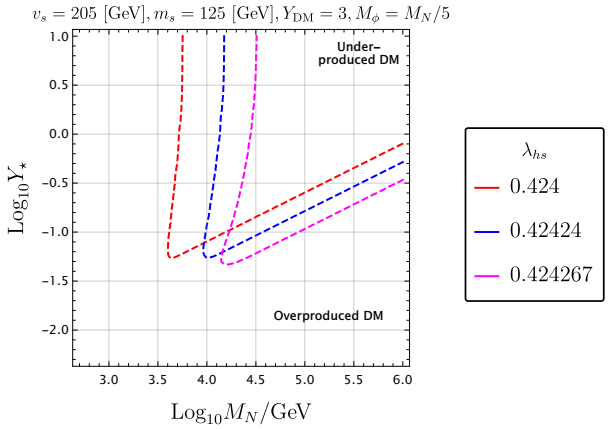

Figure 5.12: DM production in the fermionic portal model. We fix $M_{\rm DM} = M_N/5$, and $Y_{\rm DM} = 3$. Only the co-annihilation regime where $|M_\phi - M_\chi| \lesssim M_\phi/20$ appears to be viable and shown by dashed lines.

$M_{\rm DM} = M_N/5$, and $Y_{\rm DM} = 3$. However, even in this case, we see that bubble expansion tends to overproduce the DM and the relic abundance in BE can be reproduced if only the factor $\exp[-M_N^2/(2v_{EW}T_{\rm nuc}\gamma_w)]$ starts playing a role in suppressing DM relic density (left boundary of Fig.5.12 is almost vertical).

singlet DM ?

Finally, before closing this section, we comment about the possibility of considering the singlet s itself, in the limit of very precise Z_2, as DM. After the phase transition $T \sim 40$ GeV, the singlet is in thermal equilibrium and we can apply straightforwardly the freeze-out expression:

$$\Omega^{\rm today}_{s,\,\rm FO} h^2 \approx 0.1 \left(\frac{0.06}{\lambda_{hs}}\right)^2 \left(\frac{M_s(v_{EW},0)}{100\ \text{GeV}}\right)^2 . \tag{5.35}$$

From this estimate of the FO abundance for s and recalling that we considered $\lambda_{hs} \sim 0.3 - 0.6$ and $M_s(v_{EW},0) \sim 100$ GeV, we conclude that the abundance of s produced in this fashion, today, is underproduced by one or two orders of magnitude to fit the observed amount of DM $\Omega^{\rm today}_{s,\,\rm FO} h^2 \approx 0.1$. Even in this underproduced case, there are severe bounds from the direct detection experiments except for the resonant region, where (5.35) is over-estimated. However, as we will discuss in the Appendix. 5.3.5, we will have a Z_2 explicit breaking which makes s decay much before today.

5.4.3 Baryogenesis mechanism

In Chapter 4 we proposed a model of baryogenesis relying on EW relativistic bubbles. At the time, we kept the discussion generic and did not provide a model for the EW sector. In this Chapter, we studied such a model in detail and so we would like to revisit our former model. In Chapter 4 we argued that the absence of strong wash-out leads to the following conditions

$$M_{B,\chi,\eta} \gtrsim 30 T_{\rm reh} \sim 1\ \text{TeV} , \qquad \text{(suppressed wash-out)} \tag{5.36}$$

as well as experimental signatures (direct production in colliders, flavor violation, neutron oscillations) pushed the heavy particles to be

$$\boxed{M_{B,\chi,\eta} \gtrsim 2 \times 10^3 \text{ GeV}} \,. \tag{5.37}$$

In the context of singlet extension with Z_2 that we studied, this opens up the range

$$M_{B,\chi,\eta} \in [2, 10] \text{ TeV} \,, \tag{5.38}$$

where the Baryogenesis mechanism proposed is operative.

5.4.4 Impact of the heavy sector on the phase transition and the tuning

The models we are considering by construction have new heavy fields coupled to the Higgs boson. These will lead to the finite corrections to the scalar parameters of the form (assuming a Yukawa type connection $YBHb$)

$$\delta m_h^2 \sim \frac{-8 g_N M_N^2 Y^2}{64\pi^2}\Big(\log\frac{M_N^2}{v_{EW}^2} - \frac{3}{2}\Big), \qquad \delta\lambda \sim 4 g_N \frac{Y^4}{64\pi^2}\Big(\log\frac{M_N^2}{v_{EW}^2} - \frac{3}{2}\Big), \tag{5.39}$$

where g_N is the number of heavy degrees of freedom and M_N is the typical mass of the heavy sector. One can wonder how these corrections can effect the tuning of the Higgs potential. However note that in our model the Higgs mass hierarchy problem is not addressed and generically we expect the size of m_h^2 to be of the order of the cut off scale ($M_{\rm pl}$ in SM). So the corrections in Eq.(5.39) do not make the tuning worse.

In case the Higgs hierarchy problem is solved at the scale of the heavy fields in Eq.4.61 the tuning in the Higgs potential will be roughly,

$$\text{tuning} \sim \frac{m_h^2}{\Delta_{\text{Heavy physics}} m_h^2} \sim \frac{8\pi^2 m_h^2}{Y^2 M_N^2} \qquad \text{(Hierarchy problem solved)} \tag{5.40}$$

We can combine this estimate with a tuning for low nucleation temperatures (see discussion in section 5.3.1) which are necessary for the heavy field production and the tuning estimate becomes:

$$\text{tuning} \sim \frac{m_h^2}{\Delta_{\text{Heavy physics}} m_h^2}\frac{T_{\rm nuc}^2}{m_h^2} \sim \frac{T_{\rm nuc}^2}{\Delta_{\text{Heavy physics}} m_h^2} \sim \frac{8\pi^2 T_{\rm nuc}^2}{Y^2 M_N^2}. \qquad \text{(Hierarchy problem solved)} \tag{5.41}$$

Using the estimates of the maximal values of γ_w and the maximal mass of heavy particles which can be produced during the bubble-plasma collisions (see Eq.(2.152) and Eq.(3.59)) we get the following estimate for the maximal tuning in the model by taking back Eq.(5.32), saturating the bound and taking $Y \sim 1$

$$\text{tuning}^{MAX} \sim \left(\frac{T_{\rm nuc}}{20\text{GeV}}\right)^4, \tag{5.42}$$

where we remind the reader that this estimate is valid *only if the Higgs hierarchy problem is solved at the heavy fields scale*.

5.5 Gravitational waves emitted

It is well known that strong gravitational waves background will be emitted, with peak frequency around the mHz if the EWPT happens to be strongly first order. This is the optimal range of sensitivity of the forthcoming LISA detector [328, 54] and also GW detectors such as eLISA[329], LIGO[330, 331], BBO[332, 333], DECIGO[334, 335, 336], ET[337, 45, 338], AION[339], AEDGE[340].

As we have seen in sections 5.4.3-5.4.2, for the baryogenesis and DM production we need relativistic walls with relatively low nucleation temperature $\lesssim 10$ GeV. In this context, $\alpha \gg 1$ and $\kappa_{sw} \to 1$. The peak frequency and the signal amplitude are only function of the size of the bubbles at collision, which are reported in Table 5.2 and 5.3. We can observe that in this range β/H spans the value between $[50, 10^4]$, with a preference for lower values. Going back to section 1.6, emitted amplitude and frequencies will be of the order

$$\Omega^{\text{peak}}_{\text{plasma}} h^2 \in [5 \times 10^{-7}, 2 \times 10^{-9}], \qquad f_{\text{peak}} \in [10^{-4}, 0.03] \quad \text{Hz} \tag{5.43}$$

where we set $z_p = 10, g_\star = 100$. This range of frequencies and amplitude are largely in the expected sensitivity of the coming observer LISA[329, 54], as expected for this class of models[31]. We thus conclude that strong GW signal in the LISA with spectrum controlled by the plasma sound waves is a generic prediction of baryogenesis and DM production with relativistic bubble walls. This is in sharp opposition with the general expectation that usual EWBG demands slow walls, and thus suppressed signals.

As a final comment, it should however be noticed that the current simulations do not directly provide a solution for the regime of large α, and we only have an extrapolation of the numerical result. Thus, the conclusion above should be taken with a grain of salt.

5.6 Summary and outlook

In this study we have presented an explicit realization of the baryogenesis and DM production during electroweak phase transition with ultra-relativistic bubble expansion. The work is based on the proposals in [1, 2, 3, 303] where new heavy particles are produced in plasma−bubble wall collisions. We have shown that the model with SM extended by a real singlet with a Z_2 symmetry can indeed lead to ultra-relativistic bubbles, where the Lorentz factor γ_w can reach the values $\sim 10^{(5-6)}$. Such fast bubbles can appear if the symmetry breaking occurs in two steps: first discrete Z_2 is spontaneously broken and in the second step electroweak symmetry breaking is accompanied by Z_2 restoration $(0,0) \xrightarrow{SOPT} (0, v_s) \xrightarrow{FOPT} (v_{EW}, 0)$. We find that there exists a region of parameter space where the nucleation temperature can become as low as $1-2$ GeV and the collision of the bubble wall with the plasma particles can lead to the non-thermal heavy particle production with the masses up to ~ 10 TeV. Interestingly we find that the mechanism is most efficient for relatively low masses of the singlet field $M_s(v_{EW}, 0) \sim 70 - 100$ GeV, close to the region excluded by the Higgs invisible decays. Subsequently, this region of parameter space will be probed by HL-LHC ([377, 391]) in the singlet production mediated by off-shell Higgs boson. By noting the slight Z_2 breaking, s, if produced, can decay into $b\bar{b}$ in collider experiments. Depending on the size of the breaking displaced vertices of $b\bar{b}$ may be probed. We find the typical bubble radius parameter of the order of $R_\star \sim (10^{-4} - 10^{-1}) H^{-1}$ so that stochastic gravitational background signal becomes observable at GW experiments like LISA[329, 54].

The model necessarily requires tuning $\propto (T_{\text{nuc}}/m_h)^2$ which numerically turns out to be of the order of $10^{-4} - 10^{-2}$ (using Giudice-Barbieri measure) for successful baryogenesis and DM production mechanism. In spite of this we believe it can provide a useful guidance for more appealing models where these hierarchies can appear naturally.

In general we hope that more realistic realisation of the ultra-relativistic EWPT would follow the lines of this study, for example in nearly conformal completion of the EWPT and composite Higgs. The case of near conformality offers a natural realisation of the supercooling, as we already argued for example [5], though our model was not realistic, and the physical conformality is expected to occur when strongly coupled dynamics. Due to this expectation, it becomes interesting to know if our mechanisms of DM production and baryogenesis can be lifted to strongly coupled UV completion. We leave this difficult question to further studies.

Appendix A

Appendix

A.1 The membrane action

In Chapter 1, we used an effective Lagrangian for the description of the early bubble expansion, in Eq.(1.123). Since this Lagrangian is not immediately obvious, we would like to reproduce the derivation of the membrane action in the thin wall limit, following the lines of [29]. The action takes the form

$$S = \int d^4x \left(\frac{1}{2}(\partial_\mu \phi)^2 - V(\phi) \right). \tag{A.1}$$

In the context of a spherical bubble, we can introduce the radial variable $r^2 = x^2 + y^2 + z^2$. Then the derivative $\partial_r \phi$ is only non-vanishing in the vicinity of the region interpolating between the two vacua, that we call the *wall*. The wall is by definition this region of strong gradient. The action of the membrane simplifies to

$$S = 4\pi \int dt dr r^2 \left(\frac{1}{2}((\partial_t \phi)^2 - (\partial_r \phi)^2) - V(\phi) \right). \tag{A.2}$$

As already emphasized, gradients are only strong in the direct vicinity of the wall. We can thus separate the integral into two contributions: the region of the wall, containing gradients, and the rest of the space, where only the potential matters and the integral over the radius can be easily performed:

$$S = 4\pi \int_{\text{wall}} dt dr r^2 \left(\frac{1}{2}((\partial_t \phi)^2 - (\partial_r \phi)^2) - V(\phi) \right) - \frac{4\pi R^3}{3} \int dt \Delta V. \tag{A.3}$$

To make further progress, let us change the basis from $(\mathbf{e}_t, \mathbf{e}_r)$ into $(\mathbf{e}_\perp, \mathbf{e}_{||})$ defined in the following way

$$\mathbf{e}_\perp \equiv \frac{1}{\sqrt{1-\dot{R}^2}}(-\dot{R}\mathbf{e}_t + \mathbf{e}_r), \qquad \mathbf{e}_{||} \equiv \frac{1}{\sqrt{1-\dot{R}^2}}(\mathbf{e}_t + \dot{R}\mathbf{e}_r). \tag{A.4}$$

Now noticing that the wall can be approximated by a function of $\phi(r - \dot{R}t)$, with slow variation of its shape, we can expect that

$$e^\mu_\perp \partial_\mu \phi \gg e^\mu_{||} \partial_\mu \phi \qquad \Rightarrow \partial^\mu \partial_\mu \phi \approx \partial^2_\perp \phi \tag{A.5}$$

Plugging this in the equation of motion, neglecting all forms of friction, and integrating over ϕ gives

$$\int_{\phi_f}^{\phi_t} d\phi \frac{dV}{d\phi} = \int_{\infty}^{0} dr \frac{d\phi}{dr} \partial_{\perp}^2 \phi. \tag{A.6}$$

In the *thin wall* limit, the gradient are concentrated within a very thin shell, and the integral is simple

$$2V(\phi) = (\partial_{\perp}\phi)^2, \tag{A.7}$$

where $V(\phi)$ is defined as zero in the true vacuum and is positive outside the bubble. We can now finish our computation

$$\begin{aligned} 4\pi \int_{\text{wall}} dt dr r^2 \Big(\frac{1}{2}((\partial_t \phi)^2 - (\partial_r \phi)^2) - V(\phi) \Big) &= 4\pi \int_{\text{wall}} dt dr r^2 \Big(-\frac{1}{2}(\partial_{\perp}\phi)^2 - V(\phi) \Big) \\ &= 4\pi \int dt R^2(t) \int_{\text{wall}} dr \Big(-(\partial_{\perp}\phi)^2 \Big). \end{aligned} \tag{A.8}$$

Now since

$$\frac{\partial r}{\partial \phi} \approx \frac{\sqrt{1-\dot{R}^2}}{\partial_{\perp}\phi}. \tag{A.9}$$

We obtain

$$\begin{aligned} -4\pi \int dt R^2(t) \sqrt{1-\dot{R}^2} \int_{\text{wall}} d\phi (\partial_{\perp}\phi)^2 \frac{1}{\partial_{\perp}\phi} &= -4\pi \int dt R^2(t) \sqrt{1-\dot{R}^2} \int_{\text{wall}} d\phi \sqrt{2V(\phi)} \\ &= -4\pi \int dt R^2(t) \sqrt{1-\dot{R}^2} \sigma, \end{aligned} \tag{A.10}$$

with σ being the tension of the wall defined by

$$\sigma \equiv \int_{\text{wall}} d\phi \partial_{\perp}\phi = \int_{\text{wall}} d\phi \sqrt{2V(\phi)}. \tag{A.11}$$

Collecting all the terms, the action becomes

$$S = \int dt \Big(4\pi R^2(t)\sigma - \frac{4\pi}{3} R^3(t) \int dt \Delta V \Big). \tag{A.12}$$

A.2 Transition pressure

In this appendix we will review, for the sake of completeness, the pressure from transition of the particles through the wall. We will focus on the limit $\gamma_w \gg 1$ and will always assume that the mean free path of the particles is larger than the wall width, exactly as we did in the main text. In this case we can treat particles quasi-classically and consider only individual interactions with the wall. This discussion is not new and was already presented in the papers [95, 80] and recently reviewed in [92](where the analytical results for the pressure have been reported). The particle, in front of the wall, will follow the usual thermal distribution, which in the frame of the wall becomes

$$f(E,p,T) = f\left(\frac{p_\mu u^\mu}{T}\right) = f\left(\frac{\gamma_w (E + v_w p_z)}{T}\right), \tag{A.13}$$

where we have assumed like in Fig.2.3 that the wall moves along the positive z direction with velocity v_w and $u_\mu = \gamma_w(1, 0, 0, -v_w)$. We will assume that the particle is incident on the wall with mass m_s and on the other side it has mass m_h. The pressure on the wall is originating from the following three processes (we follow closely the notations of [95]).

- **Reflection from the wall**: when the incident particle does not have enough momentum or energy to pass through the wall:

$$\begin{aligned}\Delta\mathcal{P}^{\rm ref} &= \frac{2}{4\pi^2}\int_{m_s}^{m_h} dE \int_{-\sqrt{E^2-m_s^2}}^{0} dp_z \left[p_z^2 f\left(\frac{\gamma_w(E+v_w p_z)}{T}\right)\right] \\ &+ \frac{2}{4\pi^2}\int_{m_h}^{\infty} dE \int_{-\sqrt{m_h^2-m_s^2}}^{0} dp_z \left[p_z^2 f\left(\frac{\gamma_w(E+v_w p_z)}{T}\right)\right] \end{aligned} \tag{A.14}$$

  in this case the momentum transfer to the wall is $\Delta p_z = 2p_z$.

- **Transition through the wall**: the pressure is generated due to the change of momenta of the particle with $\Delta p_z = p_z + \sqrt{p_z^2 - (m_h^2 - m_s^2)}$:

$$\Delta\mathcal{P}^{t+} = \frac{1}{4\pi^2}\int_{m_h}^{\infty} dE \int_{-\sqrt{E^2-m_s^2}}^{-\sqrt{m_h^2-m_s^2}} dp_z \left[p_z(p_z + \sqrt{p_z^2 - (m_h^2 - m_s^2)}) f\left(\frac{\gamma_w(E+v_w p_z)}{T}\right)\right] \tag{A.15}$$

- **Transition in the opposite direction**: with $\Delta p_z = \sqrt{p_z^2 + m_h^2 - m_s^2} - p_z$:

$$\Delta\mathcal{P}^{t-} = \frac{1}{4\pi^2}\int_{m_h}^{\infty} dE \int_{0}^{\sqrt{E^2-m_h^2}} dp_z \left[p_z(\sqrt{p_z^2 + m_h^2 - m_s^2} - p_z) f\left(\frac{\gamma_w(E+v_w p_z)}{T}\right)\right] \tag{A.16}$$

Let us start by considering the transition pressure Eq.(A.15). Introducing the new variables

$$Y \equiv \frac{\gamma_w(E+v_w p_z)}{T}, \quad k \equiv -\frac{p_z}{T}, \tag{A.17}$$

the expression for the pressure becomes:

$$\begin{aligned}\Delta\mathcal{P}^{t+} &= \frac{T^4}{4\pi^2\gamma_w}\int_{\sqrt{m_2^2-m_s^2}/T}^{\infty} dk k\left(k - \sqrt{k^2 - (m_h^2 - m_s^2)/T^2}\right) \int_{\gamma_w(\sqrt{k^2+m_s^2/T^2}-v_w k)}^{\infty} f(Y)dY \\ &= -\frac{T^2(m_h^2 - m_s^2)}{8\pi^2\gamma_w}\int_{\sqrt{m_h^2-m_s^2}/T}^{\infty} dk \int_{\gamma_w(\sqrt{k^2+m_s^2/T^2}-v_w k)}^{\infty} f(Y)dY, \end{aligned} \tag{A.18}$$

where we have expanded the momentum difference $(k - \sqrt{k^2 - (m_h^2 - m_s^2)/T^2})$ in the large k limit. We can see that the integral is non-vanishing if the lower limit of the second integral is small

$$\left\{\gamma_w(\sqrt{k^2 + m_1^h/T^2} - v_w k)\right\} \sim \frac{k}{2\gamma_w} + \frac{m_s^2}{2T^2}\frac{\gamma_w}{k} \lesssim O(1) \Rightarrow m_s \lesssim T. \tag{A.19}$$

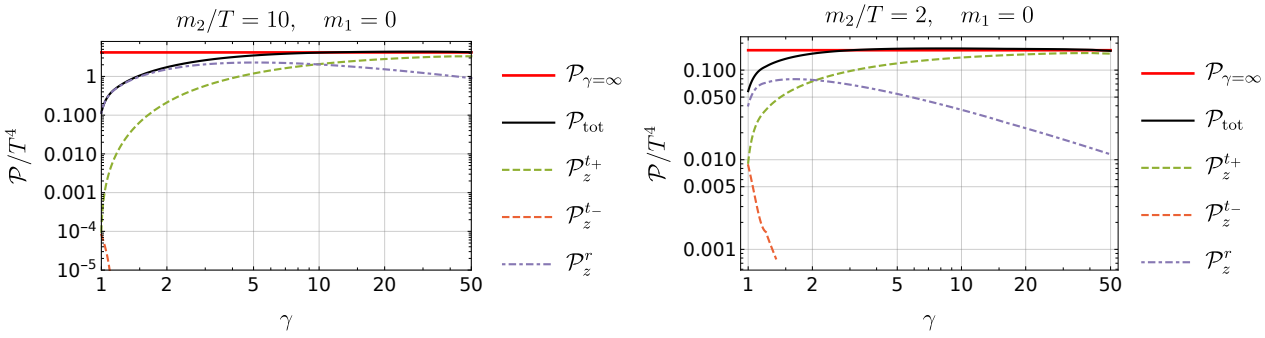

Figure A.1: Illustration of the forward transmission pressure, the reflection pressure, the total pressure and the LO order approximation. $\frac{m_h}{T} = 10, 2$ respectively on the Left and the Right.

Otherwise the pressure effects will be strongly suppressed by the Boltzmann factor $\exp[-\frac{m_s}{T}]$, which is obvious, since the energy of the massive particle is always larger than its mass. On top of this, looking at the lower limit of the k integration, we can conclude that

$$Y \lesssim 1 \Rightarrow \sqrt{m_h^2 - m_s^2} \lesssim \gamma_w T, \tag{A.20}$$

which is just the necessary condition for the particle to pass through the wall. Combining these two conditions we observe that this contribution to the friction is efficient if only

$$m_h < \gamma_w T, \quad m_s < T. \tag{A.21}$$

Performing the integration we will obtain for the friction

$$\Delta\mathcal{P}^{t+}|_{\gamma_w T/m_h \to \infty} = \frac{m_h^2 - m_s^2}{24} T^2. \tag{A.22}$$

Using a similar analysis we can argue that the reflection pressure and the transmission from the opposite side are vanishingly small in $\gamma_w \to \infty$ limit. Indeed setting $m_s \to 0$ for simplicity and using the same variable redefinition as in Eq. (A.18) we will get

$$\begin{aligned}
\Delta\mathcal{P}^{\rm ref} &= I_1 + I_2 \\
I_1 &= \frac{2}{4\pi^2}\int_0^{m_2} dE \int_{-\sqrt{E^2-m_s^2}}^{0} dp_z \left[p_z^2 f\left(\frac{\gamma_w(E+v_w p_z)}{T}\right)\right] \\
&= \frac{T^4}{2\pi^2\gamma_w}\int_0^{m_h/T} dk k^2 \int_{\frac{k}{2\gamma_w}}^{\gamma_w(m_h/T-k)} dY f(Y) \propto \gamma_w^{-1} \to 0 \\
I_2 &= \frac{T^4}{2\pi^2\gamma_w}\int_0^{m_h/T} dk k^2 \int_{\gamma_w(m_h/T-v_w k)}^{\infty} f(Y) dY \propto \gamma_w^{-2} \to 0.
\end{aligned} \tag{A.23}$$

At last the pressure from the transition in the opposite direction $\Delta\mathcal{P}^{t-}$ is always suppressed since the argument of the distribution function is always larger than one $\sim \frac{\gamma_w m_h}{T} \gg 1$. We confirm these estimates using our numerical calculation illustrated on the Figure A.1, where we plotted the various contributions to the total pressure. For the various contributions to the pressure the following approximate relations are true in the mass range $\frac{m_h}{T} \sim 1 - 10$:

$$\mathcal{P}_z^{\rm ref} \approx \mathcal{P}_z^{t+} \approx 0.4 \times \mathcal{P}_{\gamma\to\infty} \quad \text{for} \quad \gamma_w T = m_h \tag{A.24}$$

$$\mathcal{P}_z^{t-} \approx \mathcal{P}_z^{\rm ref} \approx 0, \quad \mathcal{P}_z^{t+} \approx 0.9 \times \mathcal{P}_{\gamma\to\infty} \quad \text{for} \quad \gamma_w T = 10 m_h. \tag{A.25}$$

A.3 Consequences of the shape of the wall

In the main text, we have often assumed that the wall is linear. This provided us with a suppression factor $\left(\frac{\sin\alpha}{\alpha}\right)^2$. However given a wall shape, naively, we would expect to have different types of suppression. The wall shape depends on the Higgs potential and on the specific interactions between the wall and the plasma. Here let us assume two types of wall shapes and let explicitly calculate the suppression factor from Eq.(3.18). To this end, we use first a **tanh wall shape**

$$V_{\rm tanh}(z) = \frac{v}{2}\left[\tanh\left(\frac{z}{L_w}\right)+1\right], \tag{A.26}$$

and second a **gaussian wall shape**

$$V_{\rm gaussian}(z) = \frac{v}{\sqrt{2\pi}L_w}\int_{-\infty}^{z} dz' \exp\left(-\frac{z'^2}{2L_w^2}\right) \tag{A.27}$$

to perform the integral. Here, v is the VEV inside the bubble and L_w is the length of the wall.

In general, we can perform the integral by using partial integration of

$$\mathcal{M} = -\int_{-\infty}^{\infty} dz V'(z)\frac{\exp\left(i\Delta p_z z\right)}{i\Delta p_z}. \tag{A.28}$$

For the $\tanh\left(z/L_w\right)$ case, $V'_{\rm tanh}(z) = v/(2L_w\cosh^2\left(z/L_w\right))$. By noting that z integral becomes the summation of residues at poles $z = \pi i L_w/2, 3\pi i L_w/2, \cdots$ for $\Delta p_z > 0$ or $z = -\pi i L_w/2, -3\pi i L_w/2, \cdots$ for $\Delta p_z < 0$, we obtain

$$\mathcal{M}_{\rm tanh} = {\rm sign}[\Delta p_z]\pi i v L_w \sum_{n=0}^{\infty} e^{-L_w|\Delta p_z|(n+1/2)\pi} = \frac{\pi i v L_w}{2\sinh\left(\frac{L_w\Delta p_z\pi}{2}\right)}. \tag{A.29}$$

One finds that this solution has the same behavior at $\Delta p_z \lesssim 1/L_w$ than in the linear case but the suppression is rather exponential, $\propto e^{-L_w\Delta|p_z|}$ when $L_w|\Delta p_z| \gtrsim 1$. This implies that the linear approximation is good when $L_w|\Delta p_z| \lesssim 1$ but may not be good enough when $L_w|\Delta p_z| \gtrsim 1$.

In the case of Eq. (A.27) similarly we obtain,

$$\mathcal{M}_{\rm gaussian} = -\frac{v}{\sqrt{2\pi}i\Delta p_z L_w}\int_{-\infty}^{\infty} dz \exp\left(-\frac{z^2}{2L_w^2} + i\Delta p_z z\right) = \frac{vi}{\Delta p_z}\exp\left(-\frac{L_w^2\Delta p_z^2}{2}\right) \tag{A.30}$$

where we have dropped the surface term. Again we have the same form as the linear approximation with $\Delta p_z \lesssim 1/L_w$ but the suppression factor is again exponential in the regime $\Delta p_z \gtrsim 1/L_w$. This motivates our former approximation that we set by hand the probability of production to zero in the regime $\Delta p_z \gtrsim 1/L_w$.

A.4 The bounce in one and two dimensions

In Chapter 5 we studied numerically the phase transition from the minimum $(0, v_s)$ (or in the vicinity of it) to $(v_{EW}, 0)$, so a two-fields bounce transition. The bounce computation can be done using existing codes for example `FindBounce` or `CosmoTransition`. However we have found that in the regime of long supercooling where the potential around the false vacuum is very flat and, the existing codes are often not stable and lead to numerical errors. Thus we have developed our own code (more stable for the flat potentials), following the procedure described in [266], while cross-checking the available values with `FindBounce`.

A.4.1 Computation of the bounce profile in one dimension

In this Appendix, we briefly review the standard computation of the bounce action with only one field. In order to compute the vacuum tunneling probability from the false vacuum to the true one in d dimensions, we need to minimize the Euclidean action given by

$$S_E = \int d^d x \left[\frac{1}{2} (\partial_\mu \phi)^2 + V[\phi] \right]. \tag{A.31}$$

It is known that the field configurations leading to the minimal action are the ones that exhibit an $O(d)$ spherical symmetry, then the so-called bounce solution is the solution of the following Cauchy problem

$$\frac{d^2\phi}{dr^2} + \frac{d-1}{r}\frac{d\phi}{dr} = \frac{dV[\phi]}{d\phi}, \qquad \lim_{r\to\infty} \phi(r) = 0, \qquad \left.\frac{d\phi}{dr}\right|_{r=0} = 0, \tag{A.32}$$

where we have chosen the false minimum to be at $\phi = 0$. If we interpret the parameter r as a time and ϕ as a position, this problem becomes formally equivalent to the evolution of a mechanical ball in a potential $-V[\phi]$ undergoing a friction $\frac{d-1}{r}\frac{d\phi}{dr}$, released with vanishing velocity and stopping its evolution for $r \to \infty$ at $\phi = 0$. It is well known that this problem can be solved by applying numerically an overshoot/undershoot method on the position of the released point. Releasing the ball too close to the true vacuum would induce an overshoot configuration (the ball would continue after crossing $\phi = 0$), we would thus shift the release point toward the false vacuum, while releasing it too far would end up in an undershoot configuration (the ball would never reach $\phi = 0$ and starts oscillate around the minimum of $-V[\phi]$) and we correct it by shifting the release point farther from the false vacuum. Iterating between those two situations, we are able to find the correct release point and obtain the *bounce solution*.

It is well known that the case of a PT triggered by temperature fluctuation at temperature T is formally equivalent to imposing a periodicity T^{-1} in the imaginary time t_E, as we already discussed in Chapter 1. This imposes the following constraint on the field

$$\phi[t_E, \mathbf{x}] = \phi[t_E + T^{-1}, \mathbf{x}] \tag{A.33}$$

and the computation of thermally induced phase transition thus amounts to take $d = 3$ in the above equations.

A.4.2 Bounce action in two dimensions and path deformation

The problem complexifies when the transition involves many fields. Here there is no straightforward intuition for the path followed by the fields in field space during the tunneling. One can think that a straight line, connecting the two minima, could be a reasonable guess, but it turns out that it cannot be considered as a good approximation of the euclidean action in many cases[1]. Here we thus describe the algorithm [267] to find the right path in field space. In a multi-field case, ϕ becoming a vector in the field space, the Eq.(A.32) becomes

$$\frac{d^2\phi}{dr^2} + \frac{d-1}{r}\frac{d\phi}{dr} = \nabla V[\phi], \qquad \lim_{r\to\infty} \phi(r) = 0, \qquad \left.\frac{d\phi}{dr}\right|_{r=0} = 0. \tag{A.34}$$

Since in this case an overshoot/undershoot procedure cannot be easily applied, the idea is to reduce the problem to one dimensional tunneling. In order to do so we start guessing the path, $\phi_g(x)$, where x is now to be understood as

[1]Let us emphasize that in the region of the parameter space we studied in Chapter 5, the straight line between the false and the true vacuum gives an Euclidean action which is often wrong by *orders of magnitudes!* Since the path is often very far from the straight line we cannot dispense from the effort of studying the exact 2D path in field space.

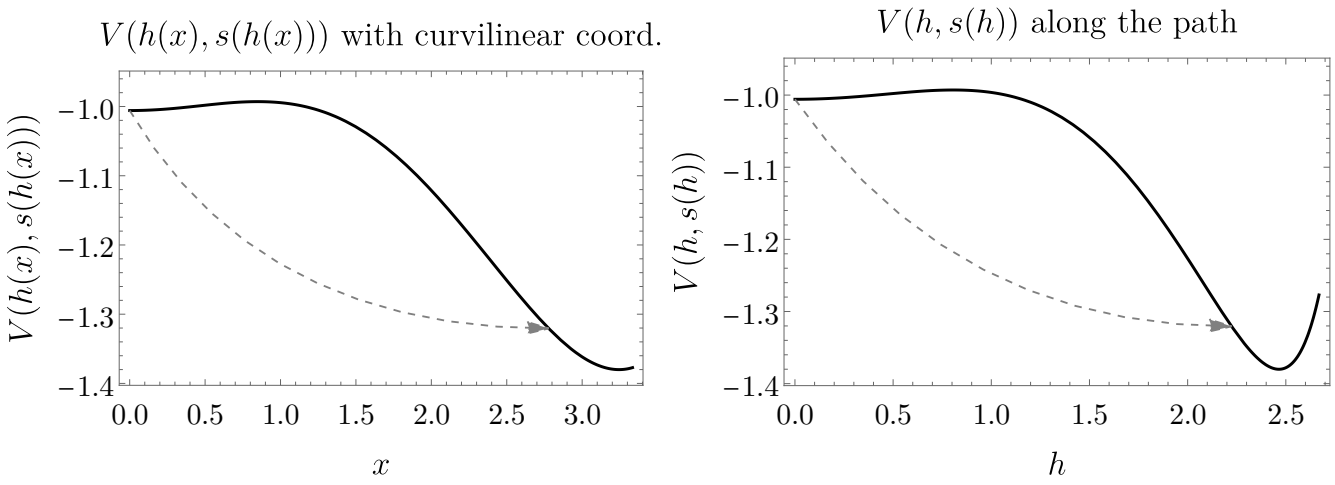

Figure A.2: On the left, the potential, along the path, experienced by the field x and the corresponding escape point $x_\star$. On the right the potential, along the path, projected on the h direction.

the parameter that measure the distance along the path, *i.e.* the so-called curvilinear abscissa. For the present case, if we parametrize the path in the field space as $(h(t), s(t)) = (t, f(t)) \equiv (h, s(h))$ it is defined as

$$x(h) = \int_{h_{fm}}^{h} \sqrt{1 + \left(\frac{ds(h')}{dh'}\right)^2}\, dh', \tag{A.35}$$

where h_{fm} is the value of the Higgs field in the false minimum. With this choice of field coordinate to parametrize the path, the condition $\left|\frac{d\phi(x)}{dx}\right|^2 = 1$ is satisfied, and the Euclidean equation of motion in Eq. (A.34) can be rewritten along the parallel and the perpendicular direction

$$\begin{aligned} &\frac{d^2x}{dr^2} + \frac{d-1}{r}\frac{dx}{dr} = \partial_x V[\phi_g(x)], \\ &\frac{d^2\phi_g(x)}{dx^2}\left(\frac{dx}{dr}\right)^2 = \nabla_\perp V[\phi_g(x)]. \end{aligned} \tag{A.36}$$

Here, we have been able to separate the dynamics along the parallel and perpendicular direction in such a way that the first equation defines a new undershoot/overshoot problem, that we solve to obtain the value of the *escape point*, $\phi_0(x_\star)$, and the Euclidean action corresponding to the potential along the path considered ϕ_g, as in Fig.A.2. On the other hand, the second equation can be seen as a condition that the bounce solution has to satisfy and can be thought as a force field acting on the path, defined as following

$$\mathbf{N} \equiv \frac{d^2\phi_g(x)}{dx^2}\left(\frac{dx}{dr}\right)^2 - \nabla_\perp V[\phi_g(x)]. \tag{A.37}$$

The right path will be the one where $\mathbf{N}$ is vanishing. The algorithm proceeds iteratively: first we guess a path, the straight line connecting the two minima, then we find the bounce solution along this path, we compute the normal force and deform the guessed path according to it. In practice, to define the path at the step n, ϕ_n, we need to solve for the bounce profile for the path at ϕ_{n-1}, extract the escape point $x_{\star,n-1}$, that is $(h(x_{\star,n-1}), s(x_{\star,n-1}))$ in field space, we then discretize the path in the interval $x \in [0, x_{\star,n-1}]$, creating a series $(\phi_{n-1})_j$, for $j = 1, ..., N$ and a

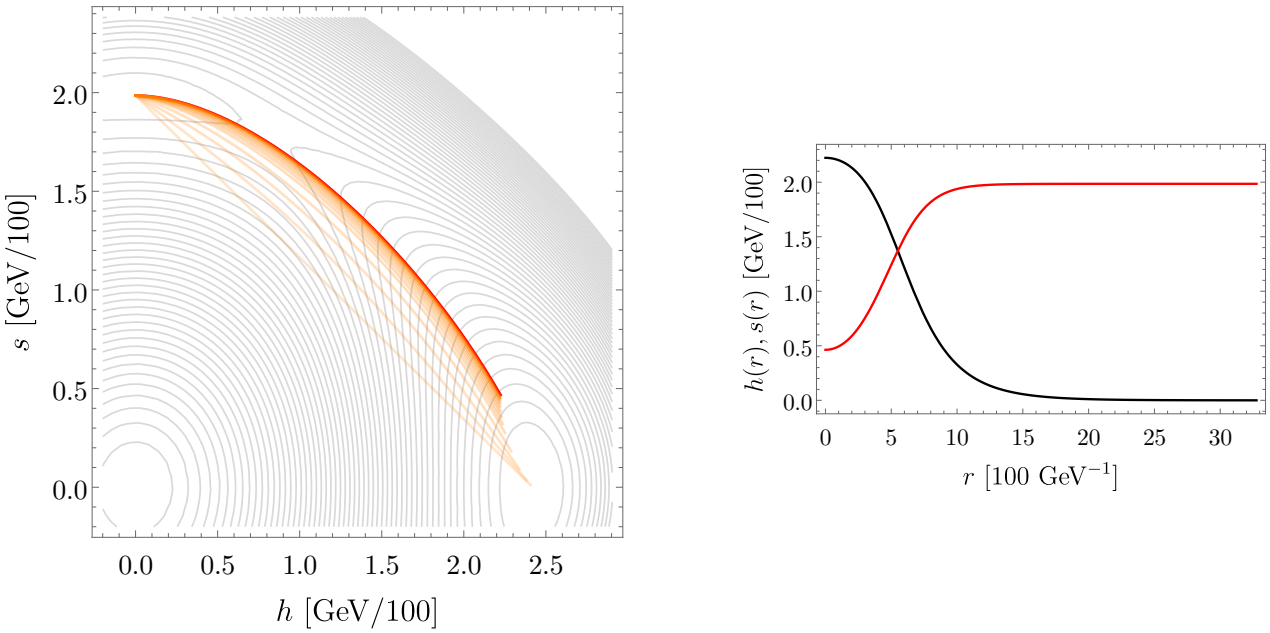

Figure A.3: **Left**: iterative procedure for the correct path, starting from the straight line connecting the two minima and then modified according to the field $\mathbf{N}$. **Right**: bounce profile of the fields (black for $h(r)$ and red for $s(r)$) on the correct path.

series of values for the normal force $(\mathbf{N}_{n-1})_j$. We then shift each point of the discretized path by

$$(\phi_n)_j = (\phi_{n-1})_j + \rho(\mathbf{N}_{n-1})_j \qquad j = 1, \dots, N. \tag{A.38}$$

In the end, we fit a path ϕ_n along the shifted points from $(\phi_{n-1})_j$. The procedure of deformation of the path will produce a series of paths $\phi_i[x]$, over which we compute the Euclidean action according to Eq.(A.31) at each step of the deformation, like in Fig.A.3. The algorithm stops when the difference in the bounce action, S_3, between two successive iterations is below some imposed precision. At a definite temperature T, we start by identifying the two minima, the false and the true ones

$$(\langle h \rangle, \langle s \rangle)_{\rm fm} = (v(T), v_s(T)) \to (v_{EW}, 0), \tag{A.39}$$

and will keep the false minimum fixed during the whole procedure of deformation. Generally, especially when we have a sizable amount of supercooling, the escape point is just behind the barrier, so the escape point $(v_\star(T_n), v_{s,\star}(T_n))$ will be different from the, zero-temperature, EWSB vacuum, but when the tunneling happens the system will classically roll down towards the global minimum, as we can see from Fig.A.3. We do not track the evolution of the fields profile after the tunneling.

A.5 WKB approximation

In many of our chapters, we have made abundant use of the WKB approximation for the quantum plane waves of particles, specially during their interaction with the bubble wall, that we considered as a background field. In this

appendix, we quickly expose the WKB[2] approximation. Developed in the early times of quantum mechanics, the WKB approximation is a method to approximate the plane waves which assumes *slowly varying potentials*.

Let us start from the Schrödinger equation in one dimension

$$\frac{d^2\psi(x)}{dx^2} + k^2(x)\psi(x) = 0 \tag{A.40}$$

where

$$k(x) = \left(\frac{2m}{\hbar^2}(E - V(x))\right)^{1/2} \text{ if } E > V(x) \tag{A.41}$$

$$k(x) = i\left(\frac{2m}{\hbar^2}(V(x) - E)\right)^{1/2} \text{ if } E < V(x) \tag{A.42}$$

The solutions of this equation for peculiar functions $k(x)$ is well known. However there is no generic solutions in the case of arbitrary $k(x)$. If we restart from the simplest case, where $k(x) = C$, thus we can easily see that one solution is given by well-known plane wave

$$\psi(x) = Ne^{ikx} \tag{A.43}$$

Now, if the potential, so k varies slowly, it becomes tempting to try to modify Eq.(A.43) by a simple

$$\psi(x) = Ne^{i\int_{x_0}^{x} k(t)dt} \tag{A.44}$$

with $k(t)$ from Eq.(A.42) and the requirement of normalisation imposes

$$\chi(z) \simeq \sqrt{\frac{k_{z,s}}{k_z(z)}} \exp\left(i\int_0^z k_z(z')dz'\right), \tag{A.45}$$

Plugging this ansatz into the Schrödinger equation (A.40) already provides the condition of validity of such an approximation

$$\frac{d^2\psi(x)}{dx^2} + k^2(x)\psi(x) = ik'(x)\psi(x) \tag{A.46}$$

which approximates (A.40) if

$$|k'| \ll k^2 \tag{A.47}$$

Applied to the problem of the phase transition, in which the Lorentz symmetry is broken along the direction of the wall, the WKB approximation demands that the states on both sides of the wall match one to one and that the plane waves smoothly interpolate from one side of the wall to the other one.

[2]The name of the WKB method comes from three physicists Wentzel, Kramers, and Brillouin that independently developed it in 1926 for the purpose of solving the Schrödinger equation. Though a mathematician, Harold Jeffreys, had already developed a similar method in 1923 for solving ODE, his name seems to have been forgotten.

A.6 Dark Matter and baryogenesis via the collision of runaway bubbles

The main purpose of this thesis was to expose and to study the cosmological consequences of particles produced in the collision of the wall with the plasma, that we showed could be very heavy. In [167], authors proposed a mechanism of production of non-thermal DM, possibly much more massive than the scale of the transition $M_{\rm DM} \gg v$, taking advantage of the collision of relativistic bubbles. This possibility was already hinted in [166] and can be easily understood from the fact that ultra-relativistic bubbles carry a typical energy $\gamma_w T_{\rm nuc}$ that is released at the collision of bubbles, possibly materializing in the form of heavy non-thermal states.

In the context of ultra-relativistic bubble wall collisions, two extremal dynamics have been analysed; *elastic* and *inelastic* wall collisions. In the first case, the walls bounce on each other multiple times, re-establishing after each collision a new region of symmetric phase in between the walls and releasing a fraction of the stored energy under the form of scalar waves and quanta. This scenario occurs when the effective potential of the symmetry breaking field has two *nearly degenerate* minima at collision instance, and the field can easily jump from one vacuum to the other. In the case of inelastic collision, the two minima are far apart and the field can not escape the broken phase. Thus all the energy is released after one collision. As a consequence, for efficient production, all the energy of the transition needs to be concentrated in the bubble wall, which is only satisfied in the regime of runaway. This rules out the EWPT as a possible model for bubble collision production, but a dark FOPT with runaway walls could make the job, this is what we will consider here.

Authors of [167] have studied Scalar, Fermion and Vector DM candidates in the case of elastic and inelastic collisions and have found vastly different DM production abundances. We focus on the case of scalar DM candidate with portal coupling similar to the one we used in Chapter 3,

$$\mathcal{L}_{\text{scalar portal}} = \frac{\lambda}{2}|\varphi|^2\phi^2, \tag{A.48}$$

where φ undergoes a transition.

Using this portal, let us review the result of [167].

Analytical estimates in the scalar portal case

Let us provide some rough analytical estimates, first in the simpler case of elastic collision and then in the case of inelastic collisions. For simplicity we remain in the case of the scalar coupling of Eq.(A.48) (which is the model we have studied) and show that the BC production is always negligible in both the case of elastic and inelastic collision with respect to BE production.

Elastic case We want to compute $\rho_{\rm DM}$ for a particle emitted with mass $M_{\rm DM}$. In order to obtain an analytically tractable expression, let us simplify the formulas of [167]. We obtain that the energy density of DM produced after the collision is roughly given by

$$\rho_{\rm DM} \approx \frac{10^3 v_\varphi^4}{4\pi^2 R_\star}\frac{\lambda^2}{8\pi}\int_{M_{\rm DM}^2}^{\infty}\frac{d\chi}{\chi^2}\sqrt{\chi - 4M_{\rm DM}^2} \approx \frac{10^3 v_\varphi^4}{4\pi^2 R_\star}\frac{\lambda^2}{8\pi}\frac{1}{M_{\rm DM}}, \qquad \text{(Produced energy density)} \tag{A.49}$$

with $\chi \equiv E^2 - p_z^2$ the invariant mass. If we plug $R_\star^{-1} \sim \beta H \sim 10\beta\frac{v_\varphi^2}{M_{\rm pl}}$ for the radius at collision and we use reasonable values for γ_w and L_w, which is any case only appear in a log Eq.(A.49) becomes

$$\Omega_{DM,\text{elastic}} \approx 6\times 10^9 \frac{\lambda^2}{g_\star(v_\varphi)}\beta\Big(\frac{v_\varphi}{T_{\rm reh}}\Big)^3\Big(\frac{T_{\rm reh}^2}{M_{\rm pl}M_{\rm DM}}\Big)\Big(\frac{v_\varphi}{\text{GeV}}\Big). \tag{A.50}$$

In order of magnitude we should have $T_{\rm reh}\sim v_\varphi$ and $g_\star(v_\varphi)\sim 100$, so

$$\Omega_{DM,\text{elastic}} \approx 6\times 10^7 \lambda^2\beta\Big(\frac{v_\varphi^2}{M_{\rm pl}M_{\rm DM}}\Big)\Big(\frac{v_\varphi}{\text{GeV}}\Big). \tag{A.51}$$

Comparing this expression with Eq.(3.34) shows that BE mechanism is always largely dominating if the scale of the transition is not to close to the Planck scale and the supercooling is not too drastic. The condition for BE domination is roughly

$$10^4\frac{\beta v_\varphi}{M_{\rm pl}} < \Big(\frac{T_{\rm nuc}}{T_{\rm reh}}\Big)^3 \qquad \text{(BE domination condition)} \tag{A.52}$$

Inelastic case Let us now treat the inelastic case. To provide an analytical estimate, we separate into two regimes: $M_{\rm DM}\ll m_\varphi$ and $M_{\rm DM}\gg m_\varphi$. Formulas simplify to

$$\rho_{\rm DM} \approx \frac{10^3 v_\varphi^4}{4\pi^2 R_\star}\frac{\lambda^2}{8\pi}\int_{M_{\rm DM}^2}^{\infty}\frac{d\chi}{\chi^2}\frac{m_\varphi^4}{(\chi-m_h^2)^2}\sqrt{\chi-4M_{\rm DM}^2} \qquad \text{(Produced energy density).} \tag{A.53}$$

For the sake of simplicity and because this is the regime of interest, we only treat the large mass $M_{\rm DM}\gg m_\varphi$. We obtain

$$\rho_{\rm DM} \approx \frac{10^3 v_\varphi^4}{4\pi^2 R_\star}\frac{\lambda^2}{8\pi}\frac{1}{M_{\rm DM}}\Big(\frac{m_\varphi}{M_{\rm DM}}\Big)^4 \qquad \text{for } M_{\rm DM}\gg m_\varphi \tag{A.54}$$

$$\Rightarrow \Omega_{\rm DM,inelastic}(M_{\rm DM}\gg m_\varphi) \sim \Omega_{\rm DM,elastic}(M_{\rm DM})\Big(\frac{m_\varphi}{M_{\rm DM}}\Big)^4$$

which consequently provides a even stronger suppression with respect to Eq.(A.49), so we conclude that the abundance from inelastic collision can be neglected generically.

Fermion and Vector cases. On the other hand, Fermions and Vectors via the couplings

$$\mathcal{L}_{\text{fermion portal}} = \underbrace{\lambda_f\varphi\bar f f}_{\text{yukawa coupling}} + \underbrace{\frac{\lambda_f}{\Lambda}|\varphi|^2\bar f f}_{\text{fermionic portal}}, \tag{A.55}$$

$$\mathcal{L}_{\text{vector portal}} = \underbrace{\lambda_V\varphi M_{\rm DM}V_\mu V^\mu}_{\text{Direct coupling}} + \underbrace{\lambda_V|\varphi|^2 V_\mu V^\mu}_{\text{effective coupling}}, \tag{A.56}$$

are usually copiously produced, even for $M_{\rm DM}\gg m_\varphi$, excepted in the case of the vector effective coupling; which is very suppressed. Let us note as well that the production of fermions, though large, depends on the UV completion in the case of the fermionic portal. However, is was subsequently claimed in[239] that even this production of fermions and vectors is not allowed due to perturbativity and unitarity argument.

A.6.1 Baryogenesis via bubble collision

Later on, a model a baryogenesis taking advantage of the same type of bubble collision production was proposed[239]. However, this model contained gauge bosons that could acquire a mass via the transition and thus excluding runaway.

However, the production of dark fermions necessary for baryogenesis was very efficient and scaling like $Y_{\rm produced} \propto \gamma_w$. As a consequence, though the production is suppressed by the Planck mass, it is however boosted by the strong γ_w dependence. We do not exclude that such a mechanism could also produce significant baryon number even in our models, assuming that the transition is elastic enough, which is not per se certain.

A.7 Freeze-out in the co-annihilation regime and Sommerfeld enhancement

In chapter 3, we presented the computation of the freeze-out in the most standard case. However, it has been noticed long time ago that the standard computation can fail in several specific cases[126]. We encounter such a case of nearly degenerate particles in section 3.6 of chapter 3 and we found out that Sommerfeld enhancement could be large in our models, due to large couplings. In this Appendix, for the purpose of completeness, we explain shortly those effects.

Sommerfeld enhancement Let us present the physics of the Sommerfeld enhancement. The Sommerfeld enhancement[182] is really an effect of non-relativistic quantum mechanics that can be understood from basic intuition: consider for example a positron and an electron. When they pass by, there is a probability of annihilation, which is encapsulated in the cross-section. Now, if we consider the electric attraction between the two particles, the cross-section is enhanced. This is really all of it. The "Sommerfeld enhancement" thus account for the effects of potential in the cross-sections.

Another interesting analogy is the case of a particle falling on a star of mass M and radius R. If we neglect the gravitation, the cross-section for the particle to end up on the star is really just $\sigma_0 = \pi R^2$, the surface of the star. However, when we switch on the gravity, the particle can be sucked onto the star via the interaction, this gives

$$\sigma = \sigma_0 \left(1 + \frac{v_{\rm escape}^2}{v_{\rm initial}^2}\right), \qquad v_{\rm escape} = \frac{2G_N M}{R} \tag{A.57}$$

where we see that if the initial velocity is small, then enhancement can be significant.

Let us go now to the quantum case, and work in the non-relativistic limit, since we have seen that the Sommerfeld enhancement is really efficient for low velocities. We consider ϕ the DM candidate and φ a mediator, with coupling strength λ. The wave function of the reduced two-body system is (v being the velocity of the particle ϕ)

$$\frac{\psi''(r)}{m_\phi} + V(r)\psi(r) = -m_\phi v^2 \psi(r) \tag{A.58}$$

and has a potential, in the non-relativistic limit, controlled by the mass of the mediator "med",

$$V = -\frac{\lambda^2}{4\pi r} e^{-m_{\rm med} r}. \tag{A.59}$$

It is shown that the Sommerfeld enhancement is given by[182, 183]

$$S \equiv |\psi(\infty)/\psi(0)|^2. \tag{A.60}$$

We can now rewrite the equation in Eq.(A.58) with

$$\begin{aligned} \alpha = \frac{\lambda^2}{4\pi}, \qquad \epsilon_v = \frac{v}{\alpha}, \qquad \epsilon_{\rm med} = \frac{m_{\rm med}}{m_\phi \alpha} \\ \Rightarrow \psi''(r) + \left(\epsilon_v^2 + \frac{e^{\epsilon_{\rm med} r}}{r}\right)\psi(r) = 0 \end{aligned} \tag{A.61}$$

We can easily solve in the limit of long range interactions, when $m_{\rm med} \to 0$ and we obtain

$$S = \frac{\pi/\epsilon_v}{1 - e^{-\pi/\epsilon_v}} \qquad \text{(Case of long-range potential)} \tag{A.62}$$

When the mass of the mediator is not zero anymore, the expression becomes more complicated, but an analytic approximation of the enhancement factor is given by[182, 183] (See also Refs [184, 185, 186, 187])

$$S_{\rm eff} = \frac{\pi}{\epsilon_v} \frac{\sinh\left(\frac{2\pi\epsilon_v}{\pi^2\epsilon_{\rm med}/6}\right)}{\cosh\left(\frac{2\pi\epsilon_v}{\pi^2\epsilon_{\rm med}/6}\right) - \cos\left(2\pi\sqrt{\frac{1}{\pi^2\epsilon_{\rm med}/6} - \frac{{\epsilon_v}^2}{(\pi^2\epsilon_{\rm med}/6)^2}}\right)}, \tag{A.63}$$

where $\epsilon_v = v/(\alpha_{\rm med})$ and $\epsilon_{\rm med} = m_{\rm med}/(\alpha_{\rm med} M_\phi)$. Specifically, we recover our result when $m_{\rm med} \to 0$. $S_{\rm eff} \to \frac{\pi\alpha_{\rm med}/v_\phi}{(1-e^{-\pi\alpha_{\rm med}/v_\phi})}$. In the context of this thesis, in Chapter 3 and 5 the mediator will be the production scalar undergoing a transition, the Higgs or the φ itself.

Co-annihilation regime Let us now present the case of freeze-out via co-annihilation, since in this case, the final abundance does not follow the usual FO abundance that we worked out in the text. The case of co-annihilation has been discussed with great details in [126] and the purpose of this section is not to reproduce their result, but to apply it to the special case discussed in section 3.6 and to answer the question: when can we apply the naive FO formula that we have been using? Our set-up was:

$$\mathcal{L} = \mathcal{L}_{\rm SM} + Y_* \bar{L}\varphi N + M_N \bar{N} N + Y_{\rm DM} \bar{N} \chi \phi \,. \tag{A.64}$$

where we are interested in the channel $\phi\chi \to \varphi L$ and ϕ is taken to be the DM candidate. The Boltzmann equations reads

$$\dot{n}_\phi + 3Hn_\phi = -\langle\sigma_{\chi\phi} v\rangle [n_\chi n_\phi - n_\chi^{\rm eq} n_\phi^{\rm eq}]. \tag{A.65}$$

Here the fact that the mass of χ does not equal the mass of ϕ brings a crucial difference. Intuitively, what happens if $M_\chi \gg M_\phi$ is that χ will be quickly depleted via other efficient channels for example $\chi\varphi \to \phi L$, and no abundance will be left for the interaction $\chi\phi \to \varphi L$. The whole process of FO will then be controlled by the heavy mass of χ and FO will occur around $T \sim M_\chi/20$, leaving most of the ϕ abundance intact. The ratio of the final abundance will scale like

$$\frac{n_\phi}{n_\chi} \sim e^{(M_\chi - M_\phi)/T_{FO}} \tag{A.66}$$

where we see that those two abundances are similar if

$$(M_\chi - M_\phi)/M_\chi < 1/20 \tag{A.67}$$

Summary and outlook

In this thesis, we studied the dynamics of first order phase transition with ultra-relativistic bubble walls in the context of production GW, production of DM and baryogenesis and we proposed physically motivated models realising ultra-relativistic bubble walls. In chapter 2 we discussed the friction on the wall in the relativistic regime. More specifically, we unveiled a new mechanism of pressure due to the production of heavy states in the collision of the plasma with the wall. We gave a first very simple model where this new pressure could change the regime from a "runaway wall" to a "terminal velocity wall" and we saw that this region could be sizable. We also discussed the friction from soft gauge bosons and confirmed the previous computation suggesting a γ_w scaling for this contribution to the pressure. We gave arguments that multi-gauge bosons emission should only produced a subleading log correction. This was further confirmed in [112]. However, we emphasized that this mechanism of production of soft bosons remains very obscure, as the copious emission of bosons with almost the same momentum seems to threaten perturbativity.

In chapter 3, we used the mechanism of production of heavy states to set the observed abundance of DM. We however found that the bubble wall tends to strongly overproduce DM and overclose the universe. As a consequence, we discussed three scenario that permit to reduce this initially strongly overproduced abundance: early annihilation, strong supercooling or very large mass. We discuss the intrication with the more usual FO mechanism and we found that at equal mass, the DM produced via bubble wall expansion is typically more strongly coupled, raising prospects of detection. We did not exhaust the possibility since the recent [195] found that this mechanism could be used to set non-thermal Hot and heavy dark matter with observed abundance.

In chapter 4, we went one step further and computed the one-loop correction to the production reaction. We proved that this loop can interfere with the tree-level diagram to induce CP-violation if there is an imaginary phase in the Yukawa matrices controlling the production and the connection to the SM. We then proposed two models taking advantage of such a mechanism to set the observed abundance of matter: in the first model, the baryon number is produced in the breaking of the lepton number phase transition, that we assume to be strongly first order. We find a large window where this mechanism can be realised while avoiding the subsequent wash-outs. In a second model, we completed the SM with a dark sector coupling strongly to the third generation of quarks and being produced during the EWPT phase transition. A cascade through the dark sector containing B violation then set the baryon number. The dark sector having to be rather low scale, TeV to tens of TeV, this model is highly detectable in $n - \bar{n}$ oscillations experiments and produced strong gravitational waves in the range of forthcoming LISA observer. Also on this side, further investigations of this baryogenesis are needed and have been performed for example in [303], where the production of a heavy scalar is used to set the baryon abundance.

In the final chapter 5, we use a well known scalar singlet extension of the SM inducing strongly first order EWPT. We find that bubbles become deeply relativistic only if the transition occurs in two-steps, first via breaking the Z_2 symmetry associated with the singlet, and then in a second step, restoring the Z_2 but breaking the EW symmetry. We found that in a tuned region, the nucleation temperature could become as low as 1 GeV. In this context, we

found that the mass of the singlet in the true vacuum had to be close to the kinematic boundary allowing $h \to ss$ transitions. We quantified this tuning and revisited our models of production of DM and baryogenesis.

A question that remains open at the end of this thesis is the possibility of a similar mechanism in the context of confinement/deconfinement phase transition, which bring more naturally deep supercooling.

Bibliography

[1] Aleksandr Azatov and Miguel Vanvlasselaer. "Bubble wall velocity: heavy physics effects". In: *JCAP* 01 (Oct. 2020), p. 058. DOI: 10.1088/1475-7516/2021/01/058. arXiv: 2010.02590 [hep-ph].

[2] Aleksandr Azatov, Miguel Vanvlasselaer, and Wen Yin. "Dark Matter production from relativistic bubble walls". In: *JHEP* 03 (2021), p. 288. DOI: 10.1007/JHEP03(2021)288. arXiv: 2101.05721 [hep-ph].

[3] Aleksandr Azatov, Miguel Vanvlasselaer, and Wen Yin. "Baryogenesis via relativistic bubble walls". In: *JHEP* 10 (2021), p. 043. DOI: 10.1007/JHEP10(2021)043. arXiv: 2106.14913 [hep-ph].

[4] Aleksandr Azatov et al. "Ultra-relativistic bubbles from the simplest Higgs portal and their cosmological consequences". In: (July 2022). arXiv: 2207.02230 [hep-ph].

[5] Aleksandr Azatov and Miguel Vanvlasselaer. "Phase transitions in perturbative walking dynamics". In: *JHEP* 09 (2020), p. 085. DOI: 10.1007/JHEP09(2020)085. arXiv: 2003.10265 [hep-ph].

[6] Mariano Quiros. "Finite temperature field theory and phase transitions". In: *ICTP Summer School in High-Energy Physics and Cosmology*. Jan. 1999, pp. 187–259. arXiv: hep-ph/9901312.

[7] Sidney Coleman and Erick Weinberg. "Radiative Corrections as the Origin of Spontaneous Symmetry Breaking". In: *Phys. Rev. D* 7 (6 Mar. 1973), pp. 1888–1910. DOI: 10.1103/PhysRevD.7.1888. URL: https://link.aps.org/doi/10.1103/PhysRevD.7.1888.

[8] Erick J. Weinberg. "Radiative corrections as the origin of spontaneous symmetry breaking". PhD thesis. Harvard U., 1973. arXiv: hep-th/0507214 [hep-th].

[9] Cedric Delaunay, Christophe Grojean, and James D. Wells. "Dynamics of Non-renormalizable Electroweak Symmetry Breaking". In: *JHEP* 04 (2008), p. 029. DOI: 10.1088/1126-6708/2008/04/029. arXiv: 0711.2511 [hep-ph].

[10] Eldad Gildener and Steven Weinberg. "Symmetry Breaking and Scalar Bosons". In: *Phys. Rev.* D13 (12 June 1976), p. 3333. DOI: 10.1103/PhysRevD.13.3333. URL: https://link.aps.org/doi/10.1103/PhysRevD.13.3333.

[11] Luigi Delle Rose et al. "Gravitational Waves from Supercool Axions". In: *JHEP* 04 (2020), p. 025. DOI: 10.1007/JHEP04(2020)025. arXiv: 1912.06139 [hep-ph].

[12] Ryusuke Jinno and Masahiro Takimoto. "Probing a classically conformal B-L model with gravitational waves". In: *Phys. Rev. D* 95.1 (2017), p. 015020. DOI: 10.1103/PhysRevD.95.015020. arXiv: 1604.05035 [hep-ph].

[13] J. I. Kapusta and Charles Gale. *Finite-temperature field theory: Principles and applications*. Cambridge Monographs on Mathematical Physics. Cambridge University Press, 2011. ISBN: 978-0-521-17322-3, 978-0-521-82082-0, 978-0-511-22280-1. DOI: 10.1017/CBO9780511535130.

[14] Michel Le Bellac. *Thermal Field Theory*. Cambridge Monographs on Mathematical Physics. Cambridge University Press, 2011. ISBN: 9780511885068, 9780521654777. DOI: 10.1017/CBO9780511721700. URL: http://www.cambridge.org/mw/academic/subjects/physics/theoretical-physics-and-mathematical-physics/thermal-field-theory?format=AR.

[15] Mikko Laine and Aleksi Vuorinen. *Basics of Thermal Field Theory*. Vol. 925. Springer, 2016. DOI: 10.1007/978-3-319-31933-9. arXiv: 1701.01554 [hep-ph].

[16] David Curtin, Patrick Meade, and Harikrishnan Ramani. "Thermal Resummation and Phase Transitions". In: *Eur. Phys. J.* C78.9 (2018), p. 787. DOI: 10.1140/epjc/s10052-018-6268-0. arXiv: 1612.00466 [hep-ph].

[17] Peter Brockway Arnold and Olivier Espinosa. "The Effective potential and first order phase transitions: Beyond leading-order". In: *Phys. Rev. D* 47 (8 Apr. 1993). [Erratum: Phys.Rev.D 50, 6662 (1994)], p. 3546. DOI: 10.1103/PhysRevD.47.3546. arXiv: hep-ph/9212235 [hep-ph]. URL: https://link.aps.org/doi/10.1103/PhysRevD.47.3546.

[18] Steven Weinberg. "Gauge and global symmetries at high temperature". In: *Phys. Rev. D* 9 (12 June 1974), pp. 3357–3378. DOI: 10.1103/PhysRevD.9.3357. URL: https://link.aps.org/doi/10.1103/PhysRevD.9.3357.

[19] Andrei D. Linde. "Infrared Problem in Thermodynamics of the Yang-Mills Gas". In: *Phys. Lett. B* 96 (1980), pp. 289–292. DOI: 10.1016/0370-2693(80)90769-8.

[20] Djuna Croon et al. "Theoretical uncertainties for cosmological first-order phase transitions". In: *JHEP* 04 (Sept. 2021), p. 055. DOI: 10.1007/JHEP04(2021)055. arXiv: 2009.10080 [hep-ph].

[21] Oliver Gould, Sinan Güyer, and Kari Rummukainen. "First-order electroweak phase transitions: a nonperturbative update". In: (May 2022). arXiv: 2205.07238 [hep-lat].

[22] Andreas Ekstedt, Oliver Gould, and Johan Löfgren. "Radiative first-order phase transitions to next-to-next-to-leading-order". In: (May 2022). arXiv: 2205.07241 [hep-ph].

[23] Sidney R. Coleman. "The Fate of the False Vacuum. 1. Semiclassical Theory". In: *Phys. Rev.* D15 (1977). [Erratum: Phys. Rev.D16,1248(1977)], pp. 2929–2936. DOI: 10.1103/PhysRevD.15.2929,10.1103/PhysRevD.16.1248.

[24] Andrei D. Linde. "Fate of the False Vacuum at Finite Temperature: Theory and Applications". In: *Phys. Lett.* 100B (1981), pp. 37–40. DOI: 10.1016/0370-2693(81)90281-1.

[25] Andrei D. Linde. "Decay of the False Vacuum at Finite Temperature". In: *Nucl. Phys.* B216 (1983). [Erratum: Nucl. Phys.B223,544(1983)], p. 421. DOI: 10.1016/0550-3213(83)90293-6,10.1016/0550-3213(83)90072-X.

[26] Thomas Banks, Carl M. Bender, and Tai Tsun Wu. "Coupled Anharmonic Oscillators. I. Equal-Mass Case". In: *Phys. Rev. D* 8 (10 Nov. 1973), pp. 3346–3366. DOI: 10.1103/PhysRevD.8.3346. URL: https://link.aps.org/doi/10.1103/PhysRevD.8.3346.

[27] Curtis G. Callan and Sidney Coleman. "Fate of the false vacuum. II. First quantum corrections". In: *Phys. Rev. D* 16 (6 Sept. 1977), pp. 1762–1768. DOI: 10.1103/PhysRevD.16.1762. URL: https://link.aps.org/doi/10.1103/PhysRevD.16.1762.

[28] Edward W. Kolb and Michael S. Turner. *The Early Universe*. Vol. 69. 1990. ISBN: 978-0-201-62674-2.

[29] Luc Darmé, Joerg Jaeckel, and Marek Lewicki. "Towards the fate of the oscillating false vacuum". In: *Phys. Rev. D* 96.5 (2017), p. 056001. DOI: 10.1103/PhysRevD.96.056001. arXiv: 1704.06445 [hep-ph].

[30] Rong-Gen Cai and Shao-Jiang Wang. "Effective picture of bubble expansion". In: (Nov. 2020). arXiv: 2011.11451 [astro-ph.CO].

[31] John Ellis et al. "Gravitational wave energy budget in strongly supercooled phase transitions". In: *JCAP* 1906.06 (2019), p. 024. DOI: 10.1088/1475-7516/2019/06/024. arXiv: 1903.09642 [hep-ph].

[32] Alan H. Guth and S. -H. H. Tye. "Phase Transitions and Magnetic Monopole Production in the Very Early Universe". In: *Phys. Rev. Lett.* 44 (14 Apr. 1980), pp. 963–963. DOI: 10.1103/PhysRevLett.44.963.2. URL: https://link.aps.org/doi/10.1103/PhysRevLett.44.963.2.

[33] John Ellis, Marek Lewicki, and Jose Miguel No. "On the Maximal Strength of a First-Order Electroweak Phase Transition and its Gravitational Wave Signal". In: *JCAP* 04 (2018). [JCAP1904,003(2019)], p. 003. DOI: 10.1088/1475-7516/2019/04/003. arXiv: 1809.08242 [hep-ph].

[34] M D Rintoul and S Torquato. "Precise determination of the critical threshold and exponents in a three-dimensional continuum percolation model". In: *Journal of Physics A: Mathematical and General* 30.16 (Aug. 1997), pp. L585–L592. DOI: 10.1088/0305-4470/30/16/005. URL: https://doi.org/10.1088%2F0305-4470%2F30%2F16%2F005.

[35] Ariel Megevand and Santiago Ramirez. "Bubble nucleation and growth in very strong cosmological phase transitions". In: *Nucl. Phys. B* 919 (2017), pp. 74–109. DOI: 10.1016/j.nuclphysb.2017.03.009. arXiv: 1611.05853 [astro-ph.CO].

[36] John Ellis, Marek Lewicki, and Jose Miguel No. "Gravitational waves from first-order cosmological phase transitions: lifetime of the sound wave source". In: *JCAP* 07 (2020), p. 050. DOI: 10.1088/1475-7516/2020/07/050. arXiv: 2003.07360 [hep-ph].

[37] Aleksandr Azatov, Daniele Barducci, and Francesco Sgarlata. "Gravitational traces of broken gauge symmetries". In: *JCAP* 07 (2020), p. 027. DOI: 10.1088/1475-7516/2020/07/027. arXiv: 1910.01124 [hep-ph].

[38] C. J. Moore, R. H. Cole, and C. P. L. Berry. "Gravitational-wave sensitivity curves". In: *Class. Quant. Grav.* 32.1 (2015), p. 015014. DOI: 10.1088/0264-9381/32/1/015014. arXiv: 1408.0740 [gr-qc].

[39] B. P. Abbott et al. "Prospects for Observing and Localizing Gravitational-Wave Transients with Advanced LIGO, Advanced Virgo and KAGRA". In: *Living Rev. Rel.* 21.1 (2018), p. 3. DOI: 10.1007/s41114-018-0012-9,10.1007/lrr-2016-1. arXiv: 1304.0670 [gr-qc].

[40] J. Aasi et al. "Advanced LIGO". In: *Class. Quant. Grav.* 32 (2015), p. 074001. DOI: 10.1088/0264-9381/32/7/074001. arXiv: 1411.4547 [gr-qc].

[41] Travis Robson, Neil J. Cornish, and Chang Liug. "The construction and use of LISA sensitivity curves". In: *Class. Quant. Grav.* 36.10 (2019), p. 105011. DOI: 10.1088/1361-6382/ab1101. arXiv: 1803.01944 [astro-ph.HE].

[42] Peter W. Graham et al. "Mid-band gravitational wave detection with precision atomic sensors". In: (Nov. 2017). arXiv: 1711.02225 [astro-ph.IM].

[43] Kent Yagi, Norihiro Tanahashi, and Takahiro Tanaka. "Probing the size of extra dimension with gravitational wave astronomy". In: *Phys. Rev.* D83 (2011), p. 084036. DOI: 10.1103/PhysRevD.83.084036. arXiv: 1101.4997 [gr-qc].

[44] Kent Yagi. "Scientific Potential of DECIGO Pathfinder and Testing GR with Space-Borne Gravitational Wave Interferometers". In: *Int. J. Mod. Phys.* D22 (2013), p. 1341013. DOI: 10.1142/S0218271813410137. arXiv: 1302.2388 [gr-qc].

[45] B. Sathyaprakash et al. "Scientific Objectives of Einstein Telescope". In: *Class. Quant. Grav.* 29 (2012). [Erratum: Class. Quant. Grav.30,079501(2013)], p. 124013. DOI: 10.1088/0264-9381/29/12/124013, 10.1088/0264-9381/30/7/079501. arXiv: 1206.0331 [gr-qc].

[46] Mark Hindmarsh et al. "Gravitational waves from the sound of a first order phase transition". In: *Phys. Rev. Lett.* 112 (2014), p. 041301. DOI: 10.1103/PhysRevLett.112.041301. arXiv: 1304.2433 [hep-ph].

[47] Mark Hindmarsh et al. "Numerical simulations of acoustically generated gravitational waves at a first order phase transition". In: *Phys. Rev. D* 92.12 (2015), p. 123009. DOI: 10.1103/PhysRevD.92.123009. arXiv: 1504.03291 [astro-ph.CO].

[48] Mark Hindmarsh et al. "Shape of the acoustic gravitational wave power spectrum from a first order phase transition". In: *Phys. Rev. D* 96.10 (2017). [Erratum: Phys.Rev.D 101, 089902 (2020)], p. 103520. DOI: 10.1103/PhysRevD.96.103520. arXiv: 1704.05871 [astro-ph.CO].

[49] Daniel Cutting, Mark Hindmarsh, and David J. Weir. "Gravitational waves from vacuum first-order phase transitions: from the envelope to the lattice". In: *Phys. Rev. D* 97.12 (2018), p. 123513. DOI: 10.1103/PhysRevD.97.123513. arXiv: 1802.05712 [astro-ph.CO].

[50] Daniel Cutting, Mark Hindmarsh, and David J. Weir. "Vorticity, kinetic energy, and suppressed gravitational wave production in strong first order phase transitions". In: *Phys. Rev. Lett.* 125.2 (2020), p. 021302. DOI: 10.1103/PhysRevLett.125.021302. arXiv: 1906.00480 [hep-ph].

[51] Oliver Gould, Satumaaria Sukuvaara, and David Weir. "Vacuum bubble collisions: From microphysics to gravitational waves". In: *Phys. Rev. D* 104.7 (2021), p. 075039. DOI: 10.1103/PhysRevD.104.075039. arXiv: 2107.05657 [astro-ph.CO].

[52] David J. Weir. "Gravitational waves from a first order electroweak phase transition: a brief review". In: *Phil. Trans. Roy. Soc. Lond. A* 376.2114 (2018), p. 20170126. DOI: 10.1098/rsta.2017.0126. arXiv: 1705.01783 [hep-ph].

[53] Mark B. Hindmarsh et al. "Phase transitions in the early universe". In: (Aug. 2020). arXiv: 2008.09136 [astro-ph.CO].

[54] Chiara Caprini et al. "Detecting gravitational waves from cosmological phase transitions with LISA: an update". In: *JCAP* 03 (2019), p. 024. DOI: 10.1088/1475-7516/2020/03/024. arXiv: 1910.13125 [astro-ph.CO].

[55] Arthur Kosowsky and Michael S. Turner. "Gravitational radiation from colliding vacuum bubbles: envelope approximation to many bubble collisions". In: *Phys. Rev.* D47 (1993), pp. 4372–4391. DOI: 10.1103/PhysRevD.47.4372. arXiv: astro-ph/9211004 [astro-ph].

[56] Marek Lewicki and Ville Vaskonen. "On bubble collisions in strongly supercooled phase transitions". In: *Phys. Dark Univ.* 30 (Dec. 2020), p. 100672. DOI: 10.1016/j.dark.2020.100672. arXiv: 1912.00997 [astro-ph.CO].

[57] Jose R. Espinosa et al. "Energy Budget of Cosmological First-order Phase Transitions". In: *JCAP* 1006 (2010), p. 028. DOI: 10.1088/1475-7516/2010/06/028. arXiv: 1004.4187 [hep-ph].

[58] Stephan J. Huber and Thomas Konstandin. "Gravitational Wave Production by Collisions: More Bubbles". In: *JCAP* 09 (2008), p. 022. DOI: 10.1088/1475-7516/2008/09/022. arXiv: 0806.1828 [hep-ph].

[59] Thomas Konstandin. "Gravitational radiation from a bulk flow model". In: *JCAP* 03.03 (2018), p. 047. DOI: 10.1088/1475-7516/2018/03/047. arXiv: 1712.06869 [astro-ph.CO].

[60] Ryusuke Jinno and Masahiro Takimoto. "Gravitational waves from bubble collisions: An analytic derivation". In: *Phys. Rev. D* 95.2 (2017), p. 024009. DOI: 10.1103/PhysRevD.95.024009. arXiv: 1605.01403 [astro-ph.CO].

[61] Ryusuke Jinno and Masahiro Takimoto. "Gravitational waves from bubble dynamics: Beyond the Envelope". In: *JCAP* 01 (2019), p. 060. DOI: 10.1088/1475-7516/2019/01/060. arXiv: 1707.03111 [hep-ph].

[62] Daniel Cutting et al. "Gravitational waves from vacuum first order phase transitions II: from thin to thick walls". In: *Phys. Rev. D* 103.2 (May 2021), p. 023531. DOI: 10.1103/PhysRevD.103.023531. arXiv: 2005.13537 [astro-ph.CO].

[63] Mark Hindmarsh. "Sound shell model for acoustic gravitational wave production at a first-order phase transition in the early Universe". In: *Phys. Rev. Lett.* 120.7 (2018), p. 071301. DOI: 10.1103/PhysRevLett.120.071301. arXiv: 1608.04735 [astro-ph.CO].

[64] Mark Hindmarsh and Mulham Hijazi. "Gravitational waves from first order cosmological phase transitions in the Sound Shell Model". In: *JCAP* 12 (2019), p. 062. DOI: 10.1088/1475-7516/2019/12/062. arXiv: 1909.10040 [astro-ph.CO].

[65] Ryusuke Jinno, Thomas Konstandin, and Henrique Rubira. "A hybrid simulation of gravitational wave production in first-order phase transitions". In: *JCAP* 04 (2021), p. 014. DOI: 10.1088/1475-7516/2021/04/014. arXiv: 2010.00971 [astro-ph.CO].

[66] John T. Giblin Jr. et al. "Gravitational Waves from Global Second Order Phase Transitions". In: *JCAP* 11 (2012), p. 006. DOI: 10.1088/1475-7516/2012/11/006. arXiv: 1111.4014 [astro-ph.CO].

[67] Daniel G. Figueroa, Mark Hindmarsh, and Jon Urrestilla. "Exact Scale-Invariant Background of Gravitational Waves from Cosmic Defects". In: *Phys. Rev. Lett.* 110.10 (2013), p. 101302. DOI: 10.1103/PhysRevLett.110.101302. arXiv: 1212.5458 [astro-ph.CO].

[68] Daniel G. Figueroa et al. "Irreducible background of gravitational waves from a cosmic defect network: update and comparison of numerical techniques". In: *Phys. Rev. D* 102.10 (2020), p. 103516. DOI: 10.1103/PhysRevD.102.103516. arXiv: 2007.03337 [astro-ph.CO].

[69] Paul Joseph Steinhardt. "Relativistic detonation waves and bubble growth in false vacuum decay". In: *Phys. Rev. D* 25 (8 Apr. 1982), pp. 2074–2085. DOI: 10.1103/PhysRevD.25.2074. URL: https://link.aps.org/doi/10.1103/PhysRevD.25.2074.

[70] Felix Giese et al. "Model-independent energy budget for LISA". In: (Oct. 2020). arXiv: 2010.09744 [astro-ph.CO].

[71] M. Laine. "Bubble growth as a detonation". In: *Phys. Rev. D* 49 (8 Apr. 1994), pp. 3847–3853. DOI: 10.1103/PhysRevD.49.3847. arXiv: hep-ph/9309242. URL: https://link.aps.org/doi/10.1103/PhysRevD.49.3847.

[72] Thomas Konstandin, Germano Nardini, and Mariano Quiros. "Gravitational Backreaction Effects on the Holographic Phase Transition". In: *Phys. Rev. D* 82 (2010), p. 083513. DOI: 10.1103/PhysRevD.82.083513. arXiv: 1007.1468 [hep-ph].

[73] L Landau and E Lifshitz. *Fluid Mechanics: Landau and Lifshitz: Course of Theoretical Physics*. Sept. 2013. ISBN: 9781483161044.

[74] Bennett Link. "Deflagration instability in the quark-hadron phase transition". In: *Phys. Rev. Lett.* 68 (16 Apr. 1992), pp. 2425–2428. DOI: 10.1103/PhysRevLett.68.2425. URL: https://link.aps.org/doi/10.1103/PhysRevLett.68.2425.

[75] Patrick Huet et al. "Hydrodynamic stability analysis of burning bubbles in electroweak theory and in QCD". In: *Phys. Rev. D* 48 (6 Sept. 1993), pp. 2477–2492. DOI: 10.1103/PhysRevD.48.2477. URL: https://link.aps.org/doi/10.1103/PhysRevD.48.2477.

[76] Ariel Megevand and Federico Agustin Membiela. "Stability of cosmological deflagration fronts". In: *Phys. Rev. D* 89.10 (2014), p. 103507. DOI: 10.1103/PhysRevD.89.103507. arXiv: 1311.2453 [astro-ph.CO].

[77] Ariel Megevand, Federico Agustin Membiela, and Alejandro D. Sanchez. "Lower bound on the electroweak wall velocity from hydrodynamic instability". In: *JCAP* 03 (2015), p. 051. DOI: 10.1088/1475-7516/2015/03/051. arXiv: 1412.8064 [hep-ph].

[78] Dietrich Bodeker and Guy D. Moore. "Can electroweak bubble walls run away?" In: *JCAP* 0905 (2009), p. 009. DOI: 10.1088/1475-7516/2009/05/009. arXiv: 0903.4099 [hep-ph].

[79] S. Yu. Khlebnikov. "Fluctuation-dissipation formula for bubble-wall velocity". In: *Phys. Rev. D* 46 (8 Oct. 1992), R3223–R3226. DOI: 10.1103/PhysRevD.46.R3223. URL: https://link.aps.org/doi/10.1103/PhysRevD.46.R3223.

[80] Peter Brockway Arnold. "One loop fluctuation - dissipation formula for bubble wall velocity". In: *Phys. Rev. D* 48 (1993), pp. 1539–1545. DOI: 10.1103/PhysRevD.48.1539. arXiv: hep-ph/9302258.

[81] Guy D. Moore and Tomislav Prokopec. "How fast can the wall move? A Study of the electroweak phase transition dynamics". In: *Phys. Rev. D* 52 (1995), pp. 7182–7204. DOI: 10.1103/PhysRevD.52.7182. arXiv: hep-ph/9506475 [hep-ph].

[82] Bao Hua Liu, Larry McLerran, and Neil Turok. "Bubble nucleation and growth at a baryon-number-producing electroweak phase transition". In: *Phys. Rev. D* 46 (6 Sept. 1992), pp. 2668–2688. DOI: 10.1103/PhysRevD.46.2668. URL: https://link.aps.org/doi/10.1103/PhysRevD.46.2668.

[83] Thomas Konstandin, Germano Nardini, and Ingo Rues. "From Boltzmann equations to steady wall velocities". In: *JCAP* 09.09 (2014), p. 028. DOI: 10.1088/1475-7516/2014/09/028. arXiv: 1407.3132 [hep-ph].

[84] Guy D. Moore and Tomislav Prokopec. "Bubble wall velocity in a first order electroweak phase transition". In: *Phys. Rev. Lett.* 75 (1995), pp. 777–780. DOI: 10.1103/PhysRevLett.75.777. arXiv: hep-ph/9503296 [hep-ph].

[85] J. Ignatius et al. "Growth of bubbles in cosmological phase transitions". In: *Phys. Rev. D* 49 (8 Apr. 1994), pp. 3854–3868. DOI: 10.1103/PhysRevD.49.3854. arXiv: astro-ph/9309059. URL: https://link.aps.org/doi/10.1103/PhysRevD.49.3854.

[86] Guy D. Moore. "Electroweak bubble wall friction: Analytic results". In: *JHEP* 03 (2000), p. 006. DOI: 10.1088/1126-6708/2000/03/006. arXiv: hep-ph/0001274.

[87] Benoit Laurent and James M. Cline. "Fluid equations for fast-moving electroweak bubble walls". In: *Phys. Rev. D* 102.6 (July 2020), p. 063516. DOI: 10.1103/PhysRevD.102.063516. arXiv: 2007.10935 [hep-ph].

[88] James M. Cline and Kimmo Kainulainen. "Electroweak baryogenesis at high bubble wall velocities". In: *Phys. Rev. D* 101.6 (2020), p. 063525. DOI: 10.1103/PhysRevD.101.063525. arXiv: 2001.00568 [hep-ph].

[89] Stefania De Curtis et al. "Bubble wall dynamics at the electroweak phase transition". In: *JHEP* 03 (Jan. 2022), p. 163. DOI: 10.1007/JHEP03(2022)163. arXiv: 2201.08220 [hep-ph].

[90] Glauber C. Dorsch, Stephan J. Huber, and Thomas Konstandin. "Bubble wall velocities in the Standard Model and beyond". In: *JCAP* 1812.12 (2018), p. 034. DOI: 10.1088/1475-7516/2018/12/034. arXiv: 1809.04907 [hep-ph].

[91] Glauber C. Dorsch, Stephan J. Huber, and Thomas Konstandin. "A sonic boom in bubble wall friction". In: (Dec. 2021). arXiv: 2112.12548 [hep-ph].

[92] Marc Barroso Mancha, Tomislav Prokopec, and Bogumila Swiezewska. "Field theoretic derivation of bubble wall force". In: *JHEP* 01 (May 2020), p. 070. DOI: 10.1007/JHEP01(2021)070. arXiv: 2005.10875 [hep-th].

[93] Wen-Yuan Ai, Bjorn Garbrecht, and Carlos Tamarit. "Bubble wall velocities in local equilibrium". In: (Sept. 2021). arXiv: 2109.13710 [hep-ph].

[94] Shyam Balaji, Michael Spannowsky, and Carlos Tamarit. "Cosmological bubble friction in local equilibrium". In: *JCAP* 03 (Oct. 2020), p. 051. DOI: 10.1088/1475-7516/2021/03/051. arXiv: 2010.08013 [hep-ph].

[95] Michael Dine et al. "Towards the theory of the electroweak phase transition". In: *Phys. Rev.* D46 (1992), pp. 550–571. DOI: 10.1103/PhysRevD.46.550. arXiv: hep-ph/9203203 [hep-ph].

[96] Dietrich Bodeker and Guy D. Moore. "Electroweak Bubble Wall Speed Limit". In: *JCAP* 1705.05 (2017), p. 025. DOI: 10.1088/1475-7516/2017/05/025. arXiv: 1703.08215 [hep-ph].

[97] S.P. Mikheev and A.Yu. Smirnov. "Neutrino Oscillations in a Variable Density Medium and Neutrino Bursts Due to the Gravitational Collapse of Stars". In: *Sov. Phys. JETP* 64 (1986), pp. 4–7. arXiv: 0706.0454 [hep-ph].

[98] Samoil Bilenky. *Introduction to the physics of massive and mixed neutrinos*. Vol. 817. 2010. DOI: 10.1007/978-3-642-14043-3.

[99] Moritz Breitbach et al. "Dark, Cold, and Noisy: Constraining Secluded Hidden Sectors with Gravitational Waves". In: *JCAP* 1907.07 (2019), p. 007. DOI: 10.1088/1475-7516/2019/07/007. arXiv: 1811.11175 [hep-ph].

[100] Stefan Höche et al. "Towards an all-orders calculation of the electroweak bubble wall velocity". In: *JCAP* 03 (July 2020), p. 009. DOI: 10.1088/1475-7516/2021/03/009. arXiv: 2007.10343 [hep-ph].

[101] Enrico Fermi. "Uber die Theorie des Stoßes zwischen Atomen und elektrisch geladenen Teilchen". In: *Zeitschrift fur Physik* 29.1 (1924), pp. 315–327. DOI: 10.1007/BF03184853.

[102] C.F. von Weizsacker. "Radiation emitted in collisions of very fast electrons". In: *Z. Phys.* 88 (1934), pp. 612–625. DOI: 10.1007/BF01333110.

[103] E.J. Williams. "Nature of the high-energy particles of penetrating radiation and status of ionization and radiation formulae". In: *Phys. Rev.* 45 (1934), pp. 729–730. DOI: 10.1103/PhysRev.45.729.

[104] Lev Landau and Evgeni Lifshitz. In: *Phys.Z.Sowjetunion* 6.1 (1934), p. 612.

[105] Michael E. Peskin and Daniel V. Schroeder. *An Introduction to quantum field theory*. Reading, USA: Addison-Wesley, 1995. ISBN: 978-0-201-50397-5.

[106] A.I. Akhiezer and V.B. Berestetskii. *Quantum electrodynamics*. New York: Interscience Publishers, Sept. 1986. ISBN: 0470018488.

[107] V.B. Berestetskii, E.M. Lifshitz, and L.P. Pitaevskii. *QUANTUM ELECTRODYNAMICS*. Vol. 4. Course of Theoretical Physics. Oxford: Pergamon Press, 1982. ISBN: 978-0-7506-3371-0.

[108] Guido Altarelli and G. Parisi. "Asymptotic Freedom in Parton Language". In: *Nucl. Phys. B* 126 (1977), pp. 298–318. DOI: 10.1016/0550-3213(77)90384-4.

[109] V.N. Gribov and L.N. Lipatov. "e+ e- pair annihilation and deep inelastic e p scattering in perturbation theory". In: *Sov. J. Nucl. Phys.* 15 (1972), pp. 675–684.

[110] Yuri L. Dokshitzer. "Calculation of the Structure Functions for Deep Inelastic Scattering and e+ e- Annihilation by Perturbation Theory in Quantum Chromodynamics." In: *Sov. Phys. JETP* 46 (1977), pp. 641–653.

[111] Alan D. Martin. "Proton structure, Partons, QCD, DGLAP and beyond". In: *Acta Phys. Polon. B* 39 (2008). Ed. by R. Fiore, A. Papa, and C. Royon, pp. 2025–2062. arXiv: 0802.0161 [hep-ph].

[112] Yann Gouttenoire, Ryusuke Jinno, and Filippo Sala. "Friction pressure on relativistic bubble walls". In: (Dec. 2021). arXiv: 2112.07686 [hep-ph].

[113] Andrea Banfi, Gavin P. Salam, and Giulia Zanderighi. "Principles of general final-state resummation and automated implementation". In: *JHEP* 03 (2005), p. 073. DOI: 10.1088/1126-6708/2005/03/073. arXiv: hep-ph/0407286.

[114] Peter Brockway Arnold, Guy D Moore, and Laurence G. Yaffe. "Transport coefficients in high temperature gauge theories. 2. Beyond leading log". In: *JHEP* 05 (2003), p. 051. DOI: 10.1088/1126-6708/2003/05/051. arXiv: hep-ph/0302165.

[115] Gianfranco Bertone and Dan Hooper. "History of dark matter". In: *Rev. Mod. Phys.* 90.4 (2018), p. 045002. DOI: 10.1103/RevModPhys.90.045002. arXiv: 1605.04909 [astro-ph.CO].

[116] F. Zwicky. "On the Masses of Nebulae and of Clusters of Nebulae". In: *apj* 86 (Oct. 1937), p. 217. DOI: 10.1086/143864.

[117] K. C. Freeman. "On the Disks of Spiral and S0 Galaxies". In: *apj* 160 (June 1970), p. 811. DOI: 10.1086/150474.

[118] D. H. Rogstad and G. S. Shostak. "Gross Properties of Five Scd Galaxies as Determined from 21-CENTIMETER Observations". In: *apj* 176 (Sept. 1972), p. 315. DOI: 10.1086/151636.

[119] V. C. Rubin, Jr. Ford W. K., and N. Thonnard. "Extended rotation curves of high-luminosity spiral galaxies. IV. Systematic dynamical properties, Sa -> Sc." In: *apjl* 225 (Nov. 1978), pp. L107–L111. DOI: 10.1086/182804.

[120] K. G. Begeman, A. H. Broeils, and R. H. Sanders. "Extended rotation curves of spiral galaxies : dark haloes and modified dynamics." In: *mnras* 249 (Apr. 1991), p. 523. DOI: 10.1093/mnras/249.3.523.

[121] N. Aghanim et al. "Planck 2018 results. VI. Cosmological parameters". In: *Astron. Astrophys.* 641 (2020). [Erratum: Astron.Astrophys. 652, C4 (2021)], A6. DOI: 10.1051/0004-6361/201833910. arXiv: 1807.06209 [astro-ph.CO].

[122] Gianfranco Bertone, Dan Hooper, and Joseph Silk. "Particle dark matter: Evidence, candidates and constraints". In: *Phys. Rept.* 405 (2005), pp. 279–390. DOI: 10.1016/j.physrep.2004.08.031. arXiv: hep-ph/0404175.

[123] Hong-Yee Chiu. "Symmetry Between Particle and Antiparticle Populations in the Universe". In: *Phys. Rev. Lett.* 17 (13 Sept. 1966), pp. 712–714. DOI: 10.1103/PhysRevLett.17.712. URL: https://link.aps.org/doi/10.1103/PhysRevLett.17.712.

[124] Mark Srednicki, Richard Watkins, and Keith A. Olive. "Calculations of Relic Densities in the Early Universe". In: *Nucl. Phys. B* 310 (1988). Ed. by M.A. Srednicki, p. 693. DOI: 10.1016/0550-3213(88)90099-5.

[125] Paolo Gondolo and Graciela Gelmini. "Cosmic abundances of stable particles: Improved analysis". In: *Nuclear Physics B* 360.1 (1991), pp. 145–179. ISSN: 0550-3213. DOI: https://doi.org/10.1016/0550-3213(91)90438-4. URL: http://www.sciencedirect.com/science/article/pii/0550321391904384.

[126] Kim Griest and David Seckel. "Three exceptions in the calculation of relic abundances". In: *Phys. Rev. D* 43 (1991), pp. 3191–3203. DOI: 10.1103/PhysRevD.43.3191.

[127] P. Hut. "Limits on Masses and Number of Neutral Weakly Interacting Particles". In: *Phys. Lett. B* 69 (1977). Ed. by M. A. Srednicki, p. 85. DOI: 10.1016/0370-2693(77)90139-3.

[128] R. Agnese et al. "New Results from the Search for Low-Mass Weakly Interacting Massive Particles with the CDMS Low Ionization Threshold Experiment". In: *Phys. Rev. Lett.* 116.7 (2016), p. 071301. DOI: 10.1103/PhysRevLett.116.071301. arXiv: 1509.02448 [astro-ph.CO].

[129] D.S. Akerib et al. "Results from a search for dark matter in the complete LUX exposure". In: *Phys. Rev. Lett.* 118.2 (2017), p. 021303. DOI: 10.1103/PhysRevLett.118.021303. arXiv: 1608.07648 [astro-ph.CO].

[130] Andi Tan et al. "Dark Matter Results from First 98.7 Days of Data from the PandaX-II Experiment". In: *Phys. Rev. Lett.* 117.12 (2016), p. 121303. DOI: 10.1103/PhysRevLett.117.121303. arXiv: 1607.07400 [hep-ex].

[131] G. Angloher et al. "Results on light dark matter particles with a low-threshold CRESST-II detector". In: *Eur. Phys. J. C* 76.1 (2016), p. 25. DOI: 10.1140/epjc/s10052-016-3877-3. arXiv: 1509.01515 [astro-ph.CO].

[132] C. Amole et al. "Dark Matter Search Results from the PICO-60 Bubble Chamber". In: *Phys. Rev. Lett.* 118.25 (2017), p. 251301. DOI: 10.1103/PhysRevLett.118.251301. arXiv: 1702.07666 [astro-ph.CO].

[133] Giorgio Arcadi et al. "The waning of the WIMP? A review of models, searches, and constraints". In: *Eur. Phys. J. C* 78.3 (2018), p. 203. DOI: 10.1140/epjc/s10052-018-5662-y. arXiv: 1703.07364 [hep-ph].

[134] Oleg Lebedev. "The Higgs Portal to Cosmology". In: (Apr. 2021). arXiv: 2104.03342 [hep-ph].

[135] Kim Griest and Marc Kamionkowski. "Unitarity limits on the mass and radius of dark-matter particles". In: *Phys. Rev. Lett.* 64 (6 Feb. 1990), pp. 615–618. DOI: 10.1103/PhysRevLett.64.615. URL: https://link.aps.org/doi/10.1103/PhysRevLett.64.615.

[136] Rupert Coy et al. "The domain of thermal dark matter candidates". In: (May 2021). arXiv: 2105.01263 [hep-ph].

[137] Chuan-Yang Xing and Shou-Hua Zhu. "Dark Matter Freeze-Out via Catalyzed Annihilation". In: *Phys. Rev. Lett.* 127.6 (2021), p. 061101. DOI: 10.1103/PhysRevLett.127.061101. arXiv: 2102.02447 [hep-ph].

[138] Eric David Kramer et al. "Heavy Thermal Dark Matter from a New Collision Mechanism". In: *Phys. Rev. Lett.* 126 (8 Feb. 2021), p. 081802. DOI: 10.1103/PhysRevLett.126.081802. URL: https://link.aps.org/doi/10.1103/PhysRevLett.126.081802.

[139] Eric David Kramer et al. "Heavy Thermal Dark Matter from a New Collision Mechanism". In: *Phys. Rev. Lett.* 126.8 (8 Feb. 2021), p. 081802. DOI: 10.1103/PhysRevLett.126.081802. arXiv: 2003.04900 [hep-ph]. URL: https://link.aps.org/doi/10.1103/PhysRevLett.126.081802.

[140] Maxim Pospelov, Adam Ritz, and Mikhail B. Voloshin. "Secluded WIMP Dark Matter". In: *Phys. Lett. B* 662 (2008), pp. 53–61. DOI: 10.1016/j.physletb.2008.02.052. arXiv: 0711.4866 [hep-ph].

[141] Hyungjin Kim and Eric Kuflik. "Superheavy Thermal Dark Matter". In: *Phys. Rev. Lett.* 123.19 (2019), p. 191801. DOI: 10.1103/PhysRevLett.123.191801. arXiv: 1906.00981 [hep-ph].

[142] R. Sekhar Chivukula et al. "A Comment on the strong interactions of color - neutral technibaryons". In: *Phys. Lett. B* 298 (1993), pp. 380–382. DOI: 10.1016/0370-2693(93)91836-C. arXiv: hep-ph/9210274.

[143] John Bagnasco, Michael Dine, and Scott D. Thomas. "Detecting technibaryon dark matter". In: *Phys. Lett. B* 320 (1994), pp. 99–104. DOI: 10.1016/0370-2693(94)90830-3. arXiv: hep-ph/9310290.

[144] Sven Bjarke Gudnason, Chris Kouvaris, and Francesco Sannino. "Dark Matter from new Technicolor Theories". In: *Phys. Rev. D* 74 (2006), p. 095008. DOI: 10.1103/PhysRevD.74.095008. arXiv: hep-ph/0608055.

[145] Roshan Foadi, Mads T. Frandsen, and Francesco Sannino. "Technicolor Dark Matter". In: *Phys. Rev. D* 80 (2009), p. 037702. DOI: 10.1103/PhysRevD.80.037702. arXiv: 0812.3406 [hep-ph].

[146] Junhai Kang and Markus A. Luty. "Macroscopic Strings and 'Quirks' at Colliders". In: *JHEP* 11 (2009), p. 065. DOI: 10.1088/1126-6708/2009/11/065. arXiv: 0805.4642 [hep-ph].

[147] Graham D. Kribs et al. "Quirky Composite Dark Matter". In: *Phys. Rev. D* 81 (2010), p. 095001. DOI: 10.1103/PhysRevD.81.095001. arXiv: 0909.2034 [hep-ph].

[148] Lawrence J. Hall et al. "Freeze-In Production of FIMP Dark Matter". In: *JHEP* 03 (2010), p. 080. DOI: 10.1007/JHEP03(2010)080. arXiv: 0911.1120 [hep-ph].

[149] Xiaoyong Chu et al. "Thermal and non-thermal production of dark matter via Z'-portal(s)". In: *JCAP* 01 (2014), p. 034. DOI: 10.1088/1475-7516/2014/01/034. arXiv: 1306.4677 [hep-ph].

[150] Luc Darmé et al. "Forbidden frozen-in dark matter". In: *JHEP* 11 (2019), p. 159. DOI: 10.1007/JHEP11(2019)159. arXiv: 1908.05685 [hep-ph].

[151] Daniel J. H. Chung, Edward W. Kolb, and Antonio Riotto. "Nonthermal supermassive dark matter". In: *Phys. Rev. Lett.* 81 (1998), pp. 4048–4051. DOI: 10.1103/PhysRevLett.81.4048. arXiv: hep-ph/9805473.

[152] Daniel J.H. Chung, Edward W. Kolb, and Antonio Riotto. "Superheavy dark matter". In: *Phys. Rev. D* 59 (1998), p. 023501. DOI: 10.1103/PhysRevD.59.023501. arXiv: hep-ph/9802238.

[153] Rouzbeh Allahverdi, Koushik Dutta, and Anshuman Maharana. "Constraining Non-thermal Dark Matter by CMB". In: *JCAP* 10 (2018), p. 038. DOI: 10.1088/1475-7516/2018/10/038. arXiv: 1808.02659 [astro-ph.CO].

[154] Dan Hooper, Gordan Krnjaic, and Samuel D. McDermott. "Dark Radiation and Superheavy Dark Matter from Black Hole Domination". In: *JHEP* 08 (2019), p. 001. DOI: 10.1007/JHEP08(2019)001. arXiv: 1905.01301 [hep-ph].

[155] Rouzbeh Allahverdi and Jacek K. Osiński. "Early Matter Domination from Long-Lived Particles in the Visible Sector". In: (Aug. 2021). arXiv: 2108.13136 [hep-ph].

[156] Michael J. Baker and Joachim Kopp. "Dark Matter Decay between Phase Transitions at the Weak Scale". In: *Phys. Rev. Lett.* 119.6 (2017), p. 061801. DOI: 10.1103/PhysRevLett.119.061801. arXiv: 1608.07578 [hep-ph].

[157] Michael J. Baker and Lukas Mittnacht. "Variations on the Vev Flip-Flop: Instantaneous Freeze-out and Decaying Dark Matter". In: *JHEP* 05 (2019), p. 070. DOI: 10.1007/JHEP05(2019)070. arXiv: 1811.03101 [hep-ph].

[158] Lucien Heurtier and Hervé Partouche. "Spontaneous freeze out of dark matter from an early thermal phase transition". In: *Phys. Rev. D* 101.4 (4 Feb. 2020), p. 043527. DOI: 10.1103/PhysRevD.101.043527. arXiv: 1912.02828 [hep-ph]. URL: https://link.aps.org/doi/10.1103/PhysRevD.101.043527.

[159] Ligong Bian and Yi-Lei Tang. "Thermally modified sterile neutrino portal dark matter and gravitational waves from phase transition: The Freeze-in case". In: *JHEP* 12 (2018), p. 006. DOI: 10.1007/JHEP12(2018)006. arXiv: 1810.03172 [hep-ph].

[160] Timothy Cohen, David E. Morrissey, and Aaron Pierce. "Changes in Dark Matter Properties After Freeze-Out". In: *Phys. Rev. D* 78 (2008), p. 111701. DOI: 10.1103/PhysRevD.78.111701. arXiv: 0808.3994 [hep-ph].

[161] David N. Schramm. "Phase transitions and dark matter problems". In: *Nuclear Physics B* 252 (1985), pp. 53–72. ISSN: 0550-3213. DOI: https://doi.org/10.1016/0550-3213(85)90425-0. URL: http://www.sciencedirect.com/science/article/pii/0550321385904250.

[162] Lam Hui and Ewan D. Stewart. "Superheavy dark matter from thermal inflation". In: *Phys. Rev. D* 60 (1999), p. 023518. DOI: 10.1103/PhysRevD.60.023518. arXiv: hep-ph/9812345.

[163] Daniel Chung, Andrew Long, and Lian-Tao Wang. "Probing the Cosmological Constant and Phase Transitions with Dark Matter". In: *Phys. Rev. D* 84 (2011), p. 043523. DOI: 10.1103/PhysRevD.84.043523. arXiv: 1104.5034 [astro-ph.CO].

[164] Daniel J.H. Chung and Andrew J. Long. "Cosmological Constant, Dark Matter, and Electroweak Phase Transition". In: *Phys. Rev. D* 84 (2011), p. 103513. DOI: 10.1103/PhysRevD.84.103513. arXiv: 1108.5193 [astro-ph.CO].

[165] Thomas Hambye, Alessandro Strumia, and Daniele Teresi. "Super-cool Dark Matter". In: *JHEP* 08 (2018), p. 188. DOI: 10.1007/JHEP08(2018)188. arXiv: 1805.01473 [hep-ph].

[166] Richard Watkins and Lawrence M. Widrow. "Aspects of reheating in first order inflation". In: *Nucl. Phys. B* 374 (1992), pp. 446–468. DOI: 10.1016/0550-3213(92)90362-F.

[167] Adam Falkowski and Jose M. No. "Non-thermal Dark Matter Production from the Electroweak Phase Transition: Multi-TeV WIMPs and 'Baby-Zillas'". In: *JHEP* 02 (2013), p. 034. DOI: 10.1007/JHEP02(2013)034. arXiv: 1211.5615 [hep-ph].

[168] Michael J. Baker, Joachim Kopp, and Andrew J. Long. "Filtered Dark Matter at a First Order Phase Transition". In: *Phys. Rev. Lett.* 125.15 (15 Oct. 2020), p. 151102. DOI: 10.1103/PhysRevLett.125.151102. arXiv: 1912.02830 [hep-ph]. URL: https://link.aps.org/doi/10.1103/PhysRevLett.125.151102.

[169] Dongjin Chway, Tae Hyun Jung, and Chang Sub Shin. "Dark matter filtering-out effect during a first-order phase transition". In: *Phys. Rev. D* 101.9 (2020), p. 095019. DOI: 10.1103/PhysRevD.101.095019. arXiv: 1912.04238 [hep-ph].

[170] Danny Marfatia and Po-Yan Tseng. "Gravitational wave signals of dark matter freeze-out". In: (June 2020). arXiv: 2006.07313 [hep-ph].

[171] Pouya Asadi et al. "Thermal Squeezeout of Dark Matter". In: (Mar. 2021). arXiv: 2103.09827 [hep-ph].

[172] Pouya Asadi et al. "Accidentally Asymmetric Dark Matter". In: (Mar. 2021). arXiv: 2103.09822 [hep-ph].

[173] Iason Baldes, Yann Gouttenoire, and Filippo Sala. "String Fragmentation in Supercooled Confinement and Implications for Dark Matter". In: *JHEP* 04 (July 2021), p. 278. DOI: 10.1007/JHEP04(2021)278. arXiv: 2007.08440 [hep-ph].

[174] Iason Baldes et al. "Supercool Composite Dark Matter beyond 100 TeV". In: (Oct. 2021). arXiv: 2110.13926 [hep-ph].

[175] Giorgio Arcadi, Abdelhak Djouadi, and Martti Raidal. "Dark Matter through the Higgs portal". In: *Phys. Rept.* 842 (2020), pp. 1–180. DOI: 10.1016/j.physrep.2019.11.003. arXiv: 1903.03616 [hep-ph].

[176] David H. Lyth and Ewan D. Stewart. "Thermal inflation and the moduli problem". In: *Phys. Rev. D* 53 (1996), pp. 1784–1798. DOI: 10.1103/PhysRevD.53.1784. arXiv: hep-ph/9510204.

[177] Katsuji Yamamoto. "Phase Transition Associated With Intermediate Gauge Symmetry Breaking in Superstring Models". In: *Phys. Lett. B* 168 (1986), pp. 341–346. DOI: 10.1016/0370-2693(86)91641-2.

[178] Ryuji Daido, Fuminobu Takahashi, and Wen Yin. "The ALP miracle: unified inflaton and dark matter". In: *JCAP* 05 (2017), p. 044. DOI: 10.1088/1475-7516/2017/05/044. arXiv: 1702.03284 [hep-ph].

[179] Fuminobu Takahashi and Wen Yin. "ALP inflation and Big Bang on Earth". In: *JHEP* 07 (2019), p. 095. DOI: 10.1007/JHEP07(2019)095. arXiv: 1903.00462 [hep-ph].

[180] Takeo Moroi and Lisa Randall. "Wino cold dark matter from anomaly mediated SUSY breaking". In: *Nucl. Phys. B* 570 (2000), pp. 455–472. DOI: 10.1016/S0550-3213(99)00748-8. arXiv: hep-ph/9906527.

[181] Kwang Sik Jeong, Masatoshi Shimosuka, and Masahiro Yamaguchi. "Light Higgsino in Heavy Gravitino Scenario with Successful Electroweak Symmetry Breaking". In: *JHEP* 09 (2012), p. 050. DOI: 10.1007/JHEP09(2012)050. arXiv: 1112.5293 [hep-ph].

[182] A. Sommerfeld. "Über die Beugung und Bremsung der Elektronen". In: *Annalen der Physik* 403.3 (1931), pp. 257–330. DOI: https://doi.org/10.1002/andp.19314030302. eprint: https://onlinelibrary.wiley.com/doi/pdf/10.1002/andp.19314030302. URL: https://onlinelibrary.wiley.com/doi/abs/10.1002/andp.19314030302.

[183] Jonathan L. Feng, Manoj Kaplinghat, and Hai-Bo Yu. "Halo Shape and Relic Density Exclusions of Sommerfeld-Enhanced Dark Matter Explanations of Cosmic Ray Excesses". In: *Phys. Rev. Lett.* 104 (2010), p. 151301. DOI: 10.1103/PhysRevLett.104.151301. arXiv: 0911.0422 [hep-ph].

[184] Junji Hisano, S. Matsumoto, and Mihoko M. Nojiri. "Unitarity and higher order corrections in neutralino dark matter annihilation into two photons". In: *Phys. Rev. D* 67 (2003), p. 075014. DOI: 10.1103/PhysRevD.67.075014. arXiv: hep-ph/0212022.

[185] Junji Hisano, Shigeki Matsumoto, and Mihoko M. Nojiri. "Explosive dark matter annihilation". In: *Phys. Rev. Lett.* 92 (2004), p. 031303. DOI: 10.1103/PhysRevLett.92.031303. arXiv: hep-ph/0307216.

[186] Marco Cirelli, Alessandro Strumia, and Matteo Tamburini. "Cosmology and Astrophysics of Minimal Dark Matter". In: *Nucl. Phys. B* 787 (2007), pp. 152–175. DOI: 10.1016/j.nuclphysb.2007.07.023. arXiv: 0706.4071 [hep-ph].

[187] Nima Arkani-Hamed et al. "A Theory of Dark Matter". In: *Phys. Rev. D* 79 (2009), p. 015014. DOI: 10.1103/PhysRevD.79.015014. arXiv: 0810.0713 [hep-ph].

[188] E. Aprile et al. "Constraining the spin-dependent WIMP-nucleon cross sections with XENON1T". In: *Phys. Rev. Lett.* 122.14 (2019), p. 141301. DOI: 10.1103/PhysRevLett.122.141301. arXiv: 1902.03234 [astro-ph.CO].

[189] E. Aprile et al. "Projected WIMP Sensitivity of the XENONnT Dark Matter Experiment". In: *JCAP* 11 (2020), p. 031. DOI: 10.1088/1475-7516/2020/11/031. arXiv: 2007.08796 [physics.ins-det].

[190] J. Aalbers et al. "DARWIN: towards the ultimate dark matter detector". In: *JCAP* 11 (2016), p. 017. DOI: 10.1088/1475-7516/2016/11/017. arXiv: 1606.07001 [astro-ph.IM].

[191] Ankit Beniwal et al. "Combined analysis of effective Higgs portal dark matter models". In: *Phys. Rev. D* 93.11 (2016), p. 115016. DOI: 10.1103/PhysRevD.93.115016. arXiv: 1512.06458 [hep-ph].

[192] Thomas Konstandin and Geraldine Servant. "Cosmological Consequences of Nearly Conformal Dynamics at the TeV scale". In: *JCAP* 1112 (2011), p. 009. DOI: 10.1088/1475-7516/2011/12/009. arXiv: 1104.4791 [hep-ph].

[193] Pietro Baratella, Alex Pomarol, and Fabrizio Rompineve. "The Supercooled Universe". In: *JHEP* 03 (2019), p. 100. DOI: 10.1007/JHEP03(2019)100. arXiv: 1812.06996 [hep-ph].

[194] Benedict von Harling and Geraldine Servant. "QCD-induced Electroweak Phase Transition". In: *JHEP* 01 (2018), p. 159. DOI: 10.1007/JHEP01(2018)159. arXiv: 1711.11554 [hep-ph].

[195] Iason Baldes, Yann Gouttenoire, and Filippo Sala. "Hot and Heavy Dark Matter from Supercooling". In: (July 2022). arXiv: 2207.05096 [hep-ph].

[196] Pasquale Di Bari. "On the origin of matter in the Universe". In: (July 2021). arXiv: 2107.13750 [hep-ph].

[197] P.A.R. Ade et al. "Planck 2015 results. XIII. Cosmological parameters". In: *Astron. Astrophys.* 594 (2016), A13. DOI: 10.1051/0004-6361/201525830. arXiv: 1502.01589 [astro-ph.CO].

[198] A. D. Sakharov. "Violation of CP Invariance, C asymmetry, and baryon asymmetry of the universe". In: *Pisma Zh. Eksp. Teor. Fiz.* 5.5 (1967). [Usp. Fiz. Nauk161,no.5,61(1991)], pp. 32–35. DOI: 10.1070/PU1991v034n05ABEH002497.

[199] Mark Trodden and Sean M. Carroll. "TASI lectures: Introduction to cosmology". In: *Theoretical Advanced Study Institute in Elementary Particle Physics (TASI 2002): Particle Physics and Cosmology: The Quest for Physics Beyond the Standard Model(s)*. Jan. 2004, pp. 703–793. arXiv: astro-ph/0401547.

[200] A. D. Dolgov. "NonGUT baryogenesis". In: *Phys. Rept.* 222 (1992), pp. 309–386. DOI: 10.1016/0370-1573(92)90107-B.

[201] Gerard 't Hooft. "Symmetry Breaking Through Bell-Jackiw Anomalies". In: *Phys. Rev. Lett.* 37 (1976). Ed. by Mikhail A. Shifman, pp. 8–11. DOI: 10.1103/PhysRevLett.37.8.

[202] Guy D. Moore. "Sphaleron rate in the symmetric electroweak phase". In: *Phys. Rev. D* 62 (8 Sept. 2000), p. 085011. DOI: 10.1103/PhysRevD.62.085011. URL: https://link.aps.org/doi/10.1103/PhysRevD.62.085011.

[203] Jeffrey A. Harvey and Michael S. Turner. "Cosmological baryon and lepton number in the presence of electroweak fermion number violation". In: *Phys. Rev. D* 42 (1990), pp. 3344–3349. DOI: 10.1103/PhysRevD.42.3344.

[204] Antonio Riotto. "Theories of baryogenesis". In: *ICTP Summer School in High-Energy Physics and Cosmology*. July 1998. arXiv: hep-ph/9807454.

[205] Dietrich Bödeker and Wilfried Buchmüller. "Baryogenesis from the weak scale to the grand unification scale". In: (Sept. 2020). arXiv: 2009.07294 [hep-ph].

[206] Ian Affleck and Michael Dine. "A new mechanism for baryogenesis". In: *Nuclear Physics B* 249.2 (1985), pp. 361–380. ISSN: 0550-3213. DOI: https://doi.org/10.1016/0550-3213(85)90021-5. URL: http://www.sciencedirect.com/science/article/pii/0550321385900215.

[207] Michael Dine, Lisa Randall, and Scott D. Thomas. "Baryogenesis from flat directions of the supersymmetric standard model". In: *Nucl. Phys. B* 458 (1996), pp. 291–326. DOI: 10.1016/0550-3213(95)00538-2. arXiv: hep-ph/9507453.

[208] Kari Enqvist and Anupam Mazumdar. "Cosmological consequences of MSSM flat directions". In: *Phys. Rept.* 380 (2003), pp. 99–234. DOI: 10.1016/S0370-1573(03)00119-4. arXiv: hep-ph/0209244.

[209] Michael Dine and Alexander Kusenko. "The Origin of the matter - antimatter asymmetry". In: *Rev. Mod. Phys.* 76 (2003), p. 1. DOI: 10.1103/RevModPhys.76.1. arXiv: hep-ph/0303065.

[210] Raymond T. Co and Keisuke Harigaya. "Axiogenesis". In: *Phys. Rev. Lett.* 124.11 (2020), p. 111602. DOI: 10.1103/PhysRevLett.124.111602. arXiv: 1910.02080 [hep-ph].

[211] Raymond T. Co et al. "Lepto-Axiogenesis". In: *JHEP* 03 (2021), p. 017. DOI: 10.1007/JHEP03(2021)017. arXiv: 2006.05687 [hep-ph].

[212] Kaloian D. Lozanov and Mustafa A. Amin. "End of inflation, oscillons, and matter-antimatter asymmetry". In: *Phys. Rev.* D90.8 (2014), p. 083528. DOI: 10.1103/PhysRevD.90.083528. arXiv: 1408.1811 [hep-ph].

[213] Graham White et al. "Detectable Gravitational Wave Signals from Affleck-Dine Baryogenesis". In: (May 2021). arXiv: 2105.11655 [hep-ph].

[214] Motohiko Yoshimura. "Unified Gauge Theories and the Baryon Number of the Universe". In: *Phys. Rev. Lett.* 41 (1978). [Erratum: Phys.Rev.Lett. 42, 746 (1979)], pp. 281–284. DOI: 10.1103/PhysRevLett.41.281.

[215] M. Fukugita and T. Yanagida. "Barygenesis without grand unification". In: *Physics Letters B* 174.1 (1986), pp. 45–47. ISSN: 0370-2693. DOI: https://doi.org/10.1016/0370-2693(86)91126-3. URL: https://www.sciencedirect.com/science/article/pii/0370269386911263.

[216] Chee Sheng Fong, Enrico Nardi, and Antonio Riotto. "Leptogenesis in the Universe". In: *Adv. High Energy Phys.* 2012 (2012), p. 158303. DOI: 10.1155/2012/158303. arXiv: 1301.3062 [hep-ph].

[217] Karin Dick et al. "Leptogenesis with Dirac neutrinos". In: *Phys. Rev. Lett.* 84 (2000), pp. 4039–4042. DOI: 10.1103/PhysRevLett.84.4039. arXiv: hep-ph/9907562.

[218] Hitoshi Murayama and Aaron Pierce. "Realistic Dirac leptogenesis". In: *Phys. Rev. Lett.* 89 (2002), p. 271601. DOI: 10.1103/PhysRevLett.89.271601. arXiv: hep-ph/0206177.

[219] George Lazarides and Q. Shafi. "Origin of matter in the inflationary cosmology". In: *Phys. Lett. B* 258 (1991), pp. 305–309. DOI: 10.1016/0370-2693(91)91090-I.

[220] T. Asaka et al. "Leptogenesis in inflaton decay". In: *Phys. Lett. B* 464 (1999), pp. 12–18. DOI: 10.1016/S0370-2693(99)01020-5. arXiv: hep-ph/9906366.

[221] Lotfi Boubekeur et al. "Leptogenesis and rescattering in supersymmetric models". In: *Phys. Rev. D* 67 (4 Feb. 2003), p. 043515. DOI: 10.1103/PhysRevD.67.043515. URL: https://link.aps.org/doi/10.1103/PhysRevD.67.043515.

[222] G. F. Giudice et al. "Production of massive fermions at preheating and leptogenesis". In: *JHEP* 08 (1999), p. 014. DOI: 10.1088/1126-6708/1999/08/014. arXiv: hep-ph/9905242.

[223] Andrew G. Cohen and David B. Kaplan. "SPONTANEOUS BARYOGENESIS". In: *Nucl. Phys. B* 308 (1988), pp. 913–928. DOI: 10.1016/0550-3213(88)90134-4.

[224] Andrew G. Cohen and David B. Kaplan. "Spontaneous baryogenesis". In: *Nuclear Physics B* 308.4 (1988), pp. 913–928. ISSN: 0550-3213. DOI: https://doi.org/10.1016/0550-3213(88)90134-4. URL: http://www.sciencedirect.com/science/article/pii/0550321388901344.

[225] Ryuji Daido, Naoya Kitajima, and Fuminobu Takahashi. "Axion domain wall baryogenesis". In: *JCAP* 07 (2015), p. 046. DOI: 10.1088/1475-7516/2015/07/046. arXiv: 1504.07917 [hep-ph].

[226] Evgeny K. Akhmedov, V. A. Rubakov, and A. Yu. Smirnov. "Baryogenesis via neutrino oscillations". In: *Phys. Rev. Lett.* 81 (1998), pp. 1359–1362. DOI: 10.1103/PhysRevLett.81.1359. arXiv: hep-ph/9803255.

[227] Brian Shuve and Itay Yavin. "Baryogenesis through Neutrino Oscillations: A Unified Perspective". In: *Phys. Rev. D* 89.7 (2014), p. 075014. DOI: 10.1103/PhysRevD.89.075014. arXiv: 1401.2459 [hep-ph].

[228] Takehiko Asaka et al. "Initial condition for baryogenesis via neutrino oscillation". In: *Phys. Rev. D* 96.8 (2017), p. 083010. DOI: 10.1103/PhysRevD.96.083010. arXiv: 1704.02692 [hep-ph].

[229] Ya. B. Zeldovich. "Charge Asymmetry of the Universe Due to Black Hole Evaporation and Weak Interaction Asymmetry". In: *Pisma Zh. Eksp. Teor. Fiz.* 24 (1976), pp. 29–32.

[230] Michael S. Turner. "Baryon production by primordial black holes". In: *Physics Letters B* 89.1 (1979), pp. 155–159. ISSN: 0370-2693. DOI: https://doi.org/10.1016/0370-2693(79)90095-9. URL: https://www.sciencedirect.com/science/article/pii/0370269379900959.

[231] Daniel Baumann, Paul J. Steinhardt, and Neil Turok. "Primordial Black Hole Baryogenesis". In: (Mar. 2007). arXiv: hep-th/0703250.

[232] Glennys R. Farrar and Gabrijela Zaharijas. "Dark matter and the baryon asymmetry". In: *Phys. Rev. Lett.* 96 (2006), p. 041302. DOI: 10.1103/PhysRevLett.96.041302. arXiv: hep-ph/0510079.

[233] David B. Kaplan. "Single explanation for both baryon and dark matter densities". In: *Phys. Rev. Lett.* 68 (6 Feb. 1992), pp. 741–743. DOI: 10.1103/PhysRevLett.68.741. URL: https://link.aps.org/doi/10.1103/PhysRevLett.68.741.

[234] S.M. Barr, R. Sekhar Chivukula, and Edward Farhi. "Electroweak fermion number violation and the production of stable particles in the early universe". In: *Physics Letters B* 241.3 (1990), pp. 387–391. ISSN: 0370-2693. DOI: https://doi.org/10.1016/0370-2693(90)91661-T. URL: https://www.sciencedirect.com/science/article/pii/037026939091661T.

[235] Hooman Davoudiasl et al. "Unified Origin for Baryonic Visible Matter and Antibaryonic Dark Matter". In: *Phys. Rev. Lett.* 105 (21 Nov. 2010), p. 211304. DOI: 10.1103/PhysRevLett.105.211304. URL: https://link.aps.org/doi/10.1103/PhysRevLett.105.211304.

[236] Xiaoyong Chu et al. "Dark freeze-out cogenesis". In: *JHEP* 03 (2022), p. 031. DOI: 10.1007/JHEP03(2022)031. arXiv: 2112.10784 [hep-ph].

[237] N. Haba and S. Matsumoto. "Baryogenesis from Dark Sector". In: *Prog. Theor. Phys.* 125 (2011), pp. 1311–1316. DOI: 10.1143/PTP.125.1311. arXiv: 1008.2487 [hep-ph].

[238] Jessie Shelton and Kathryn M. Zurek. "Darkogenesis: A baryon asymmetry from the dark matter sector". In: *Phys. Rev. D* 82 (2010), p. 123512. DOI: 10.1103/PhysRevD.82.123512. arXiv: 1008.1997 [hep-ph].

[239] Andrey Katz and Antonio Riotto. "Baryogenesis and Gravitational Waves from Runaway Bubble Collisions". In: *JCAP* 11 (2016), p. 011. DOI: 10.1088/1475-7516/2016/11/011. arXiv: 1608.00583 [hep-ph].

[240] Sebastian Bruggisser, Thomas Konstandin, and Geraldine Servant. "CP-violation for Electroweak Baryogenesis from Dynamical CKM Matrix". In: *JCAP* 11 (2017), p. 034. DOI: 10.1088/1475-7516/2017/11/034. arXiv: 1706.08534 [hep-ph].

[241] Geraldine Servant. "The serendipity of electroweak baryogenesis". In: *Phil. Trans. Roy. Soc. Lond. A* 376.2114 (2018), p. 20170124. DOI: 10.1098/rsta.2017.0124. arXiv: 1807.11507 [hep-ph].

[242] Germano Nardini, Mariano Quiros, and Andrea Wulzer. "A Confining Strong First-Order Electroweak Phase Transition". In: *JHEP* 09 (2007), p. 077. DOI: 10.1088/1126-6708/2007/09/077. arXiv: 0706.3388 [hep-ph].

[243] Chiara Caprini and Jose M. No. "Supersonic Electroweak Baryogenesis: Achieving Baryogenesis for Fast Bubble Walls". In: *JCAP* 01 (2012), p. 031. DOI: 10.1088/1475-7516/2012/01/031. arXiv: 1111.1726 [hep-ph].

[244] Jose R. Espinosa et al. "Electroweak Baryogenesis in Non-minimal Composite Higgs Models". In: *JCAP* 01 (2012), p. 012. DOI: 10.1088/1475-7516/2012/01/012. arXiv: 1110.2876 [hep-ph].

[245] Geraldine Servant. "Baryogenesis from Strong CP Violation and the QCD Axion". In: *Phys. Rev. Lett.* 113.17 (2014), p. 171803. DOI: 10.1103/PhysRevLett.113.171803. arXiv: 1407.0030 [hep-ph].

[246] A. Tranberg et al. "Cold electroweak baryogenesis with Standard Model CP violation". In: *Physics Letters B* 690.3 (2010), pp. 207–212. ISSN: 0370-2693. DOI: https://doi.org/10.1016/j.physletb.2010.05.030. URL: http://www.sciencedirect.com/science/article/pii/S0370269310006222.

[247] Jan Smit and Anders Tranberg. "Chern-Simons number asymmetry from CP violation during tachyonic preheating". In: *5th Internationa Conference on Strong and Electroweak Matter*. Oct. 2002. DOI: 10.1142/9789812704498_0071. arXiv: hep-ph/0210348.

[248] Juan Garcia-Bellido, Margarita Garcia-Perez, and Antonio Gonzalez-Arroyo. "Chern-Simons production during preheating in hybrid inflation models". In: *Phys. Rev. D* 69 (2004), p. 023504. DOI: 10.1103/PhysRevD.69.023504. arXiv: hep-ph/0304285.

[249] Anders Tranberg and Jan Smit. "Baryon asymmetry from electroweak tachyonic preheating". In: *JHEP* 11 (2003), p. 016. DOI: 10.1088/1126-6708/2003/11/016. arXiv: hep-ph/0310342.

[250] B. J. W. van Tent, Jan Smit, and Anders Tranberg. "Electroweak scale inflation, inflaton Higgs mixing and the scalar spectral index". In: *JCAP* 07 (2004), p. 003. DOI: 10.1088/1475-7516/2004/07/003. arXiv: hep-ph/0404128.

[251] Meindert van der Meulen et al. "Chern-Simons and winding number in a tachyonic electroweak transition". In: *JHEP* 02 (2006), p. 029. DOI: 10.1088/1126-6708/2006/02/029. arXiv: hep-ph/0511080.

[252] Kari Enqvist et al. "Fast Electroweak Symmetry Breaking and Cold Electroweak Baryogenesis". In: *JCAP* 09 (2010), p. 019. DOI: 10.1088/1475-7516/2010/09/019. arXiv: 1005.0752 [astro-ph.CO].

[253] Zong-Gang Mou, Paul M. Saffin, and Anders Tranberg. "Cold Baryogenesis from first principles in the Two-Higgs Doublet model with Fermions". In: *JHEP* 06 (2015), p. 163. DOI: 10.1007/JHEP06(2015)163. arXiv: 1505.02692 [hep-ph].

[254] V.A. Kuzmin, V.A. Rubakov, and M.E. Shaposhnikov. "On the Anomalous Electroweak Baryon Number Nonconservation in the Early Universe". In: *Phys. Lett. B* 155 (1985), p. 36. DOI: 10.1016/0370-2693(85)91028-7.

[255] M.E. Shaposhnikov. "Possible Appearance of the Baryon Asymmetry of the Universe in an Electroweak Theory". In: *JETP Lett.* 44 (1986), pp. 465–468.

[256] David E. Morrissey and Michael J. Ramsey-Musolf. "Electroweak baryogenesis". In: *New J. Phys.* 14 (2012), p. 125003. DOI: 10.1088/1367-2630/14/12/125003. arXiv: 1206.2942 [hep-ph].

[257] Sylvie Braibant, Yves Brihaye, and Jutta Kunz. "Sphalerons at finite temperature". In: *Int. J. Mod. Phys. A* 8 (1993), pp. 5563–5574. DOI: 10.1142/S0217751X93002198. arXiv: hep-ph/9302314.

[258] S.Yu. Khlebnikov and M.E. Shaposhnikov. "The statistical theory of anomalous fermion number non-conservation". In: *Nuclear Physics B* 308.4 (1988), pp. 885–912. ISSN: 0550-3213. DOI: https://doi.org/10.1016/0550-3213(88)90133-2. URL: https://www.sciencedirect.com/science/article/pii/0550321388901332.

[259] K. Kajantie et al. "Is there a hot electroweak phase transition at m(H) larger or equal to m(W)?" In: *Phys. Rev. Lett.* 77 (14 Sept. 1996), pp. 2887–2890. DOI: 10.1103/PhysRevLett.77.2887. arXiv: hep-ph/9605288 [hep-ph]. URL: https://link.aps.org/doi/10.1103/PhysRevLett.77.2887.

[260] M. B. Gavela et al. "Standard model CP violation and baryon asymmetry". In: *Mod. Phys. Lett. A* 9 (1994), pp. 795–810. DOI: 10.1142/S0217732394000629. arXiv: hep-ph/9312215.

[261] Patrick Huet and Eric Sather. "Electroweak baryogenesis and standard model CP violation". In: *Phys. Rev. D* 51 (1995), pp. 379–394. DOI: 10.1103/PhysRevD.51.379. arXiv: hep-ph/9404302.

[262] M. B. Gavela et al. "Standard model CP violation and baryon asymmetry. Part 2: Finite temperature". In: *Nucl. Phys. B* 430 (1994), pp. 382–426. DOI: 10.1016/0550-3213(94)00410-2. arXiv: hep-ph/9406289.

[263] A. E. Nelson, D. B. Kaplan, and Andrew G. Cohen. "Why there is something rather than nothing: Matter from weak interactions". In: *Nucl. Phys. B* 373 (1992), pp. 453–478. DOI: 10.1016/0550-3213(92)90440-M.

[264] Marcela Carena, M. Quiros, and C. E. M. Wagner. "Opening the window for electroweak baryogenesis". In: *Phys. Lett. B* 380 (1996), pp. 81–91. DOI: 10.1016/0370-2693(96)00475-3. arXiv: hep-ph/9603420.

[265] James M. Cline. "Is electroweak baryogenesis dead?" In: *Phil. Trans. Roy. Soc. Lond. A* 376.2114 (2018). Ed. by Etienne Auge, Jacques Dumarchez, and Jean Tran Thanh Van, p. 20170116. DOI: 10.1098/rsta.2017.0116. arXiv: 1704.08911 [hep-ph].

[266] Sebastian Bruggisser et al. "Electroweak Phase Transition and Baryogenesis in Composite Higgs Models". In: *JHEP* 12 (2018), p. 099. DOI: 10.1007/JHEP12(2018)099. arXiv: 1804.07314 [hep-ph].

[267] Sebastian Bruggisser et al. "Baryon Asymmetry from a Composite Higgs Boson". In: *Phys. Rev. Lett.* 121.13 (2018), p. 131801. DOI: 10.1103/PhysRevLett.121.131801. arXiv: 1803.08546 [hep-ph].

[268] Silvia Pascoli, Jessica Turner, and Ye-Ling Zhou. "Baryogenesis via leptonic CP-violating phase transition". In: *Phys. Lett. B* 780 (2018), pp. 313–318. DOI: 10.1016/j.physletb.2018.03.011. arXiv: 1609.07969 [hep-ph].

[269] Andrew J. Long, Andrea Tesi, and Lian-Tao Wang. "Baryogenesis at a Lepton-Number-Breaking Phase Transition". In: *JHEP* 10 (2017), p. 095. DOI: 10.1007/JHEP10(2017)095. arXiv: 1703.04902 [hep-ph].

[270] M. Carena et al. "The Baryogenesis Window in the MSSM". In: *Nucl. Phys. B* 812 (2009), pp. 243–263. DOI: 10.1016/j.nuclphysb.2008.12.014. arXiv: 0809.3760 [hep-ph].

[271] David Curtin, Prerit Jaiswal, and Patrick Meade. "Excluding Electroweak Baryogenesis in the MSSM". In: *JHEP* 08 (2012), p. 005. DOI: 10.1007/JHEP08(2012)005. arXiv: 1203.2932 [hep-ph].

[272] Stefan Liebler, Stefano Profumo, and Tim Stefaniak. "Light Stop Mass Limits from Higgs Rate Measurements in the MSSM: Is MSSM Electroweak Baryogenesis Still Alive After All?" In: *JHEP* 04 (2016), p. 143. DOI: 10.1007/JHEP04(2016)143. arXiv: 1512.09172 [hep-ph].

[273] S. V. Demidov, D. S. Gorbunov, and D. V. Kirpichnikov. "Split NMSSM with electroweak baryogenesis". In: *JHEP* 11 (2016). [Erratum: JHEP 08, 080 (2017)], p. 148. DOI: 10.1007/JHEP11(2016)148. arXiv: 1608.01985 [hep-ph].

[274] V. Andreev and N. Hutzler. "Improved Limit on the Electric Dipole Moment of the Electron". In: *Nature* 562.7727 (Oct. 2018). DOI: 10.1038/s41586-018-0599-8.

[275] Gilly Elor et al. "New Ideas in Baryogenesis: A Snowmass White Paper". In: *2022 Snowmass Summer Study*. Mar. 2022. arXiv: 2203.05010 [hep-ph].

[276] Apostolos Pilaftsis and Thomas E. J. Underwood. "Resonant leptogenesis". In: *Nucl. Phys. B* 692 (2004), pp. 303–345. DOI: 10.1016/j.nuclphysb.2004.05.029. arXiv: hep-ph/0309342.

[277] Apostolos Pilaftsis and Thomas E. J. Underwood. "Electroweak-scale resonant leptogenesis". In: *Phys. Rev. D* 72 (2005), p. 113001. DOI: 10.1103/PhysRevD.72.113001. arXiv: hep-ph/0506107.

[278] Koichi Hamaguchi, Hitoshi Murayama, and T. Yanagida. "Leptogenesis from N dominated early universe". In: *Phys. Rev. D* 65 (2002), p. 043512. DOI: 10.1103/PhysRevD.65.043512. arXiv: hep-ph/0109030.

[279] R. Barbier et al. "R-parity violating supersymmetry". In: *Phys. Rept.* 420 (2005), pp. 1–202. DOI: 10.1016/j.physrep.2005.08.006. arXiv: hep-ph/0406039.

[280] Savas Dimopoulos and Lawrence J. Hall. "Baryogenesis at the MeV Era". In: *Phys. Lett. B* 196 (1987), pp. 135–141. DOI: 10.1016/0370-2693(87)90593-4.

[281] K. S. Babu, R. N. Mohapatra, and S. Nasri. "Post-Sphaleron Baryogenesis". In: *Phys. Rev. Lett.* 97 (2006), p. 131301. DOI: 10.1103/PhysRevLett.97.131301. arXiv: hep-ph/0606144.

[282] David McKeen and Ann E. Nelson. "CP Violating Baryon Oscillations". In: *Phys. Rev. D* 94.7 (2016), p. 076002. DOI: 10.1103/PhysRevD.94.076002. arXiv: 1512.05359 [hep-ph].

[283] Kyle Aitken et al. "Baryogenesis from Oscillations of Charmed or Beautiful Baryons". In: *Phys. Rev. D* 96.7 (2017), p. 075009. DOI: 10.1103/PhysRevD.96.075009. arXiv: 1708.01259 [hep-ph].

[284] Gilly Elor, Miguel Escudero, and Ann Nelson. "Baryogenesis and Dark Matter from B Mesons". In: *Phys. Rev. D* 99.3 (2019), p. 035031. DOI: 10.1103/PhysRevD.99.035031. arXiv: 1810.00880 [hep-ph].

[285] Christophe Grojean et al. "Implications of an Improved Neutron-Antineutron Oscillation Search for Baryogenesis: A Minimal Effective Theory Analysis". In: *Phys. Rev. Lett.* 121.17 (2018), p. 171801. DOI: 10.1103/PhysRevLett.121.171801. arXiv: 1806.00011 [hep-ph].

[286] Yuta Hamada, Ryuichiro Kitano, and Wen Yin. "Leptogenesis via Neutrino Oscillation Magic". In: *JHEP* 10 (2018), p. 178. DOI: 10.1007/JHEP10(2018)178. arXiv: 1807.06582 [hep-ph].

[287] Aaron Pierce and Bibhushan Shakya. "Gaugino Portal Baryogenesis". In: *JHEP* 06 (2019), p. 096. DOI: 10.1007/JHEP06(2019)096. arXiv: 1901.05493 [hep-ph].

[288] Takehiko Asaka, Hiroyuki Ishida, and Wen Yin. "Direct baryogenesis in the broken phase". In: *JHEP* 07 (2020), p. 174. DOI: 10.1007/JHEP07(2020)174. arXiv: 1912.08797 [hep-ph].

[289] M. Fukugita and T. Yanagida. "Baryogenesis Without Grand Unification". In: *Phys. Lett. B* 174 (1986), pp. 45–47. DOI: 10.1016/0370-2693(86)91126-3.

[290] Peter Minkowski. "$\mu \to e\gamma$ at a Rate of One Out of 10^9 Muon Decays?" In: *Phys. Lett. B* 67 (1977), pp. 421–428. DOI: 10.1016/0370-2693(77)90435-X.

[291] Tsutomu Yanagida. "Horizontal gauge symmetry and masses of neutrinos". In: *Conf. Proc. C* 7902131 (1979). Ed. by Osamu Sawada and Akio Sugamoto, pp. 95–99.

[292] Murray Gell-Mann, Pierre Ramond, and Richard Slansky. "Complex Spinors and Unified Theories". In: *Conf. Proc. C* 790927 (1979), pp. 315–321. arXiv: 1306.4669 [hep-th].

[293] S. L. Glashow. "The Future of Elementary Particle Physics". In: *NATO Sci. Ser. B* 61 (1980), p. 687. DOI: 10.1007/978-1-4684-7197-7_15.

[294] Rabindra N. Mohapatra and Goran Senjanovic. "Neutrino Mass and Spontaneous Parity Nonconservation". In: *Phys. Rev. Lett.* 44 (1980), p. 912. DOI: 10.1103/PhysRevLett.44.912.

[295] Sacha Davidson, Enrico Nardi, and Yosef Nir. "Leptogenesis". In: *Phys. Rept.* 466 (2008), pp. 105–177. DOI: 10.1016/j.physrep.2008.06.002. arXiv: 0802.2962 [hep-ph].

[296] Tom Charnock et al. "CMB constraints on cosmic strings and superstrings". In: *Phys. Rev. D* 93.12 (2016), p. 123503. DOI: 10.1103/PhysRevD.93.123503. arXiv: 1603.01275 [astro-ph.CO].

[297] Takashi Hiramatsu, Masahiro Kawasaki, and Ken'ichi Saikawa. "On the estimation of gravitational wave spectrum from cosmic domain walls". In: *JCAP* 02 (2014), p. 031. DOI: 10.1088/1475-7516/2014/02/031. arXiv: 1309.5001 [astro-ph.CO].

[298] Marco Gorghetto, Edward Hardy, and Horia Nicolaescu. "Observing invisible axions with gravitational waves". In: *JCAP* 06 (2021), p. 034. DOI: 10.1088/1475-7516/2021/06/034. arXiv: 2101.11007 [hep-ph].

[299] Paolo Creminelli, Alberto Nicolis, and Riccardo Rattazzi. "Holography and the electroweak phase transition". In: *JHEP* 03 (2002), p. 051. DOI: 10.1088/1126-6708/2002/03/051. arXiv: hep-th/0107141 [hep-th].

[300] Marcela Carena et al. "Electroweak baryogenesis and new TeV fermions". In: *Nucl. Phys. B* 716 (2005), pp. 319–351. DOI: 10.1016/j.nuclphysb.2005.03.025. arXiv: hep-ph/0410352.

[301] Andrei Angelescu and Peisi Huang. "Multistep Strongly First Order Phase Transitions from New Fermions at the TeV Scale". In: *Phys. Rev. D* 99.5 (2019), p. 055023. DOI: 10.1103/PhysRevD.99.055023. arXiv: 1812.08293 [hep-ph].

[302] Jeff A. Dror et al. "Testing the Seesaw Mechanism and Leptogenesis with Gravitational Waves". In: *Phys. Rev. Lett.* 124.4 (2020), p. 041804. DOI: 10.1103/PhysRevLett.124.041804. arXiv: 1908.03227 [hep-ph].

[303] Iason Baldes et al. "Baryogenesis via relativistic bubble expansion". In: (June 2021). arXiv: 2106.15602 [hep-ph].

[304] Greg W. Anderson and Lawrence J. Hall. "Electroweak phase transition and baryogenesis". In: *Phys. Rev. D* 45 (8 Apr. 1992), pp. 2685–2698. DOI: 10.1103/PhysRevD.45.2685. URL: https://link.aps.org/doi/10.1103/PhysRevD.45.2685.

[305] Jarny Choi and R. R. Volkas. "Real Higgs singlet and the electroweak phase transition in the Standard Model". In: *Phys. Lett. B* 317 (1993), pp. 385–391. DOI: 10.1016/0370-2693(93)91013-D. arXiv: hep-ph/9308234.

[306] J. R. Espinosa and M. Quiros. "The Electroweak phase transition with a singlet". In: *Phys. Lett. B* 305 (1993), pp. 98–105. DOI: 10.1016/0370-2693(93)91111-Y. arXiv: hep-ph/9301285.

[307] Stefano Profumo, Michael J. Ramsey-Musolf, and Gabe Shaughnessy. "Singlet Higgs phenomenology and the electroweak phase transition". In: *JHEP* 08 (2007), p. 010. DOI: 10.1088/1126-6708/2007/08/010. arXiv: 0705.2425 [hep-ph].

[308] Jose R. Espinosa, Thomas Konstandin, and Francesco Riva. "Strong Electroweak Phase Transitions in the Standard Model with a Singlet". In: *Nucl. Phys. B* 854 (2012), pp. 592–630. DOI: 10.1016/j.nuclphysb.2011.09.010. arXiv: 1107.5441 [hep-ph].

[309] Chien-Yi Chen, Jonathan Kozaczuk, and Ian M. Lewis. "Non-resonant Collider Signatures of a Singlet-Driven Electroweak Phase Transition". In: *JHEP* 08 (2017), p. 096. DOI: 10.1007/JHEP08(2017)096. arXiv: 1704.05844 [hep-ph].

[310] Mikael Chala, Claudius Krause, and Germano Nardini. "Signals of the electroweak phase transition at colliders and gravitational wave observatories". In: *JHEP* 07 (2018), p. 062. DOI: 10.1007/JHEP07(2018)062. arXiv: 1802.02168 [hep-ph].

[311] Fa Peng Huang et al. "Testing the electroweak phase transition and electroweak baryogenesis at the LHC and a circular electron-positron collider". In: *Phys. Rev. D* 93.10 (2016), p. 103515. DOI: 10.1103/PhysRevD.93.103515. arXiv: 1511.03969 [hep-ph].

[312] Dietrich Bodeker et al. "The Baryon asymmetry in the standard model with a low cut-off". In: *JHEP* 02 (2005), p. 026. DOI: 10.1088/1126-6708/2005/02/026. arXiv: hep-ph/0412366.

[313] K$are Fridell$, Julia Harz, and Chandan Hati. "Probing baryogenesis with neutron-antineutron oscillations". In: (May 2021). arXiv: 2105.06487 [hep-ph].

[314] M. Baldo-Ceolin et al. "A New experimental limit on neutron - anti-neutron oscillations". In: *Z. Phys. C* 63 (1994), pp. 409–416. DOI: 10.1007/BF01580321.

[315] K. Abe et al. "The Search for $n - \bar{n}$ oscillation in Super-Kamiokande I". In: *Phys. Rev. D* 91 (2015), p. 072006. DOI: 10.1103/PhysRevD.91.072006. arXiv: 1109.4227 [hep-ex].

[316] Sumathi Rao and Robert Shrock. "$n \leftrightarrow \bar{n}$ Transition Operators and Their Matrix Elements in the MIT Bag Model". In: *Phys. Lett. B* 116 (1982), pp. 238–242. DOI: 10.1016/0370-2693(82)90333-1.

[317] Michael I. Buchoff, Chris Schroeder, and Joseph Wasem. "Neutron-antineutron oscillations on the lattice". In: *PoS* LATTICE2012 (2012), p. 128. DOI: 10.22323/1.164.0128. arXiv: 1207.3832 [hep-lat].

[318] Sergey Syritsyn et al. "Neutron-antineutron oscillation matrix elements with domain wall fermions at the physical point". In: *PoS* LATTICE2015 (2016), p. 132. DOI: 10.22323/1.251.0132.

[319] D. G. Phillips II et al. "Neutron-Antineutron Oscillations: Theoretical Status and Experimental Prospects". In: *Phys. Rept.* 612 (2016), pp. 1–45. DOI: 10.1016/j.physrep.2015.11.001. arXiv: 1410.1100 [hep-ex].

[320] David Milstead. "A new high sensitivity search for neutron-antineutron oscillations at the ESS". In: *PoS* EPS-HEP2015 (2015), p. 603. DOI: 10.22323/1.234.0603. arXiv: 1510.01569 [physics.ins-det].

[321] M. J. Frost. "The NNbar Experiment at the European Spallation Source". In: *7th Meeting on CPT and Lorentz Symmetry*. July 2016. DOI: 10.1142/9789813148505_0070. arXiv: 1607.07271 [hep-ph].

[322] Jeremy E. T. Hewes. "Searches for Bound Neutron-Antineutron Oscillation in Liquid Argon Time Projection Chambers". PhD thesis. Manchester U., 2017. DOI: 10.2172/1426674.

[323] Gian Francesco Giudice, Ben Gripaios, and Raman Sundrum. "Flavourful Production at Hadron Colliders". In: *JHEP* 08 (2011), p. 055. DOI: 10.1007/JHEP08(2011)055. arXiv: 1105.3161 [hep-ph].

[324] Jonathan Engel, Michael J. Ramsey-Musolf, and U. van Kolck. "Electric Dipole Moments of Nucleons, Nuclei, and Atoms: The Standard Model and Beyond". In: *Prog. Part. Nucl. Phys.* 71 (2013), pp. 21–74. DOI: 10.1016/j.ppnp.2013.03.003. arXiv: 1303.2371 [nucl-th].

[325] D. Chang et al. "QCD Corrections to CP Violation From Color Electric Dipole Moment of b Quark". In: *Phys. Lett. B* 241 (1990), pp. 589–592. DOI: 10.1016/0370-2693(90)91875-C.

[326] Hector Gisbert and Joan Ruiz Vidal. "Improved bounds on heavy quark electric dipole moments". In: *Phys. Rev. D* 101.11 (2020), p. 115010. DOI: 10.1103/PhysRevD.101.115010. arXiv: 1905.02513 [hep-ph].

[327] Stephen M. Barr and A. Zee. "Electric Dipole Moment of the Electron and of the Neutron". In: *Phys. Rev. Lett.* 65 (1990). [Erratum: Phys.Rev.Lett. 65, 2920 (1990)], pp. 21–24. DOI: 10.1103/PhysRevLett.65.21.

[328] Pau Amaro-Seoane et al. *Laser Interferometer Space Antenna*. 2017. arXiv: 1702.00786 [astro-ph.IM].

[329] Chiara Caprini et al. "Science with the space-based interferometer eLISA. II: Gravitational waves from cosmological phase transitions". In: *JCAP* 1604.04 (2016), p. 001. DOI: 10.1088/1475-7516/2016/04/001. arXiv: 1512.06239 [astro-ph.CO].

[330] Benedict Von Harling et al. "Peccei-Quinn Phase Transition at LIGO". In: *JHEP* 04 (2020), p. 195. DOI: 10.1007/JHEP04(2020)195. arXiv: 1912.07587 [hep-ph].

[331] Vedran Brdar, Alexander J. Helmboldt, and Jisuke Kubo. "Gravitational Waves from First-Order Phase Transitions: LIGO as a Window to Unexplored Seesaw Scales". In: *JCAP* 02 (2019), p. 021. DOI: 10.1088/1475-7516/2019/02/021. arXiv: 1810.12306 [hep-ph].

[332] Vincent Corbin and Neil J. Cornish. "Detecting the cosmic gravitational wave background with the big bang observer". In: *Class. Quant. Grav.* 23 (2006), pp. 2435–2446. DOI: 10.1088/0264-9381/23/7/014. arXiv: gr-qc/0512039.

[333] Jeff Crowder and Neil J. Cornish. "Beyond LISA: Exploring future gravitational wave missions". In: *Phys. Rev. D* 72 (2005), p. 083005. DOI: 10.1103/PhysRevD.72.083005. arXiv: gr-qc/0506015.

[334] Naoki Seto, Seiji Kawamura, and Takashi Nakamura. "Possibility of direct measurement of the acceleration of the universe using 0.1-Hz band laser interferometer gravitational wave antenna in space". In: *Phys. Rev. Lett.* 87 (2001), p. 221103. DOI: 10.1103/PhysRevLett.87.221103. arXiv: astro-ph/0108011.

[335] Kent Yagi and Naoki Seto. "Detector configuration of DECIGO/BBO and identification of cosmological neutron-star binaries". In: *Phys. Rev. D* 83 (2011). [Erratum: Phys.Rev.D 95, 109901 (2017)], p. 044011. DOI: 10.1103/PhysRevD.83.044011. arXiv: 1101.3940 [astro-ph.CO].

[336] Soichiro Isoyama, Hiroyuki Nakano, and Takashi Nakamura. "Multiband Gravitational-Wave Astronomy: Observing binary inspirals with a decihertz detector, B-DECIGO". In: *PTEP* 2018.7 (2018), 073E01. DOI: 10.1093/ptep/pty078. arXiv: 1802.06977 [gr-qc].

[337] S. Hild et al. "Sensitivity Studies for Third-Generation Gravitational Wave Observatories". In: *Class. Quant. Grav.* 28 (2011), p. 094013. DOI: 10.1088/0264-9381/28/9/094013. arXiv: 1012.0908 [gr-qc].

[338] Michele Maggiore et al. "Science Case for the Einstein Telescope". In: *JCAP* 03 (2020), p. 050. DOI: 10.1088/1475-7516/2020/03/050. arXiv: 1912.02622 [astro-ph.CO].

[339] L. Badurina et al. "AION: An Atom Interferometer Observatory and Network". In: *JCAP* 05 (2020), p. 011. DOI: 10.1088/1475-7516/2020/05/011. arXiv: 1911.11755 [astro-ph.CO].

[340] Yousef Abou El-Neaj et al. "AEDGE: Atomic Experiment for Dark Matter and Gravity Exploration in Space". In: *EPJ Quant. Technol.* 7 (2020), p. 6. DOI: 10.1140/epjqt/s40507-020-0080-0. arXiv: 1908.00802 [gr-qc].

[341] Georges Aad et al. "Search for squarks and gluinos in final states with jets and missing transverse momentum using 139 fb^{-1} of $\sqrt{s}$ =13 TeV pp collision data with the ATLAS detector". In: *JHEP* 02 (2021), p. 143. DOI: 10.1007/JHEP02(2021)143. arXiv: 2010.14293 [hep-ex].

[342] Albert M Sirunyan et al. "Search for supersymmetry in proton-proton collisions at 13 TeV in final states with jets and missing transverse momentum". In: *JHEP* 10 (2019), p. 244. DOI: 10.1007/JHEP10(2019)244. arXiv: 1908.04722 [hep-ex].

[343] David N. Schramm. "Phase Transitions and Dark Matter Problems". In: *Nucl. Phys. B* 252 (1985). Ed. by R. Baier and H. Satz, pp. 53–71. DOI: 10.1016/0550-3213(85)90425-0.

[344] Lucien Heurtier and Hervé Partouche. "Spontaneous Freeze Out of Dark Matter From an Early Thermal Phase Transition". In: *Phys. Rev. D* 101.4 (2020), p. 043527. DOI: 10.1103/PhysRevD.101.043527. arXiv: 1912.02828 [hep-ph].

[345] Kalliopi Petraki, Mark Trodden, and Raymond R. Volkas. "Visible and dark matter from a first-order phase transition in a baryon-symmetric universe". In: *JCAP* 02 (2012), p. 044. DOI: 10.1088/1475-7516/2012/02/044. arXiv: 1111.4786 [hep-ph].

[346] Iason Baldes. "Gravitational waves from the asymmetric-dark-matter generating phase transition". In: *JCAP* 05 (2017), p. 028. DOI: 10.1088/1475-7516/2017/05/028. arXiv: 1702.02117 [hep-ph].

[347] Eleanor Hall et al. "Asymmetric Matters from a Dark First-Order Phase Transition". In: (Nov. 2019). arXiv: 1911.12342 [hep-ph].

[348] Nathaniel Craig et al. "Ripples in Spacetime from Broken Supersymmetry". In: *JHEP* 21 (Nov. 2020), p. 184. DOI: 10.1007/JHEP02(2021)184. arXiv: 2011.13949 [hep-ph].

[349] F. Csikor, Z. Fodor, and J. Heitger. "Endpoint of the hot electroweak phase transition". In: *Phys. Rev. Lett.* 82 (1999), pp. 21–24. DOI: 10.1103/PhysRevLett.82.21. arXiv: hep-ph/9809291 [hep-ph].

[350] K. Kajantie et al. "A Nonperturbative analysis of the finite T phase transition in SU(2) x U(1) electroweak theory". In: *Nucl. Phys. B* 493 (1997), pp. 413–438. DOI: 10.1016/S0550-3213(97)00164-8. arXiv: hep-lat/9612006.

[351] Michela D'Onofrio and Kari Rummukainen. "Standard model cross-over on the lattice". In: *Phys. Rev. D* 93.2 (2016), p. 025003. DOI: 10.1103/PhysRevD.93.025003. arXiv: 1508.07161 [hep-ph].

[352] A.I. Bochkarev, S.V. Kuzmin, and M.E. Shaposhnikov. "Electroweak baryogenesis and the Higgs boson mass problem". In: *Physics Letters B* 244.2 (1990), pp. 275–278. ISSN: 0370-2693. DOI: https://doi.org/10.1016/0370-2693(90)90069-I. URL: http://www.sciencedirect.com/science/article/pii/037026939090069I.

[353] Zoltan Fodor and Arthur Hebecker. "Finite temperature effective potential to order g^4, λ^2 and the electroweak phase transition". In: *Nucl. Phys. B* 432 (1994), pp. 127–146. DOI: 10.1016/0550-3213(94)90596-7. arXiv: hep-ph/9403219.

[354] Micha Berkooz, Yosef Nir, and Tomer Volansky. "Baryogenesis from the Kobayashi-Maskawa phase". In: *Phys. Rev. Lett.* 93 (2004), p. 051301. DOI: 10.1103/PhysRevLett.93.051301. arXiv: hep-ph/0401012.

[355] Iason Baldes, Thomas Konstandin, and Geraldine Servant. "A first-order electroweak phase transition from varying Yukawas". In: *Phys. Lett. B* 786 (2018), pp. 373–377. DOI: 10.1016/j.physletb.2018.10.015. arXiv: 1604.04526 [hep-ph].

[356] Archil Kobakhidze, Adrian Manning, and Jason Yue. "Gravitational waves from the phase transition of a nonlinearly realized electroweak gauge symmetry". In: *Int. J. Mod. Phys. D* 26.10 (2017), p. 1750114. DOI: 10.1142/S0218271817501140. arXiv: 1607.00883 [hep-ph].

[357] Archil Kobakhidze et al. "Gravitational waves from a supercooled electroweak phase transition and their detection with pulsar timing arrays". In: *Eur. Phys. J. C* 77.8 (2017), p. 570. DOI: 10.1140/epjc/s10052-017-5132-y. arXiv: 1703.06552 [hep-ph].

[358] P. Basler et al. "Strong First Order Electroweak Phase Transition in the CP-Conserving 2HDM Revisited". In: *JHEP* 02 (2017), p. 121. DOI: 10.1007/JHEP02(2017)121. arXiv: 1612.04086 [hep-ph].

[359] Christophe Grojean, Geraldine Servant, and James D. Wells. "First-order electroweak phase transition in the standard model with a low cutoff". In: *Phys. Rev. D* 71 (2005), p. 036001. DOI: 10.1103/PhysRevD.71.036001. arXiv: hep-ph/0407019.

[360] Ligong Bian, Yongcheng Wu, and Ke-Pan Xie. "Electroweak phase transition with composite Higgs models: calculability, gravitational waves and collider searches". In: *JHEP* 12 (2019), p. 028. DOI: 10.1007/JHEP12(2019)028. arXiv: 1909.02014 [hep-ph].

[361] James M. Cline, Matti Järvinen, and Francesco Sannino. "Electroweak phase transition in nearly conformal technicolor". In: *Phys. Rev. D* 78 (7 Oct. 2008), p. 075027. DOI: 10.1103/PhysRevD.78.075027. URL: https://link.aps.org/doi/10.1103/PhysRevD.78.075027.

[362] Jose Ramon Espinosa and Mariano Quiros. "Novel Effects in Electroweak Breaking from a Hidden Sector". In: *Phys. Rev. D* 76 (2007), p. 076004. DOI: 10.1103/PhysRevD.76.076004. arXiv: hep-ph/0701145.

[363] Andrew Noble and Maxim Perelstein. "Higgs self-coupling as a probe of electroweak phase transition". In: *Phys. Rev. D* 78 (2008), p. 063518. DOI: 10.1103/PhysRevD.78.063518. arXiv: 0711.3018 [hep-ph].

[364] A. Ashoorioon and T. Konstandin. "Strong electroweak phase transitions without collider traces". In: *JHEP* 07 (2009), p. 086. DOI: 10.1088/1126-6708/2009/07/086. arXiv: 0904.0353 [hep-ph].

[365] Poul H. Damgaard et al. "Constraints on New Physics from Baryogenesis and Large Hadron Collider Data". In: *Phys. Rev. Lett.* 111.22 (2013), p. 221804. DOI: 10.1103/PhysRevLett.111.221804. arXiv: 1305.4362 [hep-ph].

[366] Tommi Alanne, Kimmo Tuominen, and Ville Vaskonen. "Strong phase transition, dark matter and vacuum stability from simple hidden sectors". In: *Nucl. Phys. B* 889 (2014), pp. 692–711. DOI: 10.1016/j.nuclphysb.2014.11.001. arXiv: 1407.0688 [hep-ph].

[367] Peisi Huang, Andrew J. Long, and Lian-Tao Wang. "Probing the Electroweak Phase Transition with Higgs Factories and Gravitational Waves". In: *Phys. Rev. D* 94.7 (2016), p. 075008. DOI: 10.1103/PhysRevD.94.075008. arXiv: 1608.06619 [hep-ph].

[368] Ankit Beniwal et al. "Gravitational wave, collider and dark matter signals from a scalar singlet electroweak baryogenesis". In: *JHEP* 08 (2017), p. 108. DOI: 10.1007/JHEP08(2017)108. arXiv: 1702.06124 [hep-ph].

[369] Vernon Barger et al. "LHC Phenomenology of an Extended Standard Model with a Real Scalar Singlet". In: *Phys. Rev. D* 77 (2008), p. 035005. DOI: 10.1103/PhysRevD.77.035005. arXiv: 0706.4311 [hep-ph].

[370] Jonathan Kozaczuk, Michael J. Ramsey-Musolf, and Jessie Shelton. "Exotic Higgs boson decays and the electroweak phase transition". In: *Phys. Rev. D* 101.11 (2020), p. 115035. DOI: 10.1103/PhysRevD.101.115035. arXiv: 1911.10210 [hep-ph].

[371] Zhen Wang et al. "Study of Electroweak Phase Transition in Exotic Higgs Decays at the CEPC". In: Mar. 2022. arXiv: 2203.10184 [hep-ex].

[372] Gowri Kurup and Maxim Perelstein. "Dynamics of Electroweak Phase Transition In Singlet-Scalar Extension of the Standard Model". In: *Phys. Rev. D* 96.1 (2017), p. 015036. DOI: 10.1103/PhysRevD.96.015036. arXiv: 1704.03381 [hep-ph].

[373] Zhaofeng Kang, P. Ko, and Toshinori Matsui. "Strong first order EWPT & strong gravitational waves in Z_3-symmetric singlet scalar extension". In: *JHEP* 02 (2018), p. 115. DOI: 10.1007/JHEP02(2018)115. arXiv: 1706.09721 [hep-ph].

[374] Lauri Niemi, Philipp Schicho, and Tuomas V. I. Tenkanen. "Singlet-assisted electroweak phase transition at two loops". In: *Phys. Rev. D* 103.11 (2021), p. 115035. DOI: 10.1103/PhysRevD.103.115035. arXiv: 2103.07467 [hep-ph].

[375] Ben Gripaios et al. "Beyond the Minimal Composite Higgs Model". In: *JHEP* 04 (2009), p. 070. DOI: 10.1088/1126-6708/2009/04/070. arXiv: 0902.1483 [hep-ph].

[376] Stefania De Curtis, Luigi Delle Rose, and Giuliano Panico. "Composite Dynamics in the Early Universe". In: *JHEP* 12 (2019), p. 149. DOI: 10.1007/JHEP12(2019)149. arXiv: 1909.07894 [hep-ph].

[377] David Curtin, Patrick Meade, and Chiu-Tien Yu. "Testing Electroweak Baryogenesis with Future Colliders". In: *JHEP* 11 (2014), p. 127. DOI: 10.1007/JHEP11(2014)127. arXiv: 1409.0005 [hep-ph].

[378] Albert M Sirunyan et al. "A measurement of the Higgs boson mass in the diphoton decay channel". In: *Phys. Lett. B* 805 (2020), p. 135425. DOI: 10.1016/j.physletb.2020.135425. arXiv: 2002.06398 [hep-ex].

[379] Martin B. Einhorn and D. R. Timothy Jones. "A NEW RENORMALIZATION GROUP APPROACH TO MULTISCALE PROBLEMS". In: *Nucl. Phys. B* 230 (1984), pp. 261–272. DOI: 10.1016/0550-3213(84)90127-5.

[380] James M. Cline and Kimmo Kainulainen. "Electroweak baryogenesis and dark matter from a singlet Higgs". In: *JCAP* 01 (2013), p. 012. DOI: 10.1088/1475-7516/2013/01/012. arXiv: 1210.4196 [hep-ph].

[381] Ville Vaskonen. "Electroweak baryogenesis and gravitational waves from a real scalar singlet". In: *Phys. Rev. D* 95.12 (2017), p. 123515. DOI: 10.1103/PhysRevD.95.123515. arXiv: 1611.02073 [hep-ph].

[382] Dario Buttazzo, Filippo Sala, and Andrea Tesi. "Singlet-like Higgs bosons at present and future colliders". In: *JHEP* 11 (2015), p. 158. DOI: 10.1007/JHEP11(2015)158. arXiv: 1505.05488 [hep-ph].

[383] Hiren H. Patel and Michael J. Ramsey-Musolf. "Stepping Into Electroweak Symmetry Breaking: Phase Transitions and Higgs Phenomenology". In: *Phys. Rev. D* 88 (2013), p. 035013. DOI: 10.1103/PhysRevD.88.035013. arXiv: 1212.5652 [hep-ph].

[384] Weicong Huang et al. "New insights in the electroweak phase transition in the NMSSM". In: *Phys. Rev. D* 91.2 (2015), p. 025006. DOI: 10.1103/PhysRevD.91.025006. arXiv: 1405.1152 [hep-ph].

[385] Minyuan Jiang et al. "Impact of a complex singlet: Electroweak baryogenesis and dark matter". In: *Phys. Rev. D* 93.6 (2016), p. 065032. DOI: 10.1103/PhysRevD.93.065032. arXiv: 1502.07574 [hep-ph].

[386] Cheng-Wei Chiang, Michael J. Ramsey-Musolf, and Eibun Senaha. "Standard Model with a Complex Scalar Singlet: Cosmological Implications and Theoretical Considerations". In: *Phys. Rev. D* 97.1 (2018), p. 015005. DOI: 10.1103/PhysRevD.97.015005. arXiv: 1707.09960 [hep-ph].

[387] Victor Guada, Miha Nemevsek, and Matevz Pintar. "FindBounce: Package for multi-field bounce actions". In: *Comput. Phys. Commun.* 256 (2020), p. 107480. DOI: 10.1016/j.cpc.2020.107480. arXiv: 2002.00881 [hep-ph].

[388] Riccardo Barbieri and G. F. Giudice. "Upper Bounds on Supersymmetric Particle Masses". In: *Nucl. Phys. B* 306 (1988), pp. 63–76. DOI: 10.1016/0550-3213(88)90171-X.

[389] K. Enqvist et al. "Nucleation and bubble growth in a first order cosmological electroweak phase transition". In: *Phys. Rev.* D45 (10 May 1992), pp. 3415–3428. DOI: 10.1103/PhysRevD.45.3415. URL: https://link.aps.org/doi/10.1103/PhysRevD.45.3415.

[390] Simone Blasi and Alberto Mariotti. "Domain walls seeding the electroweak phase transition". In: (Mar. 2022). arXiv: 2203.16450 [hep-ph].

[391] Spyros Argyropoulos, Oleg Brandt, and Ulrich Haisch. "Collider Searches for Dark Matter through the Higgs Lens". In: *Symmetry* 2021 (Sept. 2021), p. 13. DOI: 10.3390/sym13122406. arXiv: 2109.13597 [hep-ph].